NASA CR - 135141

(NASA-CR-135141) ADVANCED HIGH PRESSURE ENGINE STUDY FOR MIXED-MODE VEHICLE APPLICATIONS Final Report (Aerojet Liquid Rocket Co.) 319 p HC A14/MF A01 CSCL 21H
N77-23194
Unclas
G3/20 29065

NASA

ADVANCED HIGH PRESSURE ENGINE STUDY FOR MIXED-MODE VEHICLE APPLICATIONS

Final Report

by

W. P. Luscher and J. A. Mellish

AEROJET LIQUID ROCKET COMPANY

Prepared for

NATIONAL AERONAUTICS AND SPACE ADMINISTRATION

NASA Lewis Research Center

Contract NAS 3-19727

1. Report No.	2. Government Accession No.	3. Recipient's Catalog No.
NASA CR-135141		

4. Title and Subtitle	5. Report Date
Advanced High Pressure Engine Study for Mixed-Mode Vehicle Applications, Final Report	January 1977
	6. Performing Organization Code

7. Author(s)

W. P. Luscher and J. A. Mellish

8. Performing Organization Report No.

9. Performing Organization Name and Address

Aerojet Liquid Rocket Company
Post Office Box 13222
Sacramento, California 95813

10. Work Unit No.

11. Contract or Grant No.

NAS3-19727

13. Type of Report and Period Covered

Contractor Report, Final

12. Sponsoring Agency Name and Address

National Aeronautics and Space Administration
Washington, D. C. 20546

14. Sponsoring Agency Code

15. Supplementary Notes

Project Manager, D. D. Scheer, Chemical Energy Division, NASA-Lewis Research Center, Cleveland, Ohio

16. Abstract High pressure liquid rocket engine design, performance, weight, envelope and operational characteristics were evaluated for a variety of candidate engines for use in mixed-mode, single-stage-to-orbit applications.

Propellant property and performance data were obtained for candidate Mode 1 fuels which included; RP-1, RJ-5, hydrazine, monomethyl-hydrazine, and methane. The common oxidizer was liquid oxygen. Oxygen, the candidate Mode 1 fuels, and hydrogen were evaluated as thrust chamber coolants. Oxygen, methane and hydrogen were found to be the most viable cooling candidates. Water, lithium and sodium-potassium were also evaluated as auxiliary coolant systems. Water proved to be the best of these but the system was heavier than those systems which cooled with the engine propellants.

Engine weight and envelope parametric data were established for candidate Mode 1, Mode 2 and dual-fuel engines. Delivered engine performance data was also calculated for all candidate Mode 1 and dual-fuel engine.

Engines carried into preliminary design were; (1) LOX cooled, LOX/RP-1 Mode 1, staged combustion cycle, (2) hydrogen cooled, LOX/RP-1 Mode 1, gas-generator cycle, and (3) dual-fuel LOX cooled, LOX/RP-1 Mode 1/LH_2 Mode 2, staged combustion cycle.

17. Key Words (Suggested by Author(s))

Single-Stage-to-Orbit
Mixed-Mode Propulsion
High Pressure Liquid Rocket Engine
Mode 1 and Mode 2
Dual-Fuel

18. Distribution Statement

Unclassified - Unlimited

19. Security Classif. (of this report)	20. Security Classif. (of this page)	21. No. of Pages	22. Price*
Unclassified	Unclassified	304	

*For sale by the National Technical Information Service, Springfield, Virginia 22151

FOREWORD

The work described herein was performed at the Aerojet Liquid Rocket Company under NASA Contract NAS3-19727 with Mr. Dean D. Scheer, NASA-Lewis Research Center, as Project Manager. The ALRC Program Manager was Mr. Werner P. Luscher and the Project Engineer was Mr. Joseph A. Mellish.

The technical period performance for the study was from 30 June 1975 to 30 June 1976.

The authors wish to acknowledge the efforts of the following ALRC engineering personnel who contributed significantly to this report:

R. E. Anderson
L. L. Bickford
A. T. Caffo
R. L. Ewen
J. W. Hidahl
M. C. Huppert
G. R. Janser
J. E. Jellison
C. J. O'Brien
J. W. Salmon
D. H. Saltzman
M. Short
K. Y. Wong

We also wish to thank Mr. Rudi Beichel, ALRC Senior Scientist, for his comments and assistance throughout the study effort.

TABLE OF CONTENTS

TABLE OF CONTENTS (cont.)

TABLE OF CONTENTS (cont.)

LIST OF TABLES

LIST OF TABLES (cont.)

LIST OF TABLES (cont.)

LIST OF TABLES (cont.)

LIST OF TABLES (cont.)

LIST OF FIGURES

LIST OF FIGURES (cont.)

LIST OF FIGURES (cont.)

LIST OF FIGURES (cont.)

SECTION I
SUMMARY

A. STUDY OBJECTIVES AND SCOPE

The major objectives of this study program were to provide parametric data, preliminary designs and identify technology requirements of advanced high pressure engines for use in mixed-mode single-stage-to-orbit vehicles.

The two sets of liquid rocket engines used as the propulsion for the mixed-mode vehicle concept are called Mode 1 and Mode 2. Mode 1 engines use relatively low performance, high density propellants while the Mode 2 engines use high performance, low density oxygen/hydrogen propellants. A third engine type, called the dual-fuel, uses both high density fuel and low density hydrogen sequentially in a common thrust chamber. This study was primarily concerned with the Mode 1 and dual-fuel engines.

To accomplish the objectives, the six task study program summarized on Figure 1 was conducted.

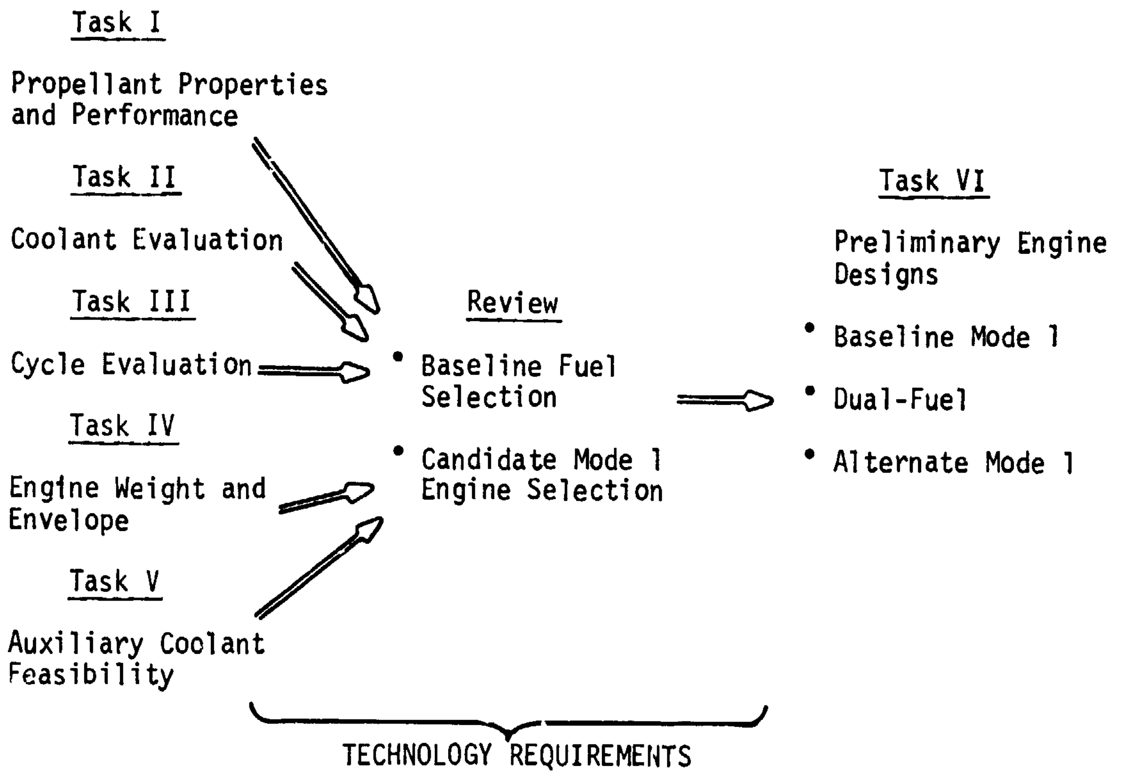

Figure 1. Advanced High Pressure Engine Study Program Summary

High pressure engine design, performance, weight, envelope and operational characteristics were evaluated for a variety of candidate engines.

Propellant property, performance and characteristic data were obtained for candidate Mode 1 fuels which included; kerosene (RP-1), SHELLDYNE-H[R] (RJ-5), hydrazine (N_2H_4), monomethyly-hydrazine (MMH), and methane (CH_4). Liquid oxygen was the common oxidizer.

Oxygen, the candidate Mode 1 fuels, and hydrogen were evaluated as thrust chamber coolants for the Mode 1 engines. The dual-fuel engine was oxygen cooled and the baseline Mode 2 engine was a hydrogen cooled configuration similar to the Space Shuttle Main Engine (SSME). Water, lithium, and sodium potassium (NaK 56%) were also evaluated as auxiliary systems for cooling the chamber.

Engine weight and envelope parametric data were established for the candidate Mode 1 engine, the oxygen/hydrogen Mode 2 engine and the dual-fuel engine. Delivered engine specific impulse data were also calculated at the most practical thrust chamber pressure for all candidate Mode 1 and the dual-fuel engines.

Based upon the results of Task I through V and the study guidelines, three engines were carried into a preliminary design phase. These engines were; (1) baseline Mode 1, LOX cooled, LOX/RP-1, staged combustion cycle, (2) dual-fuel, LOX cooled, LOX/RP-1 (Mode 1) and LH_2 (Mode 2), staged combustion cycle, and (3) alternate Mode 1, hydrogen cooled, LOX/RP-1, gas generator cycle.

Throughout the entire study effort, basic data gaps and areas requiring technology work were identified.

B. RESULTS AND CONCLUSIONS

Oxygen, methane and hydrogen were found to be the most viable candidates for cooling the Mode 1 engine. RP-1 and RJ-5 are unfeasible for cooling at chamber pressures above 136 atmospheres (2,000 psia) because of coking and gumming in the coolant channels. For long term use, N_2H_4 and MMH are incompatible with zirconium copper, ZrCu, which was the specified thrust chamber material for the study effort. In addition, the fuel-rich combustion products of LOX/MMH and LOX/N_2H_4 create a turbine design life problem because the combustion temperatures are in excess of 1000°F (1800°R). Water proved to be the best auxiliary coolant but the system was heavier than those using one of the main propellants as a coolant.

The Task I through V review resulted in the following major decisions:

- Change the baseline fuel from RJ-5 to RP-1.

• Select the hydrogen cooled, gas generator cycle engine as the candidate Mode 1 for preliminary design.

• Include methane (CH_4) in the first four study tasks.

Current RJ-5 propellant costs are 4.41 \$/Kg (2.00 \$/Lb). This cost appeared to be probibitive and RP-1 was selected as the baseline Mode 1 fuel for the preliminary engine designs. However, the higher density of RJ-5 still makes this fuel attractive for use if the cost goes down when purchased in large quantities.

The current cost of CH_4 is similar to that of RP-1, 0.132 \$/Kg (0.06 \$/Lb) and offers about 10 secs. greater specific impulse for an engine weight penalty of approximately 218 Kg (480 Lb). Because of the late entry of the CH_4 into the study, a preliminary design of a LOX/CH_4 engine could not be incorporated within the remaining study time span. However, because of the potential benefits previously mentioned, the LOX/CH_4 engine should be studied further in a preliminary design phase.

The hydrogen cooled, gas generator cycle engine was selected as the candidate Mode 1 engine because preliminary trade-off studies showed potential improvements in either vehicle gross lift-off weight or dry weight when compared to the baseline.

The engine design data summary for the three engines carried into the preliminary design phase is shown on Table I.

Supporting research and technology programs are recommended to fill basic data gaps or provide critical information prior to entering a high pressure, Mode 1 or dual-fuel engine development. These programs are required to verify propellant and combustion gas property data at high pressure, provide heat transfer information on liquid oxygen as a coolant, obtain engine and component life data and to verify engine performance at high thrust chamber pressure.

TABLE I. - ENGINE PRELIMINARY DESIGN DATA SUMMARY

	ENGINE CONFIGURATION			
	Baseline Mode 1	Alternate Mode 1	Dual-Fuel	
			Mode 1	Mode 2
Main Propellants Oxidizer Fuel	 Oxygen RP-1	 Oxygen RP-1	 Oxygen RP-1	 Oxygen LH2
Coolant	Oxygen	Hydrogen	Oxygen	Oxygen
Cycle	Staged Combustion	Gas Generator	Staged Combustion	Staged Combustion
Thrust, N (Lb) Sea-Level Vacuum	 2.70×10^6 (607,000) 2.926×10^6 (657,700)	 2.70×10^6 (607,000) 2.927×10^6 (658,000)	 2.70×10^6 (607,000) 2.926×10^6 (657,700)	 -- 2.292×10^6 (515,250)
Specific Impulse, sec. Sea-Level Vacuum	 323.6 350.6	 323.5 350.7	 322.9 349.9	 -- 459.2
Thrust Chamber Pressure, Atm. (psia)	272 (4000)	289 (4250)	272 (4000)	204 (3000)
Engine Mixture Ratio, O/F	2.9	2.9[a]	2.9	7.0
Nozzle Area Ratio, ε	40	42.7	40	200
LOX Flow Rate, Kg/sec (lb/sec)	632.7 (1394.8)	626.1 (1380.4)	634.0 (1397.8)	445.3 (981.8)
RP-1 Flow Rate, Kg/sec (lb/sec)	218.2 (481.0)	215.9 (476.0)	218.6 (482.0)	--
H_2 Flow Rate, Kg/sec (lb/sec)	--	9.07 (20.0)	--	63.64 (140.3)
Engine Dry Weight, Kg (lb)	2112 (4657)	1758 (3935)	4183 (9223)	--
Engine Length, CM (in.)	277 (109)	315 (124)	307 (121)[b]	734/879 (289/346)[c]
Maximum Diameter, CM (in.)	224 (88)[d]	208 (81.5)[d]	392 (154.5)[d]	392 (154.5)[e]

[a]LOX/RP-1

[b]Fixed ε = 40 Nozzle

[c]Extenible Nozzle, Retracted/Deployed

[d]Powerhead

[e]Mode 2 Nozzle Exit Dia.

SECTION II
INTRODUCTION

A. BACKGROUND

The NASA is currently conducting studies of advanced recoverable vehicle concepts for the post 1990 time period in order to identify technology needs and provide guidance in agency planning. One of the concepts under study is a vertical takeoff, horizontal landing (VTOHL) single-stage-to-orbit (SSTO) vehicle which utilizes mixed-mode ascent propulsion. Mixed-mode propulsion involves the sequential or parallel use of high density impulse propellants and high specific impulse propellants in a single stage to increase vehicle performance and reduce vehicle weight. The concept has been described in the literature (e.g., "Reusable One-Stage-to-Orbit Shuttles: Brightening Prospects" by Robert Salkeld and Rudi Beichel, Astronautics and Aeronautics, June, 1973) and theoretically provides the performance necessary for a VTOHL-SSTO Space Transportation Vehicle.

The propulsion system for the vehicle concepts under study consists of two sets of engines (herein called Mode 1 and Mode 2 engines) which utilize oxygen as a common oxidizer. Mode 1 engines burn a high bulk density fuel during lift-off and early ascent to minimize the performance penalty associated with carrying the weight of Mode 1 fuel tanks to orbit. Mode 2 engines burn hydrogen and complete the trajectory to orbit. In some concepts the Mode 1 and Mode 2 engines are burned sequentially (series burn concept) while other concepts have both the Mode 1 and Mode 2 engines in operation during lift-off and early ascent (parallel burn concept). An engine variation introduced in the previously cited reference integrates hydrogen turbopump system hardware with the basic oxygen-high bulk density fuel engine thus permitting sequential burn of both fuels with the common oxidizer in an engine which shares common components such as the thrust chamber (dual-fuel engine). In all of the concepts, the engines must be lightweight and operate at high chamber pressure to permit high expansion area ratio within the confine of the VTOHL vehicle base area.

B. PURPOSE AND SCOPE

The feasibility of the mixed-mode single-stage-to-orbit vehicle is heavily dependent on the delivered performance of the engine systems. It was the purpose of this effort to analytically determine the performance of candidate engine systems and to identify technology needs in the propulsion area.

Parametric studies and engine preliminary designs were conducted based upon currently achievable component performance levels and currently available materials.

C. GENERAL REQUIREMENTS

For purposes of this study, a parallel burn vehicle with the requirements and operating conditions given in Table II and a series burn vehicle with the requirements and operating conditions given in Table III were assumed as baseline vehicle concepts. Basic requirements for the baseline Mode 1, Mode 2, and dual-fuel engines, consistent with the baseline vehicles, are given in Table IV.

The initial baseline Mode 1 engine for both the parallel burn vehicle and the series burn vehicle was a fixed 40:1 area ratio 90% bell nozzle, staged-combustion turbine drive cycle engine utilizing RJ-5/oxygen as propellants. The thrust chamber is regeneratively cooled with oxygen.

The baseline Mode 2 engine for the parallel burn vehicle is a staged combustion cycle hydrogen-oxygen engine with a fixed 40:1 area ratio 90% bell nozzle for sea level operation and an extendible 200:1 area ratio 90% bell nozzle for vacuum operation. The chamber is regeneratively cooled with hydrogen.

The baseline dual-fuel engine for the series burn vehicle is a basic Mode 1 engine which incorporates those design features and components necessary to provide capability for sequential in-flight operation as a hydrogen-oxygen Mode 2 engine with a 200:1 area ratio 90% bell nozzle. The chamber is regeneratively cooled with oxygen during both operational modes.

D. APPROACH

To accomplish the program objectives, a study involving six technical tasks was conducted. The results of the first five tasks were reviewed to select a baseline fuel, update the baseline engine requirements and performance, and to select a Mode 1 engine concept, in addition to the baseline Mode 1 and dual-fuel, for preliminary design. Tasks conducted were:

1. TASK I: PROPELLANT PROPERTIES AND PERFORMANCE

Property data and characteristics of various candidate propellants were obtained and established as a result of this task.

Oxygen is assumed as the common oxidizer for the Mode 1 engines and the hydrogen-fueled Mode 2 engines. Candidate Mode 1 fuels are kerosene (RP-1), SHEELDYNE-H[R] (RJ-5), hydrazine, monomethyl-hydrazine (MMH) and methane (CH_4).

The data includes:

a. Physical and thermodynamic property data for the candidate fuels.

b. Logistics and safety aspects such as projected availability and cost, handling, chemical and thermal stability, material compatibility, corrosivity and toxicity.

TABLE II. - PARALLEL BURN MIXED-MODE VEHICLE DEFINITION

Gross Weight: 1,448,400 kg (3,193,200 lb.)

Dry Weight: 135,400 kg (298,600 lb.)

Propulsion System

Mode 1

No. of Engines	4	
Vacuum Specific Impulse, Sec.	345.6	
Vacuum Level Thrust per Engine, N (lb)	2.92×10^6	(656,400)
Sea Level Thrust per Engine, N (lb)	2.70×10^6	(607,000)
Ideal Velocity, m/sec (ft/sec)	1,208	(3,962)
Fuel Density, kg/m^3 (lb/ft^3)	1,102	(68.8)
Oxidizer Density, kg/m^3 (lb/ft^3)	1,137	(71.0)
Mixture Ratio	2.4	
Area Ratio	40	

Mode 2

No. of Engines	3	
Vacuum Specific Impulse, Sec.	466.5	
Vacuum Level Thrust per Engine, N (lb)	3.318×10^6	(746,000)
Sea Level Thrust per Engine, N (lb)	2.793×10^6	(628,000)
Ideal Velocity, m/sec (ft/sec)	7,805	(25,608)
Fuel Density, kg/m^3 (lb/ft^3)	70.5	(4.4)
Oxidizer Density, kg/m^3 (lb/ft^3)	1,137	(71.0)
Mixture Ratio	7.0	
Area Ratio (Sea Level/Vacuum)	40/200	

TABLE III. - SERIES BURN MIXED-MODE VEHICLE DEFINITION (DUAL-FUEL ENGINE)

Gross Weight: 1,598,500 kg (3,524,000 lb.)

Dry Weight: 132,900 kg (293,000 lb.)

Propulsion System

Mode 1

No. of Engines	8	
Vacuum Specific Impulse, sec.	3[illegible].6	
Vacuum Level Thrust per Engine, N (lb)	2.92×10^6	(656,400)
Sea Level Thrust per Engine, N (lb)	2.70×10^6	(607,000)
Ideal Velocity, m/sec (ft/sec)	2,462	(8,076)
Fuel Density, kg/m^3 (lb/ft^3)	1,102	(68.8)
Oxidizer Density, kg/m^3 (lb/ft^3)	1,137	(71.0)
Mixture Ratio	2.4	
Area Ratio	40	

Mode 2

No. of Engines	4	
Vacuum Specific Impulse, sec.	466.5	
Vacuum Level Thrust per Engine, N (lb)	2.29×10^6	(515,250)
Ideal Velocity, m/sec (ft/sec)	6,586	(21,608)
Fuel Density, kg/m^3 (lb/ft^3)	70.5	(4.4)
Oxidizer Density, kg/m^3 (lb/ft^3)	1,137	(71.0)
Mixture Ratio	7.0	
Area Ratio (vacuum)	200	

TABLE IV. - BASELINE ENGINE DEFINITIONS

	Parallel Burn		Series Burn, Dual-Fuel	
	Mode 1	Mode 2	Mode 1	Mode 2
Propellants: Oxidizer	Oxygen	Oxygen	Oxygen	Oxygen
Fuel	RJ-5	Hydrogen	RJ-5	Hydrogen
Mixture Ratio, (O/F)	2.4	7.0	2.4	7.0
Sea Level Thrust, N (lb)	2.70×10^6 (607,000)	2.793×10^6 (628,000)	2.70×10^6 (607,000)	--
Vacuum Thrust, N (lb)	2.92×10^6 (656,400)	3.318×10^6 (746,000)	2.92×10^6 (656,400)	2.29×10^6 (515,250)
Vacuum Impulse, Sec.	345.6	466.5	345.6	466.5
Drive Cycle	Staged Comb.	Staged Comb.	Staged Comb.	Staged Comb.
Nozzle Type	90% Bell	90% Bell	90% Bell	90% Bell
Nozzle Expansion Ratio	40	40 SL/200 Vac	40	200
Propellant Inlet Temp.: Oxidizer °K(°R)	90.3 (162.5)	90.3 (162.5)	90.3 (162.5)	90.3 (162.5)
Fuel, °K (°R)	300 (540)	20.3 (36.5)	300 (540)	20.3 (36.5)
NPSH @ Engine Inlet: Oxidizer, m (ft)	4.88 (16)	4.88 (16)	4.88 (16)	4.88 (16)
Fuel, m (ft)	14.0 (46)	19.8 (65)	14.0 (46)	19.8 (65)
Chamber Pressure, Atm. (psia)	272 (4,000)	204 (3,000)	272 (4,000)	204 (3,000)
Service Life Between Overhauls	250 Cycles or 20 Hours Run Time	250 Cycles or 20 Hours Run Time	250 Cycles or 20 Hours Run Time	250 Cycles or 20 Hours Run Time
Gimbal Angle (Square Pattern), Degrees	± 10	± 7	± 10	± 7

c. Main chamber and preburner propellant combination combustion gas thermodynamic and transport property parametric data.

d. Main chamber theoretical rocket performance parametric data.

2. TASK II: COOLANT EVALUATION

The relative coolant capability of candidate Mode 1 fuels, oxygen and hydrogen were determined. Concepts considered are:

Propellant Combination	Coolant
RJ-5/Oxygen	Oxygen
RJ-5/Oxygen	RJ-5
RJ-5/Oxygen	Hydrogen
RP-1/Oxygen	RP-1
Hydrazine/Oxygen	Hydrazine
MMH/Oxygen	MMH
CH_4/Oxygen	CH_4

The relative merit of the various coolants is established on the basis of the attainable thrust chamber pressure, as reflected in the coolant pressure drop, with consideration of potential propellant property problems and limitations.

3. TASK III: CYCLE EVALUATION

Engine cycle pressures, temperatures and delivered performance for various candidate Mode 1 engine concepts were established. Concepts are:

Main Chamber Injector Propellant Combination	Coolant	Description
RJ-5/Oxygen	Oxygen	Gas-Gas, Staged Combustion Cycle
RJ-5/Oxygen	RJ-5	Gas-Gas, Staged Combustion Cycle
RJ-5/Oxygen	Hydrogen	Gas-Gas, Staged Combustion Cycle, Parallel Burn H_2/O_2
RJ-5/Oxygen	Hydrogen	Liquid-Liquid, Gas Generator (H_2/O_2) Cycle
RP-1/Oxygen	RP-1	Gas-Gas, Staged Combustion Cycle
Hydrazine/Oxygen	Hydrazine	Gas-Gas, Staged Combustion Cycle
MMH/Oxygen	MMH	Gas-Gas, Staged Combustion Cycle
CH_4/Oxygen	CH_4	Gas-Gas, Staged Combustion Cycle

The candidate Mode 1 concepts were studied over a practical, achievable chamber pressure range.

4. TASK IV: ENGINE WEIGHT AND ENVELOPE

Weight and envelope estimates for candidate Mode 1 engine concepts and the baseline Mode 2 engine concept were established over ranges of thrust,

thrust chamber pressure and nozzle area ratios.

5. TASK V: AUXILIARY COOLANT FEASIBILITY

The relative merit of auxiliary coolants which include water, lithium, and sodium-potassium (NaK 56%) for an RJ-5/Oxygen Mode 1 engine concept were determined. The relative merit of the auxiliary coolants was established on the basis of coolant capability, auxiliary system weight and complexity, and propellant property considerations.

6. TASK VI: ENGINE PRELIMINARY DESIGN

Preliminary designs and associated data were prepared for three candidate engine concepts and their major components. Engines carried into the design phase were: (1) baseline Mode 1, (2) dual-fuel, and (3) candidate Mode 1 resulting from the study.

SECTION III

TASK I - PROPELLANT PROPERTIES AND PERFORMANCE

A. OBJECTIVES AND GUIDELINES

The objectives of this task were to provide propellant and combustion gas property data, operational characteristics, and theoretical performance for the various candidate propellants and propellant combinations considered in this study. To accomplish these objectives, literature surveys and analyses were conducted. Much of the propellant property data is readily available in the literature and the best references are cited herein. Analytically derived data or relatively new information, such as the data on RJ-5, is presented in this report.

Theoretical performance and combustion gas property data were calculated for the following parametric ranges.

- Preburners (Fuel and Oxidizer-Rich)

Chamber Pressure:	136 to 476 atm. (2000 to 10000 psia)
Mixture Ratio:	defined by the combustion temperature range of 700° to 1367°K (800 to 2000°F)

- Thrust Chamber

Chamber Pressure:	68 to 340 atm. (1000 to 5000 psia)
Area Ratio:	1 to 400
Mixture Ratio:	corresponding to stoichiometric ±50%

Propellant Combination	Stoichiometric O/F
O_2/RJ-5	3.13
O_2/RP-1	3.42
O_2/MMH	1.74
O_2/N_2H_4	1.00
O_2/H_2	7.94
O_2/CH_4	4.00

B. PHYSICAL AND THERODYNAMIC PROPERTY DATA

A summary of propellant property data for the candidate fuels and oxygen is shown on Table V. Each of the various propellants are discussed in the paragraphs which follow and appropriate references cited.

TABLE V. - PROPERTIES OF CANDIDATE PROPELLANTS

	Oxygen	Hydrogen	RP-1	RJ-5	MMH	Hydrazine	Methane
Formula	O_2	H_2	$(CH_2)_{12.37}$	$C_{14}H_{18.15}$	CH_6N_2	N_2H_4	CH_4
Molecular Weight	31.9988	2.01594	172.5151	186.45	46.07237	32.04528	16.043
Freezing Point, °K (°F)	54.372 (-361.818)	13.835 (-434.767)	224.8 (-55)	268.2[a] (23)	220.78 (-62.27)	274.68 (34.75)	90.68 (-296.4)
Boiling Point, °K (°F)	90.188 (-297.346)	20.268 (-423.187)	~492.6 (~427)	517-547 (470-525)	360.80 (189.77)	387.4 (237.6)	111.64 (-258.7)
Critical Temperature, °K (°F)	154.581 (-181.433)	32.976 (-400.313)	679 (763)	780 (944.33)	585 (593)	653 (716)	190.6 (-116.7)
Critical Pressure, MN/m^2 (psia)	5.043 (731.4)	1.2928 (187.51)	2.344 (340)	2.551 (370)	8.239 (1195)	14.69 (2131)	4.60 (667)
Critical Density, kg/m^3 (lb/ft^3)	436.1 (27.23)	31.43 (1.962)	-- --	300 (18.73)	290 (18.1)	231 (14.42)	160.43 (10.015)
Vapor Pressure at 298.15°K, kN/m^2 (at 77°F, psia)	-- --	-- --	1.8 (.26)	.048 (.0070)	6.595 (0.957)	1.892 (0.274)	-- --
Density, liquid at 298.15°K, kg/m^3 (at 77°F, lb/ft^3)	1140.8[b] (71.23)	70.78[b] (4.419)	800 (49.94)	1067.4 (66.636)	870.2 (54.325)	1003.7 (62.659)	422.6[b] (26.38)
Heat Capacity, liquid at 298.15°K, J/g-°K (at 77°F, Btu/lb-°F)	1.696[b] (.405)	9.690[b] (2.316)	1.98 (.474)	1.28 (.307)	2.930 (.6998)	3.078 (.7351)	3.50[b] (0.835)
Viscosity, liquid at 298.15°K, mN/m^2 (at 77°F, lb_m/ft-sec)	.1958[b] (1.316×10^{-4})	.0132[b] ($.887 \times 10^{-5}$)	1.53 (1.04×10^{-3})	22.76 (1.530×10^{-2})	0.775 (5.21×10^{-4})	0.913 (6.135×10^{-4})	0.1155[b] (7.76×10^{5})
Thermal Conductivity, liq. at 298.15°K, W/m-°K (at 77°F, Btu/ft-sec-°F)	.1515[b] (2.433×10^{-5})	.0989[b] (1.589×10^{-5})	.137 (2.2×10^{-5})	.1617 (2.60×10^{-5})	.248 (3.98×10^{-5})	.490 (7.86×10^{-5})	.193[b] (3.10)
Heat of Formation, liquid at 298.15°K, kcal/mol (at 77°F, Btu/lb)	-3.093[b] (-174.0)	-2.134[b] (-1905)	-6.2[c] (-796)	+13.0 (+126)	13.106 (511.67)	12.054 (676.57)	-21.37[b] (-2400)

a The highest temperature at which any solid Phase RJ-5 can remain in equilibrium with the liquid phase.
b At NBP
c kcal/g CH_2 unit

1. Properties of Oxygen

Detailed properties of oxygen are available in a number of sources and all the preferred ones are directly traceable to the Cryogenics Division of the National Bureau of Standards. The best sources of oxygen data are Ref's. 1, 2, and 3. For the thermal conductivity data, in the vicinity of the critical point where anomalous behavior occurs, Table VI of Ref. 4 was used.

2. Properties of Hydrogen

The detailed properties of parahydrogen are available in a number of source documents but are generally all traceable to the Cryogenics Division of the National Bureau of Standards. In this study program, Ref. 5 was used as the primary data source.

3. Properties of RP-1

The properties of RP-1 used, were taken from Ref. 6. These properties are dominantly obtained from Ref. 7 which is an alternate data source.

4. Properties of Monomethylhydrazine (MMH)

The primary source of properties data on MMH is Ref. 8. References 9 and 10 are supplementary data sources.

5. Properties of Hydrazine

The primary source of properties data on N_2H_4 is also Ref. 8. Reference 11 is a supplementary data source.

6. Properties of RJ-5 (Shelldyne-H^R)

The most comprehenisve compilation of properties data on RJ-5 has been prepared by the Fuels Branch, Air Force Aero Propulsion Laboratory and is the primary data source, Ref. 12. However, because of data gaps and inconsistencies in the available information, the various recommended properties of RJ-5 are discussed.

a. Empirical Formula, Molecular Weight and Heat of Formation

Various heats of formation and empirical formula were derived based upon literature searches, communications with the Sun Oil Company and communications with NASA/LeRC. The data is summarized herein to show the sensitivity to the available information. The latest data (Sept. 1975) obtained from the Air Force Aero Propulsion Laboratory at Wright-Patterson AFB by the Lewis Research Center was used in this study. This data is based upon the average of analyses on three batches of RJ-5.

Source	Chemical Composition Isomer	% Wt.
I Literature Search (Ref. 13)	$C_{14}H_{18}$	85.3
	$C_{14}H_{20}$	10.3
	$C_{14}H_{22}$	4.4
II Communication with Sun Oil	$C_{14}H_{18}$	85.3
	$C_{14}H_{20}$	14.7
III Communication with NASA/LeRC (Recommended)	$C_{14}H_{18}$	92.45
	$C_{14}H_{20}$	7.55

Based upon the compositions, the following can be derived for each case:

Source	Mean Molecular Weight	Empirical Formula
I	186.703	$C_{14}H_{18.4}$
II	186.593	$C_{14}H_{18.29}$
III (Recommended)	186.450	$C_{14}H_{18.15}$

The net heats of combustion and formation obtained for each of the calculations are:

Source	Net Heat of Combustion k cal/g-mole	(BTU/lb)	Heat of Formation* k cal/g-mole
I	1829.065	(17,634)	-19.4
II	1829.650	(17,650)	-15.6
III (Recommended)	1854.250	(17,901)	+13.0

*Liquid RJ-5 at 298.15°K (77°F)

The effect of all calculated heats of formation and empirical formula on theoretical specific impulse is only approximately 3 to 4 secs. A positive heat of formation value results in higher specific impulse.

All of the cited calculations appear to be approximately valid for thermochemically characterizing RJ-5. Previous values were based on an extremely small data base. Therefore, the latest values obtained by NASA/Lewis from the Aero Propulsion Lab were recommended. Further carbon and hydrogen analyses should be performed on various available lots of RJ-5 and heats of combustion determined on each of those lots. With this extended data base, a more reliable empirical formula and heat of formation could be established as well as the variability and precision of the values.

b. Freezing Point

RJ-5 does not exhibit a sharp freezing point but rather complex supercooling and fractional crystallization behavior. RJ-5 undergoes essentially complete crystallization at temperatures lower than 231°K (-45°F) followed by partial melting on warming to 250°K (-10°F), resolidification on holding at this temperature and remelting on warming to 253°K (-5°F) with the last crystal disappearing at 268°K (+23°F) (Ref. 13). Assuming that 268°K (+23°F) is the highest temperature at which any solid phase can exist in equilibrium with the liquid phase, 268°K (+23°F) is recommended as the "threshold freezing point," a value of most importance in rocketry.

c. Boiling Point

Since RJ-5 consists of a mixture of compounds, it exhibits a boiling range rather than a specific boiling point. The range of 517 to 547°K (470 to 525°F) (Ref. 12) was recommended for use.

d. Critical Temperature

The critical temperatures given in Ref. 12, 945°F and 504°C, are inconsistent with each other (i.e., 945°F = 507.2°C). Although not specified, these values are probably estimates. Analyses were performed which resulted in an estimated value of 780°K (506.85°C or 944.33°F). These values are consistent, close to those in the reference, and hence, were used. The inaccuracy in this value is estimated to be ± 15°K.

e. Critical Volume and Critical Density

No values for critical volume or density of RJ-5 were found in the literature. Therefore, these values were estimated through analytical techniques. The estimated values used in this study are:

Critical Volume = 622.4 cm^3/g Mol
Critical Density = 0.300 g/cm^3

The probable inaccuracies in these estimates are ±5%.

f. Critical Pressure and Compressibility

The critical pressure values of Ref. 12 were also inconsistent and presumably are estimated values. Analyses were again performed to arrive at a consistent set of values. This resulted in the following estimated values:

Critical Pressure = 25.2 atm (370 psia)
Critical Compressibility (Z_c) = 0.2448

g. Vapor Pressure

The vapor pressure of RJ-5 has been measured by Atlantic Research (Ref. 14) at 373, 398, 423, and 350°K with duplicate vapor pressure measurements taken at each temperature. A least-squares curve fit of the eight data points, wherein the pressure measurements using the Bourdon tube gage are given twice the weight of those using a mercury manometer, yields the following equation:

$$\text{Log } P(\text{psia}) = 4.817675 - \frac{3741.925}{459.67 + {}^\circ F} \quad (1)$$

This equation was used for the temperature range of 373 to 448°K (212-347°F).

For higher temperatures, the vapor pressure at 448°K (347°F), the normal average boiling point, and the critical point were used to define the three constants for an Anotoine-type vapor pressure equation which is given below for the temperature range $448 \leq T \leq 780°K$ ($347 \leq T \leq 944.33°F$).

$$\text{Log } P(\text{psia}) = 4.751597 - \frac{2496.043}{198.863 + {}^\circ F} \quad (2)$$

The above equations were used in this program to define the vapor pressure of RJ-5. Values calculated from these equations are shown on Table VI.

h. Density

The density of RJ-5 (ambient pressure) has been measured by Atlantic Research (Ref. 14) over the temperature range of 0 to 150°C (32°F - 302°F). The nine values reported were curve-fit to give the following equivalent equation:

$$\rho(\text{g/ml}) = 1.08716 - .00079288(°C) \text{ for } 0 \leq T \leq 150°C \quad (3)$$

$$\rho(\text{lb/ft}^3) = 68.75385 - .02750753(°F) \text{ for } 32 \leq T \leq 302°F \quad (3a)$$

ρ = density

For densities in the compressed liquid state and at temperatures substantially above 150°C, the density can be estimated by the following equation:

$$\rho(\text{lb/ft}^3) = 19.931\ (\rho_R) \quad (4)$$

where ρ_R = reduced density (density/critical density)

Values of ρ_R were obtained from Table 3-6 of Ref. 15.

Density values calculated from the equations above are summarized in Table VII.

TABLE VI. - VAPOR PRESSURE OF RJ-5

Temperature °K	(°F)	Vapor Pressure Atm.	(psia)
366.7	(200)	0.00952	(0.14)
394.4	(250)	0.0238	(0.35)
422.2	(300)	0.053	(0.78)
450.0	(350)	0.109	(1.6)
477.8	(400)	0.259	(3.8)
405.6	(450)	0.544	(8.0)
533.3	(500)	1.02	(15)
561.1	(550)	1.77	(26)
588.9	(600)	2.86	(42)
616.7	(650)	4.42	(65)
644.4	(700)	6.39	(94)
672.2	(750)	8.98	(132)
700.0	(800)	12.18	(179)
727.8	(850)	15.99	(235)
755.6	(900)	20.54	(302)
780.0	(944.33)	25.17	(370)

TABLE VII. - DENSITY OF RJ-5

Temperature °K	Density kg/m^3 Sat. Liq.	At 340 Atm.	At 680 atm.
255.6	1101	1111	1118
311.1	1057	1075	1084
366.7	1013	1039	1051
422.2	969	1004	1018
477.8	922	971	988
533.3	870	938	955
588.9	813	907	935
644.4	747	874	910
700.0	666	842	888
755.6	543	811	868

English Units

Temperature °F	Density, lb(m)/ft^3 Sat. Liq.	At 5000 Psia	At 10000 Psia
0	68.75	69.36	69.81
100	66.00	67.14	67.69
200	63.25	64.89	65.60
300	60.50	62.70	63.57
400	57.55	60.59	61.67
500	54.31	58.58	59.64
600	50.74	56.61	58.38
700	46.64	54.55	56.84
800	41.60	52.54	55.44
900	33.91	50.60	54.16

i. Viscosity

The viscosity of RJ-5 has been measured by Atlantic Research (Ref. 14) at low shear rates with Cannon-Fenske viscometers in the temperature range of 250 to 448°K (-10.3 to 347°F).

The rheology of RJ-5 was also investigated in detail by Atlantic Research (Ref. 14) with an extrusion rheometer in the low temperature range, 219 to 296°K (-65 to 72°F), where RJ-5 exhibits a transition from Newtonian to pseudoplastic behavior as temperature decreases.

The viscosity of RJ-5 has been estimated by Shell Development Company (Ref. 16) over a range of conditions using the well-known Jossi-Stiel-Thodos correlation of residual viscosity and a critical properties function with reduced density.

The viscosity used was a smoothed combination of; (1) the experimental viscosity data (Ref. 14), (2) a graphical extrapolation of that data, and (3) the estimated viscosity data at the higher temperatures (Ref. 16). The data are summarized on Table VIII.

j. Heat Capacity and Thermal Conductivity

The heat capacity and thermal conductivity of RJ-5 apparently have not been experimentally determined. Estimated values are reported by Atlantic Research (Ref. 14) which are attributable to Shell Development (Ref. 16). The accuracy of these data are quite uncertain but were used in this program for lack of any other data. These data are summarized in Table IX.

7. Properties of Methane (CH_4)

a. Triple Point

The triple point values of methane were obtained from a recent NBS compilation (Ref. 17) and are shown below.

<u>Triple Point Values of Methane</u>

Temperature:	90.680°K(163.224°R, -296.446°F)
Pressure:	11743.57 N/m^2 (1.70326 psia, 0.11590 atm)
Density:	
Liquid:	451.562 kg/m^3 (28.1901 lb/ft^3)
Vapor:	0.2515326 kg/m^3 (0.01570268 lb/ft^3)

b. Critical Point

The critical point values of methane obtained from Ref. 17 and are:

TABLE VIII. - VISCOSITY OF RJ-5

Temperature °K	Temperature (°F)	Viscosity N-sec/m^2	Viscosity (lbm/ft-sec)
255.6	(0)	0.231	0.155
298.2	(77)	0.0228	0.0153
311.1	(100)	0.0146	0.0098
366.7	(200)	0.00357	0.0024
422.2	(300)	0.00149	0.0010
477.8	(400)	0.00083	0.00056
533.3	(500)	0.00054	0.00036
588.9	(600)	0.00037	0.00025

TABLE IX. - HEAT CAPACITY AND THERMAL CONDUCTIVITY OF RJ-5

Temperature °K	Temperature (°F)	Heat Capacity (liquid) J/g-°K	Heat Capacity (liquid) (BTU/lb-°F)	Thermal Conductivity W/m-°K	Thermal Conductivity (BTU/ft-sec-°F)
255.6	(0)	1.08	0.257	.166	2.67×10^{-5}
311.1	(100)	1.35	0.322	.161	2.58×10^{-5}
366.7	(200)	1.62	0.387	.156	2.50×10^{-5}
422.2	(300)	1.89	0.452	.147	2.36×10^{-5}
477.8	(400)	2.12	0.507	.136	2.19×10^{-5}
533.3	(500)	2.34	0.559	.125	2.00×10^{-5}
588.9	(600)	2.54	0.606	.111	1.78×10^{-5}

Critical Point Values of Methane

Temperature:	190.555°K(342.999°R, -116.671°F)
Pressure:	4.598825 MN/m^2 (667.003 psia, 45.3869 atm)
Density:	160.43 kg/m^3 (10.015 lb/ft^3)
Compressibility:	0.29027

c. P-V-T and Derived Thermodynamic Properties

The pressure-volume-temperature data and derived thermodynamic properties of methane (internal energy, enthalpy, entropy, specific heats at constant pressure and constant volume, and speed of sound) are available in Ref. 17 for the range of pressures from the triple point pressure to 680 atm (10,000 psia) and for the range of temperatures from the melting line to 500°K (440°F).

Values of density and heat capacity at constant pressure, Cp, are not readily available above 500°K (440°F) and at high pressures, 136 to 680 atm (2,000 to 10,000 psia). Because values in this pressure range and to temperatures near 922°K (1200°F) were necessary to conduct heat transfer analyses, such values were estimated. These extrapolated values are given in Tables X and XI and are intended to supplement the data available in Ref. 17. The heat capacities were estimated based upon the ideal gas heat capacities given in Ref. 18 and heat capacity corrections for the effect of pressure given by Gambill (Ref. 19).

Densities were extended into the higher temperature and pressure region utilizing estimated compressibility factors from Lydersen's generalized tables (Ref. 20) and then adjusting those estimated values upward or downward slightly so that the resulting estimated fluid densities agreed with those given in Ref. 17 at 500°K (900°R) for each pressure being considered.

d. Viscosity

The viscosity of many substances can be closely approximated by the following expression:

$$\eta = \eta_o + \Delta\eta \tag{5}$$

where η_o = the gas viscosity at low pressure and is a function of temperature only

$\Delta\eta = \eta - \eta_o$, the so-called residual viscosity which is a function of density only, as a first good approximation (except near the critical point)

Recommended values of η_o from Ref. 21 are given in Table XII. These reference values are based on an analysis of 27 sets of experimental data.

TABLE X. - EXTRAPOLATED HEAT CAPACITIES OF METHANE

Temperature °K	C_p, J/g - °K 136 atm	272 atm	408 atm	544 atm	680 atm
600	3.38	3.51	3.63	3.69	3.74
700	3.68	3.76	3.84	3.92	4.00
800	3.97	4.03	4.08	4.13	4.19
900	4.25	4.29	4.33	4.36	4.40
1000	4.50	4.53	4.55	4.59	4.61

English Units

Temp., °R	C_p, Btu/lb °R 2000 psia	4000 psia	6000 psia	8000 psia	10,000 psia
1080	0.808	0.838	0.868	0.881	0.894
1260	0.880	0.899	0.918	0.937	0.956
1440	0.950	0.963	0.976	0.988	1.001
1620	1.016	1.025	1.034	1.043	1.052
1800	1.076	1.083	1.089	1.096	1.102

TABLE XI. - EXTRAPOLATED DENSITIES OF METHANE

Temperature °K	Density, kg/m^3				
	136 atm	272 atm	408 atm	544 atm	680 atm
600	43.3	87.4	118.0	147.4	172.2
700	37.0	74.8	101. 6	128.0	151.1
800	32.3	65.4	89.1	113.0	134.6
900	28.7	58.1	79.5	101.4	121.0
1000	25.8	52.3	71.7	92.0	110.4

English Units

Temp, °R	Density, lb/ft^3				
	2000 psia	4000 psia	6000 psia	8000 psia	10,000 psia
1080	2.702	5.456	7.369	9.203	10.750
1260	2.311	4.672	6.340	7.988	9.430
1440	2.019	4.084	5.565	7.057	8.403
1620	1.792	3.629	4.960	6.330	7.554
1800	1.611	3.264	4.474	5.743	6.891

TABLE XII. - VISCOSITY OF METHANE

$\eta = \eta_o \pm \Delta\eta$

Temp., °K	(°R)	η_o, Micropoise
70	(126)	30.0
80	(144)	33.6
90	(162)	37.2
100	(180)	40.6
110	(198)	44.2
120	(216)	47.8
130	(234)	51.1
140	(25[illegible])	55.3
150	(270	59.0
160	(288)	62.8
170	(306)	66.5
180	(324)	70.2
190	(342)	73.9
200	(360)	77.6
210	(378)	81.2
220	(396)	84.8
240	(432)	91.9
260	(468)	98.7
280	(504)	105.4
300	(540)	112.0
320	(576)	118.4
340	(612)	124.6
360	(648)	130.7

Temp., °K	(°R)	η_o, Micropoise
380	(684)	136.6
400	(720)	142.4
420	(756)	148.1
440	(792)	153.7
460	(828)	159.1
480	(864)	164.4
500	(900)	169.6
520	(936)	175
540	(972)	180
560	(1008)	185
580	(1044)	190
600	(1080)	194
620	(1116)	199
640	(1152)	204
660	(1188)	208
680	(1224)	213
700	(1260)	217
750	(1350)	228
800	(1440)	238
850	(1530)	248
900	(1620)	257
950	(1710)	267
1000	(1800)	276

Density, Kg/m^3	(lb/ft^3)	$\Delta\eta$, Micropoise
0	0	0
8	(0.5)	1.24
16	(1)	2.79
32	(2)	6.77
48	(3)	11.96
64	(4)	18.35
80	(5)	25.94
96	(6)	34.72
112	(7)	44.71
128	(8)	55.9
144	(9)	68.3
160	(10)	81.9
176	(11)	96.7
192	(12)	113
208	(13)	131
224	(14)	152
240	(15)	176
256	(16)	203
272	(17)	234
288	(18)	269
304	(19)	311
320	(20)	358

Density, Kg/m^3	(lb/ft^3)	$\Delta\eta$, Micropoise
336	(21)	413
352	(22)	476
360	(22.5)	513
368	(23)	553
376	(23.5)	598
384	(24)	656
392	(24.5)	726
400	(25)	810
408	(25.5)	906
416	(26)	1015
424	(26.5)	1140
432	(27)	1290
440	(27.5)	1480
444	(27.75)	1600
448	(28)	1730
452	(28.25)	1870
456	(28.5)	2020
460	(28.75)	[illegible]
464	(29)	[illegible]

Values of $\Delta\eta$ versus density are presented graphically in Ref. 22. Difficulty in reading the graph accurately led to the decision to recorrelate the most comprehensive experimental data. This was accomplished using values of η_o (Ref. 21) and experimental values of η (Ref. 22 and 23). The corresponding values of density were determined from Ref. 17. A good graphical correlation of $\Delta\eta$ versus density was then obtained. The original values of η were obtained at temperatures from 103 to 273°K (-274° to 32°F) and at pressures up to 340 atm (5000 psia). More than 100 data points were utilized in the correlation. The resulting values of $\Delta\eta$ versus density are listed in Table XII.

e. Thermal Conductivity

The thermal conductivity of methane has been correlated in a manner similar to that used in correlating the viscosity data, i.e.,

$$k = k_o + \Delta k \qquad (6)$$

where k_o = the gas thermal conductivity of low pressure which is a function of temperature only

$\Delta k = k - k_o$, the so-called residual thermal conductivity which is primarily a function of density, as a first good approximation (except near the critical point).

Values of k_o were obtained from Ref. 24 and are given in Table XIII. These values are based on an analysis of eleven sets of experimental data by the authors of Ref. 24.

Values of Δk versus density are based on a graphical correlation which was developed in this study. The Δk's, as defined by Eq. (6), were obtained using values of k_o (Ref. 24) and values of k primarily from Ref. 25. The corresponding values of density were determined from Ref. 17. The original values of k were obtained at temperatures from 99 to 235°K (-281-to -37°F) and at pressures up to 500 atm (7360 psia). Forty-five data points were utilized in the correlation. Enhanced thermal conductivities in the vicinity of the critical point have been neglected in the correlation because of insufficient data and because expected operating pressures are anticipated to be very substantially greater than the critical pressure.

The resulting values of Δk versus density are listed in Table XIII.

TABLE XIII. - THERMAL CONDUCTIVITY OF METHANE

$k = k_o + \Delta k$

Temp., °K	Temp., °R	k_o, cal/cm-s-°k x 10^4
100	(180)	0.2533
180	(324)	0.4661
190	(342)	0.4947
200	(360)	0.5210
240	(432)	0.6358
250	(450)	0.6620
270	(486)	0.7194
280	(504)	0.7505
300	(540)	0.8198
320	(576)	0.8867
340	(612)	0.9536
360	(648)	1.018
380	(684)	1.087
400	(720)	1.157
420	(756)	1.248
440	(792)	1.338
460	(828)	1.424
480	(864)	1.515
500	(900)	1.604
520	(936)	1.697
540	(972)	1.790
560	(1008)	1.879

Temp., °K	Temp., °R	k_o, cal/cm-s-°k x 10^4
580	1044	1.967
600	1080	2.051
620	1116	2.137
640	1152	2.223
660	1188	2.311
680	1224	2.400
700	1260	2.488
750	1350	2.717
800	1440	2.964
850	1530	3.227
900	1620	3.489
950	1710	3.752
1000	1800	4.039

Density, Kg/m^3	Density, (lb/ft^3)	Δk, cal/cm-s-°k x 10^4
0	(0)	0
16	(1)	0.038
32	(2)	0.084
48	(3)	0.142
64	(4)	0.211
80	(5)	0.282
96	(6)	0.364
112	(7)	0.452
128	(8)	0.543
144	(9)	0.640
160	(10)	0.739
176	(11)	0.839
192	(12)	0.943
208	(13)	1.048
224	(14)	1.160
240	(15)	1.280
256	(16)	1.413
272	(17)	1.556
288	(18)	1.716
304	(19)	1.899
320	(20)	2.109
336	(21)	2.355

Density, Kg/m^3	Density, (lb/ft^3)	Δk, cal/cm-s-°k x 10^4
352	(22)	2.632
368	(23)	2.942
376	(23.5)	3.116
384	(24)	3.296
392	(24.5)	3.483
400	(25)	3.677
408	(25.5)	3.877
416	(26)	4.083
424	(26.5)	4.297
432	(27)	4.517
440	(27.5)	4.744
448	(28)	4.978
456	(28.5)	5.220
464	(29)	5.468

ORIGINAL PAGE IS
OF POOR QUALITY

C. OPERATIONAL CONSIDERATIONS

Operational considerations include those propellant properties or characteristics that have a significant impact upon the reliability and cost of the engine and its potential impact on the environment such as; (1) cost and availability, (2) safety and ground handling, (3) chemical and/or thermal stability, (4) corrosivity/materials compatibility, and (5) environmental effects.

1. Cost and Availability

Three factors that strongly affect the cost of the candidate propellants are the cost of; (1) petroleum and/or natural gas, (2) energy to produce, and (3) added operating and/or capital costs arising from new environmental and/or occupational health requirements. Recent changes of significant magnitude in some of these cost factors and uncertainty as to the magnitude of further changes in the near-term makes propellant cost projections very difficult. However, an attempt to estimate propellant "hard" cost was made in this study. Two methods of approach were tried. These are:

- Extrapolation of historical data
- Use of cost escalation indices

The historical propellant cost data on oxygen, hydrogen, RP-1, N_2H_4 and MMH were provided by the NASA/LeRC Project Manager as costs to the government for mid 1966 and 1975. The RJ-5 cost estimate is based upon telephone communications between ALRC and Air Force Aero Propulsion Laboratory, Wright-Patterson Air Force Base personnel. The base point historical cost for methane was obtained from NASA/MSFC by ALRC to support the "Phase A/B Study for a Pressure-Fed Engine on a Reuseable Space Shuttle Booster," Contract NAS8-28217. These data, obtained in October 1971, indicated that methane and propane were expected to cost about 0.055$/kg (0.025 $/lb) while RP-1 was approximately 0.066 $/kg (0.03 $/lb). For purposes of this study, these costs were considered to be equal. Extrapolation of this data to 1976 results in a cost of approximately 0.132 $/kg (0.06 $/lb) which agrees with the data shown in Ref. 26.

The historical data and estimates were plotted on semi-logarithmic graph paper and linearly extrapolated to 1990 as shown in Figure 2. It is realized that there have been step changes in some of the propellant costs over the past years. However, the assumption is that a straight line averages out these steps. The historical data on hydrogen indicates that the cost has remained constant. An article in the July 14, 1975 issue of Aviation Week and Space Technology (Page 21) indicates that the price of hydrogen will grow to 3.31 $/kg ($1.50/lb) over the remainder of a 12-year NASA contract with Air Products to 1987.

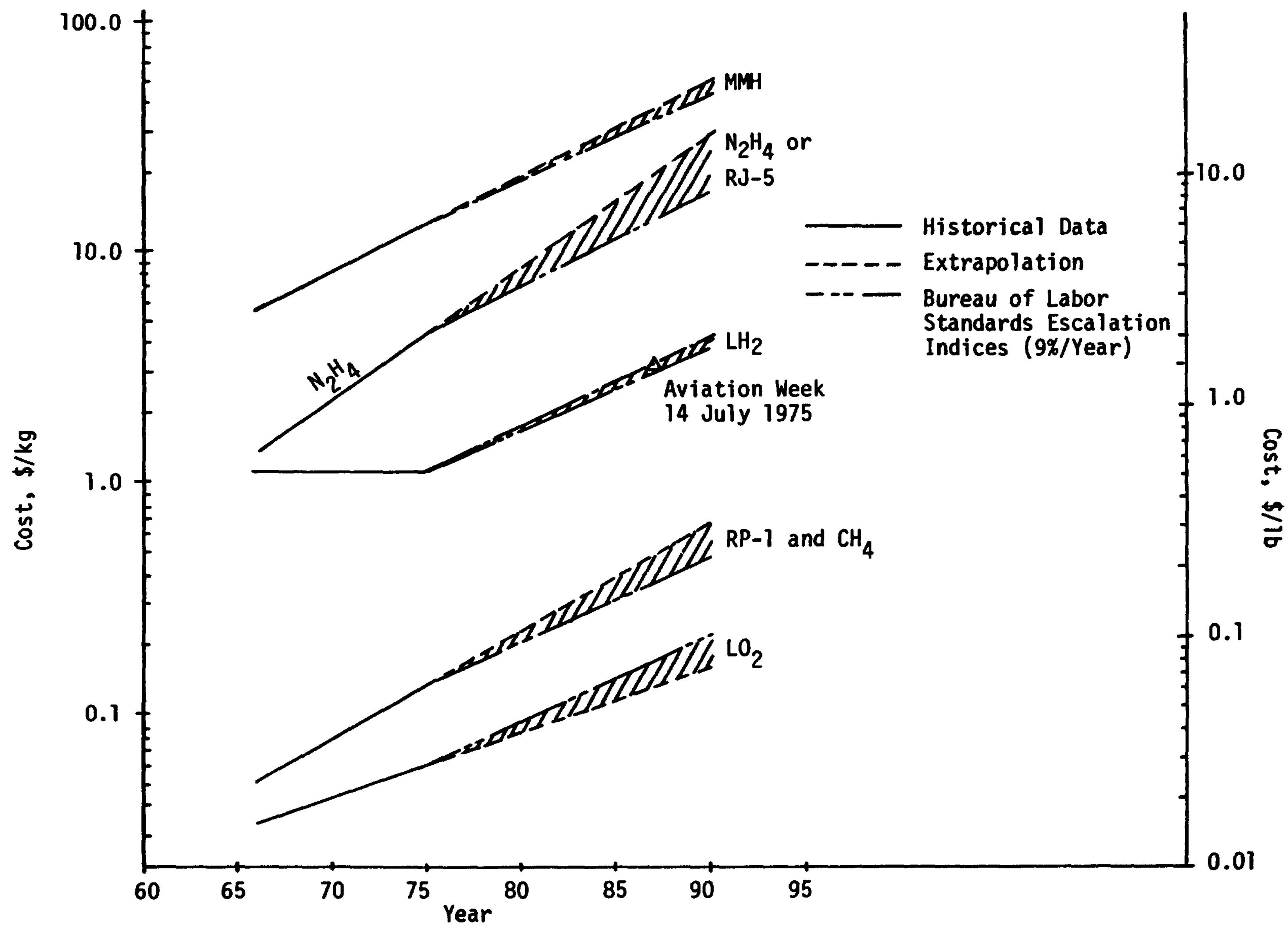

Figure 2. Propellant Cost Projections

The escalation indices used was obtained from the Bureau of Labor Standards as of 1 October 1975. A rate of 9%/year is currently being used by procurement people at ALRC.

The historical data extrapolation and the escalated costs are within reasonable agreement as shown by the figure. The data is summarized on Table XIV. The projected cost for 1990 shown on this table is based upon the escalation factor.

Both the extrapolation and escalated cost projections assume that current manufacturing methods will be used to produce the propellants.

2. Safety and Ground Handling

The safety and ground handling characteristics of the candidate propellants are conveniently summarized in detail in CPIA Publication No. 194 (Ref. 27). This report is a standard data source for such information.

Because O_2/H_2 was defined as the only Mode 2 engine propellant combination and O_2/RJ-5 as the baseline Mode 1 engine propellant combination for this program, the ranking of candidate propellants with respect to safety and handling characteristics reduces to the ranking of RP-1, N_2H_4, MMH, and CH_4 versus RJ-5 as alternative Mode 1 fuels. RP-1 and CH_4 compared with RJ-5 tend to be ranked slightly below RJ-5 from the safety and handling standpoint primarily because of their higher volatility (flammability and toxic hazards). However, experience with RP-1 would indicate that all three can be handled safely. Hydrazine and MMH present a significantly greater safety and handling problem than RJ-5, RP-1 or CH_4 for a number of reasons: (1) higher volatility, (2) very toxic, (3) highly flammable, (4) higher reactivity with air and materials of construction, and (5) their ability to decompose rapidly and exothermically from certain thermal or catalytic stimuli.

Oxygen, the oxidizer for both Mode 1 and Mode 2 engines, has several safety and handling characteristics important to note: (1) its cryogenic nature, and (2) its strong tendency to react oxidatively with many materials. By itself, oxygen is a very stable material, but many organic contaminants in a dense oxygen phase can yield explosive mixtures which can be initiated by a variety of stimuli such as shock, friction, etc. Gaseous oxygen contaminated by gaseous organics, or finely divided solid organics, or metal, can similarly form explosive materials that are sensitive to thermal stimuli. Oxygen, at high temperatures, will cause almost any organic material to burn and readily causes a fast surface oxidation of metals. Most metals will actively burn in oxygen at sufficiently high temperature/pressure conditions.

TABLE XIV. - PROPELLANT COST SUMMARY

Propellant	Current Cost, $/kg	Current Cost, ($/lb)	Estimated[a] 1990 Cost, $/kg	Estimated[a] 1990 Cost, ($/lb)
LH_2	1.10	(0.50)	3.97	(1.80)
LO_2	0.060	(0.027)	0.022	(0.10)
MMH	13.23	(6.00)	48.50	(22.00)
N_2H_4	4.41	(2.00)	16.09	(7.30)
RP-1	0.132	(0.06)	0.49	(0.22)
RJ-5	4.41	(2.00)	16.09	(7.30)
CH_4	0.132	(0.06)	0.49	(0.22)

[a] Based upon escalation factor.

Hydrogen, the fuel for the Mode 2 engine, also exhibits several safety and handling characteristics worthy of special consideration: (1) its very low density and extreme volatility which are attributable to its very low molecular weight and boiling point, (2) its high flammability in air and other oxidizers, (3) its very high heat of combustion, and (4) its adverse effect on certain metals due to hydrogen embrittlement phenomenon.

Although each propellant exhibits many unique characteristics, all have been safely handled in past rocket engine programs. Therefore, safety is not a single major propellant selection criteria.

3. Chemical and/or Thermal Stability

Oxygen and hydrogen are both thermally stable but they are highly reactive in oxidation and reduction reactions, respectively. As previously mentioned, oxygen will form explosive mixtures with a wide variety of both organic and inorganic materials having fuel value. These mixtures will react exothermically when exposed to certain thermal or shock stimuli. The violence of the reaction will depend upon the mixture, the degree of confinement, and the interfacial area of the oxygen/material mixture. Hydrogen behaves quite similarly except its potentially dangerous mixtures form with materials having oxidative capabilities (e.g., air and oxygen.)

The hydrocarbon fuels, RJ-5, RP-1, and CH_4 are relatively stable but they do have tendencies to gum, crack, or coke at elevated temperatures. These tendencies are increased when contaminated by water and/or oxygen. Because these fuels are flammable, their mixtures with oxidizers such as air or oxygen are subject to the burning or explosive chemical reactions typical of heavy hydrocarbons.

The gumming, cracking, and coking characteristics of RP-1 and RJ-5 are of particular concern when they are used as regenerative coolants, or in fuel-rich gas generators (preburners.) Comprehensive comparative thermal stability testing of these two fuels by the same test procedures in the same test equipment are not known to have been conducted, so their relative thermal stabilities are difficult to assess. It would appear, however, that RJ-5 has the potential for the better thermal stability because it is a synthetic fuel and can be purified to remove unstable components to almost any degree desirable (only a military specification draft presently exists for it). RP-1 is a specially purified kerosene, but nonetheless, may contain certain specified maximum quantities of "impurities" (as existent and potential gums, sulfur, mercaptan, aromatics, and olefins) which are known to have a considerable influence on thermal stability.

On the basis of thermal stability tests by the JFTOT (Jet Fuel Thermal Oxidation Test, ASTM D 3241-73T) test method on RJ-5 and Jet A-1 fuels (Ref. 28), and the close similarities between Jet A-1 and RP-1, RJ-5 is thermally stable (in terms of deposit formation on heated surfaces) to a temperature of approximately 561°K (550°F) while RP-1 is probably stable to about 547 to 561°K (525-550°F) using similar criteria. From this, it can be estimated that liquid-side wall temperatures in excess of 589°K (600°F) will lead to the fouling of the coolant flow passages, particularly with repeated engine cycles.

Methane is thermally stable at temperatures up to approximately 978°K (1300°F), Ref. 29. Therefore, coolant passage fouling would not be expected with this propellant.

The use of RP-1, RJ-5, or CH_4 in fuel-rich preburners can present a thermal stability problem manifested as coking. Coking of heated hydrocarbon fuel was studied under the Titan I (LR91-AJ-3) engine development contract because the fuel was used as the regenerative coolant, and a fuel-rich gas generator was utilized, Ref. 30. JPL conducted tests by flowing jet propulsion fuel through a heated tube and exhausting the heated vapors through a known orifice. It was noted that at approximately 994°K (1330°F), coking suddenly became so pronounced that the tests could not be continued due to complete choking of the tube. On the basis of these tests,it was recommended that any jet propulsion fuel-rich gas generator be run at temperatures below 978°K (1300°F), the time at which any fuel may be above this temperature be minimized, and any local temperatures over 978°K (1300°F) be eliminated by uniformly mixing the propellants during the injection process. Similar tests conducted by Aerojet, using RP-1 fuel, showed that little coke formed at a temperature of 922°K (1200°F); a light amount formed at 978°K (1300°F), and a heavy amount formed at 1033°K (1400°F).

On the basis of these test results and experience with hydrocarbon fuels in Atlas, Titan I, and the F-1 engines, it would appear that coking problems with either RP-1 or RJ-5 in fuel-rich preburners present no major difficulty provided the gas temperature is controlled below 922°K (1200°F). This assessment should, however, be experimentally verified in the case of RJ-5. For study purposes, a fuel-rich gas turbine inlet temperature of 867°K (1100°F) was selected.

The candidate fuels, hydrazine and monomethylhydrazine, have unique thermal stability characteristics which can have important bearings on their suitability for use in high-pressure, staged-combustion-cycle engines. Both of these fuels exhibit certain thresholds of stability and these thresholds are dependent upon the materials of construction and the nature of the stimuli that imparts energy to the fuel.

The thermal stability of MMH and N_2H_4 and N_2H_4-MMH (90/10) was the subject of a comprehensive experimental evaluation (Ref. 31). The materials of construction, the physical state of the fuel, and the nature of the sensitizing stimulus have important influences on the threshold sensitivity temperatures of these fuels. The liquid/vapor phase for MMH undergoes initial exothermic decomposition at an average temperature of 499°K (438°F) in the ten metals studied but variations in temperature of nearly $\pm$33°K ($\pm$ 60°F) occur because of the nature of the various metals. Similarly, the average threshold temperature for explosive decomposition is 547°K (524°F) with metal-caused variations of about -214 to 283°K (-75 to +50°F). The presence of MMH only in the vapor phases decreases the threshold sensitivity temperature about 289 to 306°K (60 to 90°F). A comparison of the sensitivity of mixed liquid/vapor phases of MMH or N_2H_4 to moderate heating rates versus a combination of heating followed by adiabatic compression of the vapor phase, shows that MMH vapor is not appreciably sensitive to compression while N_2H_4 vapor is generally very sensitive to compression and is further sensitized by some metals. In view of the marked difference in the sensitivity of MMH and N_2H_4 vapors to compression, it is important to note that even a small addition of MMH to N_2H_4 (i.e., 10% wt) greatly reduces the sensitivity of N_2H_4 to compression. The effectiveness of ammonia (NH_3) in reducing N_2H_4 sensitivity is also established, although less succinctly documented.

The use of MMH as a coolant will necessitate designs that insure the bulk temperature of MMH does not exceed about 478°K (400°F). The use of hydrazine imposes similar thermal limits under normal conditions, but a much more severe limit, about 367°K (200°F), if simultaneous exposure to vapor phase adiabatic compression occurs such as during start or shutdown transients. The fact that a copper alloy is used to form a part of the coolant passage, and the effect of copper alloys on the thermal stability of MMH and N_2H_4 has not been established, points up the need for further experimental work.

4. Materials Compatibility/Corrosivity

a. Oxygen

Oxygen incompatibility is manifested either by loss of toughness at low temperatures, reduction of fatigue life, or catastrophic oxidation.

In the case of most common structural alloys, the oxidative attack becomes appreciable only at high temperature because the reaction is inhibited by the formation of a protective oxide layer. In the case of organic materials, the choice of acceptable materials is very limited, as is the application of the materials to various engine uses. While the above indicates a significant possible problem in using oxygen, the long-standing experience with oxygen in a variety of vehicles (e.g., Atlas, Titan I, Saturn, etc.) has lead to a well established group of materials and corresponding engine uses that permit reliable application of oxygen. Several reports provide good compilations of materials acceptable for use in oxygen service (Ref. 32, 33, and 34.) Titanium and its alloys and aluminum and its alloys are incompatible from an oxidation standpoint when they are subject to high energy inputs.

The aluminum, austenitic iron, copper, nickel and cobalt base alloys all posess adequate toughness for applications to 94°K (-290°F). The effect of oxygen and water vapor as found in oxygen combustion products on fatigue life has been investigated (Ref. 35). The strain utilized in these tests (Ref. 35) suggests that both high cycle and low cycle fatigue are deleteriously affected. Limited fracture toughness tests have been performed in oxygen. Inconel 718 did not exhibit environmentally enhanced subcritical flaw growth when tested in 68 atm (1000 psi) oxygen at room temperature (Ref. 36). Considerable testing remains to be done to establish the effects of gaseous oxygen on fracture toughness and high and low cycle fatigue of candidate materials.

b. Hydrogen

One of the most important materials consideration in the use of liquid hydrogen fuel is embrittlement. The susceptibility of metals to embrittlement by high purity, high pressure, 272 to 510 atm (4000-7500 psi) gaseous hydrogen has been extensively investigated for candidate alloys for Space Shuttle main engine (SSME) components (Ref. 37 and 38).

Hydrogen incompatibility is manifested by loss of toughness both with decreasing temperature and by hydrogen absorption. Embrittlement by hydrogen absorption is the most severe at room temperature except for those materials which are affected by hydrogen reactions within the metals such as hydride formation, hydrocarbon gas formation through the reduction of carbides or water vapor formation through the reduction of oxides.

Materials such as Inconel 718, a material which is susceptible to hydrogen embrittlement, are used extensively in hydrogen fuel systems. However, they are limited to low temperature applications where embrittlement effects are minimal. These applications include engine components which are at ambient as well as chilled temperatures at engine start; and hence, the former experience transition from an embrittling to a nonembrittling condition. A similar condition exists in the hot gas system where nickel base alloys are heated from low temperature to elevated temperatures in an embrittling environment during engine start. The suitability of these materials in these applications depends upon surface chilling of the material prior to reaching design stresses or rapid transition to the nonembrittling elevated operating temperature. The total time that the material will be subjected to the embrittling temperature range will be extremely short from the standpoint of the application of fracture mechanics to the design.

The influence of hydrogen in a fuel-rich hot gas system composed of the hydrogen-oxygen combustion products is uncertain. The effect of hydrogen purity has been investigated (Ref. 39). This reference shows that the introduction of 0.6% O_2 completely arrested hydrogen induced crack growth in an alloy steel. A similar effect is reported for the introduction of moisture into hydrogen. However, these results are inconsistent with the data of Ref. 37 which shows increased embrittling effects with the introduction of water vapor. In view of these inconsistencies, hydrogen embrittlement must be considered from the standpoint of pure gas effects until more definitive information becomes available. The current design of the hot gas system of the SSME calls for the protection of susceptible materials with platings and weld overlays of unaffected materials to avoid embrittlement.

c. RP-1, RJ-5, and CH_4

The hydrocarbon fuels, RJ-5, RP-1 and CH_4 do not present any significant corrosivity/materials compatibility problems. They exhibit excellent compatibility to a variety of steels, stainless steels, aluminum alloys, and titanium alloys and to a variety of elastomeric materials such as Viton, nitrite, and fluorosilicone rubber compounds. However, a carburization potential exists in their fuel-rich combustion products. Carburization should not occur below approximately 1000°K (1350°F) (Ref. 40). Where temperature poses a carburization problem, nickel base alloys can be employed to reduce carburization.

d. MMH and Hydrazine

Metals in contact with the hydrazine fuel can be subject to stress corrosion cracking and can catalyze decomposition. Stress corrosion is caused by the reaction of the metal with impurities in the fuel to produce hydrogen on the metal surface.

The titanium and aluminum alloys are unaffected while the martensitic (CRES 410 and 4130 alloy steel) and the nickel base alloy (Inconel 718) display crack growth after varying incubation periods (Ref. 41). The incubation period for crack growth in MMH is ten times that of hydrazine. Although Inconel 718 is susceptible to stress corrosion in hydrazine, the incubation period for crack growth is 600 hours; a time well beyond the current requirements of liquid rocket engines. Additional testing in hydrazine and MMH at elevated temperatures is required to establish compatibility limits. Although maximum embrittlement effects for several materials occurs at room temperature, the effect of incresed hydrogen activity not higher temperature could further influence stress corrosion cracking and must be determined.

The compatibility of uncoated zirconium copper (Z_RC_U) with N_2H_4 and MMH is questionable at elevated propellant temperatures, 333°K (140°F), for long term use.

5. Environmental Effects.

The use of oxygen and hydrogen in rocket engines will have no significant adverse effect on the environment because both are normal components in the air and their only stable reaction product is water.

The use of hydrocarbon fuels such as RJ-5, RP-1, and CH_4 will produce minimal environmental effects, the effects being generally similar to those of jet aircraft.

The use of the hydrazine fuels, N_2H_4 or MMH, add two additional points that may present environmental constraints: (1) these fuels are very toxic and some unburned fuel will locally enter the atmosphere or the earth's surface and (2) the reaction products of oxygen and N_2H_4 or MMH will yield some nitrogen compounds of environmental concern (nitrogen oxides and incompletely burned nitrogen compounds such as ammonia and amines.)

D. COMBUSTION GAS PROPERTY DATA

The TRAN 72 computer program described in Ref. 42, was used to calculate theoretical one-dimensional equilibrium and frozen main chamber and preburner gas property data. These data are summarized herein.

1. Main Chamber

Main chamber gas stagnation temperature, characteristic exhaust velocity, molecular weight, thermal conductivity, viscosity, specific heat, specific heat ratio, and Dittus-Boelter factor data were parametrically calculated for six study propellant combinations (LOX/RJ-5, LOX/RP-1, LOX/CH_4, LOX/N_2H_4, LOX/MMH and LOX/LH_2). The data were calculated at chamber pressures of 68, 136, 272 and 408 atm (1000, 2000, 4000, and 6000 psia.) The mixture ratios ranged from 0.5 to 1.5 the stoichiometric value. A sufficient number of mixture ratio points for each propellant combination were run to permit accurate interpolation of data when stored in the computer data routine. The computer program used (Ref. 42) is similar to the JANNAF One Dimensional Equilibrium (ODE) model but has been extended to include transport property calculations. The data were calculated for the following mixture ratio values:

Propellant Combination	Mixture Ratio, O/F
LOX/RJ-5	1.6, 2.0, 2.3, 2.6, 2.9, 3.2, 3.5, 3.8, 4.3, 4.8
LOX/RP-1	1.7, 2.1, 2.5, 2.8, 3.1, 3.4, 3.7, 4.0, 4.5, 5.1
LOX/MMH	0.8, 1.1, 1.4, 1.7, 2.0, 2.3, 2.6
LOX/N_2H_4	0.5, 0.7, 0.8, 0.9, 1.0, 1.2, 1.5
LOX/LH_2	4, 5, 6, 7, 8, 10, 12
LOX/CH_4	2.0, 2.4, 2.8, 3.2, 3.6, 4.0, 4.5, 5.0, 6.0

The properties are summarized on Tables XV through XX for each of the propellant combinations and a representative set of mixture ratio values covering the total range analyzed. The data show that the chamber pressure influence is small and increases with increasing mixture ratio.

2. Preburners

The combustion gas properties were also calculated for fuel-rich and oxidizer-rich preburner operation with all six study propellant combinations. These data were developed over a chamber pressure range of 136 to 680 atm. (2000 to 10,000 psia) and mixture ratio ranges corresponding to combustion gas temperatures between at least 700 to 1367°K (1260°R to 2460°R). It should be noted that for the hydrazine based fuels, (hydrazine and monomethyl-hydrazine) the existence of a monopropellant flame makes operation below a certain minimum flame temperature impossible. The monopropellant flame temperatures for N_2H_4 and MMH at 408 atm (6000 psia) are approximately 1000 and 1333°K (1800°R and 2400°R), respectively. In addition, the effect of pressure (for the range investigated) upon the properties of the oxidizer-rich combustion products is insignificant and can be neglected.

TABLE XV. - LOX/RJ-5 MAIN CHAMBER GAS PROPERTY SUMMARY

Chamber Pressure Atm.	Chamber Pressure (psia)	Mixture Ratio O/F	Combustion Temperature, °K	Combustion Temperature, (°R)	Characteristic Velocity m/sec	Characteristic Velocity (ft/sec)	Ratio of Specific Heats Equilibrium	Ratio of Specific Heats Frozen	Molecular Weight
68	(1000)	1.6	3109	(5596)	1709	(5608)	1.23	1.25	20.8
		2.6	3777	(6798)	1746	(5727)	1.14	1.22	25.5
		3.5	3719	(6695)	1665	(5461)	1.13	1.21	27.8
		4.8	3553	(6395)	1571	(5154)	1.13	1.21	29.8
136	(2000)	1.6	3132	(5637)	1711	(5612)	1.22	1.25	20.8
		2.6	3891	(7003)	1761	(5776)	1.14	1.21	25.8
		3.5	3833	(6899)	1679	(5509)	1.13	1.21	28.1
		4.8	3647	(6564)	1583	(5193)	1.13	1.20	30.0
272	(4000)	1.6	3149	(5668)	1711	(5615)	1.23	1.25	20.8
		2.6	4007	(7212)	1775	(5824)	1.14	1.21	26.1
		3.5	3948	(7106)	1693	(5555)	1.14	1.20	28.4
		4.8	3742	(6735)	1594	(5231)	1.14	1.20	30.3
408	(6000)	1.6	3158	(5684)	1712	(5616)	1.23	1.25	20.8
		2.6	4074	(7334)	1783	(5851)	1.14	1.21	26.3
		3.5	4016	(7228)	1701	(5582)	1.14	1.20	28.5
		4.8	3797	(6834)	1601	(5252)	1.14	1.20	30.5

TABLE XVI. - LOX/RP-1 MAIN CHAMBER GAS PROPERTY DATA

Chamber Pressure Atm.	Chamber Pressure (psia)	Mixture Ratio O/F	Combustion Temperature, °K	Combustion Temperature, (°R)	Characteristic Velocity m/sec	Characteristic Velocity (ft/sec)	Ratio of Specific Heats Equilibrium	Ratio of Specific Heats Frozen	Molecular Weight
68	(1000)	1.7	2884	(5192)	1724	(5657)	1.22	1.25	18.9
		2.8	3696	(6652)	1783	(5850)	1.13	1.21	24.0
		3.7	3664	(6595)	1701	(5581)	1.13	1.21	26.2
		5.1	3501	(6301)	1597	(5239)	1.13	1.20	28.4
136	(2000)	1.7	2898	(5216)	1725	(5658)	1.23	1.25	18.9
		2.8	3802	(6843)	1797	(5897)	1.14	1.21	24.2
		3.7	3771	(6787)	1715	(5628)	1.13	1.20	26.5
		5.1	3589	(6461)	1608	(5277)	1.13	1.20	28.6
272	(4000)	1.7	2908	(5234)	1725	(5659)	1.23	1.25	18.9
		2.8	3908	(7034)	1811	(5943)	1.14	1.20	24.5
		3.7	3879	(6983)	1714	(5624)	1.14	1.20	26.7
		5.1	3678	(6620)	1619	(5313)	1.14	1.20	28.9
408	(6000)	1.7	2912	(5241)	1725	(5660)	1.23	1.25	18.9
		2.8	3971	(7147)	1819	(5969)	1.14	1.20	24.6
		3.7	3944	(7099)	1737	(5700)	1.14	1.20	26.9
		5.1	3451	(6212)	1625	(5333)	1.14	1.20	29.0

TABLE XVII. - LOX/MMH MAIN CHAMBER GAS PROPERTY SUMMARY

Chamber Pressure Atm.	Chamber Pressure (psia)	Mixture Ratio O/F	Combustion Temperature, °K	Combustion Temperature, (°R)	Characteristic Velocity m/sec	Characteristic Velocity (ft/sec)	Ratio of Specific Heats Equilibrium	Ratio of Specific Heats Frozen	Molecular Weight
68	(1000)	0.8	2797	(5034)	1811	(5942)	1.23	1.25	16.5
		1.4	3553	(6395)	1875	(6150)	1.14	1.22	20.8
		2.0	3538	(6368)	1772	(5815)	1.13	1.21	23.3
		2.6	3406	(6130)	1679	(5507)	1.13	1.21	24.9
136	(2000)	0.8	2808	(5054)	1811	(5943)	1.23	1.25	16.5
		1.4	3639	(6550)	1887	(6191)	1.14	1.21	20.9
		2.0	3627	(6528)	1784	(5856)	1.14	1.21	23.4
		2.6	3479	(6262)	1688	(5539)	1.14	1.21	25.1
272	(4000)	0.8	2816	(5068)	1812	(5944)	1.24	1.25	16.6
		1.4	3722	(6699)	1898	(6228)	1.15	1.21	21.1
		2.0	3714	(6686)	1797	(5896)	1.14	1.20	23.6
		2.6	3549	(6388)	1697	(5569)	1.14	1.20	25.3
408	(6000)	0.8	2819	(5075)	1812	(5944)	1.24	1.25	16.6
		1.4	3769	(6784)	1905	([illegible]9)	1.15	1.21	21.2
		2.0	3766	(6778)	1804	(5918)	1.14	1.20	23.8
		2.6	3589	(6460)	1703	(5586)	1.14	1.20	25.4

TABLE XVIII. - LOX/N_2H_4 MAIN CHAMBER GAS PROPERTY SUMMARY

Chamber Pressure Atm.	(psia)	Mixture Ratio O/F	Combustion Temperature, °K	(°R)	Characteristic Velocity m/sec	(ft/sec)	Ratio of Specific Heats Equilibrium	Frozen	Molecular Weight
68	(1000)	0.5	2791	(5023)	1845	(6052)	1.22	1.24	16.0
↓	↓	0.8	3338	(6008)	1906	(6254)	1.15	1.22	18.7
		1.0	3417	(6150)	1873	(6144)	1.14	1.21	20.0
		1.5	3254	(5858)	1732	(5684)	1.15	1.22	22.1
136	(2000)	0.5	2802	(5043)	1845	(6053)	1.22	1.24	16.0
↓	↓	0.8	3396	(6112)	1914	(6279)	1.16	1.22	18.8
		1.0	3489	(6281)	1884	(6181)	1.15	1.21	20.1
		1.5	3304	(5948)	1739	(5706)	1.15	1.21	22.2
272	(4000)	0.5	2809	(5057)	1845	(6054)	1.23	1.24	16.0
↓	↓	0.8	3449	(6208)	1920	(6300)	1.16	1.22	18.8
		1.0	3562	(6411)	1894	(6215)	1.15	1.21	20.3
		1.5	3351	(6031)	1745	(5724)	1.15	1.21	22.3
408	(6000)	0.5	2814	(5065)	1845	(6054)	1.23	1.24	16.0
↓	↓	0.8	3477	(6258)	1923	(6310)	1.17	1.21	18.9
		1.0	3602	(6483)	1900	(6233)	1.15	1.21	20.3
		1.5	3376	(6076)	1748	(5734)	1.16	1.21	22.4

TABLE XIX. - LOX/LH_2 MAIN CHAMBER GAS PROPERTY SUMMARY

Chamber Pressure Atm.	Chamber Pressure (psia)	Mixture Ratio O/F	Combustion Temperature, °K	Combustion Temperature, (°R)	Characteristic Velocity m/sec	Characteristic Velocity (ft/sec)	Ratio of Specific Heats Equilibrium	Ratio of Specific Heats Frozen	Molecular Weight
68	(1000)	4.0	2959	(5327)	2422	(7945)	1.19	1.22	10.0
		6.0	3498	(6296)	2310	(7579)	1.16	1.21	13.4
		8.0	3601	(6481)	2150	(7054)	1.13	1.19	16.1
		12.0	3419	(6154)	1892	(6207)	1.14	1.20	19.7
136	(2000)	4.0	2979	(5363)	2424	(7952)	1.20	1.22	10.0
		6.0	3574	(6433)	2323	(7620)	1.15	1.20	13.5
		8.0	3699	(6658)	2182	(7160)	1.13	1.19	16.3
		12.0	3489	(6281)	1903	(6242)	1.14	1.20	19.8
272	(4000)	4.0	2996	(5392)	2425	(7957)	1.20	1.22	10.0
		6.0	3646	(6562)	2334	(7656)	1.15	1.20	13.6
		8.0	3794	(6830)	2181	(7156)	1.14	1.19	16.4
		12.0	3557	(6402)	1912	(6273)	1.14	1.19	19.9
408	(6000)	4.0	3004	(5407)	2426	(7959)	1.20	1.22	10.0
		6.0	3684	(6632)	2339	(7674)	1.15	1.19	13.7
		8.0	3851	(6931)	2190	(7184)	1.14	1.19	16.5
		12.0	3594	(6469)	1917	(6290)	1.15	1.19	20.0

TABLE XX. - LOX/CH_4 MAIN CHAMBER GAS PROPERTY SUMMARY

Chamber Pressure Atm.	(psia)	Mixture Ratio O/F	Combustion Temperature, °K	(°R)	Characteristic Velocity m/sec	(ft/sec)	Ratio of Specific Heats Equilibrium	Frozen	Molecular Weight
68	(1000)	2.0	2557	(4602)	1758	(5768)	1.23	1.24	16.0
		2.8	3391	(6103)	1871	(6139)	1.15	1.21	19.7
		3.6	3569	(6425)	1825	(5989)	1.13	1.20	22.2
		4.5	3534	(6361)	1745	(5726)	1.13	1.20	24.0
		6.0	3379	(6082)	1634	(5361)	1.13	1.20	26.1
136	(2000)	2.0	2562	(4611)	1758	(5768)	1.23	1.24	16.0
		2.8	3451	(6211)	1878	(6162)	1.16	1.21	19.8
		3.6	3666	(6598)	1839	(6034)	1.13	1.20	22.4
		4.5	3627	(6528)	1759	(5770)	1.13	1.19	24.2
		6.0	3453	(6215)	1644	(5394)	1.13	1.20	26.3
272	(4000)	2.0	2564	(4616)	1758	(5768)	1.24	1.24	16.0
		2.8	3504	(6307)	1884	(6182)	1.16	1.21	19.9
		3.6	3762	(6771)	1853	(6078)	1.14	1.19	22.6
		4.5	3721	(6697)	1771	(5811)	1.13	1.19	24.5
		6.0	3526	(6346)	1654	(5425)	1.14	1.19	26.5
408	(6000)	2.0	2566	(4618)	1758	(5768)	1.24	1.24	16.0
		2.8	3532	(6357)	1887	(6191)	1.17	1.20	20.0
		3.6	3818	(6872)	1860	(6103)	1.14	1.19	22.7
		4.5	3774	(6794)	1779	(5835)	1.14	1.19	24.6
		6.0	3567	(6420)	1659	(5442)	1.14	1.19	26.6

The preburner gas properties were also calculated using the previously referenced (TRAN 72) computer program. The preburner transport property calculation were limited to the frozen condition because the low gas stagnation temperatures limit thermal disassociation of the combustion products.

Properties were calculated for nominal inlet temperatures of 298°K (77°F) for RJ-5, RP-1, N_2H_4 and MMH and the normal boiling point (NBP) for LOX, LH_2 and CH_4. If a propellant is used to cool the combustion chamber, the effect of propellant preheating was accounted for by adjusting the heat of formation in the computer program. That is, the fuel heat of formation was increased for fuel-rich preburners when the fuel or oxidizer is used to cool the chamber and the LOX heat of formation is increased for oxidizer-rich preburners when LOX is used as a coolant. Because of the proportionally small fuel mass injected in the oxidizer-rich preburners, the effect of fuel preheating was neglected.

Propellant preheating can be shown as enthalpy increase above the nominal propellant inlet conditions. The range of coolant enthalpy increases evaluated was varied for each propellant to account for the available flow rate differences.

The ODE equilibrium combustion temperature, characteristic velocity, ratio of specific heats and molecular weight data are summarized on Tables XXI through XXIX at a chamber pressure of 408 atm (6000 psia) for all preburners except the fuel-rich LOX/RJ-5, LOX/RP-1 and LOX/CH_4 preburners. Chamber pressures of approximately 408 to 544 atm (6000 to 8000 psia) are typical of the operating requirements resulting from this study.

The fuel-rich LOX/hydrocarbon preburner data has been adjusted from the ODE equilibrium values to reflect the experimentally observed nonequilibrium performance of these mixtures. This nonequilibrium performance has been empirically verified by many researchers, including data reported during the Titan I engine development program (Ref. 43).

Figure 3 compares experimental fuel-rich performance (Ref. 43) to ODE performance for LOX/RP-1 at a chamber pressure of 37.4 atm (550 psia). These data were used to develop the following formulas for ODE data adjustment.

$$T_{o_{exp}} = T_{o_{ODE}} \times \underset{\text{const. } \emptyset}{\eta_{T_o}} \qquad (7)$$

$$C^*_{exp} = C^*_{ODE} \times \underset{\text{const. } \emptyset}{\eta_{C^*}} \qquad (8)$$

TABLE XXI. - LOX RJ-5 OXIDIZER-RICH PREBURNER GAS PROPERTY DATA SUMMARY

Pressure = 408 atm (6000 psia)
Chamber Coolant: LOX

Mixture Ratio	Propellant Preheating (Change in Enthalpy) Cal.	(Btu/lb)	Combustion Temperature °K	(°R)	Characteristic Velocity, m/sec	(ft/sec)	Ratio of Specific Heats	Molecular Weight
25	0	(0)	1383	(2490)	902	(2960)	1.275	32.3
40	↓	↓	883	(1590)	710	(2330)	1.31	32.2
60			600	(1080)	585	(1920)	1.325	32.1
25	27.8	(50)	1461	(2630)	930	(3050)	1.275	32.3
40	↓	↓	983	(1770)	757	(2485)	1.31	32.2
60			694	(1250)	628	(2060)	1.325	32.1
25	55.6	(100)	1567	(2820)	962	(3155)	1.275	32.3
40			1083	(1950)	797	(2615)	1.31	32.2
60			800	(1440)	677	(2220)	1.325	32.1

TABLE XXII. - LOX/RP-1 OXIDIZER-RICH PREBURNER GAS PROPERTY DATA SUMMARY

Pressure = 408 atm (6000 psia)
Chamber Coolant: RP-1

Mixture Ratio	Propellant Preheating (Change in Enthalpy) Cal.	(Btu/lb)	Combustion Temperature °K	(°R)	Characteristic Velocity, m/sec	(ft/sec)	Ratio of Specific Heats	Molecular Weight
25	0	(0)	1444	(2600)	930	(3050)	1.27	31.8
40	↓	↓	931	(1675)	733	(2405)	1.302	31.9
55			689	(1240)	631	(2070)	1.325	31.9

TABLE XXIII. - LOX/MMH OXIDIZER-RICH PREBURNER GAS PROPERTY DATA SUMMARY

Pressure = 408 atm (6000 psia)
Chamber Coolant: MMH

Mixture Ratio	Propellant Preheating (Change in Enthalpy)		Combustion Temperature		Characteristic Velocity,		Ratio of Specific Heats	Molecular Weight
	Cal.	(Btu/lb)	°K	(°R)	m/sec	(ft/sec)		
15	0	(0)	1364	(2455)	917	(3009)	1.28	30.6
20			1063	(1913)	801	(2628)	1.30	30.9
25			864	(1555)	717	(2351)	1.31	31.1
30			722	(1299)	651	(2136)	1.33	31.3

TABLE XXIV. - LOX/N_2H_4 OXIDIZER-RICH PREBURNER GAS PROPERTY DATA SUMMARY

Pressure = 408 atm (6000 psia)
Chamber Coolant: N_2H_4

Mixture Ratio	Propellant Preheating (Change in Enthalpy)		Combustion Temperature		Characteristic Velocity,		Ratio of Specific Heats	Molecular Weight
	Cal.	(Btu/lb)	°K	(°R)	m/sec	(ft/sec)		
10	0	(0)	1288	(2318)	907	(2977)	1.29	29.3
15			913	(1643)	749	(2457)	1.31	30.1
20			594	(1069)	645	(2116)	1.33	30.5

TABLE XXV. - LOX/LH_2 OXIDIZER-RICH PREBURNER GAS PROPERTY DATA SUMMARY

Pressure = 408 atm (6000 psia)
Chamber Coolant: LH_2

Mixture Ratio	Propellant Preheating (Change in Enthalpy) Cal.	(Btu/lb)	Combustion Temperature °K	(°R)	Characteristic Velocity, m/sec	(ft/sec)	Ratio of Specific Heats	Molecular Weight
70	0	(0)	1334	(2402)	929	(3047)	1.28	29.2
110			900	(1620)	748	(2455)	1.31	30.1
150			656	(1180)	625	(2050)	1.34	30.8

TABLE XXVI. - LOX/CH_4 OXIDIZER-RICH PREBURNER GAS PROPERTY DATA SUMMARY

Pressure = 408 atm (6000 psia)
Chamber Coolant: CH_4

Mixture Ratio	Propellant Preheating (Change in Enthalpy) Cal.	(Btu/lb)	Combustion Temperature °K	(°R)	Characteristic Velocity, m/sec	(ft/sec)	Ratio of Specific Heats	Molecular Weight
20	0	(0)	1882	(3387)	1088	(3569)	1.25	30.5
40			1043	(1877)	790	(2591)	1.295	31.2
60			701	(1261)	639	(2097)	1.325	31.5

TABLE XXVII. - LOX/MMH FUEL-RICH PREBURNER GAS PROPERTY DATA SUMMARY

Pressure = 408 atm (6000 psia)
Chamber Coolant: MMH

Mixture Ratio	Propellant Preheating (Change in Enthalpy)		Combustion Temperature		Characteristic Velocity,		Ratio of Specific Heats	Molecular Weight
	Cal.	(Btu/lb)	°K	(°R)	m/sec	(ft/sec)		
0.01	0	(0)	1344	(2419)	1325	(4348)	1.21	15.?
0.05	↓	↓	1394	(2509)	1359	(4458)	1.22	15.0
0.10	↓	↓	1449	(2608)	1395	(4576)	1.23	14.8
0.01	55.6	(100)	1382	(2488)	1353	(4440)	1.21	15.2
0.05	↓	↓	1429	(2573)	1385	(4545)	1.22	15.0
0.10	↓	↓	1483	(2670)	1420	(4660)	1.23	14.8
0.01	111	(200)	1419	(2555)	1383	(4538)	1.21	15.2
0.05	↓	↓	1464	(2635)	1413	(4635)	1.22	15.0
0.10	↓	↓	1517	(2730)	1445	(4740)	1.23	14.8

TABLE XXVIII. LOX/N_2H_4 FUEL-RICH PREBURNER GAS PROPERTY DATA SUMMARY

Pressure = 408 atm (6000 psia)
Chamber Coolant: N_2H_4

Mixture Ratio	Propellant Preheating (Change in Enthalpy)		Combustion Temperature		Characteristic Velocity,		Ratio of Specific Heats	Molecular Weight
	Cal.	(Btu/lb)	°K	(°R)	m/sec	(ft/sec)		
0.01	0	(0)	1014	(1826)	1285	(4217)	1.34	11.4
0.05	↓	↓	1157	(2082)	1359	(4459)	1.34	11.5
0.10	↓	↓	1361	(2449)	1452	(4763)	1.33	11.9
0.01	27.8	(50)	1042	(1875)	1304	(4278)	1.34	11.4
0.05	↓	↓	1189	(2140)	1380	(4527)	1.34	11.5
0.10	↓	↓	1395	(2512)	1472	(4828)	1.33	11.9
0.01	55.6	(100)	1071	(1928)	1326	(4350)	1.34	11.4
0.05	↓	↓	1222	(2200)	1401	(4595)	1.34	11.5
0.10	↓	↓	1431	(2575)	1490	(4890)	1.33	11.9

TABLE XXIX. - LOX/LH_2 FUEL-RICH PREBURNER GAS PROPERTY DATA SUMMARY

Pressure = 408 atm (6000 psia)
Chamber Coolant: LH_2

Mixture Ratio	Propellant Preheating (Change in Enthalpy)		Combustion Temperature		Characteristic Velocity,		Ratio of Specific Heats	Molecular Weight
	Cal.	(Btu/lb)	°K	(°R)	m/sec	(ft/sec)		
0.5	0	(0)	503	(905)	1770	(5807)	1.39	3.04
1.0	↓	↓	979	(1763)	2095	(6873)	1.36	4.03
1.5			1414	(2545)	2275	(7463)	1.32	5.04
0.5	253	(455)	572	(1030)	1832	(6010)	1.39	3.04
1.0	↓	↓	1047	(1885)	2170	(7120)	1.35	4.03
1.5			1478	(2660)	2327	(7635)	1.31	5.04
0.5	462	(831)	628	(1130)	1923	(6310)	1.39	3.04
1.0	↓	↓	1100	(1980)	2228	(7310)	1.35	4.03
1.5			1525	(2745)	2370	(7775)	1.31	5.04

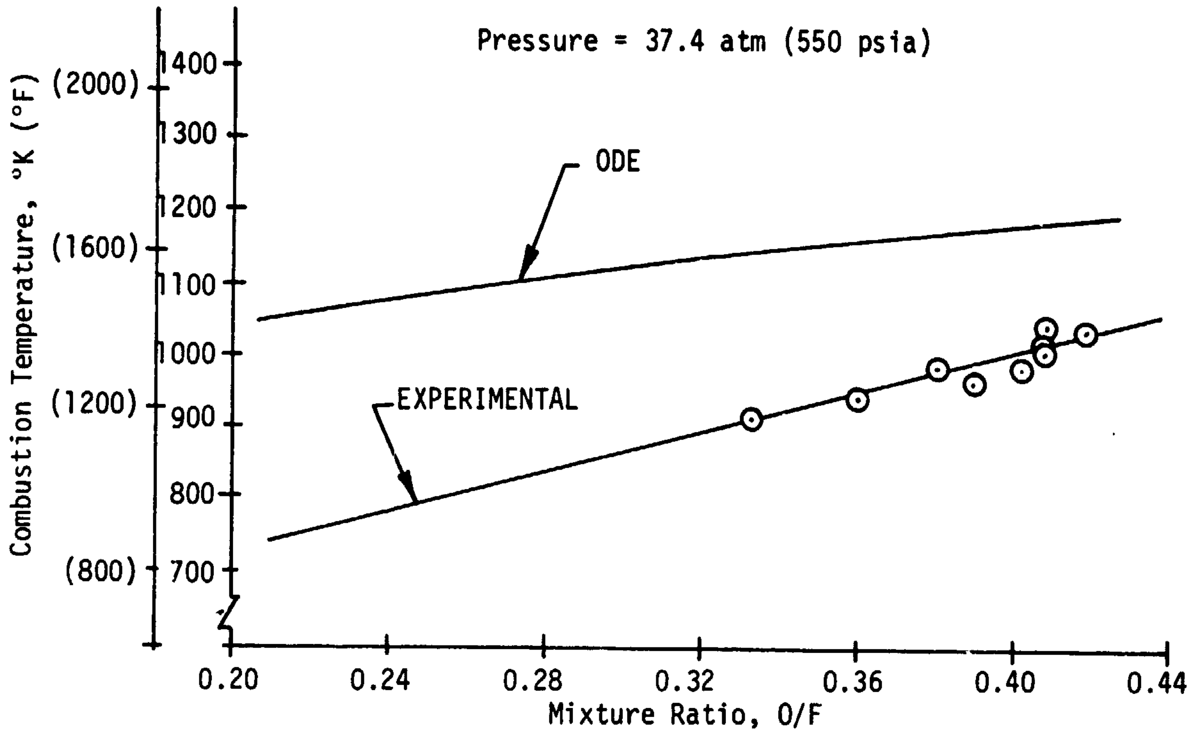

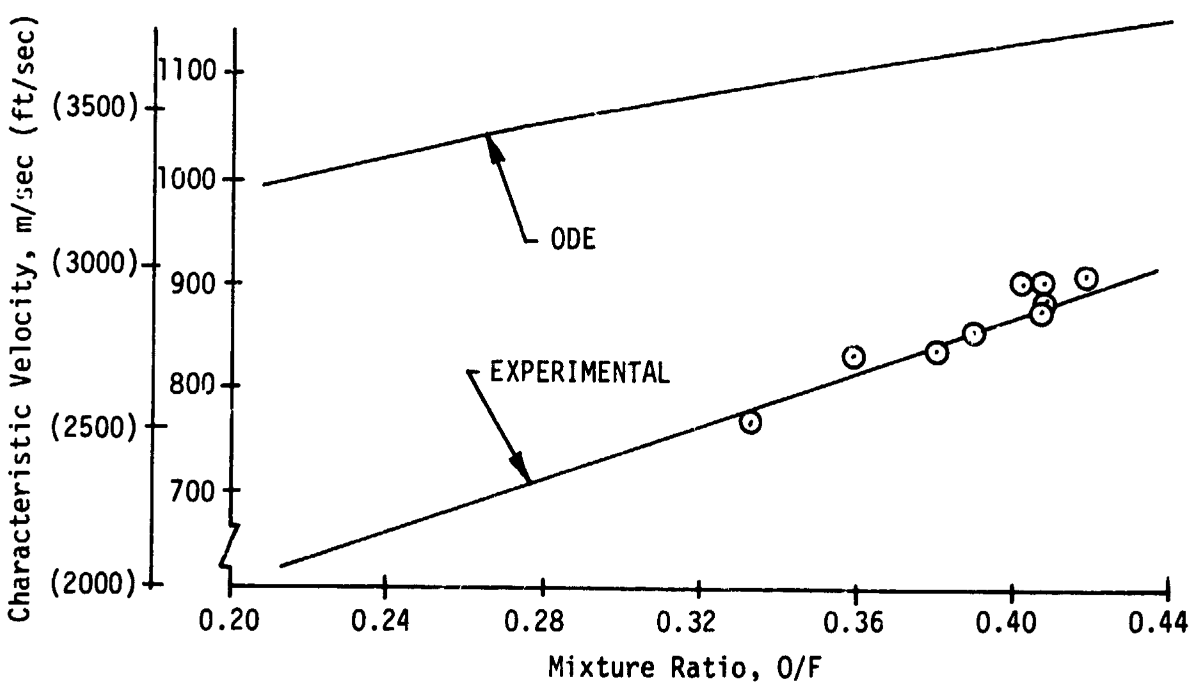

Figure 3. LOX/RP-1 Experimental Preburner Characteristics

where:

$T_{o_{exp}}$ (or C^*_{exp}) = corrected experimentally based combustion temperature or characteristic velocity value

$T_{o_{ODE}}$ (or C^*_{ODE}) = ODE combustion temperature or characteristic velocity value

η_{T_o} const. ϕ = experimental efficiency factor defined at any equivalence ratio by dividing the experimental T_O (or C*) value by the ODE T_O (or C*) value

Equivalence ratio = Stoichiometric O/F divided by design O/F.

Efficiency factors were developed versus equivalence ratio from the data of Figure 3 and used to predict T_O and C* values at higher chamber pressures. The LOX/RP-1 factors were also assumed to be valid for both the LOX/RJ-5 and LOX/CH_4 propellant combinations. This data is presented on Tables XXX, XXXI and XXXII. The empirical fuel-rich gas generator property data, which has been derived from test results, also results in a much lower ratio of specific heats and a higher molecular weight than are predicted by the ODE analytical model. For example, the analytical and experimental data at a design point of 408 atm (6000 psia) are compared below:

	LOX/RP-1	
	Experimental	Theoretical
Mixture Ratio	0.22	0.22
Combustion Temp., °K (°R)	867 (1560)	1172 (2110)
Molecular Weight	29.83	24.2
Ratio of Specific Heats, γ	1.095	1.172

The experimental data differs because the analytical models cannot accurately predict the composition of the exhaust products. The experimental data shown on Figure 4 has been empirically derived from the results of Titan I and Atlas type engine gas generator testing in a pressure range from 27.2 to 68 atm (400 to 1,000 psia). However, component designers familiar with the past work feel that the experimentally derived γ is conservative. Because no experimental data exists at high pressure, the low pressure data has been used to adjust the theroetical property data predictions. The experimentally derived molecular weight was not assumed to vary with pressure and the specific heat at constant pressure was calculated from the perfect gas law.

TABLE XXX. - LOX/RJ-5 FUEL-RICH PREBURNER GAS PROPERTY DATA SUMMARY

Pressure = 408 atm (6000 psia)
Chamber Coolant: RJ-5

Mixture Ratio	Propellant Preheating (Change in Enthalpy) Cal.	(Btu/lb)	Combustion Temperature °K	(°R)	Characteristic Velocity, m/sec	(ft/sec)	Ratio of Specific Heats	Molecular Weight
0.10	0	(0)	736	(1325)	482	(1580)	1.06	42.7
0.30	↓	↓	1111	(2000)	738	(2420)	1.135	33.8
0.50			1450	(2610)	997	(3270)	1.185	23.0
0.10	55.6	(100)	775	(1395)	512	(1680)	1.06	42.7
0.30	↓	↓	1128	(2030)	762	(2500)	1.135	33.8
0.50			1478	(2660)	1012	(3320)	1.185	23.0
0.10	111	(200)	817	(1470)	536	(1760)	1.06	42.7
0.30	↓	↓	1161	(2090)	780	(2560)	1.135	33.8
0.50			1511	(2720)	1036	(3400)	1.185	23.0

TABLE XXXI. - LOX/RP-1 FUEL-RICH PREBURNER GAS PROPERTY DATA SUMMARY

Pressure = 408 atm (6000 psia)
Chamber Coolant: RP-1

Mixture Ratio	Propellant Preheating (Change in Enthalpy) Cal.	(Btu/lb)	Combustion Temperature °K	(°R)	Characteristic Velocity, m/sec	(ft/sec)	Ratio of Specific Heats	Molecular Weight
0.1	0	(0)	611	(1100)	488	(1600)	1.05	33.7
0.3	↓	↓	986	(1775)	753	(2470)	1.115	27 2
0.5	↓	↓	1267	(2280)	988	(3240)	1.155	20.7
0.1	55.6	(100)	656	(1180)	515	(1690)	1.05	33.7
0.3	↓	↓	1011	(1820)	777	(2550)	1.115	27.2
0.5	↓	↓	1294	(2330)	1006	(3300)	1.155	20.7
0.1	111	(200)	700	(1260)	543	(1780)	1.05	33.7
0.3	↓	↓	1033	(1860)	797	(2615)	1.115	27.2
0.5	↓	↓	1317	(2370)	1024	(3360)	1.155	20.7

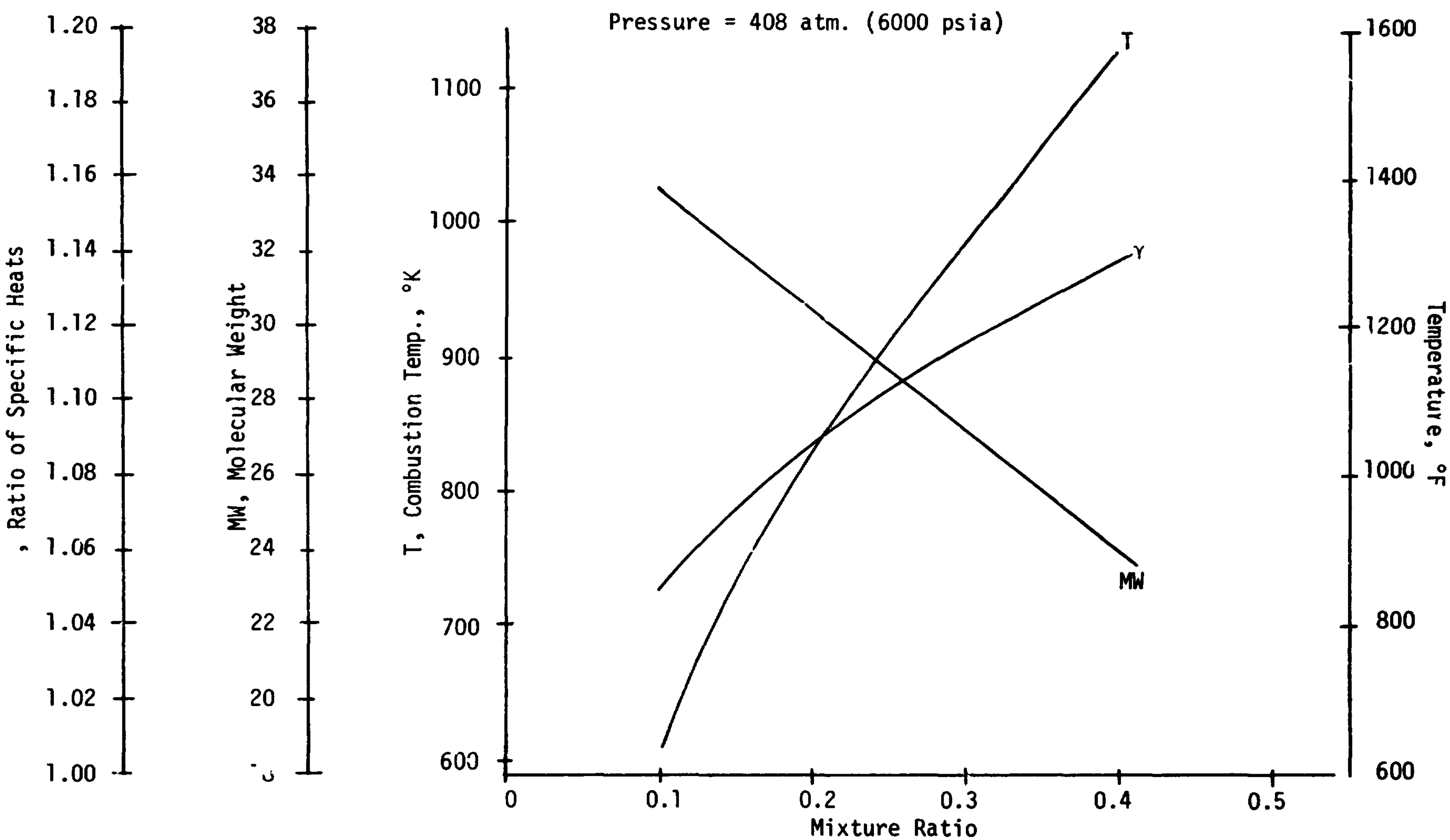

Figure 4. Empirically Derived LOX/RP-1 Fuel-Rich Gas Properties

PRECEDING PAGE BLANK NOT FILMED

E. MAIN CHAMBER THEORETICAL PERFORMANCE DATA

One-dimensional equilibrium (ODE) and frozen (ODF) sea-level and vacuum specific impulse were calculated over the same chamber pressure and mixture ratio ranges as the main chamber combustion gas property data. Performance was calculated for expansion area ratios ranging from 1:1 to 400:1. ODF performance is between five and eight percent below ODE performance for all propellant combinations. ODF performance would yield erroneous specific impulse values and nonoptimum TCA mixture ratios if utilized. A typical comparison of ODE and ODF performance is shown on Figure 5 for LOX/RP-1. Therefore, the ODE performance was used to conduct all analyses in this study effort.

For each study propellant combination, ODE vacuum specific impulse was initially plotted versus mixture ratio for various values of chamber pressure. At high thrust chamber pressure, 272 atm (4000 psia), the optimum sea-level performance occurs at nozzle area ratio of approximately 40:1. Therefore, this was the specified baseline area ratio in the study. ODE vacuum specific impulse vs mixture ratio for all six propellant combinations is presented on Figures 6 through 11.

Sea-level and vacuum ODE performance is presented as a function of nozzle area ratio for approximately optimum mixture ratios for the Mode 1 propellants and at an O/F = 7.0 for LOX/LH_2 on Figures 12 through 17.

The propellant temperature used in this performance evaluation were:

- Oxygen, NBP: 90.2°K (162.4°R)
- RP-1: 298°K (537°R)
- RJ-5: 298°K (537°R)
- MMH : 298°K (537°R)
- Hydrazine: 298°K (537°R)
- Hydrogen, NBP: 20.3°K (36.5°R)
- Methane, NBP: 112°K (201.6°R)

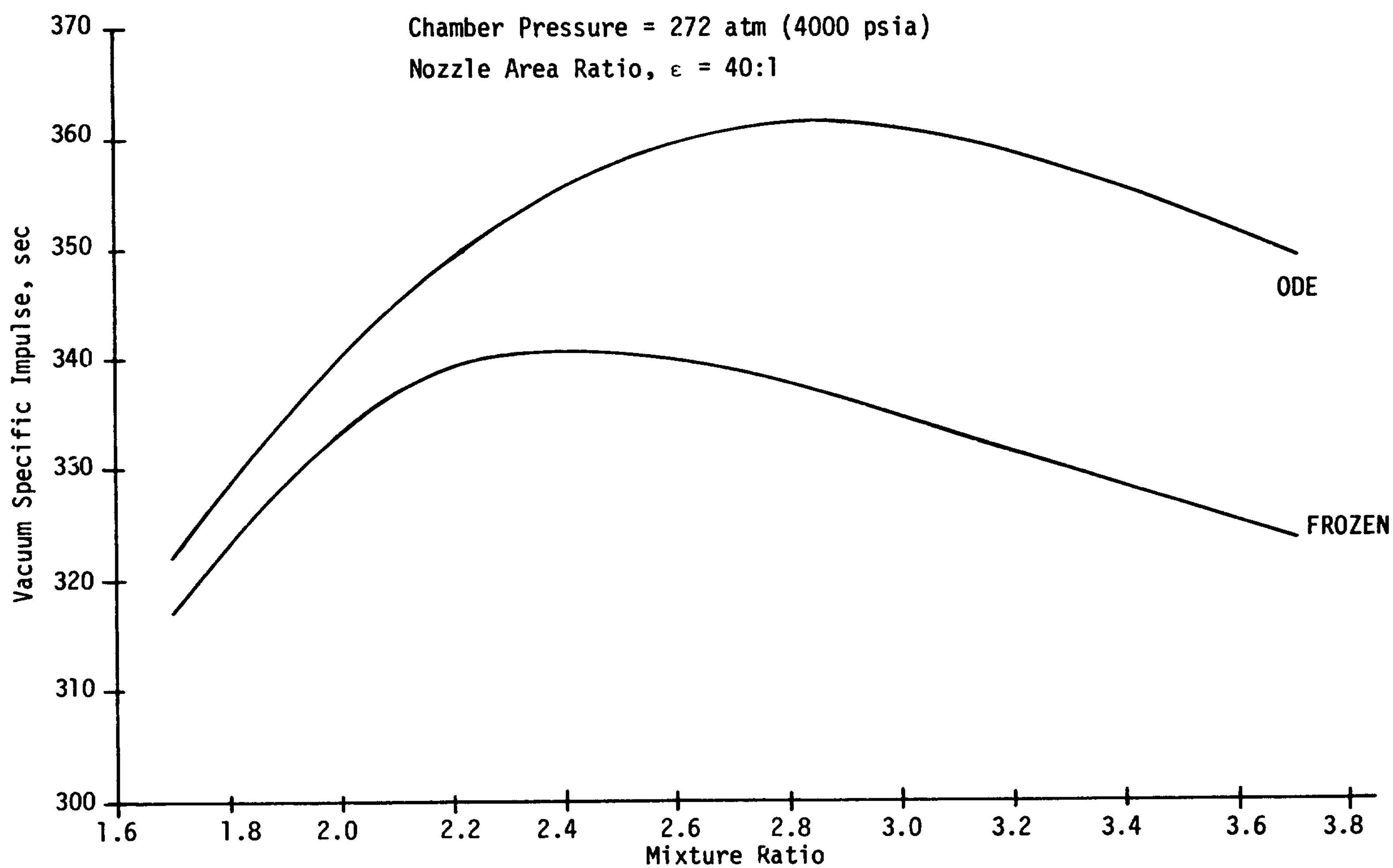

Figure 5. LOX/RP-1 ODE and Frozen Performance Comparison

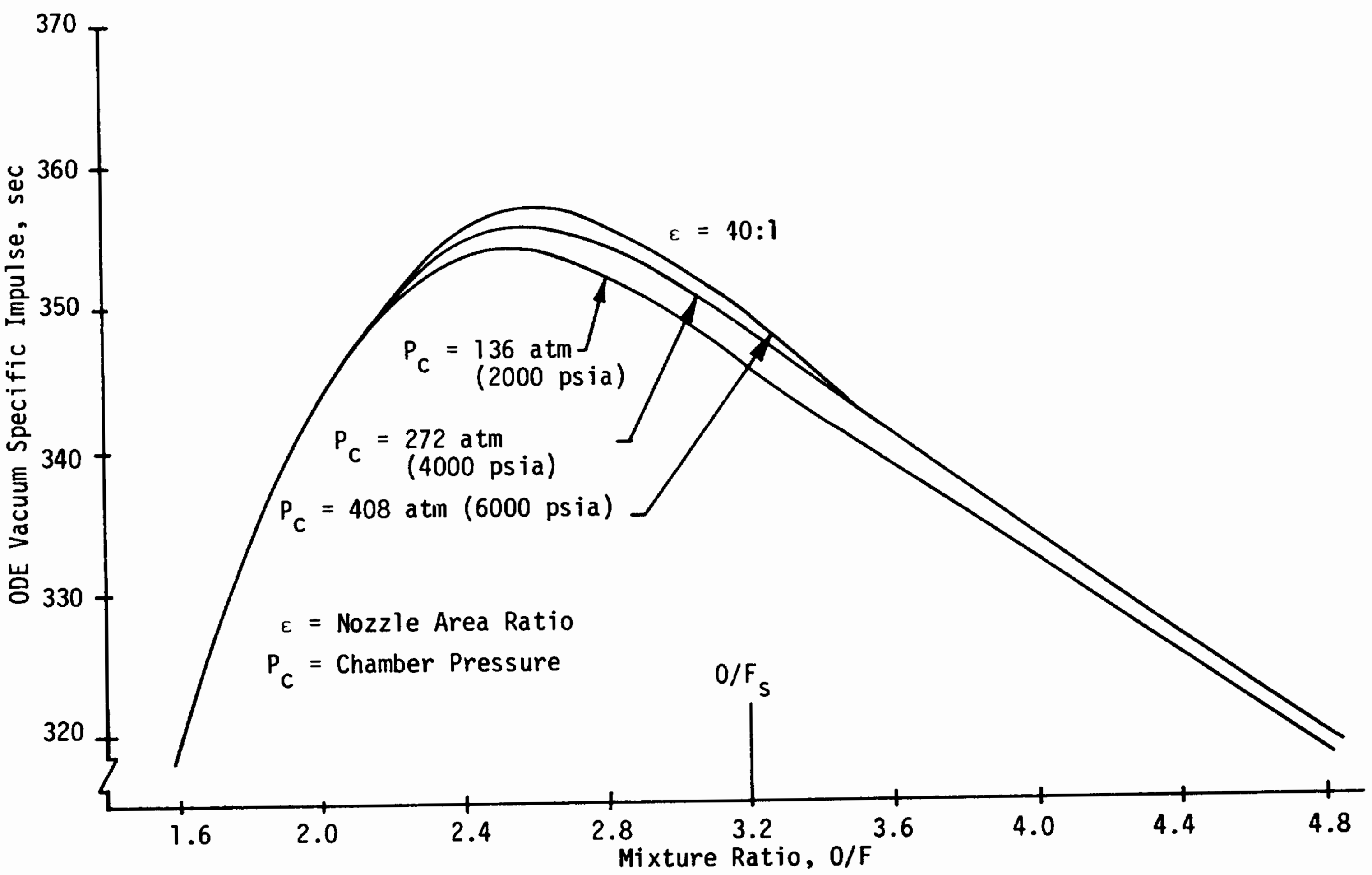

Figure 6. LOX/RJ-5 ODE Vacuum Performance Versus O/F

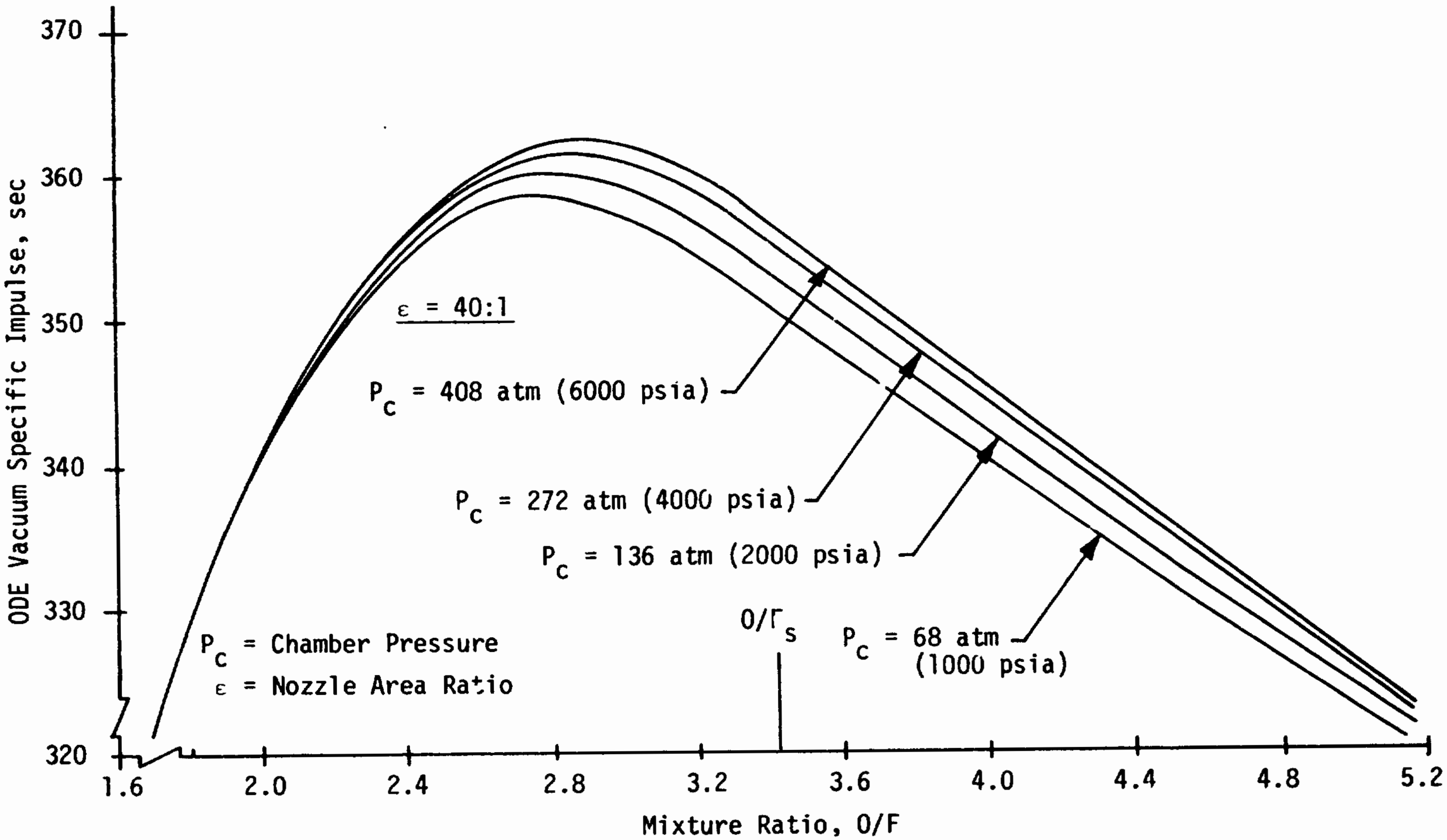

Figure 7. LOX/RP-1 ODE Vacuum Performance Versus O/F

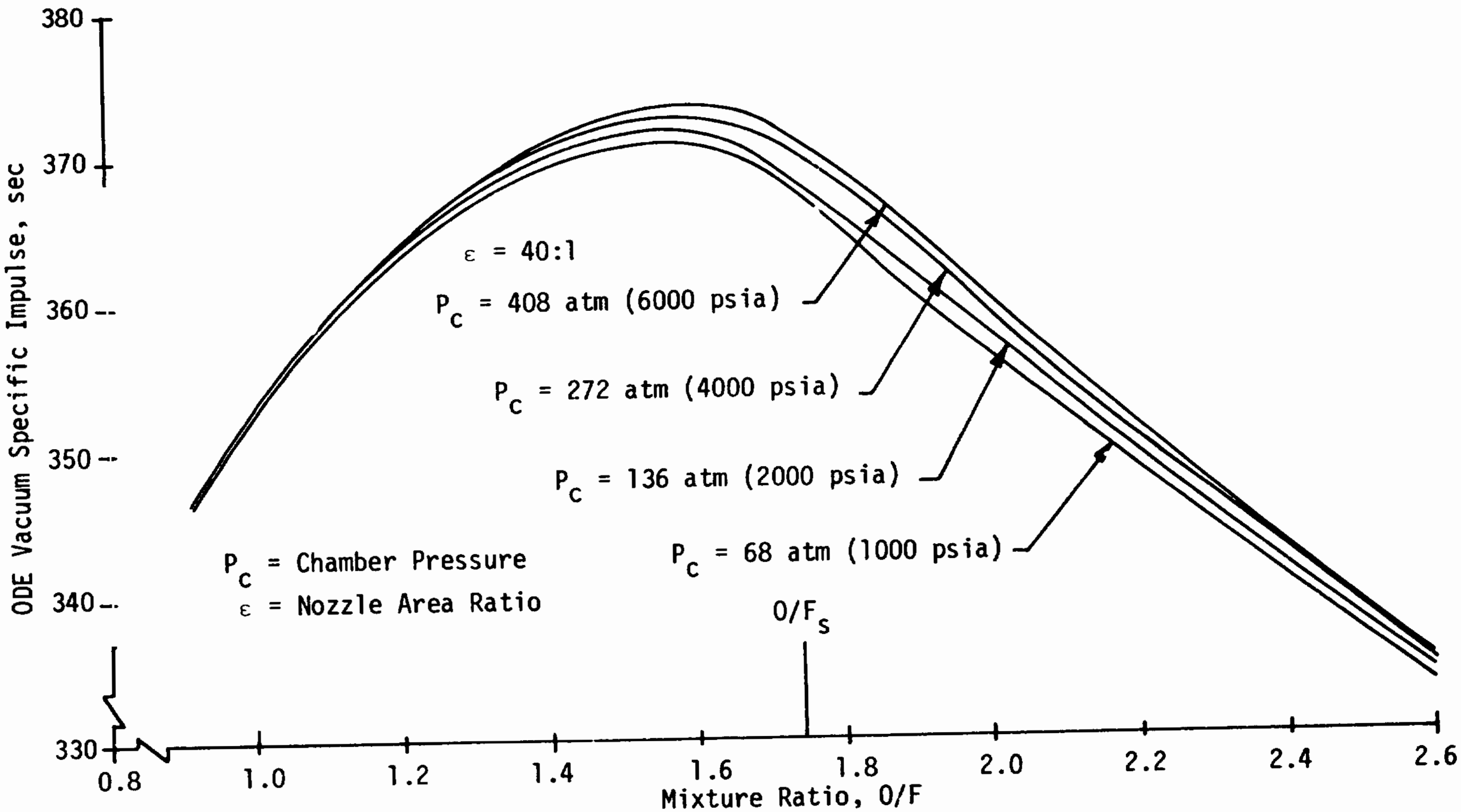

Figure 8. LOX/MMH ODE Vacuum Performance Versus O/F

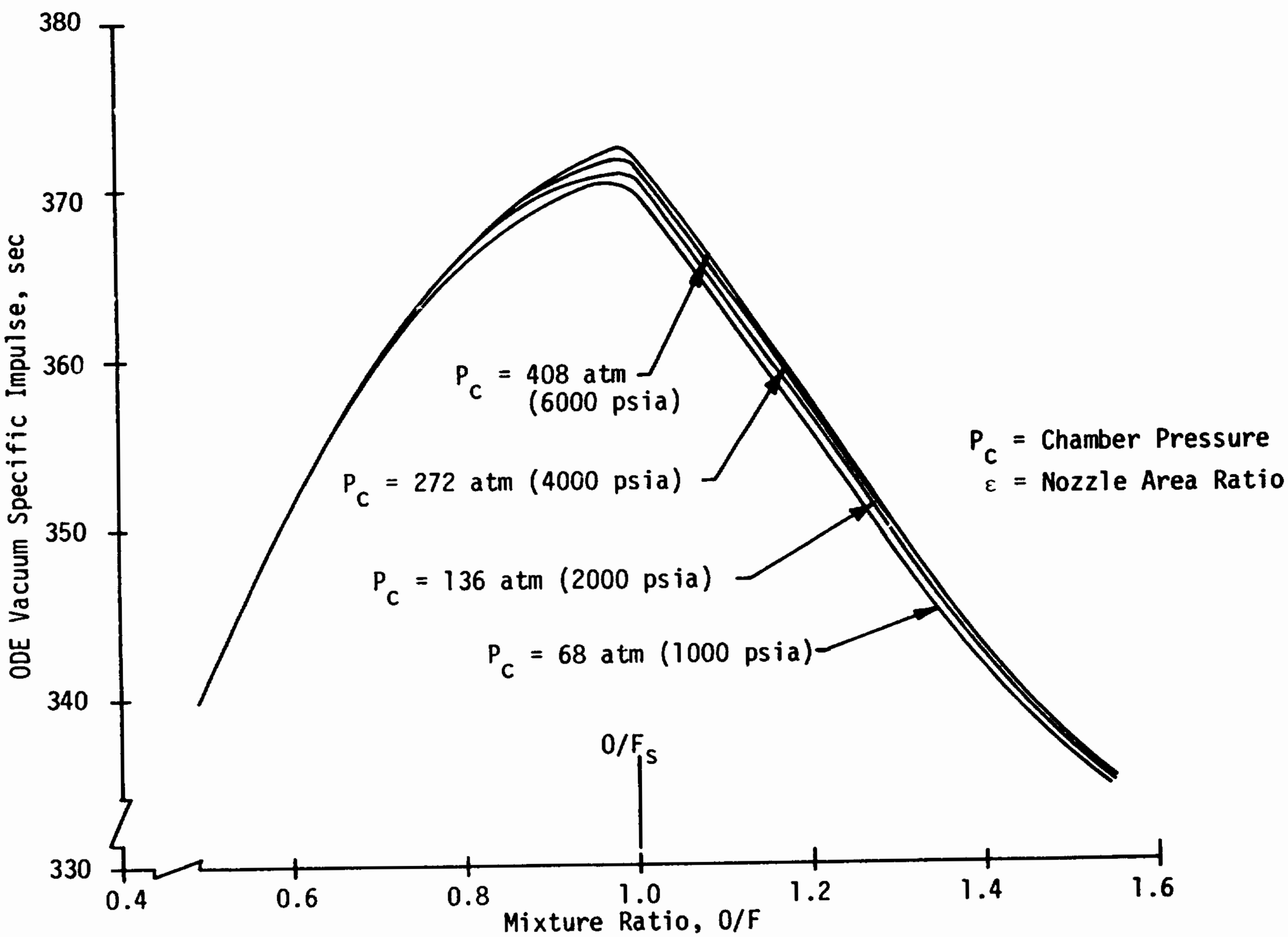

Figure 9. LOX/N_2H_4 ODE Vacuum Performance Versus O/F

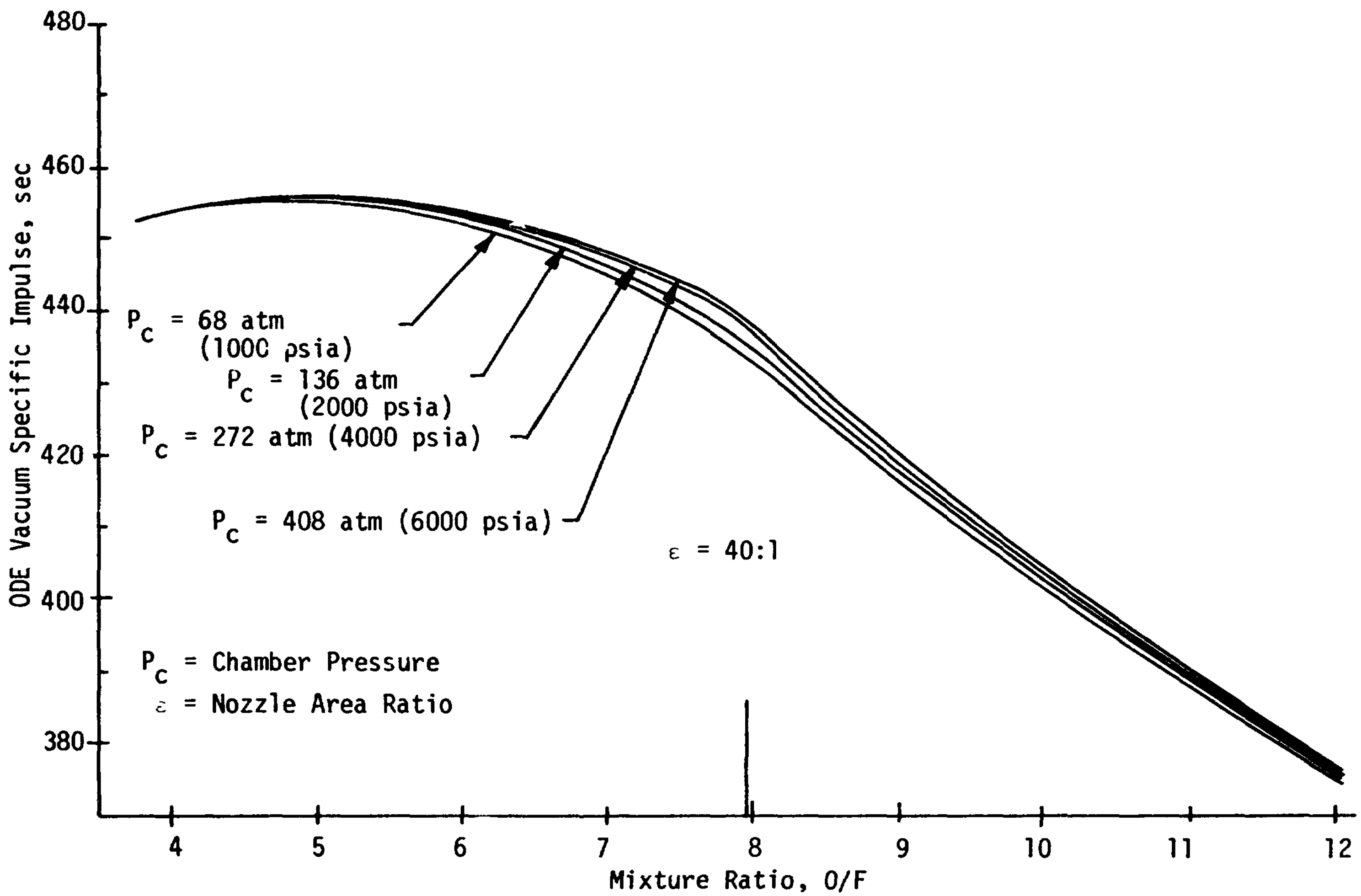

Figure 10. LOX/LH_2 ODE Vacuum Performance Versus O/F

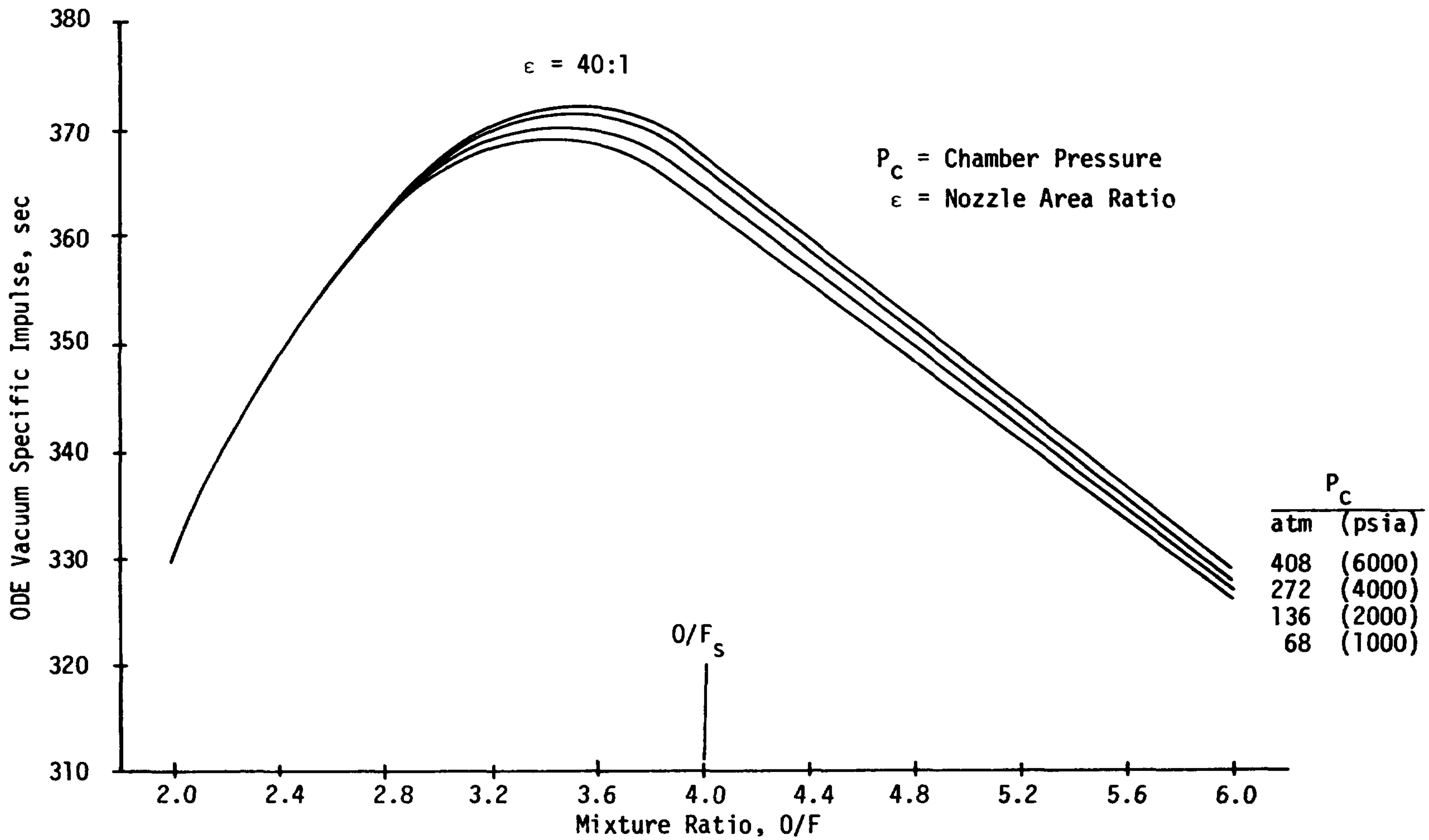

Figure 11. LOX/CH_4 ODE Vacuum Performance Versus O/F

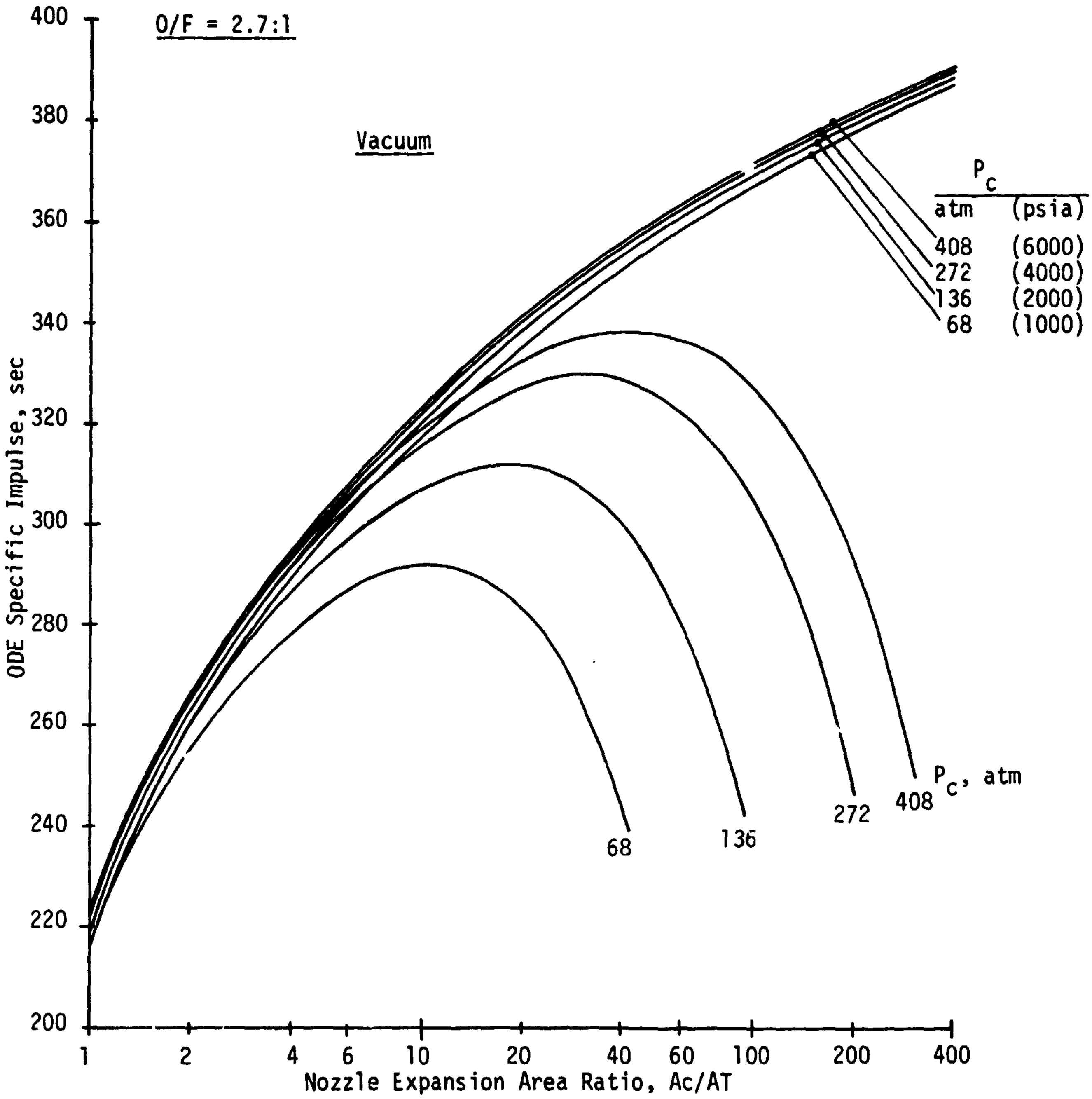

Figure 12. LOX/RJ-5 ODE Performance Versus Area Ratio

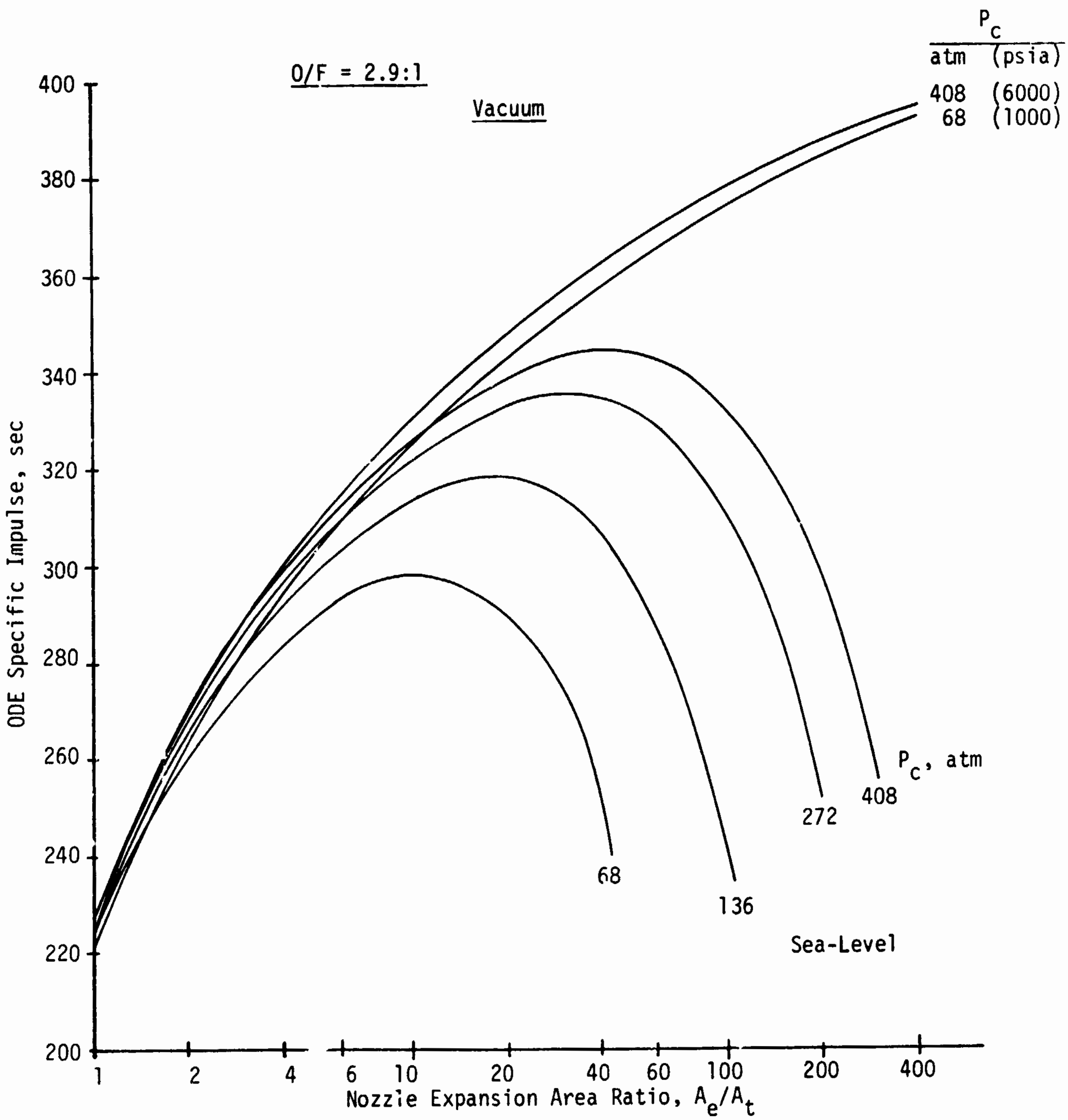

Figure 13. LOX/RP-1 ODE Performance Versus Area Ratio

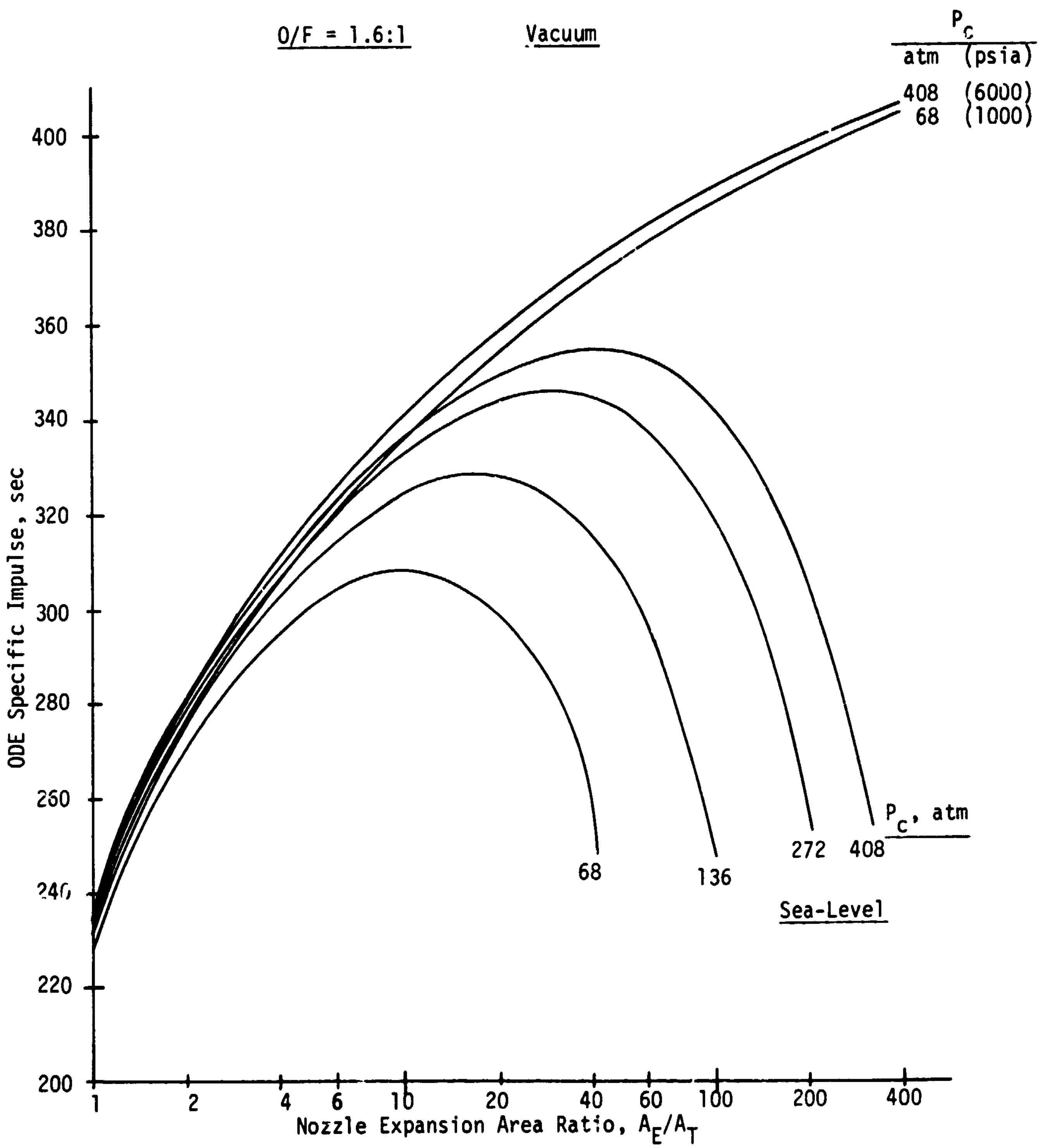

Figure 14. LOX/MMH ODE Performance Versus Area Ratio

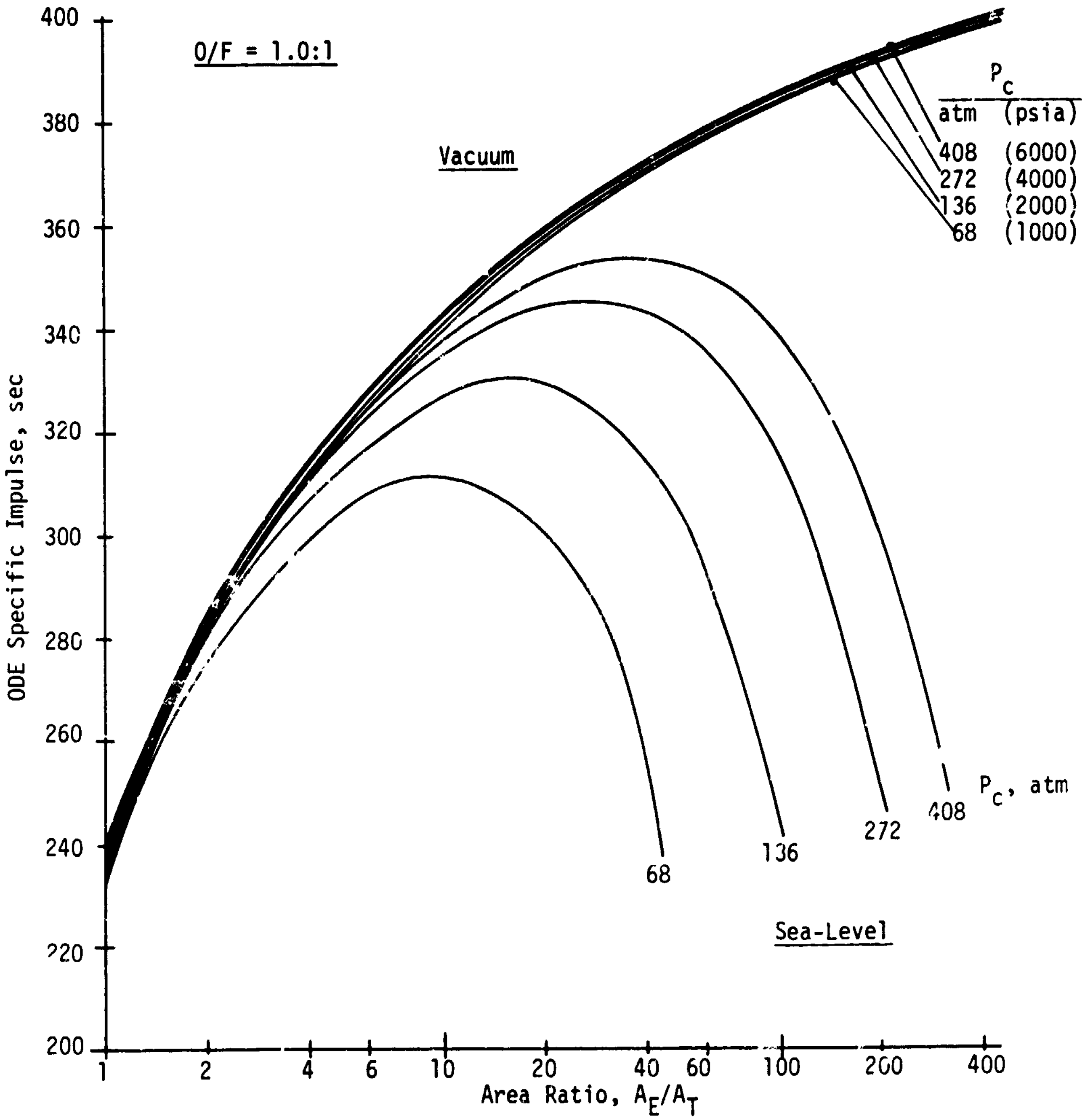

Figure 15. LOX/N_2H_4 ODE Performance Versus Area Ratio

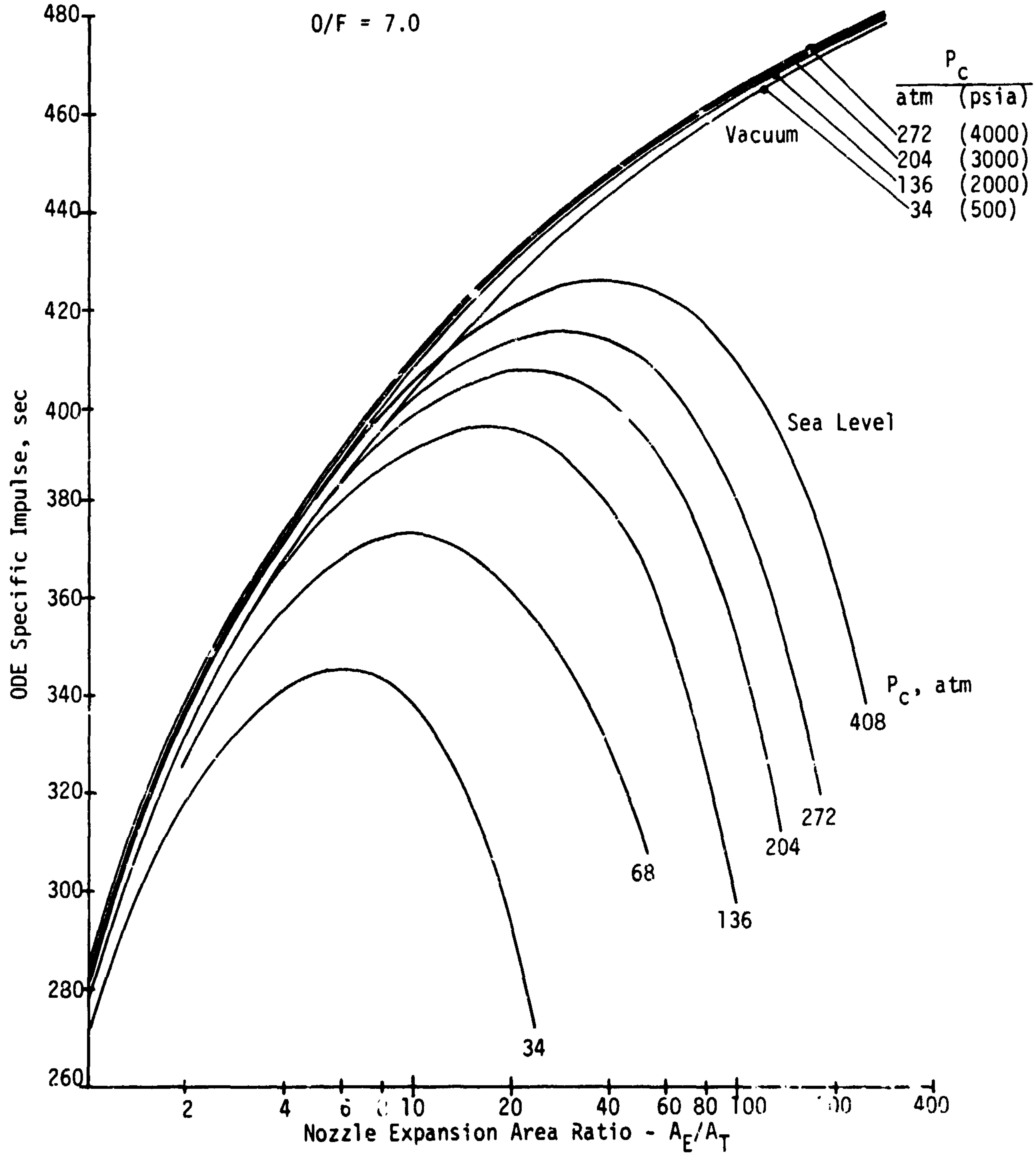

Figure 16. LOX/LH_2 ODE Performance Versus Area Ratio

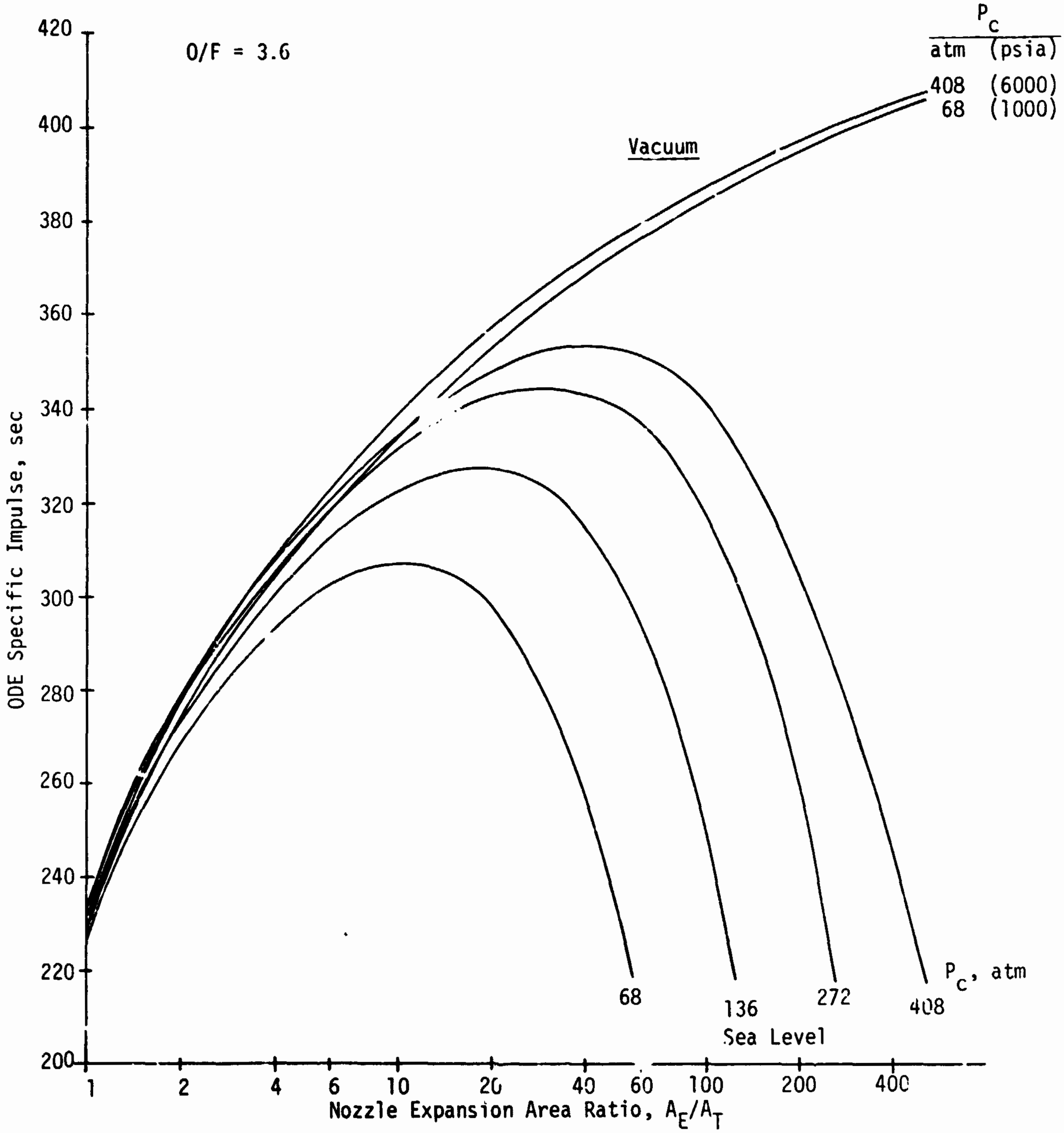

Figure 17. LOX/CH_4 ODE Performance Versus Area Ratio

SECTION IV

TASK II - COOLANT EVALUATION

A. OBJECTIVES AND GUIDELINES

The objectives of this task were to: (1) define the thrust chamber geometry and mixture ratio for the various candidate Mode 1 propellant combinations and engine cycles, and (2) to establish the relative cooling capability of the candidate Mode 1 fuels, oxygen and hydrogen.

The following propellant combinations and coolants were considered:

Propellants	Coolant	Cycle
LOX/RJ-5	Oxygen	Staged Combustion
LOX/RJ-5	Hydrogen	Staged Combustion
LOX/RJ-5	Hydrogen	Gas Generator
LOX/RJ-5	RJ-5	Staged Combustion
LOX/RP-1	RP-1	Staged Combustion
LOX/Hydrazine	Hydrazine	Staged Combustion
LOX/MMH	MMH	Staged Combustion
LOX/CH_4	CH_4	Staged Combustion

The two hydrogen cooling studies differed only in the length of the combustion chamber; the gas generator cycle required 22.9 cm (9 inches) additional length to accommodate high density propellant injection.

Parametric studies over the chamber pressure range from 136 atm to 340 atm (2000 psia to 5000 psia) were required, with the relative merit of the various coolants based on the attainable chamber pressure as determined by pressure drop requirements. A service life of 250 cycles was specified; design criteria and coolant evaluation also considered limitations such as coking of the hydrocarbon fuels and catalytic decomposition of MMH and hydrazine.

Additional Task II guidelines provided by NASA/LeRC are given in Table XXXIII and Figures 18 through 21. Rectangular channel construction was specified in the high heat flux part of the chamber using a zirconium-copper alloy. Table XXXIII provides channel dimension and wall thickness limits plus inlet pressures and temperatures. Figures 18 through 21 show the zirconium-copper properties used in the study.

B. TCA GEOMETRY AND MIXTURE RATIO SELECTION

The TCA geometry and mixture ratio were initially selected for the Mode 1 LOX/RJ-5 baseline engine. The approach and results are discussed herein.

TABLE XXXIII. - COOLANT EVALUATION STUDY GUIDELINES

Propellant Combination	Coolant	Available Coolant	Coolant Inlet Temp. °K	(°R)
RJ-5/Oxygen	Oxygen	Total Flow	111	(200)
RJ-5/Oxygen	RJ-5	Total Flow	311	(560)
RJ-5/Oxygen	Hydrogen	(Minimize)	61	(110)
RP-1/Oxygen	RP-1	Total Flow	311	(560)
Hydrazine/Oxygen	Hydrazine	Total Flow	311	(560)
MMH/Oxygen	MMH	Total Flow	311	(560)
CH_4/Oxygen	CH_4	Total Flow	144	(260)

THRUST CHAMBER

- Regeneratively Cooled
- Inlet Pressure = 2.25 Times Chamber Pressure
- High Heat Flux Portion of Chamber Shall be of Nontubular Construction with the Following Dimensional Limits:

  Minimum Slot Width = 0.762 mm (0.03 in.)

  Maximum Slot Depth/Width = 4 to 1*

  Minimum Land Thickness = 0.762 mm (0.03 in.)

  Minimum Wall Thickness = 0.635 mm (0.025 in.)

- Material (Nontubular Portion): Copper Alloy (Zirconium Copper) Conforming to the properties given Figures 18, 19, 20 and 21
- Service Free Life: 250 Cycles Times a Safety Factor of 4
- Possible Benefit of Carbon Deposition on Hot Gas Side Wall shall be Neglected

*Applied Herein from the Injector End to Area Ratio 1.5:1.

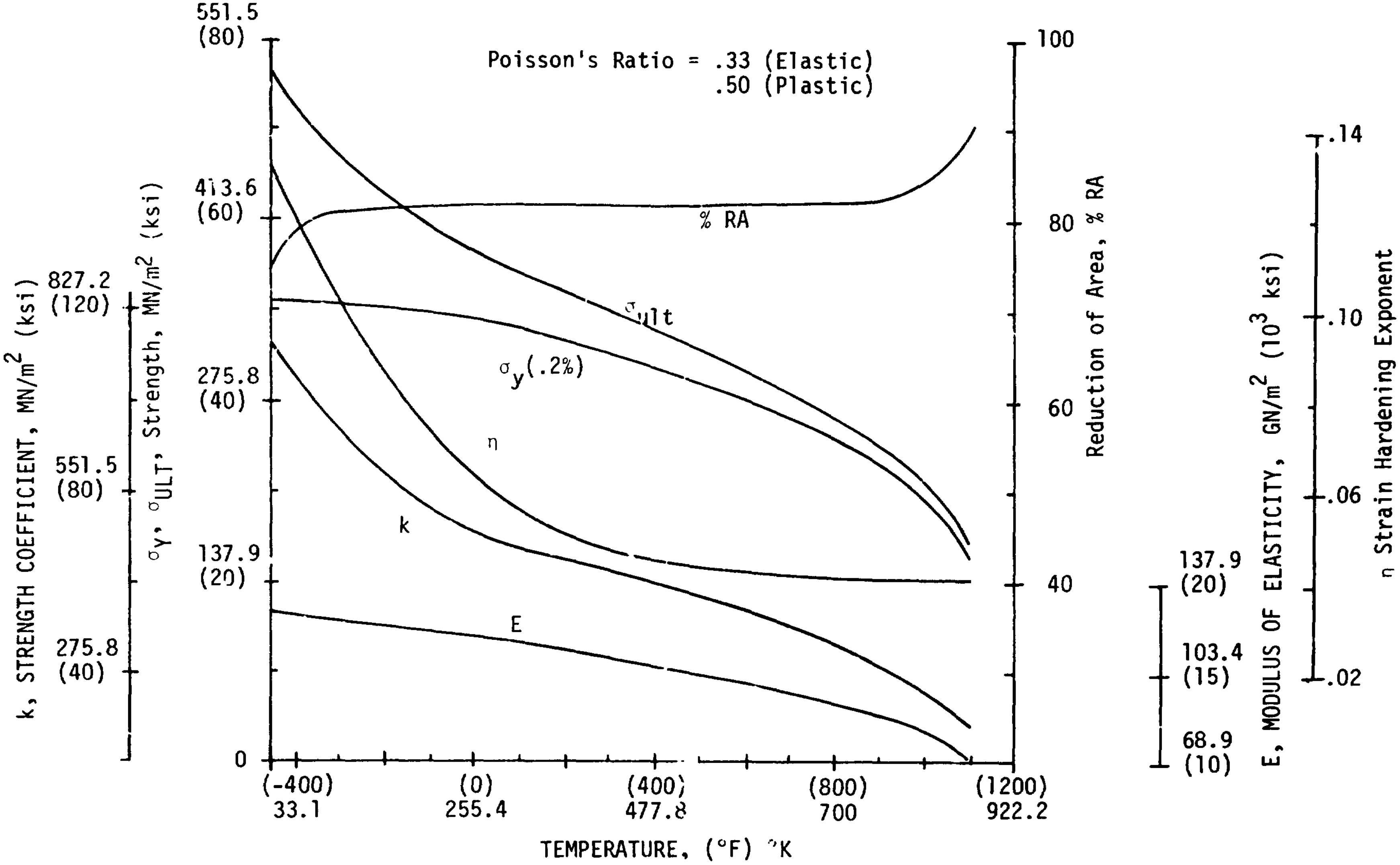

Figure 18. Tensile Properties (Zirconium Copper)

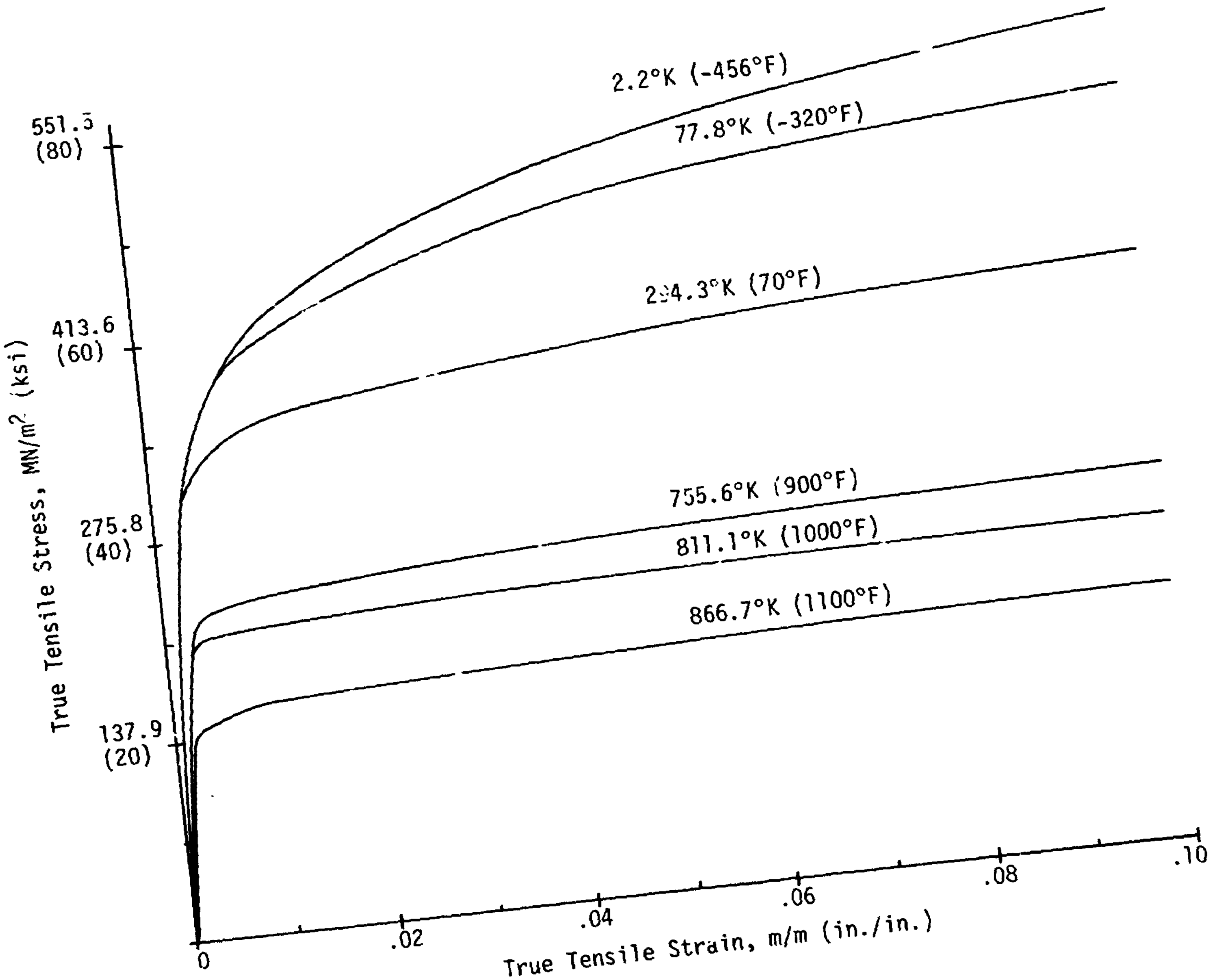

Figure 19. Tensile Stress-Strain

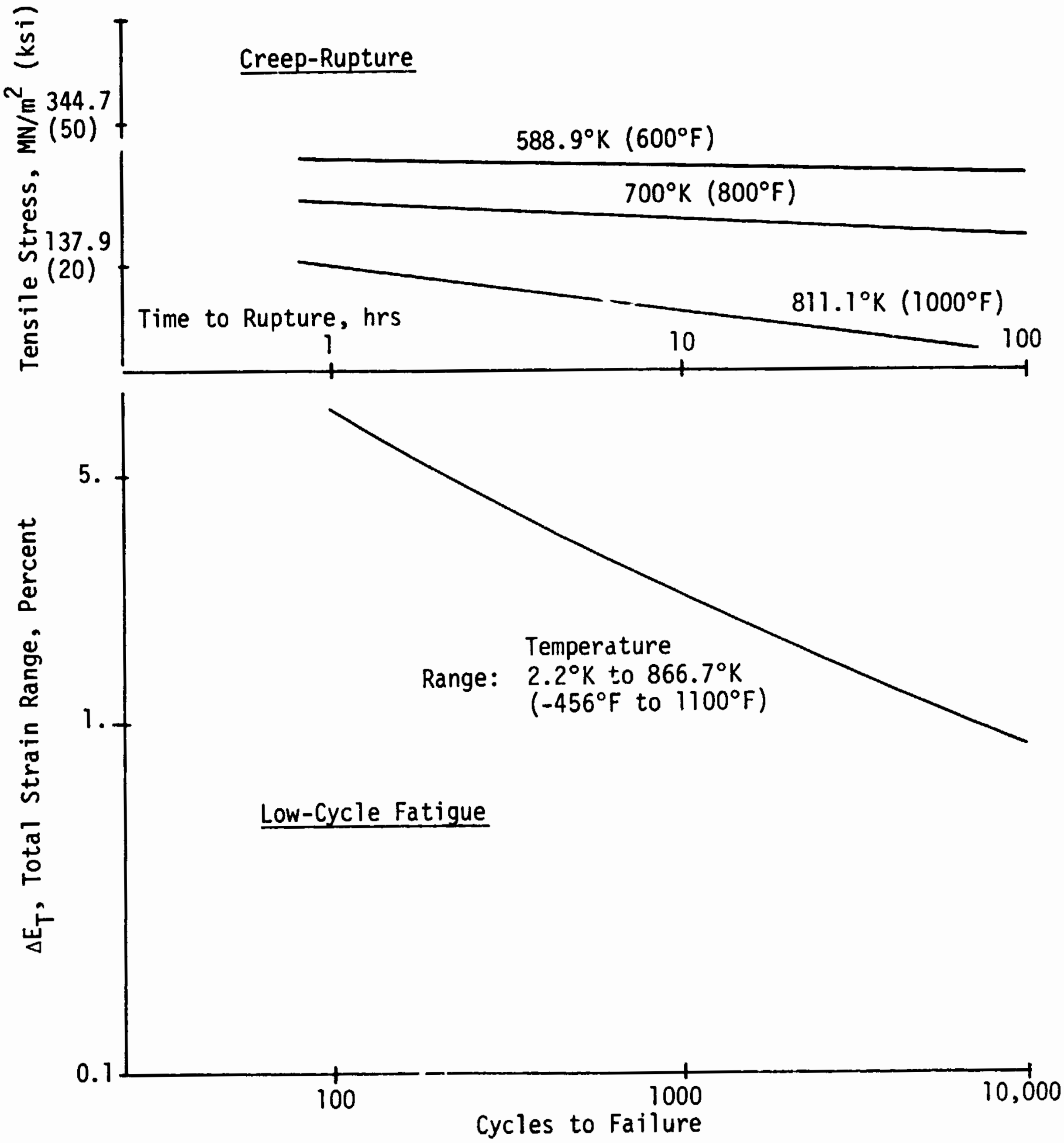

Figure 20. Creep-Rupture and Low Cycle Fatigue

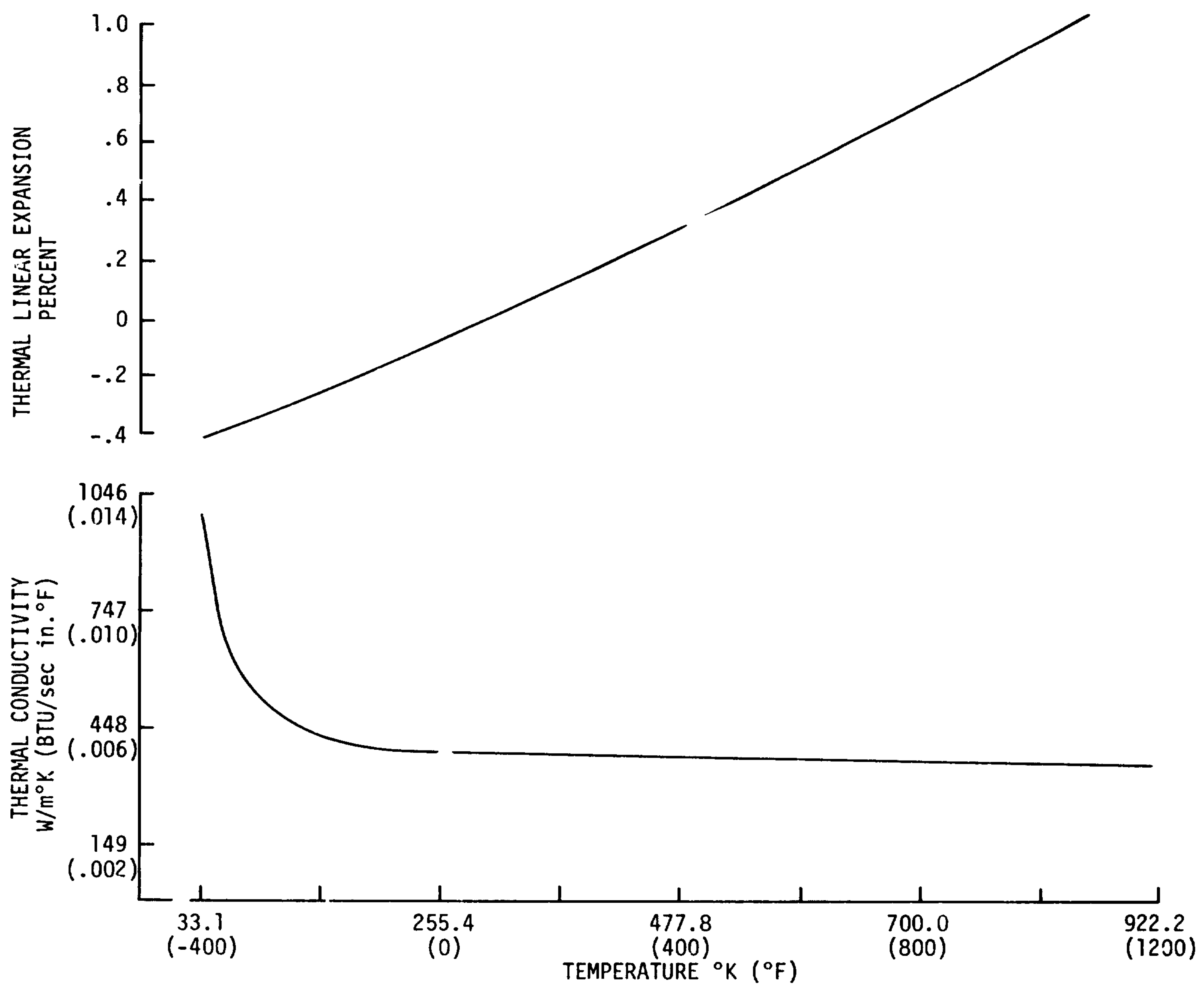

Figure 21. Conductivity and Expansion

The Mode 1 LOX/RJ-5 engine utilizes a staged combustion cycle comprised of parallel fuel-rich and oxidizer-rich preburners and a gas/gas injected primary thrust chamber. Simplified gas/gas mixing analyses were conducted with an ALRC developed gas/gas mixing model (Ref. 44). Injector energy release efficiency (ERE) was evaluated as a function of chamber length (L'), chamber pressure (Pc), chamber contraction ratio (ε_c), mixture ratio, and injector element type and pressure drop. The ERE goal used in the study is 98%.

The analysis was initiated by selecting an initial design point and evaluating injector ERE as a function of chamber length for three injector element types. The elements evaluated were a shear coaxial, a fuel-oxidizer-fuel (F-O-F) external impinging triplet, and a premix triplet. Injector element size (i.e., thrust per element), of course, also affects performance. The chamber length study was conducted for a constant thrust per element of 2233N (502 lb_f) which results in 1309 elements at a vacuum thrust level of 2.92 MN (656.400 lb_f). This element size was selected based on ALRC SSME and M-1 design experience.

Figure 22 shows ERE versus chamber length for the shear coaxial element and also notes the assumed initial design conditions. Minimum coaxial performance is predicted for the equal pressure drops in the fuel and oxidizer injection orifices. This occurs because the fuel-rich and oxidizer-rich gases have near equal densities resulting in near equal injection velocities which limits turbulent shear mixing. Engine pressure schedule criteria also dictate equal pressure drops. Therefore, this case was selected for analysis. Figure 22 indicates a maximum chamber length requirement of 20.3 to 22.9 cm (8 to 9 inches) to achieve a 98% ERE goal.

Similar analyses were conducted for the F-O-F triplet and premix triplet elements. The F-O-F triplet chamber length requirement is approximately 15.2 cm (six inches). The premix element impinges two rectangular fuel slots normal to the circular oxidizer element below the injector face plane. The fuel and oxidizer then mix in the orifice cup for 2 to 3 cup diameters before being injected. The premix element shows high performance requiring only 8.9 to 14 cm (3.5 to 5.5 inches) to reach the study performance goal.

The results indicate that for a given performance level, the longest and hence, heaviest chamber is required by the shear coaxial element. However, this element has the advantage of producing excellent chamber compatibility and is well modeled empirically. This would result in relatively low DDT&E cost. The triplet and premix elements require shorter and lighter chambers to achieve the performance goal but are also higher risk. Both can produce heat transfer problems; the external impinging triplet can produce chamber streaking and the premix produces relatively high injector face heat fluxes. The premix presents an additional problem for the Mode 1 engine; the 811°K (1000°F) oxidizer-rich and fuel-rich gases are nearly hypergolic, according to preliminary analysis. Any combustion in the face mixing cup would result in element development problems. An additional consideration is that for the large Mode 1 engine thrust level,

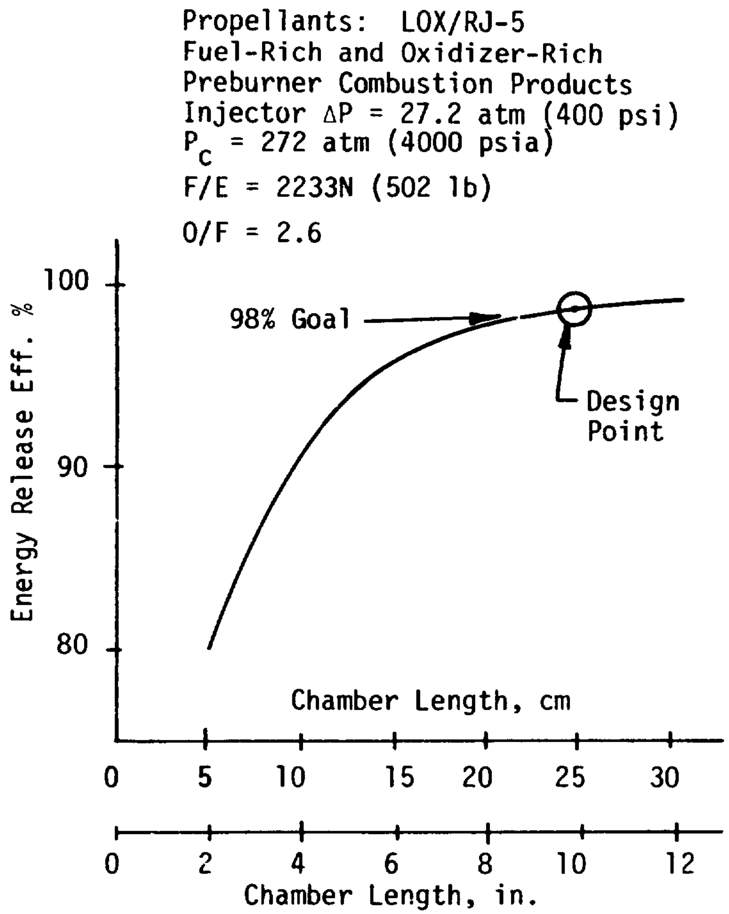

Figure 22. Shear Coaxial Element Performance

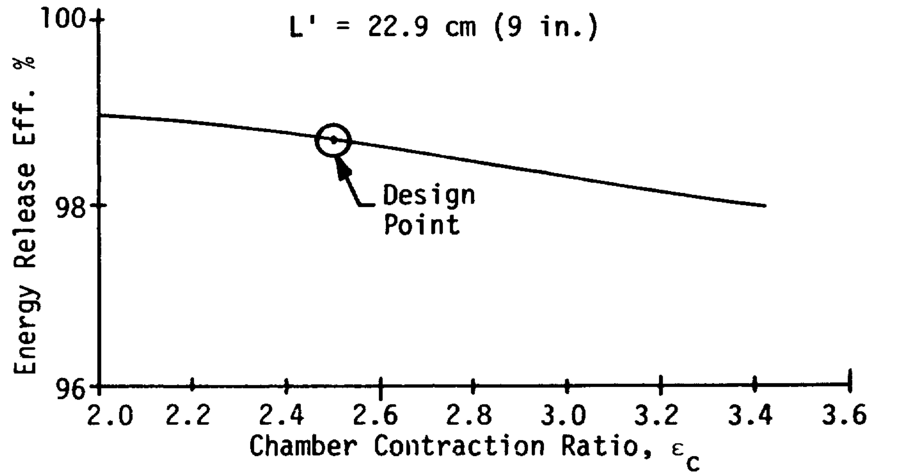

Figure 23. Effect of Chamber Contraction Ratio on Energy Release Efficiency

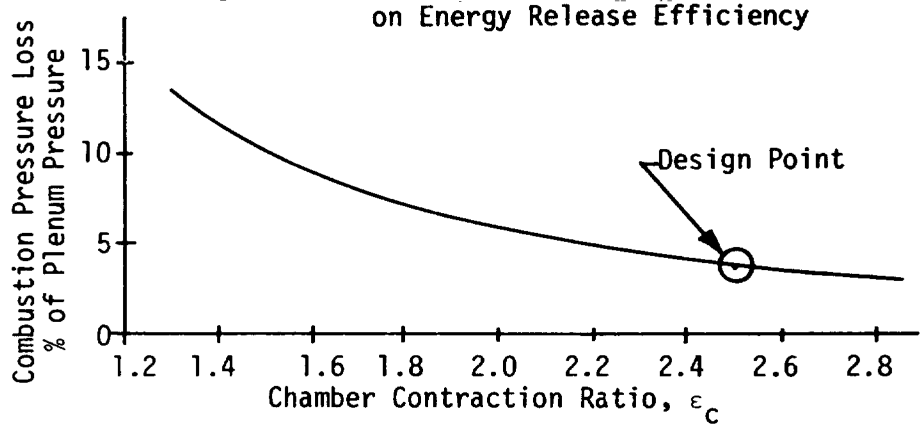

Figure 24. Effect of Chamber Contraction Ratio on Combustion Pressure Loss

the shear coaxial element would by far be the easiest element to incorporate into a non-complex manifold/pattern design. For the reasons mentioned, the shear coaxial element and associated chamber length was selected.

Figure 22 shows that the required chamber length to achieve an energy release efficiency of 98% is approximately 9". The chamber consists of a cylindrical section and a 30° convergent section. Preliminary layouts of the chamber using proper radii of curvature in the corners and at the throat results in a slight chamber length increase to 24.7 cm (9.74"). This small increase in overall length is preferred to reducing the cylindrical section length any further. Hence, for the parametric study, the chamber was split into a constant length cylindrical section and a variable length convergent section which is proportional to the throat radius. In this fashion, the convergent angle remains approximately constant.

The influences of mixture ratio, chamber contraction ratio, and chamber pressure on ERE were also determined for a fixed chamber length. Mixture ratio does not affect ERE significantly from 2.0 to 3.0:1 (the anticipated design range). Figure 23 shows that ERE increases as chamber contraction ratio (ϵ_c) decreases. The selection of the design chamber contraction ratio was tempered with the knowledge that the Rayleigh line combustion pressure loss increases sharply with decreasing contraction ratio as shown on Figure 24. A design contraction ratio value of 2.5:1 was selected to minimize the combustion pressure loss and chamber weight and to attain near maximum performance.

The TCA geometry selection process summarized herein for the LOX/RJ-5 Mode 1 baseline was repeated for the other Task II propellant combinations. The shear coaxial element was used for all engine performance studies except the hydrogen-cooled gas generator cycle which utilizes liquid/liquid TCA propellant injection. Injectors for this engine cycle must have the ability to produce finely atomized propellant sprays to maximize performance. This results in an increased chamber length requirement.

Mixture ratio selections were made on the basis of maximum delivered performance. For the Task II analyses, delivered performance was assumed to be 97% (98% ERE plus 1% for other losses) of the theoretical vacuum value. This was substantiated in later detailed analyses.

The mixture ratio selections for the various propellant combinations are based upon the delivered performance (I_S) curves shown on Figures 25, 26 and 27. Both engine and vehicle design considerations favor operating the LOX cooled engine to the "right" of the peak since this results in both more LOX for cooling and a higher bulk density. From an engine design viewpoint, it is more desirable to operate the fuel cooled engines to the "left" of the peak to increase the fuel available for cooling. This, however, results in reduced propellant bulk density. In order to avoid biasing the cooling study in favor of either the LOX or fuel cooled systems, mixture ratios were selected at the maximum specific impulse magnitudes.

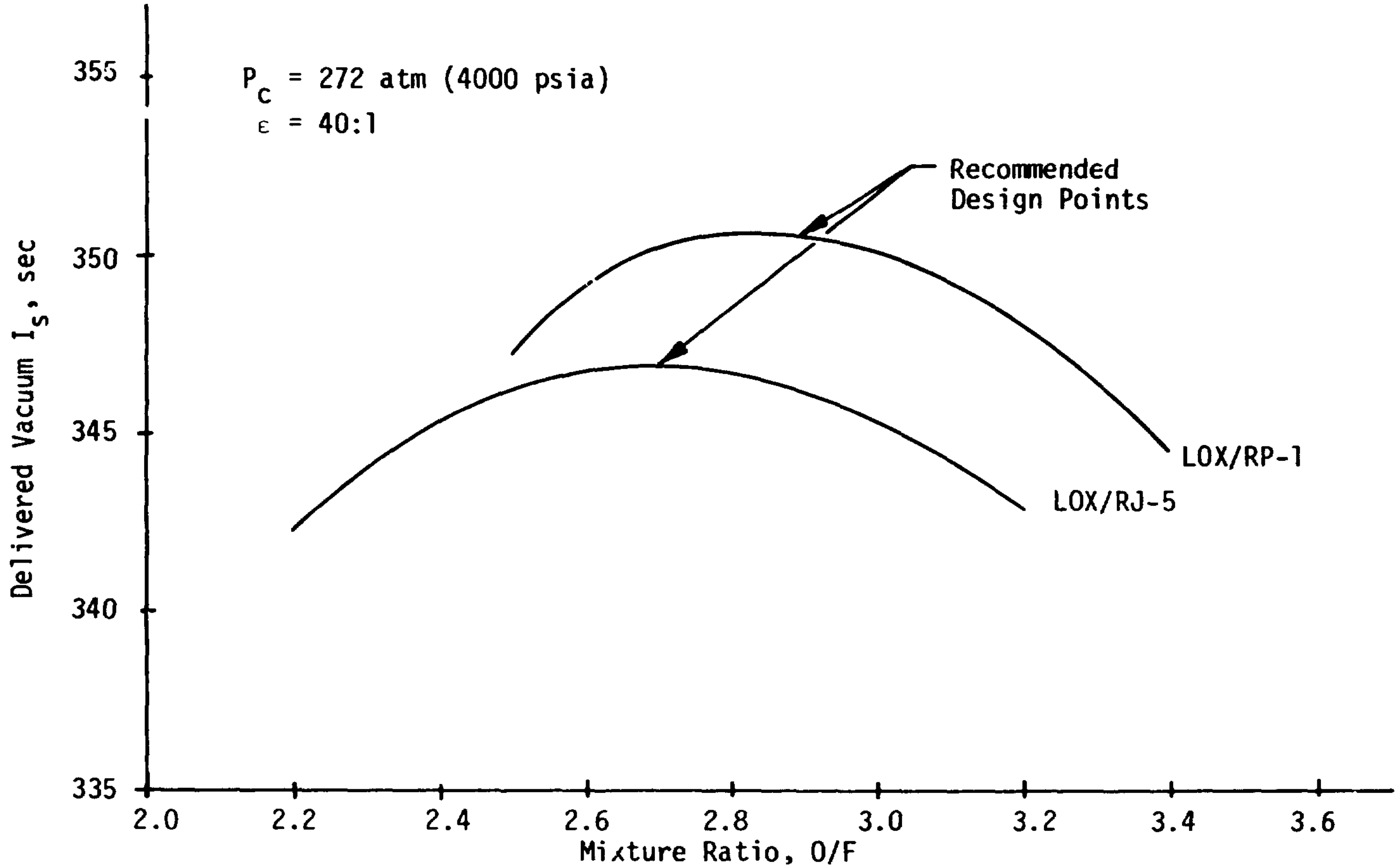

Figure 25. Task II LOX/RJ-5 and LOX/RP-1 Delivered Vacuum Performance vs Mixture Ratio

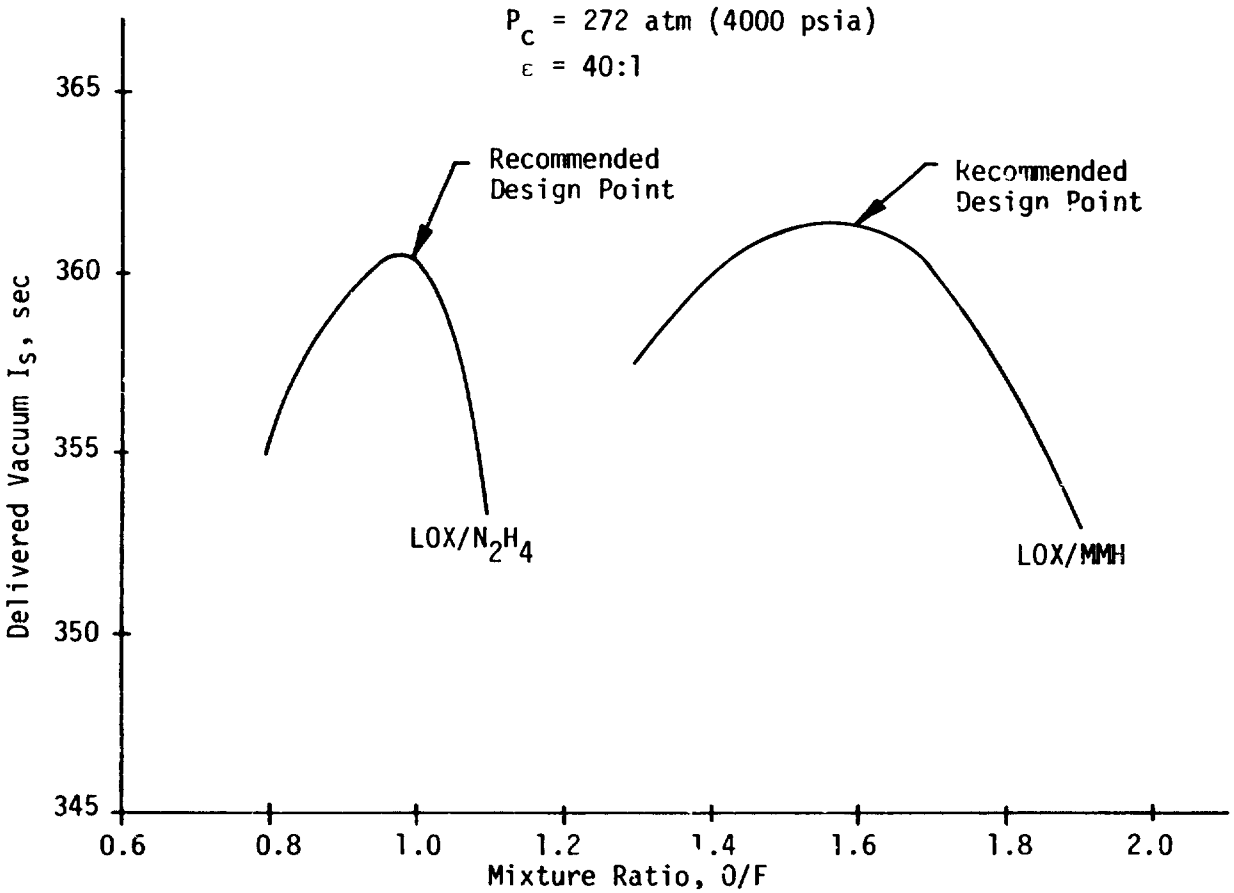

Figure 26. Task II LOX/MMH and LOX/N_2H_4 Delivered Vacuum Performance vs Mixture Ratio

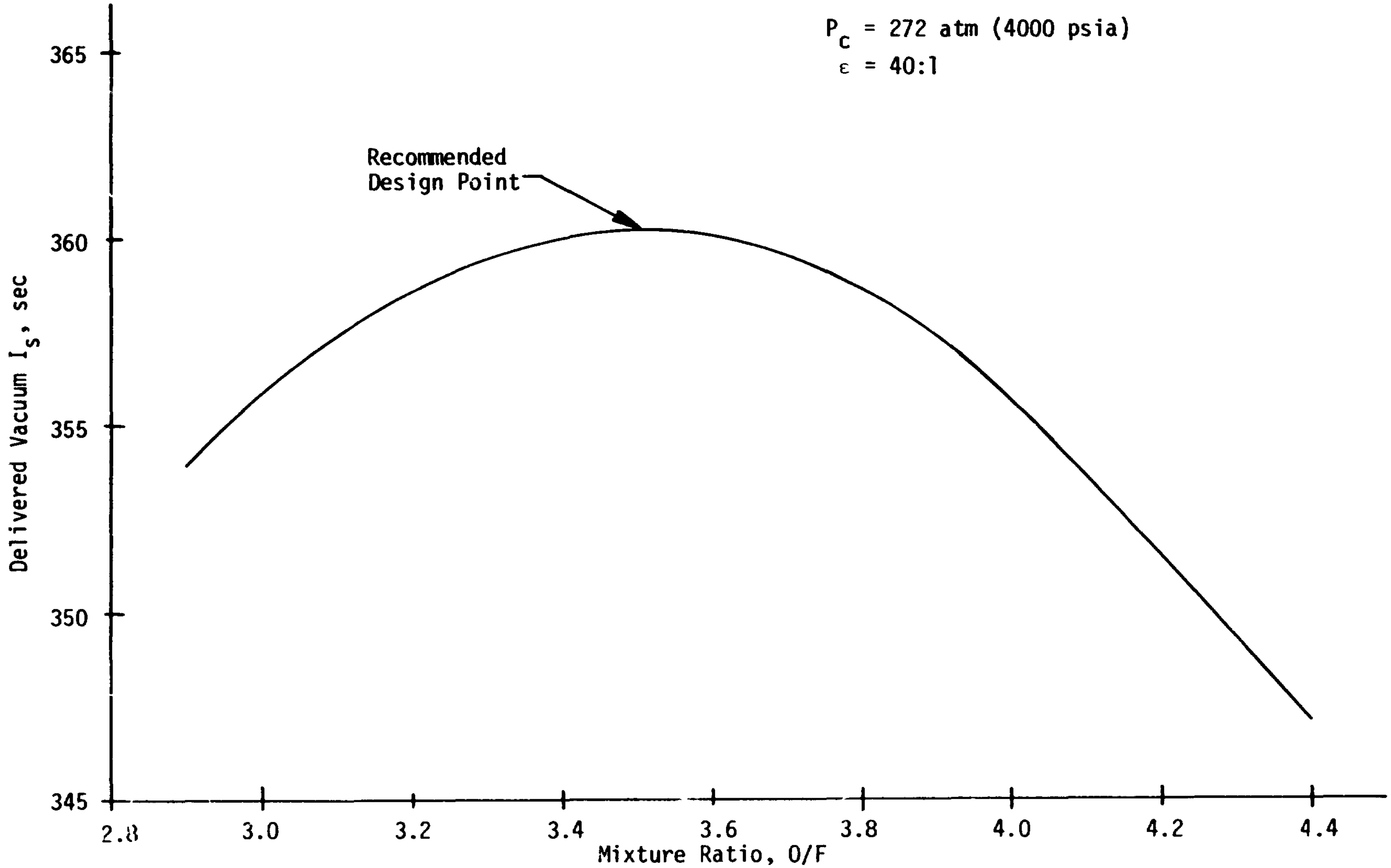

Figure 27. Task II LOX/CH_4 Delivered Vacuum Performance vs Mixture Ratio

The TCA geometry criteria and mixture ratio selections are summarized on Table XXXIV.

C. LOW CYCLE FATIGUE ANALYSIS

Low cycle thrust chamber thermal fatigue analyses were conducted in conjunction with the coolant heat transfer evaluation to establish the chamber pressure upper limit, if any, created by the chamber life requirement.

Past experience has shown that the throat region is the most critical area from a fatigue life standpoint. Therefore, analyses to determine the maximum allowable wall temperature for a design chamber life of 1000 cycles (250 cycles times a safety factor of four) were concentrated at a section through the chamber throat. The properties of chamber material, ZRCu (zirconium copper), are shown on Figures 18 through 21.

The initial analysis was conducted for the LOX/RJ-5 baseline engine at a chamber pressure of 272 atm (4000 psia). An approximate channel cross-section was selected and the pressures and temperature estimated. The stress and strain were calculated along with estimates of creep damage and cycle life. The assumed channel geometry was then modified until a satisfactory design was achieved. The thermal gradients were defined by the heat transfer analysis and a plane strain finite element model was constructed. Maximum effective strains were determined for thermal gradients and compared to the cycle life data for ZRCu. From these comparisons, the expected cycle life was established. This procedure was repeated for the other chamber pressures, 136-340 atm (2000-5000 psia) and the other study propellant combinations.

The results of the low cycle fatigue analyses are summarized on Figure 28 for the baseline LOX/RJ-5 engine at 272 atm (4000 psia). This figure shows the maximum permissible temperature difference between the hot gas side wall surface and the propellant bulk temperature (essentially the backside wall temperature) for a variation in cycle life. For a design cycle life requirement of 1000 cycles, the maximum ΔT is 867°K (1100°F). In order to contain the high pressure involved, the structural closeout would have to be approximately 0.762 cm (0.30 in.) thick. The recommended closeout material is nickel.

Further calculations at a chamber pressure of 340 atm (5000 psia) revealed that the maximum effective strain was only minimally affected. Therefore, Figure 28 was considered to be valid for the chamber pressure parametric analyses. The limiting temperature differential criteria was also found to be valid for the other propellant combinations considered parametrically in the Task II thermal analysis.

TABLE XXXIV. - TASK II MODE 1 ENGINE GEOMETRY AND MIXTURE RATIO SELECTION SUMMARY

F_{SL} = 2.7 mn (607,000 lb)

Propellant Combination	Engine Cycle	O/F	Chamber Contraction Ratio	Main Propellant Injection	L' cm	L' (Inches)
LOX/RJ-5	Stg. Comb.	2.7	2.5	Gas-Gas	7.62+1.303 R_t	(3+1.303 R_t)
LOX/RP-1	Stg. Comb.	2.9	2.5	Gas-Gas	7.62+1.303 R_t	(3+1.303 R_t)
LOX/MMH	Stg. Comb.	1.6	2.5	Gas-Gas	7.62+1.303 R_t	(3+1.303 R_t)
LOX/N_2H_4	Stg. Comb.	1.0	2.5	Gas-Gas	7.62+1.303 R_t	(3+1.303 R_t)
LOX/CH_4	Stg. Comb.	3.5	2.5	Gas-Gas	7.62+1.303 R_t	(3+1.303 R_t)
LOX/RJ-5	Gas Gen.	2.7	2.5	Liquid-Liquid	30.5+1.303 R_t	(12+1.303 R_t)

L' = Chamber Length = Cylindrical Length + Conical Section Length

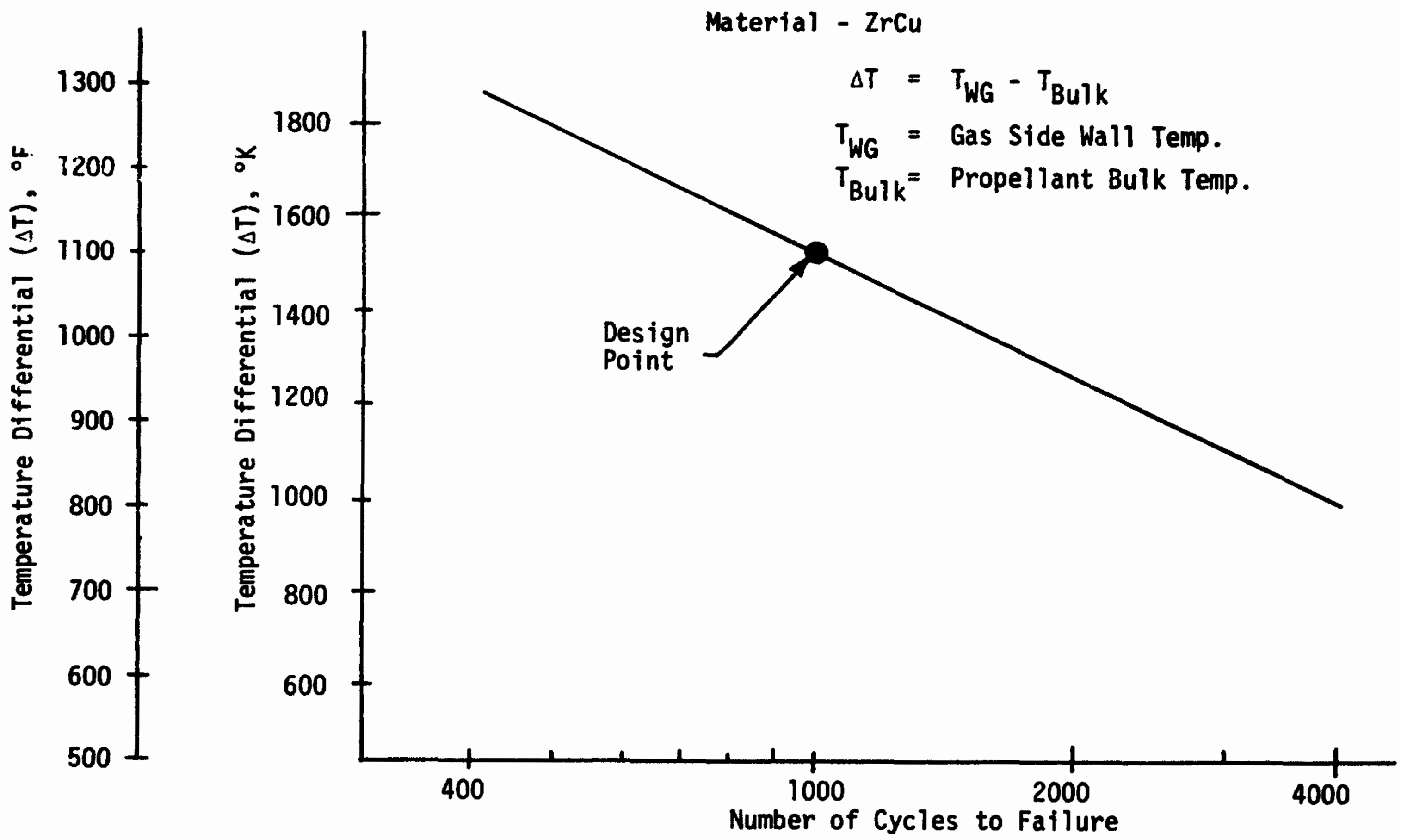

Figure 28. Low Cycle Fatigue Life Requirement

D. THERMAL ANALYSIS

Detailed chamber designs were developed for the following combinations of coolant and chamber pressure:

Coolant	Pressure Atm.	(PSIA)
Oxygen	136, 204, 272, 340	(2000, 3000, 4000, 5000)
Hydrogen (S.C. Cycle)	136, 238, 340	(2000, 3500, 5000)
Hydrogen (G.G. Cycle)	238	(3500)
Hydrazine	136, 238, 340	(2000, 3500, 5000)
MMH	136, 238, 340	(2000, 3500, 5000)
Methane	136, 272, 340	(2000, 4000, 5000)

The chamber geometry and operating mixture ratios were established as described previously in this section.

Results for the hydrogen-cooled gas generator cycle at chamber pressures other than 3500 psia were obtained by scaling the 3500 psia data based on the corresponding staged combustion cycle results.

All designs are based on straddle-mill machining with a constant land width of 1.02 mm (0.040 in.) Based on channel optimization studies for oxygen cooling, the 4:1 channel depth/width limit of the guidelines was applied in the throat region. Therefore, applying the thermal design criteria for each concept to the throat region determined the number of channels, and applying them elsewhere determined the local channel depth. The design criteria which controlled the various concepts are summarized in Table XXXV. Plane strain finite element analyses by the indicated cycle life criterion, could be satisfied by limiting the local difference between the maximum gas-side wall temperature and the essentially uniform external wall temperature to 867°K (1100°F). The 589°K (600°F) coking limit on coolant-side wall temperature prevented the development of practical designs with RJ-5 or RP-1 cooling.

TABLE XXXV. - TASK II CHAMBER DESIGN LIMITS

Coolant	Criteria
Oxygen and CH_4	$\Delta T_w \leq 867°K$ (1100°F) Cycle Life
Hydrogen	$\Delta T_w \leq 867°K$ (1100°F) Cycle Life
	$T_{wg} \leq 867°K$ (1100°F) Strength
RJ-5, RP-1	$T_{wc} \leq 589°K$ (600°F) Coking
MMH, N_2H_4	$T_{wc} \leq 644°K$ (700°F) Coolant Critical Temperature

ΔT_w = Wall temperature differential

T_{wg} = Gas-side wall temperature

T_{wc} = Coolant side wall temperature

1. Chamber Wall Construction

Although tubes could be used to save weight in the low heat flux part of the nozzle, rectangular channel construction was assumed throughout to simplify the Task II analyses. A design was selected which is practical to fabricate yet provides the flow area variation desired for efficient cooling within the channel depth/width constraint of 4:1. Straddle-mill machining, which yields a constant land width, is used except in the aft end where constant width channels are proposed. The number of channels is doubled when the channel width becomes too large from a structural standpoint. For this task, this point was selected at an area ratio of 7.6:1. Straddle milling would be terminated when the channel width again becomes too large, or else at the point where straddle milling cannot form the entire channel. However, to simplify this analyses, a constant land width was used over the entire length.

A land width of 1.02 mm (0.040 in.) was selected for all designs along with the minimum specified gas-side wall thickness of 0.635 mm (0.025 in.) per the study guidelines and an external wall thickness of 1.52 mm (0.060 in.) Channel optimization studies with oxygen cooling indicated there was a relatively small advantage in going to the minimum specified land width of 0.762 mm (0.030 in.). Structural analyses indicate a much thicker external wall is required, but it is likely this wall would be made of a lower conductivity material such as nickel. In that case, the conductance of the external wall might be less than assumed herein; however, this change would have no effect on the designs with oxygen, hydrazine, methane, and MMH cooling and only a small effect on the hydrogen-cooled designs.

The channel geometry parameters which remained to be determined for each design were the number of channels and the channel depth axial profile. With the land width fixed and the channel depth limited to four times the channel width, the maximum local coolant flow area was set by the number of channels. Channel optimization studies with oxygen cooling indicated that it was desirable to design at the channel depth/width limit of four. However, this could be accomplished at only one axial position. At other locations it was necessary to satisfy the thermal design criteria with lower depth/width ratios or to overcool, i.e., not reach the applicable wall temperature limits. In order to avoid overcooling in high flux regions, the number of channels in each design was set by satisfying the design criteria at the throat with a channel depth/width ratio close to four. Lower ratios then resulted from satisfying the design criteria between the throat and the injector end. The resultant number of channels for each design is given in Table XXXVI.

In all designs the coolant enters at area ratio 1.5:1, flows through the throat region to the injector end and then through the nozzle from 1.5:1 to 40:1. Straight-through flow paths from each end were investigated for oxygen cooling but required much higher pressure drops. All pressure drop calculations were based on a surface roughness of .002 mm (80 microinches.)

TABLE XXXVI. - NUMBER OF COOLANT CHANNELS IN COMBUSTION CHAMBER*

	Chamber Pressure, atm (psia)				
Coolant	136 (2000)	204 (3000)	238 (3500)	272 (4000)	340 (5000)
Oxygen	250	260		260	260
Hydrogen (S.C. Cycle) (Parallel Burn)	450		450		425
Hydrogen (G.G. Cycle)			425		
Hydrazine	280		250		230
MMH	400		350		330
Methane	270			270	270

*The number of channels is doubled in the nozzle at area ratio 7.6:1

2. Methods of Analysis

Design data presented herein were generated with a regenerative-cooling program similar to the computer program supplied to NASA-Lewis under Contract NAS3-17813 (Ref. 45). Two-dimensional conduction effects and the spatial variation of the coolant heat transfer coefficient were simulated in this program. A program option represents the not wall, the land and that part of the external wall adjacent to the channel as fins. That part of the external wall adjacent to the land is assumed to be isothermal. The land fin can be split into two segments with different coolant heat transfer coefficients. One coefficient is applied to the hot wall and the first part of the land fins. The other coefficient is applied to the rest of the land fin and the external wall fin. The interface between segments of the land fin corresponds to a specified coolant-side wall temperature.

A limited number of two-dimensional mode network analyses were performed at the maximum heat flux location near the throat. These studies accomplished the following:

- Provided detailed temperature distributions for the cycle life analysis.

- Provided the basis for determining the computer model simulation parameters for oxygen methane and hydrogen cooling.

- Established the optimum channel geometry for a fixed coolant flow area with oxygen cooling.

- Defined local coolant velocity requirements for RJ-5 and RP-1 cooling.

- Determined the accuracy of the computer model for MMH and hydrazine cooling.

Gas side heat transfer was handled in the following manner. A two-dimensional nozzle expansion analysis and a TRAN 72 computer program (Ref. 42) calculation were used to determine pertinent parameters at the edge of the wall boundary layer for LOX/RJ-5. Parameters established were; (1) the ratio of two-dimensional to one-dimensional mass velocities, (2) the ratio of static to stagnation temperatures and, (3) the ratio of adiabatic wall to stagnation temperatures. A recovery factor equal to the 1/3 power of the Prandtl number was used in this analysis. All ratios determined were assumed to apply to the other propellant combinations under investigation. All combustion product properties were evaluated using the TRAN 72 computer program.

Maximum heat flux occurs slightly upstream of the throat. Heat transfer from the combustion products to the chamber wall was calculated as:

$$\phi = 0.026\, C_g\, \rho_f\, u_e\, Re_f^{-0.2}\, Pr_f^{-0.6}\, C_{p_f}\, (Taw\text{-}Twg) \qquad (9)$$

where:

$$\rho_f = \rho_e \left(\frac{T_e}{T_f}\right) \qquad (10)$$

$$Re_f = \rho_f\, u_e\, D/\mu_f \qquad (11)$$

$$T_f = 0.5\, (Taw\text{-}Twg) \qquad (12)$$

The coefficient C_g accounts for flow acceleration effects. Nomenclature is as follows:

- English Letters

  C_g gas-side heat transfer correlation coefficient

  c_p specific heat; $\overline{C}_p$ is an integrated average between the coolant bulk temperature and the wall temperature

  D Local chamber diameter

  Pr Prandtl number

  Re Reynolds number

  T temperature

  u Axial velocity

- Greek Letters

  μ viscosity

  ρ density

  ϕ gas-side heat flux

- Subscripts

  aw adiabatic wall

  e freestream

  f film temperature

  wg gas-side wall surface

3. Oxygen Cooling

A recently developed ALRC correlation (Ref. 46) for supercritical oxygen was used. This correlation yields heat transfer coefficients which are sensitive to bulk temperature, wall temperature and pressure.

Oxygen properties for temperatures below 333°K (600°R) were taken from NBS data (Refs. 1 and 3), and extrapolations of this data. Russian data, (Ref. 47), for density, specific heat and enthalpy were used for temperatures above 333°K (600°R). Transport properties for this temperature range were taken from ALRC predictions for pressures up to 340 atm (5000 psia). A table of these values is included in Ref. 46. Extrapolation to higher pressures was based on the dense gas correlations of Ref. 1 with the dilute gas contribution inferred from the properties at 340 atm (5000 psia).

A channel optimization study was conducted early in the Task II effort to define the channel geometry which minimizes the local gas-side wall temperature for a fixed coolant velocity. This study assumed a local throat static pressure of 204 atm (3000 psia), a bulk temperature of 153°K (275°R) and a total flow area of 35.9 cm^2 (5.56 $in.^2$). These assumptions give an oxygen velocity of 198 m/sec (650 ft/sec) and a heat tranfer coefficient which varies with wall temperature as shown in Figure 29. Because the heat transfer coefficient is much higher at low wall temperatures, the land is a very effective fin and maximum wall temperatures occurred at the channel centerline. Two-dimensional network analyses with a hot wall thickness of 0.762 mm (0.030 in.) were used for this study. The optimum configuration is that with minimum channel width, which is defined by the land width and channel depth/width constraints. The results showed that the channel depth affects the maximum wall temperature much less than channel width, so the advantage in reducing the land width comes primarily from the channel width reduction allowed. Use of a 1.02 mm (0.040 in.) land in the analysis, instead of the 7.62 mm (0.030 in.) minimum guideline, results in a 278°K (40°F) higher optimum wall temperature.

Determination of the simulation parameters in the simplified Ref. 45 computer model was also based on the coolant conditions assumed above, but with a somewhat lower coolant velocity and the hot wall thickness reduced to 0.635 mm (0.025 in.). Due to wall temperature dependence shown on Figure 29, the coolant heat transfer coefficient varies by more than factor or two. It was found that the maximum temperature of the two dimensional analyses is matched by the simplified analysis by: (1) using a coefficient on the hot wall which is 11 percent greater than that calculated from the centerline wall temperature and (2) evaluating the coefficient for the external wall and the entire land with a wall temperature equal to the bulk temperature.

Channel depths from the injector end through the throat were determined by the cycle life criterion and varied from about 6.35 mm (0.25 in.) at the injector face to 7.62 mm (0.30 in.) at the throat to 25.4 mm (1.0 in.) at the exit. Note that with the straddle-mill design selected

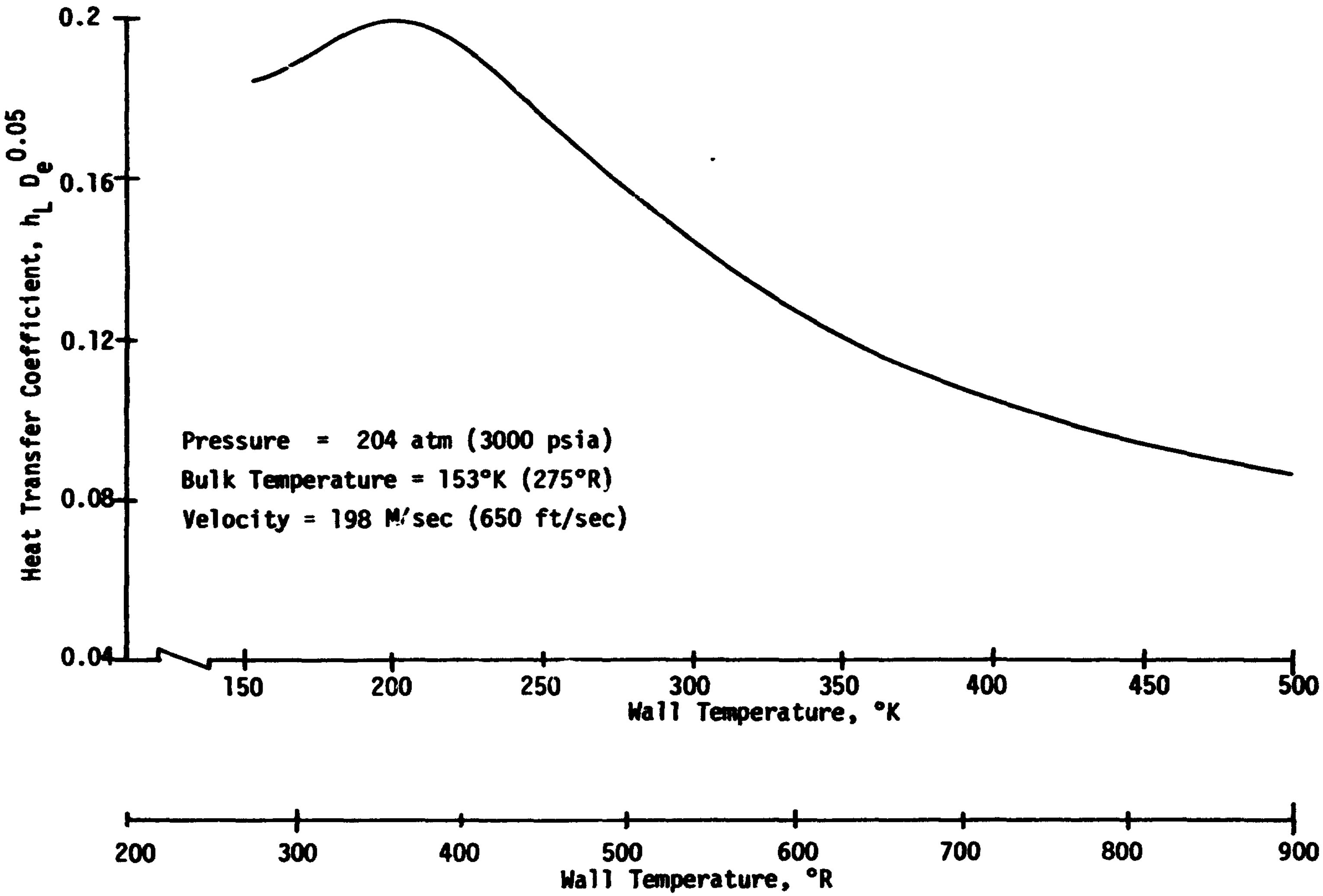

Figure 29. Oxygen Heat Transfer Coefficient Variation with Wall Temperature

herein, the channel depth does not have to change significantly from the injector through the throat.

Figure 30 shows the required oxygen pressure drop as a function of chamber pressure.

4. Hydrogen Cooling

Two hydrogen cooling concepts were investigated: the parallel burn, staged-combustion cycle and the gas generator cycle. The latter requires a 22.9 cm (9 in.) longer combustion chamber to accommodate high density liquid propellant injection. Coolant heat transfer coefficients were based on the Hess and Kunz correlation (Ref. 48), and the flow path was the same as in the oxygen-cooled design. The simplified computer model provided excellent simulation of two-dimensional conduction analyses using a coolant coefficient variation similar to that for oxygen, but with the hot wall coefficient equal to (rather than 11 percent greater than) that for the centerline wall temperature.

Local wall temperature differentials were again limited to 867°K (1100°F) to satisfy the cycle life criterion. In addition, local maximum wall temperatures were limited to 867°K (1100°F) in view of the significant structural property degradation above this value. This consideration restricts the coolant bulk temperature rise in order to cool the nozzle without excessive pressure drop, and thus sets the minimum coolant flow rate.

Detailed design studies were conducted with hydrogen flow rates of 6.35 and 9.07 kg/sec (14 and 20 lb/sec) for the parallel burn, staged combustion and gas generator cycles, respectively. These flow rates were chosen from preliminary heat transfer and cycle balance analyses. Coolant flow rates did not vary with chamber pressure, since the total heat load variation is small. Resultant required pressure drops are plotted in Figure 31. A staged combustion cycle flow rate is 7.26 kg/sec (16 lb/sec) would give bulk temperature rises comparable to the gas generator cycle values and significantly reduce nozzle pressure losses at low chamber pressures. However, since pressure drops are so low in general with hydrogen cooling, studies of pressure drop vs. flow rate for this cycle were not undertaken since they would not materially affect the study results.

5. RP-1 and RJ-5 Cooling

Cooling with RJ-5 or RP-1 was found to be impractical based on limiting coolant-side wall temperatures to 589°K (600°F) in order to prevent significant coking. Two-dimensional conduction network analyses in the throat region determined the maximum coolant velocities required for a chamber pressure of 136 atm (2000 psia) based on the Hines correlation (Ref. 49), RP-1 is the better coolant, but still required a

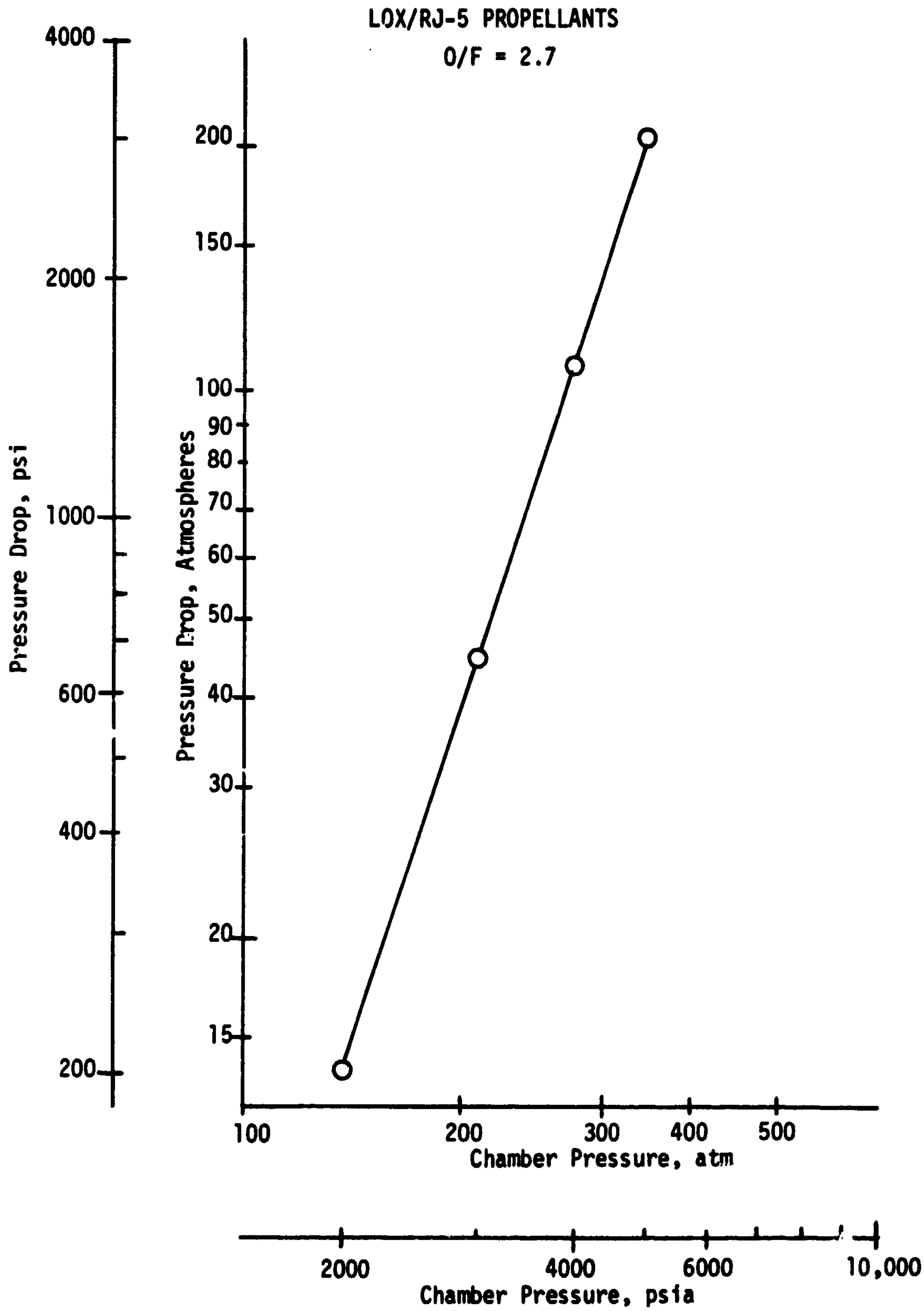

Figure 30. Coolant Pressure Drop with Oxygen Cooling

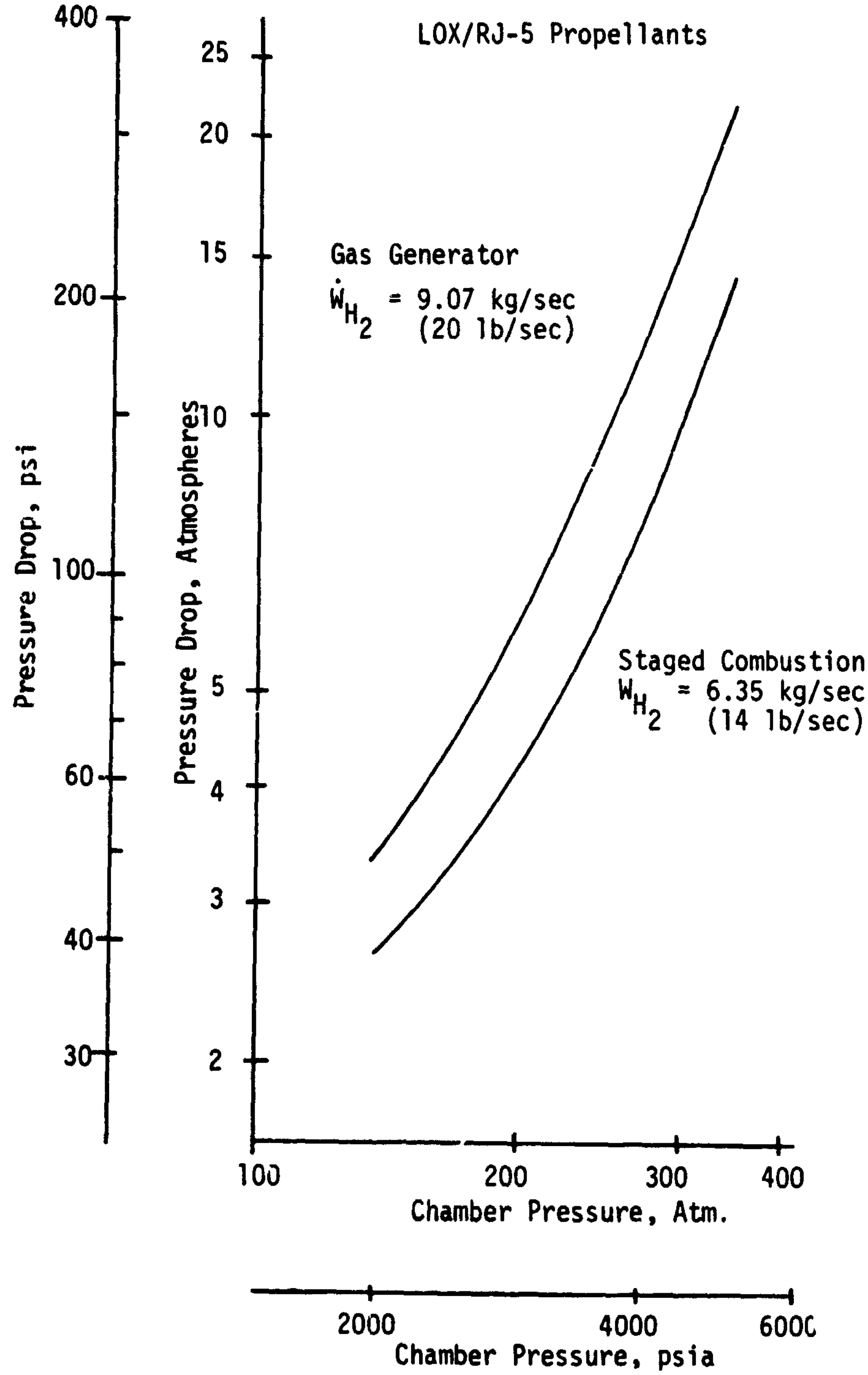

Figure 31. Coolant Pressure Drop with Hydrogen Cooling

velocity of 175 m/sec (575 ft/sec). The resultant dynamic head and friction losses preclude maintaining positive static pressures.

6. Hydrazine and MMH Cooling

Design studies for the hydrazine and MMH systems were based on limiting the coolant-side wall temperature to 644°K (700°F). Supercritical MMH tests reported in Ref. 50 indicate significant reductions in heat transfer coefficient for wall temperatures above 644°K (700°F). These and other tests with storable supercritical fluids indicate that standard bulk temperature correlations, e.g., the Hines correlation used herein, are applicable until the wall temperature reaches the critical temperature. Since no data are available for supercritical hydrazine, the limiting wall temperature was set just below the critical temperature, 653°K (716°F). Resulting outlet temperatures for MMH are well below the decomposition temperatures observed with most wall materials. However, the hydrazine outlet temperatures are at the threshold sensitivity temperatures observed with liquid/vapor samples subjected to adiabatic compression. It should be noted that adding a small amount of MMH to hydrazine increases this threshold temperature significantly. Figure 32 shows the pressure drops required for chamber cooling with MMH and hydrazine. Hydrazine pressure drops are reasonable, but MMH pressure drops are high. ZrCu was assumed as the chamber material throughout these studies in accordance with the guidelines. However, materials investigations show that uncoated ZrCu is incompatible with both MMH and N_2H_4 at temperatures above 330°K (140°F) for long term use and may not be feasible for even short term use.

7. Methane Cooling

The supercritical oxygen correlation (Ref. 46) developed at ALRC in 1975 was used to predict the heat transfer coefficients for the supercritical methane coolant. In addition, a CLF-5 supercritical correlation which is also described in Ref. 46 was used as a cross reference. The CLF-5 correlation does not contain a pressure factor which reduces the heat transfer coefficient at pressures above 212 atm (3120 psia) as the oxygen correlation does. Thus, it resulted in higher coefficients and lower cooling requirements. The oxygen correlation was chosen because no supercritical methane correlation could be located, and the oxygen data approached the same pressure range as the methane coolant pressures studied.

The coolant flow path and channel construction assumptions were identical to those previously described, and resulted in the selection of 270 channels for the combustion chamber.

The required coolant jacket pressure drop as a function of chamber pressure using methane as a coolant is shown on Figure 33.

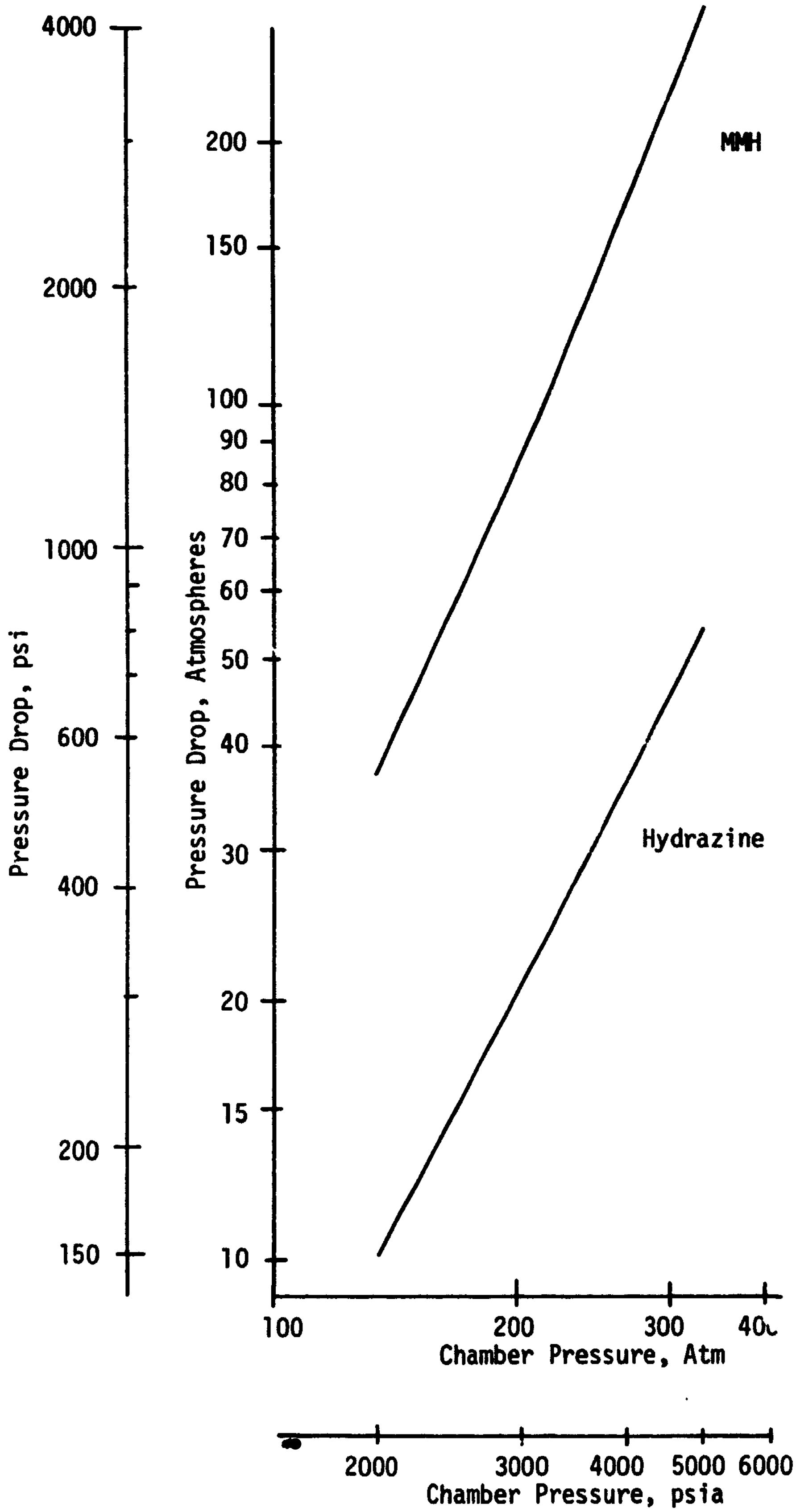

Figure 32. Coolant Pressure Drop with Hydrazine Compounds

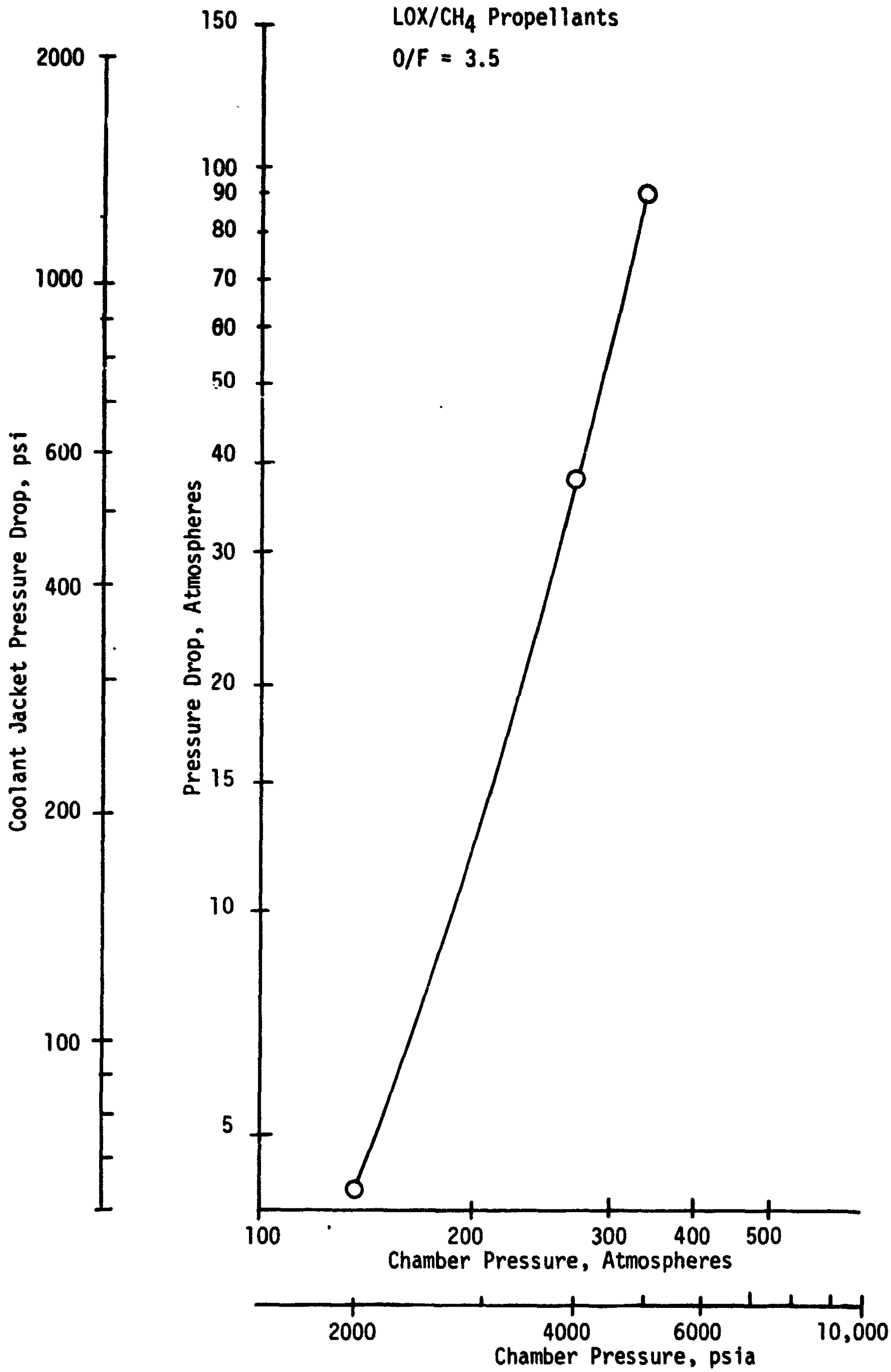

Figure 33. Coolant Pressure Drop with Methane Cooling

8. Summary of Results and Conclusions

Coolant jacket pressure drops, coolant bulk temperature rises and outlet temperatures resulting from this study are summarized on Table XXXVII.

Based upon the results of this task, the following conclusions were reached:

- Hydrocarbon fuels such as RJ-5 and RP-1 are not practical coolants for high pressure application due to the low wall temperature which must be maintained to prevent significant coking.

- Oxygen cooling is feasible for chamber pressures up to at least 272 atm (4000 psia).

- Hydrogen cooling requires the smallest pressure drop and is practical for chamber pressures beyond 340 atm (5000 psia). Flow rates as low as 7.26 kg/sec (16 lb/sec) for the staged combustion cycle and 9.07 kg/sec (20 lb/sec) for the gas generator cycle are sufficient.

- Cooling with MMH requires the highest pressure drop, but is feasible providing that the copper can be coated with a compatible material which does not significantly alter the conductivity of the chamber walls.

- Cooling with hydrazine is feasible from a pressure drop standpoint for chamber pressure beyond 340 atm (5000 psia) but coolant bulk temperatures are close to the adiabatic compression sensitivity threshold. Addition of a small amount of MMH would provide a much more stable mixture and should retain much of the heat transfer advantage of hydrazine.

- Use of methane as a regenerative coolant is feasible for thrust chamber pressures beyond 340 atm (5000 psia).

TABLE XXXVII. - TASK II COOLANT EVALUATION SUMMARY

Chamber Pressure = 272 atm (4000 psia)
Coolant Inlet Pressure = 612 atm (9000 psia)

Coolant	Pressure Drop, Atm	(psi)	Inlet Temp, °K	(°F)	Bulk Temp Rise, °K	(°F)	Outlet Temp, °K	(°F)	Flow Rate, kg/sec	(lb/sec)
O_2	106	(1560)	111	(-260)	329	(132)	184	(-128)	626	(1379)
MMH	167	(2450)	311	(100)	335	(143)	391	(243)	317	(698)
N_2H_4	37	(540)	311	(100)	311	(100)	367	(200*)	413	(910)
RP-1			IMPRACTICAL AT $P_c \geq$ 136 ATM (2000 PSIA)							
RJ-5			IMPRACTICAL AT $P_c \geq$ 136 ATM (2000 PSIA)							
H_2 (Parallel Burn)	8.2	(120)	61	(-350)	968	(1282)	773	(932)	6.35	(14)
H_2 (G.G. Cycle)	12.6	(185)	61	(-350)	872	(1110)	678	(760)	9.07	(20)
CH_4	38	(560)	144	(-200)	416	(288)	304	(88)	184	(405)

*Explosive Decomposition Threshold Temp.

SECTION V

TASK III CYCLE EVALUATION

A. OBJECTIVES AND GUIDELINES

The objectives of this task were to determine engine cycle pressures, temperatures and delivered performance for the candidate Mode 1 engines. Each candidate was evaluated over a chamber pressure range of 136 to 340 atm (2000 to 5000 psia) or at the maximum value corresponding to a cycle power balance, thrust chamber cooling or propellant property limit.

Candidate engine concepts considered were:

Propellant Combination	Coolant	Reference Schematic
RJ-5/Oxygen	Oxygen	Figure 34
RJ-5/Oxygen	RJ-5	Figure 35
RJ-5/Oxygen (Parallel Burn)	Hydrogen	Figure 36
RJ-5/Oxygen (Gas Gen Cycle)	Hydrogen	Figure 37
RP-1/Oxygen	RP-1	Figure 35
Hydrazine/Oxygen	Hydrazine	Figure 35
MMH/Oxygen	MMH	Figure 35
CH_4/Oxygen	CH_4	Figure 35
RJ-5 & LH_2/Oxygen	Oxygen	Figure 38

The engine cycle power balances were performed at a sea-level thrust of 2.70 MN (607,000 lb), with the engine mixture ratios and coolant jacket pressure drops as determined in Task II. Engine performance data were evaluated for a combustion efficiency of 98%. Additional study guidelines are presented on Tables XXXVIII, XXXIX and XL and below.

- System Pressure Losses ($\Delta P/P$ upstream)
  - Injectors:
    - Liquid - 15% min.
    - Gas - 8% min.
  - Valves:
    - Shutoff - 1%
    - Liquid Control - 5% min.
    - Gas Control 10% min.
- Boost Pump Drive Requirements not Considered
- Main Pump Suction Specific Speed = 20,000

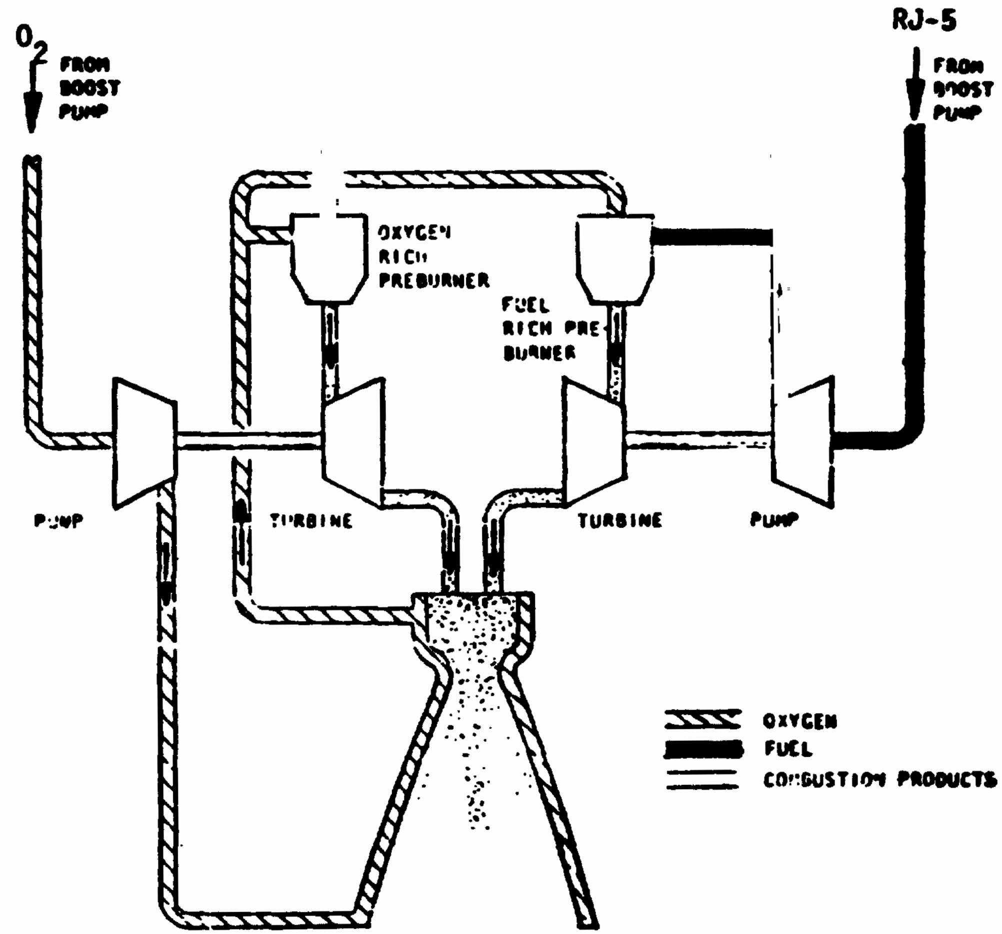

Figure 34. Task III Mode 1 Oxygen Cooled Engine Cycle Schematic

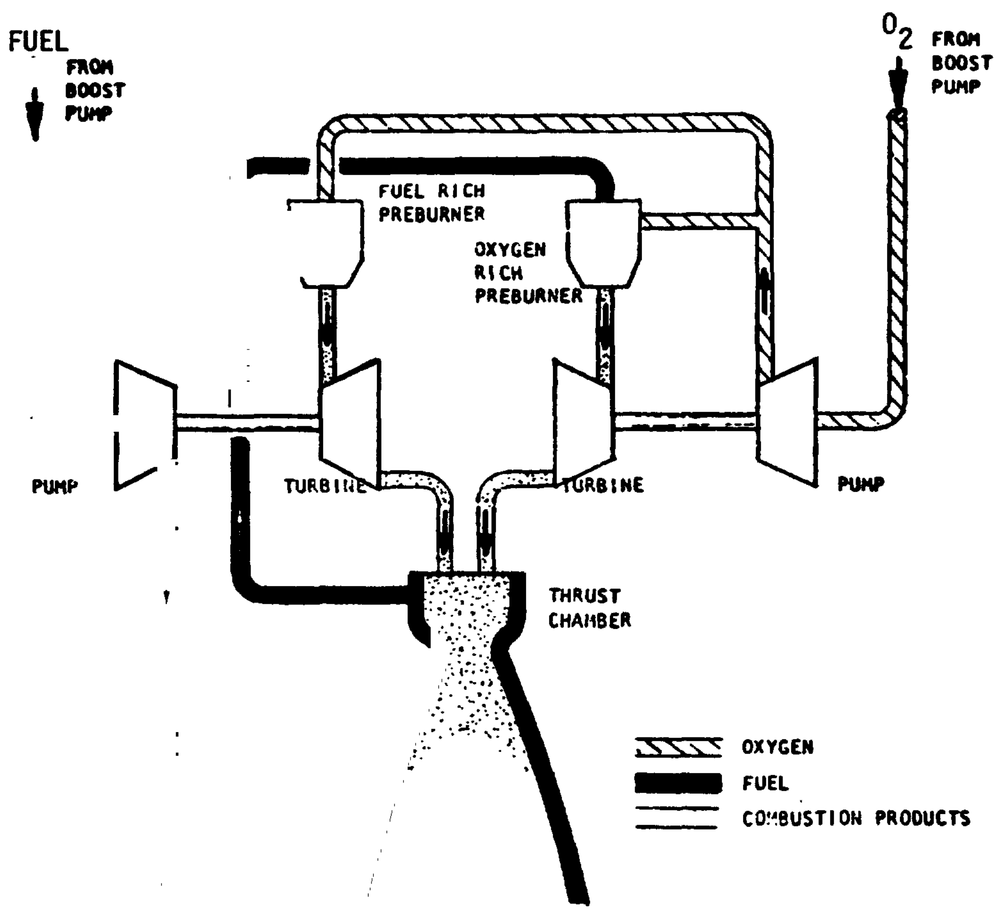

Figure 35. Task III Mode 1 Fuel Cooled Engine Cycle Schematic

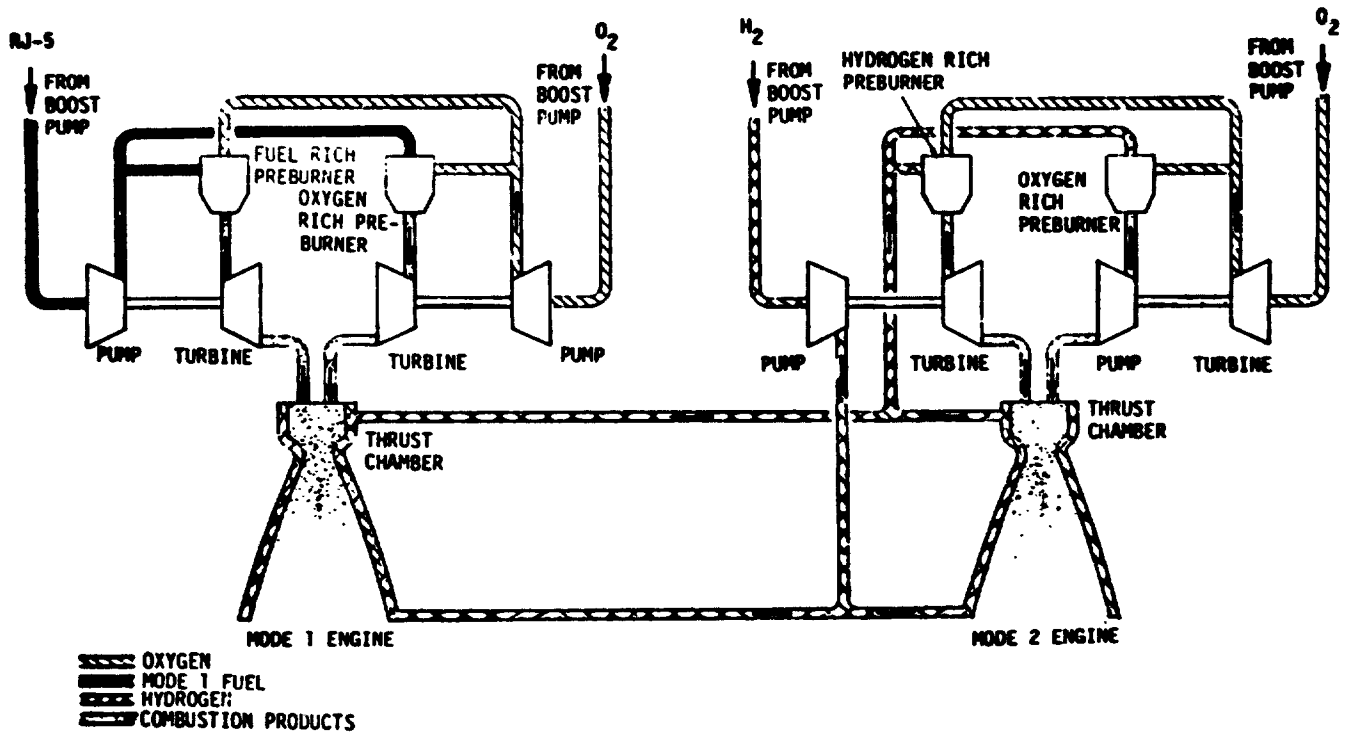

Figure 36. Task III Parallel Burn, Hydrogen Cooled Mode 1 Engine Cycle Schematic

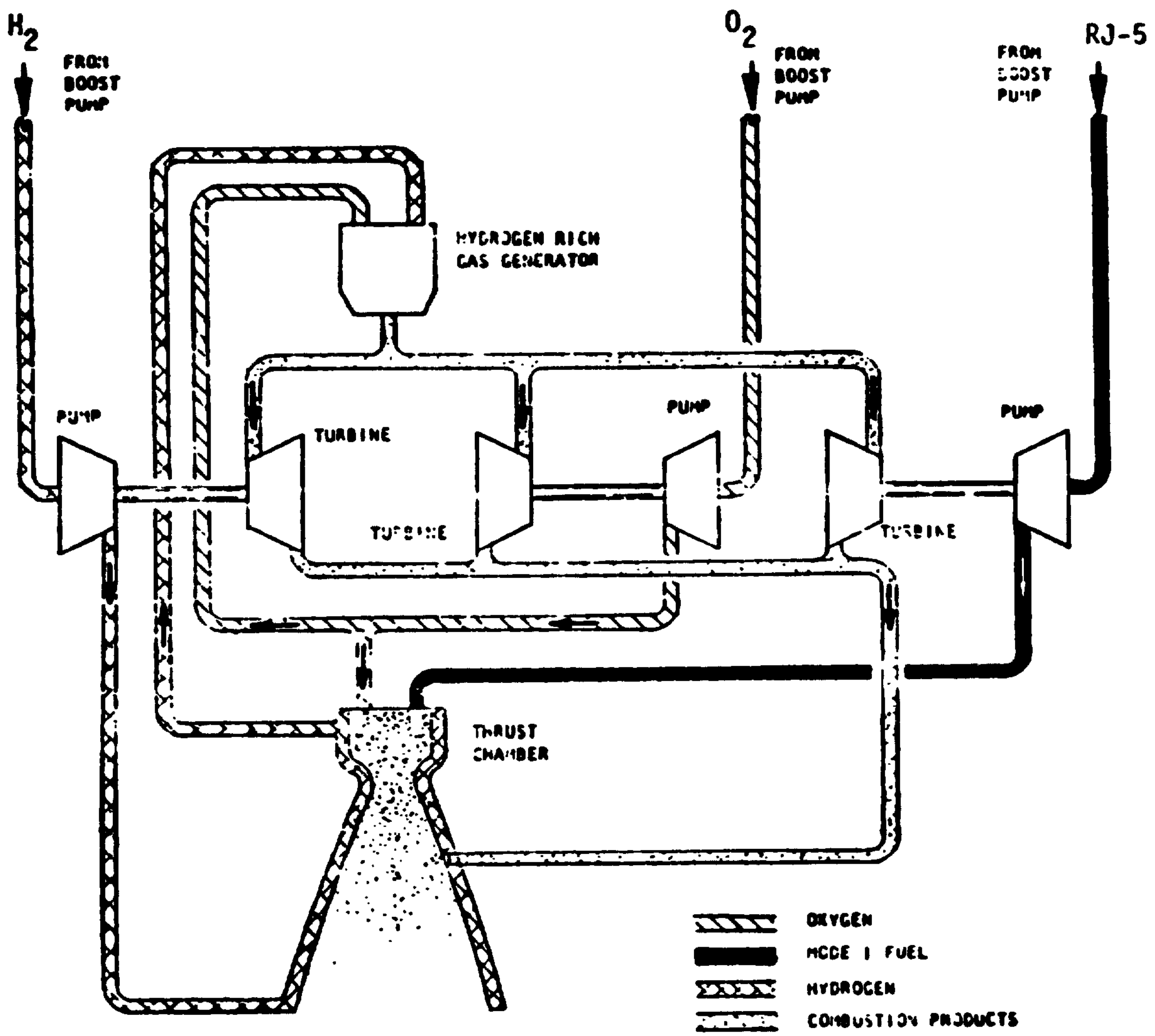

Figure 37. Task III Mode 1 Hydrogen Cooled Gas Generator Cycle Schematic

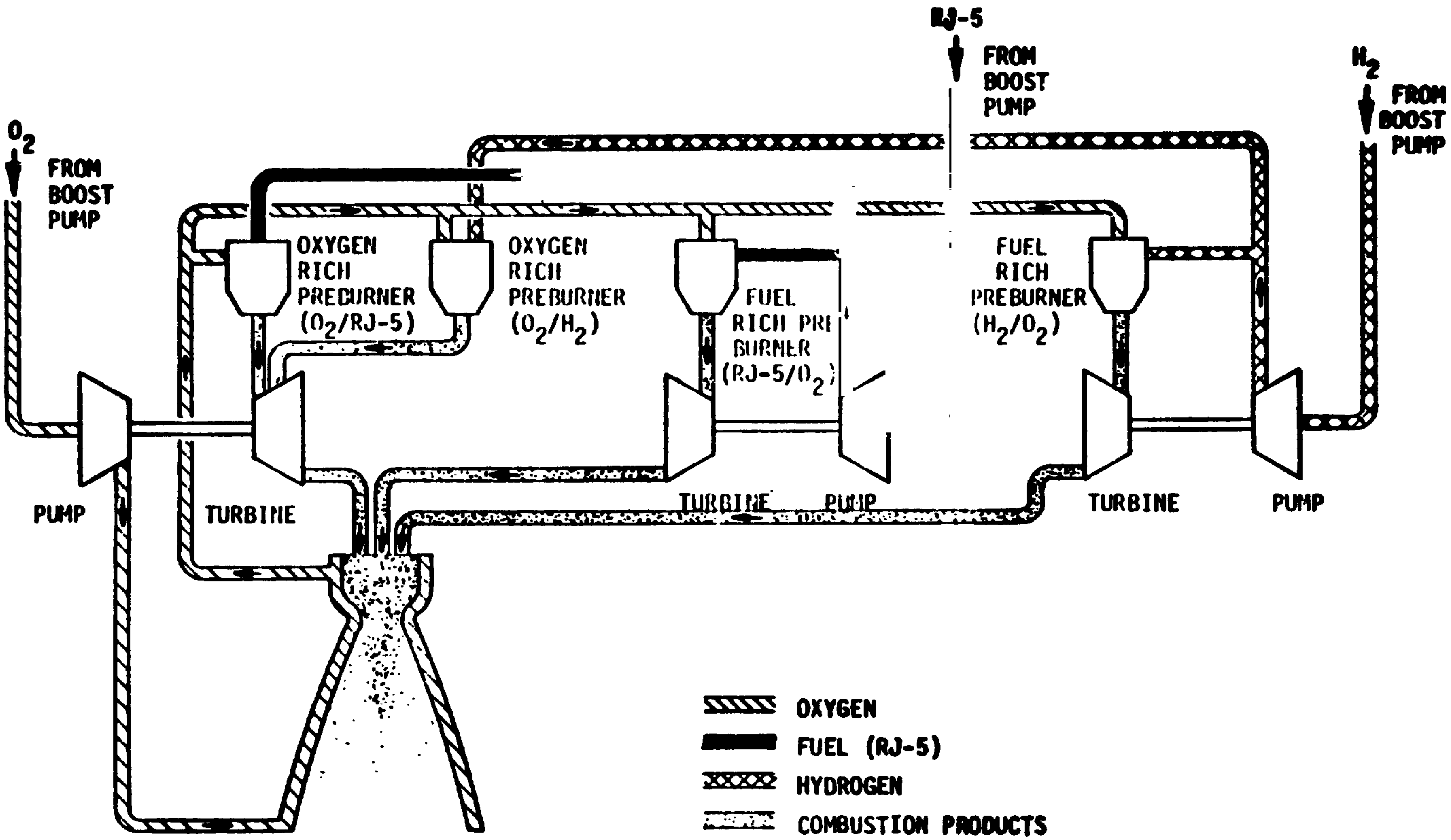

Figure 38. Task III Dual-Fuel, Oxygen Cooled Engine Cycle Schematic

TABLE XXXVIII. - MAXIMUM BEARING DN VALUES

Bearings

Turbopump design shall utilize rolling element bearings

Maximum DN:

	LH_2	LOX	RP-1	RJ-5	Hydrazine	MMH	CH_4
Roller	2.0×10^6	1.5×10^6	1.8×10^6	1.8×10^6	1.4×10^6	1.4×10^6	1.9×10^6
Ball	2.0×10^6	1.5×10^6	1.8×10^6	1.8×10^6	1.4×10^6	1.4×10^6	1.9×10^6

B_{10} Life $\geq$ 500 Hours

TABLE XXXIX. - FACE CONTACT SEAL MAXIMUM PV, FV AND P_fV FACTORS*

		LH_2	LOX	RP-1	RJ-5	Hydrazine	MMH	CH_4
PV	Metric	1037	518	518	518	133	133	726
	English	(50,000)	(25,000)	(25,000)	(25,000)	(6,400)	(6,400)	(35,000)
FV	Metric	218	109	136	136	38	38	174
	English	(4,000)	(2,000)	(2,500)	(2,500)	(700)	(700)	(3,200)
P_fV	Metric	4147	1244	1659	1659	415	415	2488
	English	(200,000)	(60,000)	(80,000)	(80,000)	(20,000)	(20,000)	(120,000)

*PV = unit load times rubbing velocity atm x m/sec ($lb/in.^2$ x ft/sec)
FV = face load per unit length times rubbing velocity kg/cm x m/sec (lb/in. x ft/sec)
P_fV = fluid pressure differential times rubbing velocity atm x m/sec (psig x ft/sec)

TABLE XL. - TASK III TURBINE INLET TEMPERATURE SELECTIONS

Propellant Combination	Turbine Drive Gas	Turbine Inlet Temp. °K	(°R)	Criteria
O_2/RJ-5	Ox-Rich	922	(1660)	Life
	Fuel-Rich	867	(1560)	Coking
O_2/RP-1	Ox-Rich	922	(1660)	Life
	Fuel-Rich	867	(1560)	Coking
O_2/MMH	Ox-Rich	922	(1660)	Life
	Fuel-Rich	922	(1660)(1)	Life
O_2/N_2H_4	Ox-Rich	922	(1660)	Life
	Fuel-Rich	922	(1660)(2)	Life
O_2/H_2	Fuel-Rich & Ox-Rich	922	(1660)	Life
O_2/CH_4	Ox-Rich	922	(1660)	Life
	Fuel-Rich	867	(1560)	Coking

(1) Preburner Temp. = 1383°K (2490°R)
(2) Preburner Temp. = 1028°K (1850°R)

The turbine inlet temperature criteria listed on Table XL were selected to meet the life requirements of the engine and to prohibit turbine coking problems in the case of the fuel-rich hydrocarbon preburners. Experimental data at lower pressures has shown that coking is insignificant at a temperature of 867°K (1100°F). For the fuel-rich LOX/MMH and LOX/N_2H_4 combinations, the monopropellant temperature exceeds practical turbine inlet temperature limits for long life. Therefore, for these cycles, it was assumed that a heat exchange device can be used to reduce the temperature of the fuel-rich preburner combustion gases.

B. TASK III DELIVERED PERFORMANCE

Delivered performance was calculated for all the engines over a chamber pressure range of 136 to 340 atm (2000 to 5000 psia). Delivered vacuum and sea-level performance was calculated as follows:

$$I_{sp\ vac\ Del} = I_{sp\ vac\ ODE} - \Sigma\, I_{sp\ Losses} \tag{13}$$

$$I_{sp\ Sea\text{-}level\ Del} = I_{sp\ vac\ Del} - \frac{P_A A_E}{\dot{W}_T} \tag{14}$$

where:

$I_{sp\ vac\ Del}$ = vacuum delivered impulse

$I_{sp\ vac\ ODE}$ = ODE vacuum impulse

$I_{sp\ Losses}$ = Real engine performance losses including chemical kinetics, boundary layer, nozzle divergence, and injector energy release

$I_{sp\ Sea\text{-}level\ Del}$ = Sea-level delivered impulse

$\frac{P_A A_E}{\dot{W}_T}$ = Sea-level nozzle exit force performance decrement

The real engine performance losses considered in the analyses are summarized below:

$\Delta I_{sp_{KL}}$ = Kinetics loss accounting for incomplete chemical recombination in the chamber convergent and expansion sections

$\Delta I_{sp_{BL}}$ = Boundary layer loss accounting for nozzle friction

$\Delta I_{sp_{HL}}$ = Loss accounting for nozzle heat transfer. This loss is zero for all the TCA fuel or ozidizer cooled engines since heat is recycled to the preburners. The loss is positive for the hydrogen cooled Mode 1 concepts

$\Delta I_{sp_{DL}}$ = Divergence loss accounting for non-axial nozzle exit momentum

$\Delta I_{sp_{ERL}}$ = Injector energy release loss assumed to be 2% of ODE performance which is consistent with the Task II geometry selection to achieve this value.

$\Delta I_{sp_{GG}}$ = Gas generator cycle loss. GG flow assumed to be dumped in TCA nozzle cycle at area ratio consistent with turbine static exit pressure

ODE performance is documented in Section III for all the Mode 1 engine propellant combinations. The nozzle chemical kinetics loss was calculated with the One-Dimensional Kinetic (ODK) option of the JANNAF TDK reference program (Ref. 51). The chamber boundary layer friction loss was calculated with an ALRC computerized formulation of the JANNAF boundary layer chart technique described in Ref. 52. The nozzle divergence loss was calculated from a Rao nozzle design program. The program predicted a divergence efficiency of 99.8% for a contoured 90% Bell length, area ratio equal to 40:1 nozzle.

The resulting delivered performance, for the staged combustion cycle engine concepts, is presented on Figures 39 through 44. The data are shown for the mixture ratios selected in Task II.

The parallel burn, hydrogen cooled staged combustion engine concept has a 1.2 sec lower delivered performance than the baseline LOX/RJ-5 engine. This occurs because the heat input into the hydrogen coolant is transferred to the Mode 2 engine preburners. The 1.2 secs performance loss can be subtracted as a constant value from the performance of Figure 39.

The hydrogen cooled, gas generator cycle Mode 1 engine concept has one additional performance loss compared to the staged combustion concepts. The gas generator flowrate is dumped in the nozzle downstream of the throat and thus, delivers something less than 40:1 expansion performance. The specific impulse of the gas generator flow was calculated assuming the gases will be expanded in the nozzle from the turbine exit static pressure to the nozzle 40:1 wall exit pressure. This pressure was obtained from a perfect gas method of characteristics solution for a 40:1, 90 percent Bell contoured nozzle. The gas generator cycle performance loss was calculated by subtracting the summed TCA and gas generator flow mass weighted performances from ODE performance for the fuel and oxidizer at nominal mixture ratio (O/F = 2.7 for LO_2/RJ-5). The calculated gas generator performance losses are 0.5, 1.0, 1.5 and 2.4 seconds for TCA chamber pressures of 136, 204, 272, and 340 atm (2000, 3000, 4000, and 5000 psia), respectively.

The gas generator performance loss plus the 1.2 sec heat loss must be subtracted from Figure 39 to obtain the delivered performance for the hydrogen cooled, gas generator cycle engine concept.

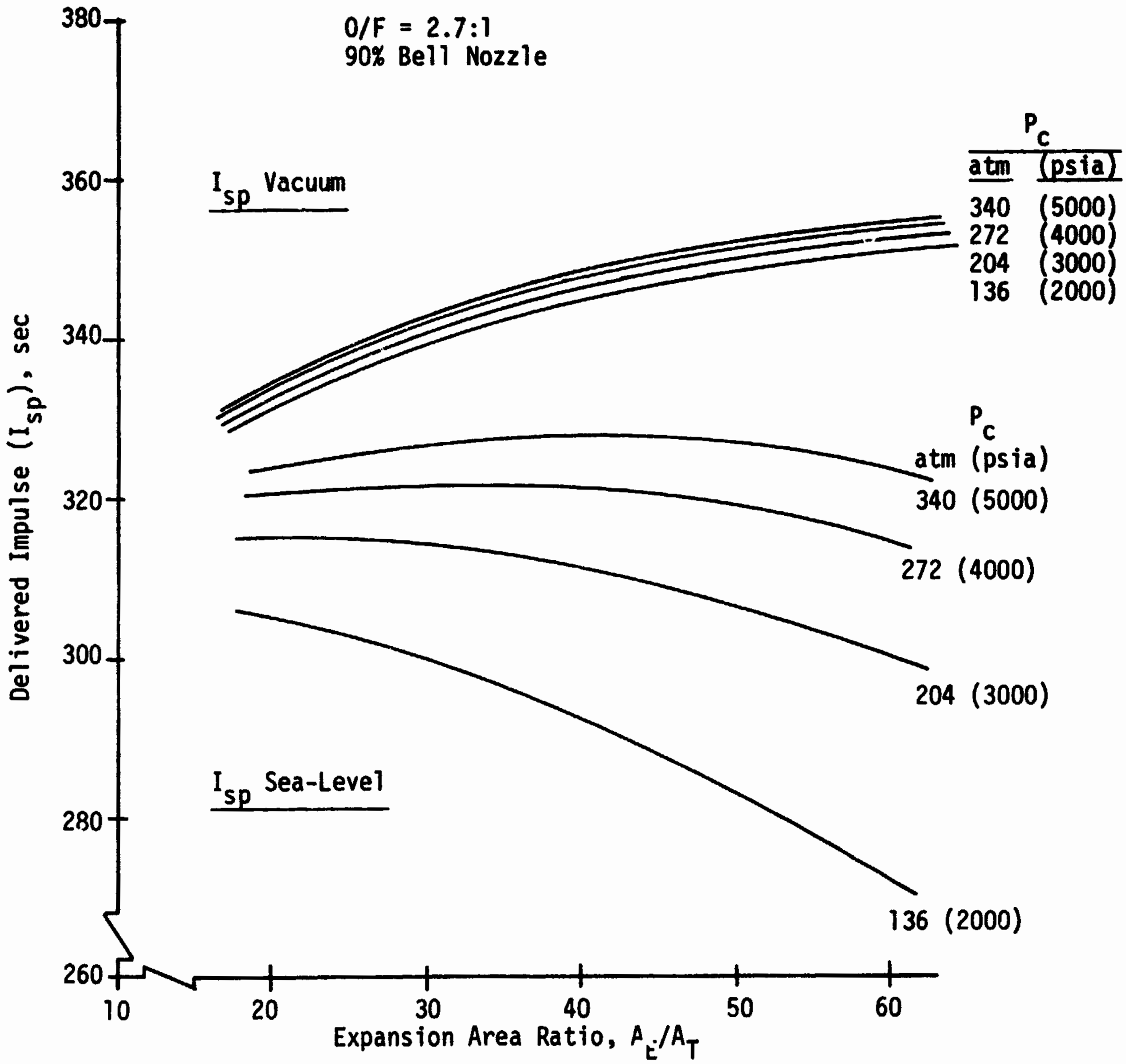

Figure 39. LOX/RJ-5 Staged Combustion Delivered Performance vs Area Ratio

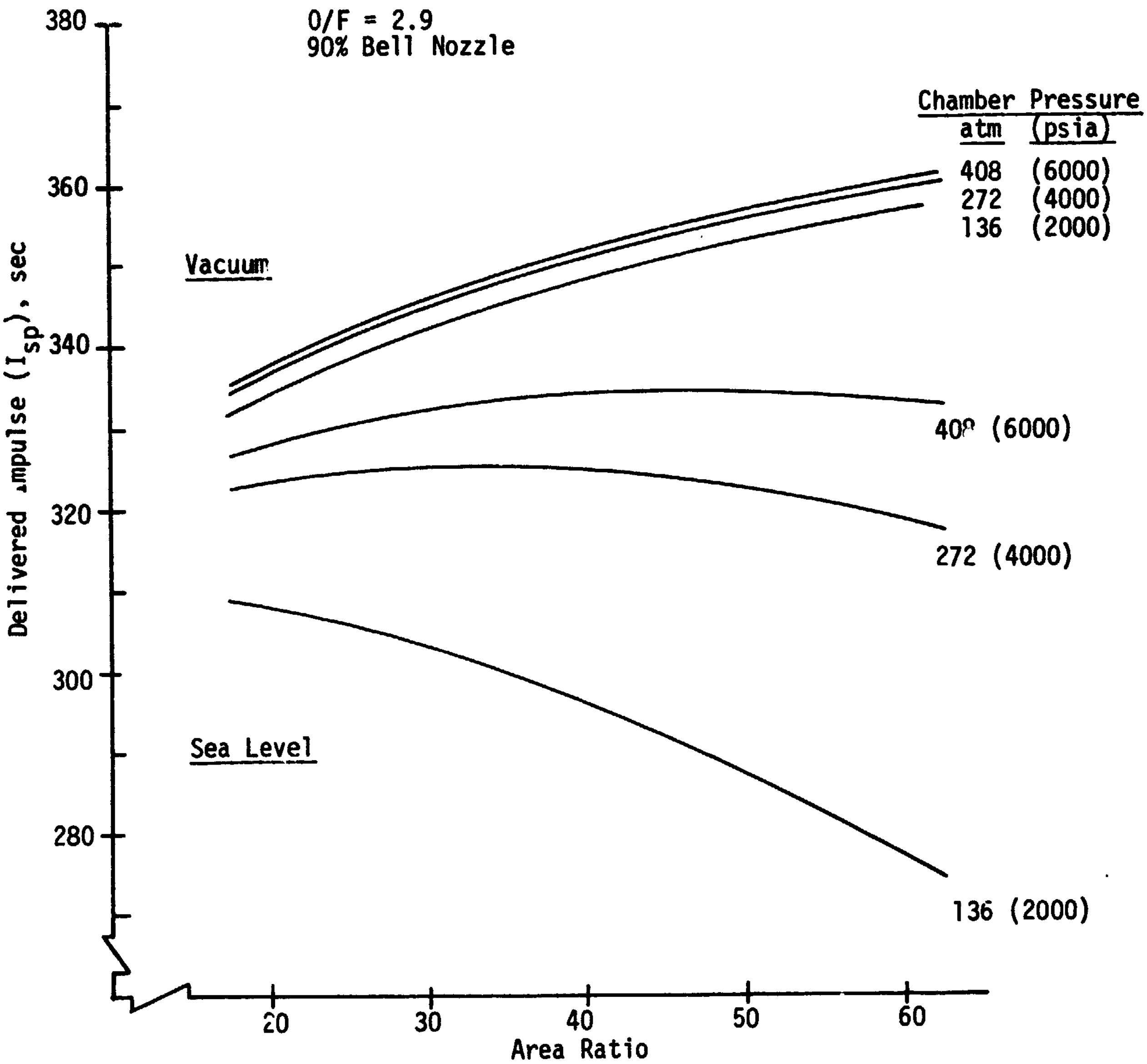

Figure 40. LOX/RP-1 Staged Combustion Delivered Performance vs Area Ratio

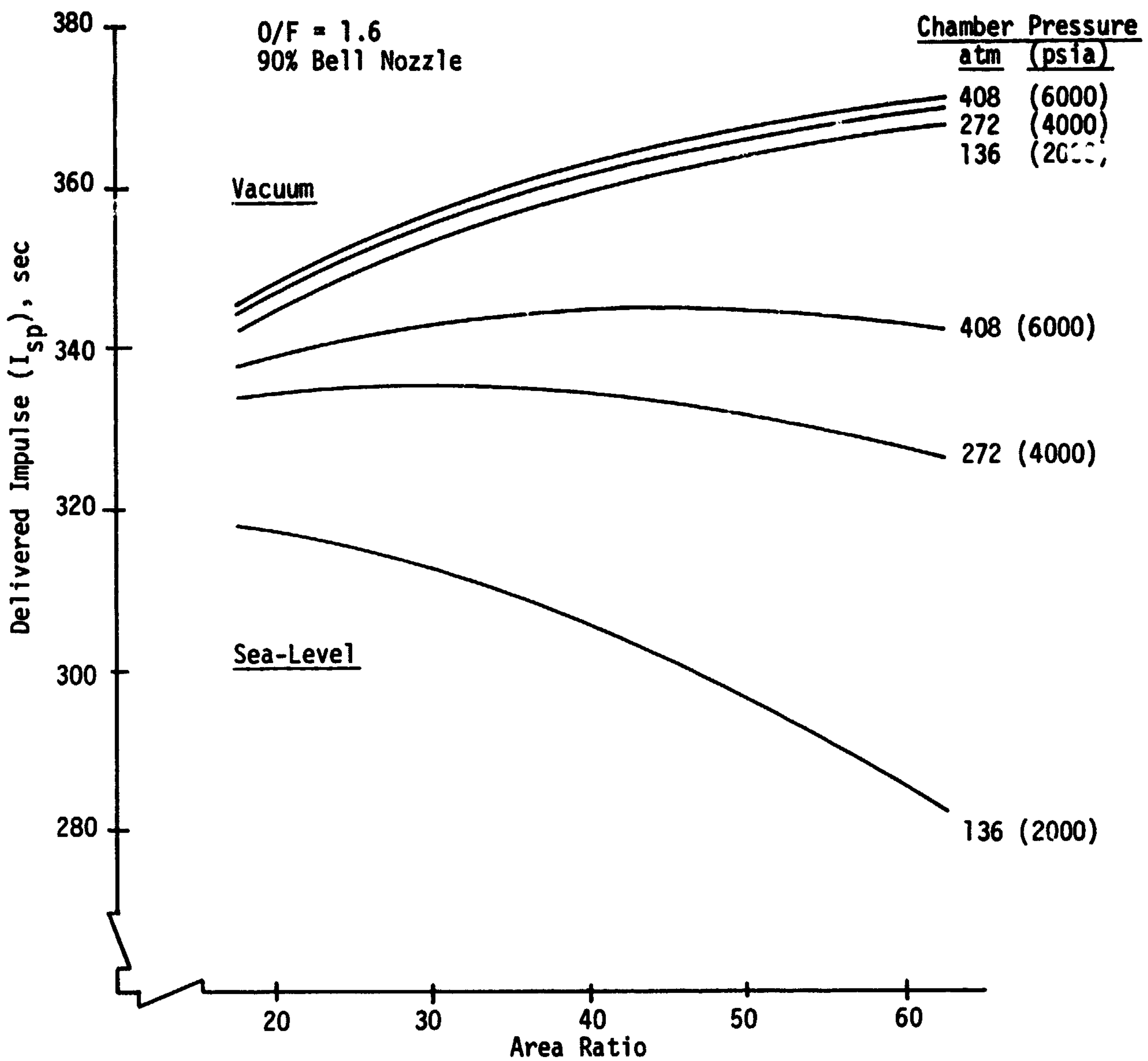

Figure 41. LOX/MMH Staged Combustion Delivered Performance vs Area Ratio

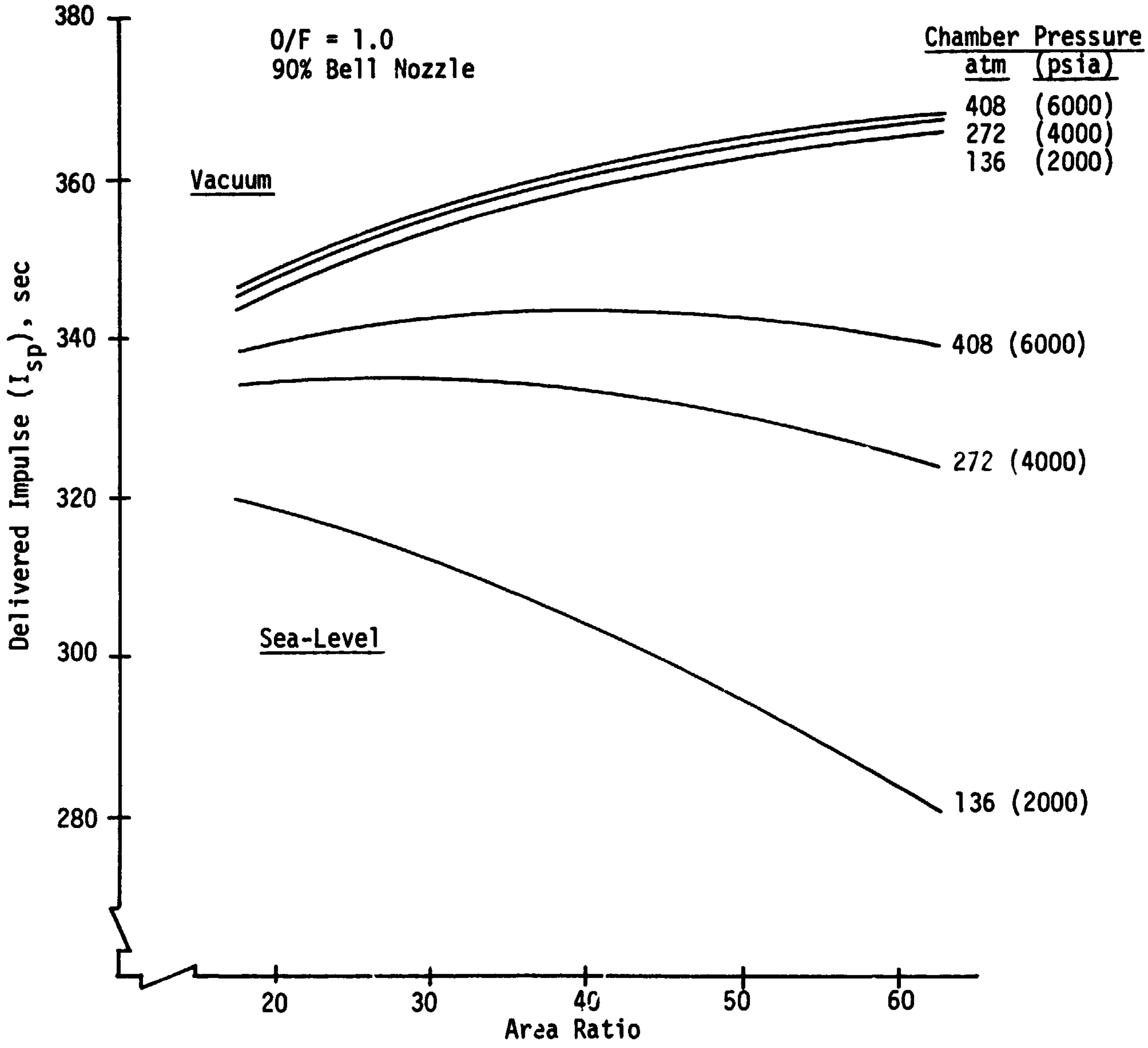

Figure 42. LOX/N_2H_4 Staged Combustion Delivered Performance vs Area Ratio

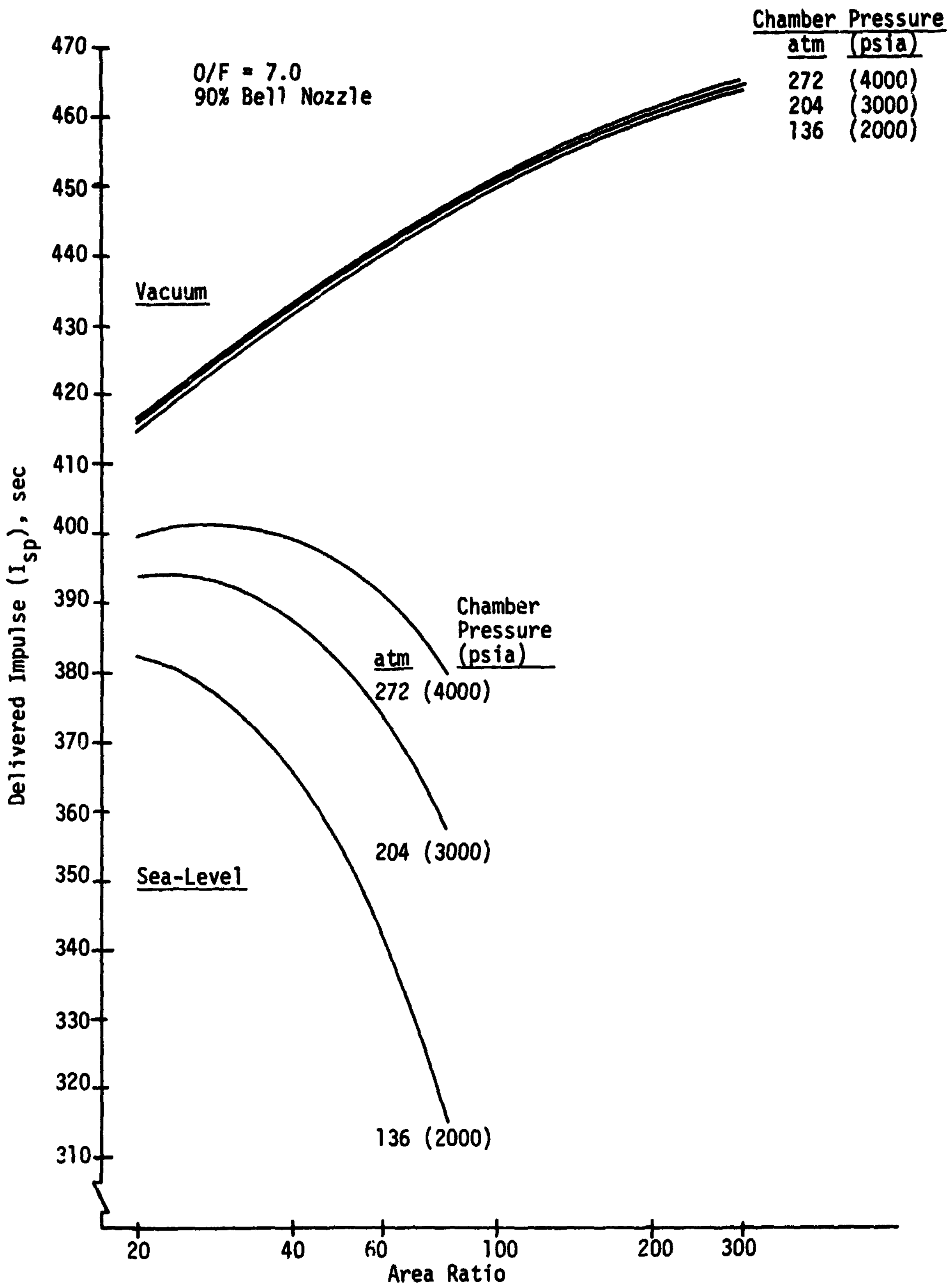

Figure 43. O_2/H_2 Staged Combustion Delivered Performance vs Area Ratio

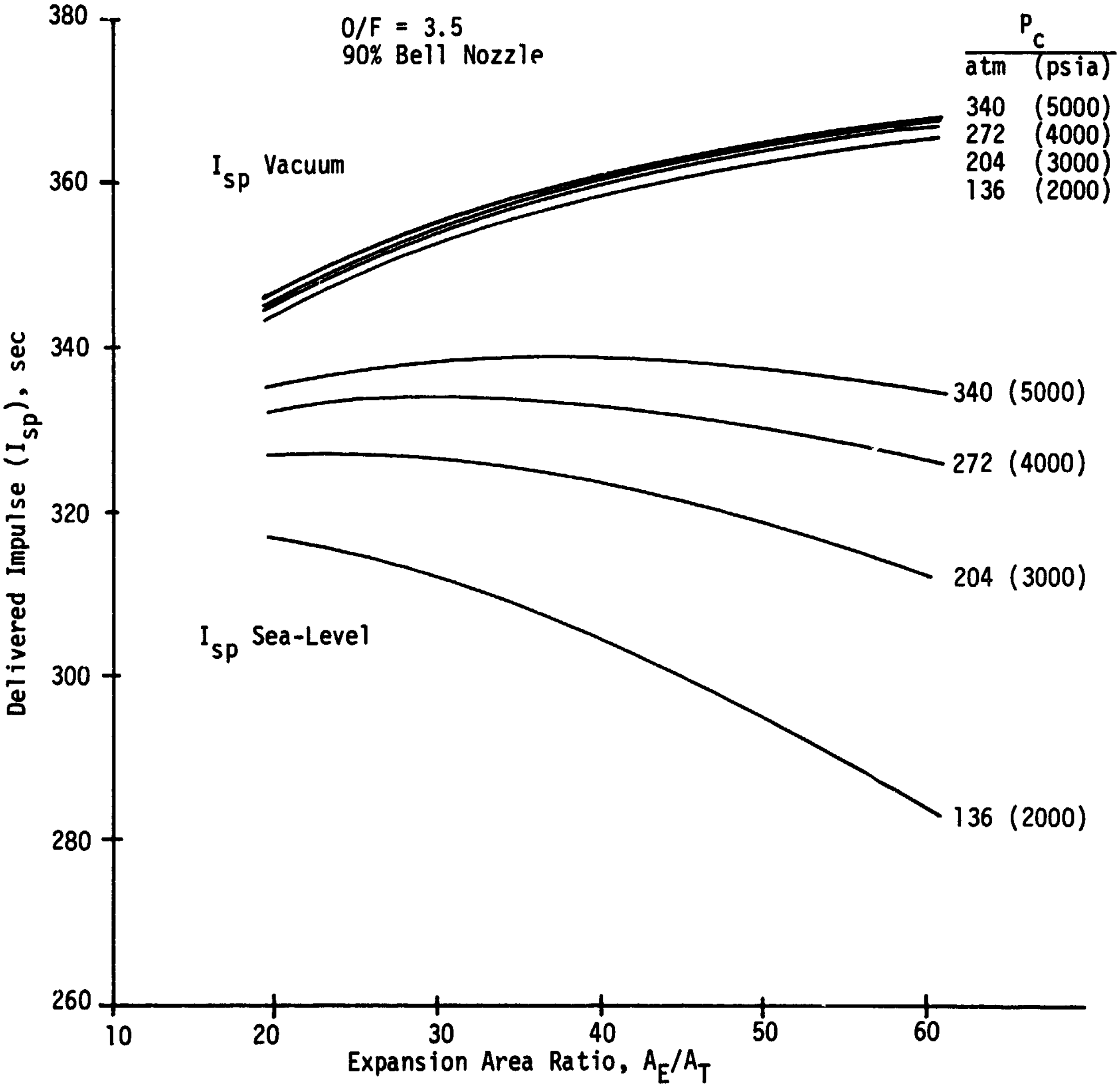

Figure 44. LOX/CH_4 Staged Combustion Delivered Performance vs Area Ratio

C. ENGINE CYCLE POWER BALANCES

Engine pump discharge pressure versus chamber pressure relationships were evaluated for the various candidate coolants and engine cycles. Cycles using RJ-5 and RP-1 as coolants were not evaluated because the coolant evaluation study results showed that operation in a reusable engine would be limited to pressures below 136 atm (2000 psia).

The results of the coolant evaluation studies, coolant jacket ΔP and flow rate, were used to conduct these analyses in conjunction with the system pressure drop criteria.

The cycle evaluation assumes that the boost pumps will produce sufficient discharge pressure to maintain a main pump suction specific speed of 3000 rpm x $m^{3/4}$ x min $^{-1/2}$ (20,000 rpm x gpm x $ft^{-3/4}$). The boost pump drive requirements were not considered in the power balances.

Parametric pump performance curves for head coefficient vs specific speed and pump efficiency vs impeller diameter were used to calculate the pump efficiencies. In general, pump efficiencies in the range of 75 to 80% were obtained depending upon the size of the impeller. The performance of the RJ-5 pumping system was lowered by 2 percentage points to account for the extremely high viscosity of the propellant.

Design point turbine efficiencies used in conducting the power balance calculations for the staged combustion cycle engines are as follows:

LOX Rich Turbines	-	80%
Candidate Fuel-Rich Turbines	-	74%
Hydrogen-Rich Turbines	-	81%

For the low flow, high pressure ratio turbines of the gas generator cycle engine, turbine efficiencies of 60% were assumed. This efficiency corresponds to that obtainable with a two-stage turbine at a velocity ratio of 0.2. Efficiency, in this case, is not critical in establishing the main propellant pump discharge pressure and does not materially affect the power balance.

Maximum pump discharge pressure requirements for the candidates are presented on Figure 45. The maximum feasible operating pressure for the staged combustion cycle engines is considered to be 80% of the chamber pressure at which the curve is asymptotic. For example, the baseline LOX cooled engine asymptote is approximately 354 atm (5200 psia) which results in a maximum recommended pressure of 283 atm (4160 psia) with the 20% margin.

Pertinent conclusions derived from the cycle evaluations along with operational considerations are summarized on Table XLI. It should be noted that the majority of the propellant combinations (particularly RJ-5 and RP-1) are viable candidates if oxygen, rather than the fuel, is used to cool the combustion chamber.

A summary of engine data at a thrust chamber pressure of 272 atm (4000 psia) is shown on Table XLII.

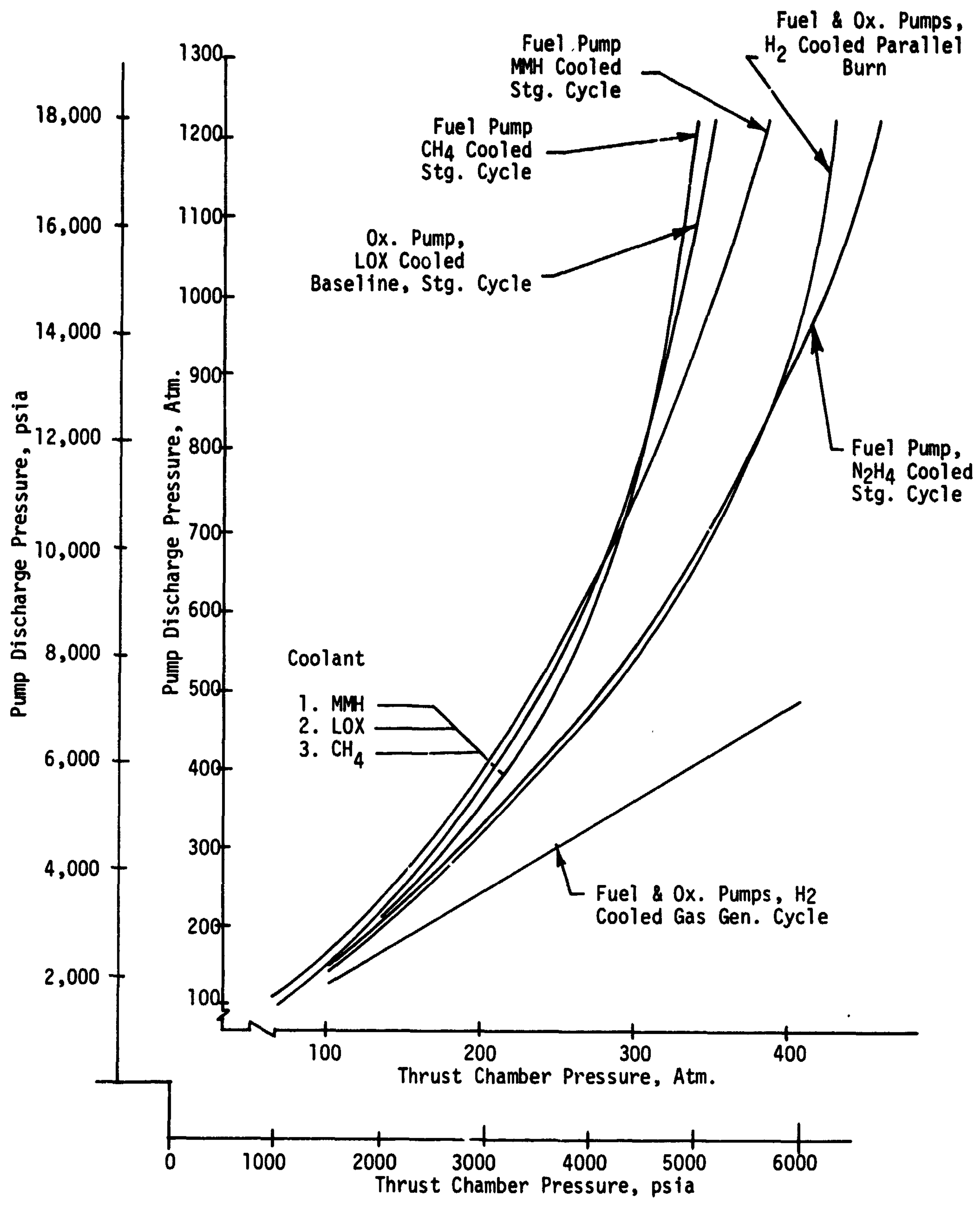

Figure 45. Maximum Pump Discharge Pressure Requirements for Candidate Mode 1 Engines

TABLE XLI. - TASK III CYCLE EVALUATION SUMMARY

Propellant Combination	Coolant	Cycle	Max P_c, Atm	(psia)	Remarks
O_2/RJ-5	O_2	S.C.	285	(4200)[a]	Viable Candidate
O_2/RJ-5	H_2	Parallel Burn	340	(5000)[a]	Viable Candidate
O_2/RJ-5	H_2	G.G.	>340	(>5000)	Viable Candidate
O_2/MMH	MMH	S.C.	306	(4500)[a]	Material compatibility questionable Fuel-Rich gas combustion temp. problem
O_2/N_2H_4	N_2H_4	S.C.	>340	(>5000)	Material compatibility questionable, Explosive decomposition of N_2H_4 vapors, Fuel-rich gas combustion temp. problem.
O_2/RJ-5	RJ-5	S.C.	<136	(<2000)[b]	Coking in channels
O_2/RP-1	RP-1	S.C.	<136	(<2000)[b]	Coking in channels
O_2/CH_4	CH_4	S.C.	272	(4000)[a]	Viable Candidate

[a]Based upon 20% power margin
[b]Propellant property limited

TABLE XLII. - TASK III CANDIDATE MODE I ENGINE COMPARISONS

Chamber Pressure = 272 atm (4000 psia)
Nozzle Area Ratio = 40:1

		Staged Combustion LOX/RJ-5 Baseline		Staged Combustion LOX/MMH		Staged Combustion LOX/N_2H_4		LOX/RJ-5 Parallel Burn		LOX/RJ-5 Gas Gen. Cycle		Staged Combustion LOX/CH_4	
Thrust, MN (lb)	S.L.	2.70	(607,000)	2.70	(607,000)	2.70	(607,000)	2.70	(607,000)	2.70	(607,000)	2.70	(607,000)
	Vac.	2.92	(656,400)	2.92	(656,900)	2.93	(657,600)	2.92	(656,500)	2.92	(656,700)	2.92	(656,800)
I_s, Sec	S.L.		321.3		334.7		333.4		320.1		318.6		333.1
	Vac.		347.4		362.2		361.2		346.2		344.7		360.4
Total Flow Rate, kg/sec (lb/sec)		857	(1889.2)	823	(1813.6)	826	(1820.6)	860	(1896.3)	864	(1905.2)	827	(1822.3)
Mixture Ratio			2.7		1.6		1.0		2.7		2.7[a]		3.5
Ox. Flow Rate, kg/sec (lb/sec)		625	(1378.6)	506	(1116.1)	413	(910.3)	628	(1383.8)	624	(1375.7)	643	(1417.3)
Fuel Flow Rate, kg/sec (lb/sec)		232	(510.6)	317	(69[illegible].5)	413	(910.3)	232	(512.5)	231	(509.5)	184	(405.0)
LH_2 Flow Rate, kg/sec (lb/sec)			--		--		--		--	9	(20.0)		--
Coolant			LOX		MMH		N_2H_4		LH_2		LH_2		CH_4
Coolant Jacket ΔP, atm (psi)		106	(1560)	167	(2450)	37	(540)	8.2	(120)	12.6	(185)	38	(560)
Coolant Exit Temp, °K (°R)		184	(332)	391	(703)	367	(660)	773	(1392)	678	(1220)	304	(548)
Ox. Pump Discharge Pressure, atm (psia)		626	(9200)	463	(6800)	442	(6500)	469	(6900)	327	(4800)	565	(8300)
Fuel Pump Discharge Pressure, atm (psia)		517	(7600)	633	(9300)	483	(7100)	469	(6900)	327	(4800)	605	(8900)
LH_2 Pump Discharge Pressure, atm (psia)			--		--		--		--	333	(4900)		--
LOX Turbopump Speed, RPM			15,100		13,300		14,300		12,100		15,400		13,700
Fuel Turbopump Speed, RPM			21,600		23,900		15,800		20,100		25,500		34,500
LH_2 Turbopump Speed, RPM			--		--		--		--		104,000		--
LOX Pump Horsepower			57,400		34,200		27,100		42,900		29,500		52,400
Fuel Pump Horsepower			19,600		39,700		33,700		17,800		12,400		45,300
LH_2 Pump Horsepower			--		--		--		--		9,600		--

[a] LOX/RJ-5

ORIGINAL PAGE IS OF POOR QUALITY

SECTION VI

TASK IV - ENGINE WEIGHT AND ENVELOPE

A. OBJECTIVE AND GUIDELINES

The objective of this task was to provide parametric engine weight and envelope data for the candidate Mode 1 engines, the dual-fuel engine and the baseline Mode 2 engine.

The parametric ranges considered were:

Parameter	Mode 1 Engines	Mode 2 Engines
Thrust, MN (Lb)	1.78 to 4.0 Sea-Level (400K to 900K Sea Level)	2.22 to 4.45 Vac. (500K to 1000K Vac.)
Chamber Pressure, Atm. (psia)	136 to 340 (2000) to (5000)	136 to 340 (2000) to (5000)
Nozzle Area Ratio	10:1 to 60:1	100:1 to 300:1

Parameter	Dual-Fuel Mode 1	Dual-Fuel Mode 2
Thrust, MN (Lb)	2.7 to 4.0 Sea-Level (607K to 900K Sea-Level)	2.16 to 3.44 Vac. (486K to 774K Vac.)
Chamber Pressure, Atm. (psia)	182 to 363 (2670 to 5330)	136 to 272 (2000 to 4000)
Nozzle Area Ratio	40:1	100:1 to 300:1

B. BASELINE ENGINE WEIGHT STATEMENTS

For purpose of the parametric study, it was necessary to establish the elements of engine weight to be included in the scaling study and to establish baseline engine weight statements. Table XLIII lists the engine components included in the parametric analyses. Those items not included are also listed.

Engine weight statements are shown on Table XLIV. Included are the three engines on which preliminary designs were completed in Task VI, the Mode 2 engine, and the LOX/CH_4 methane cooled candidate Mode 1 engine.

In the Task IV effort, it was necessary to initially generate weights and parametric data for use in the evaluation and selection of candidate Mode 1 engines for preliminary design. These data were based on

TABLE XLIII. - TASK IV - ENGINE WEIGHT DEFINITIONS

Included	Not Included
Regeneratively Cooled Combustion Chamber	Gimbal Actuators and Actuation System
Regeneratively Cooled Thrust Chamber Fixed Nozzle	Engine Controller
Thrust Chamber Nozzle Extension (Mode 2)	Pre-Valves
NozzleExtension Deployment System (Mode 2)	Tank Pressurant Heat Exchangers and Associated Equipment
Main Injector	Contingency (a total contingency is normally included in the vehicle weight statement)
Main Turbopumps	
Boost Pumps	
Preburners (or Gas Generator)	
Propellant Valves and Actuation	
Gimbal	
Hot Gas Manifold (if required)	
Propellant Lines	
Ignition System	
Miscellaneous (Electrical Harness, Instrumentation, Brackets, Auxiliary Lines and Controls)	

ORIGINAL PAGE IS
OF POOR QUALITY

TABLE XLIV. - TASK IV - BASELINE ENGINE WEIGHT STATEMENTS

Component	LOX/RP-1 Mode 1[1]		Weight, kg (lb) Mode 2[2]		Dual-Fuel[1]		LOX/CH_4 Mode 1[3]		LOX/RP-1 H_2 Cooled G.G. Cycle[1]	
Gimbal	96	(211)	94	(208)	96	(211)	95	(209)	95	(211)
Main Injector and Manifold	385	(848)	757	(1668)	385	(848)	348	(767)	349	(769)
Main Chamber	124	(274)	258	(568)	124	(274)	127	(281)	157	(347)
Fixed Nozzle	113	(249)	342	(755)	89	(197)	249	(550)	92	(203)
Extendible Nozzle		--	390	(860)	592	(1306)		--		--
Ext. Nozzle Deploy. System		--	265	(585)	292	(644)		--		--
Preburners	181	(398)	158	(349)	411	(905)	121	(267)	9	(20) G.G.
Valves and Actuation	91	(200)	328	(724)	305	(672)	268	(590)	133	(293)
Boost Pumps	159	(351)	288	(634)	209	(461)	151	(333)	167	(368)
Main Pumps	528	(1164)	1062	(2340)	986	(2174)	585	(1289)	394	(869)
Lines	209	(460)	597	(1316)	449	(989)	206	(454)	160	(353)
Miscellaneous	227	(502)	274	(605)	246	(542)	227	(502)	227	(502)
Total Dry	2113	(4657)	4813	(10,612)	4184	(9223)	2377	(5242)	1784	(3935)
Vac Thrust/Wt.		141		70.3	71 (LOX/RP-1) 56 (LOX/LH_2)			125		167

(1)Based upon calculated weights from preliminary design layouts
(2)Based upon scaling of SSME
(3)Based upon scaling of in-house IR&D conceptual design and historical data

scaling of historical weights of similar components and/or estimates obtained from conceptual designs. A fixed 90% bell nozzle was assumed for the Mode 1 engines and a fixed 90% bell nozzle to an area ratio of 40:1 and an extendible 90% bell nozzle beyond was assumed for the Mode 2 and dual-fuel engines. Upon completion of the preliminary design effort in Task VI, the weight statements and parametric data were updated for the three preliminary design engines to reflect weights and dimensions as calculated from the preliminary design layouts.

Mode 2 engine baseline weight was obtained by modifying the SSME engine target weight (Ref. 53) for the study guidelines and assumptions, and then scaling to the required thrust level. The SSME weight was modified by: (1) eliminating the contingency and miscellaneous components excluded in this study, (2) calculating the SSME nozzle weight per unit surface area and adjusting the fixed nozzle weight for a 40:1, 90% bell and, (3) adding a nozzle extension and deployment system weight which is based upon the ALRC SSME design (Ref. 54).

It should be noted that adjustments in individual components were not made to account for the mixture ratio change from 6 to 7. Past studies of hydrogen cooled, LOX/LH_2 engines have shown that variations in component weights with mixture ratio tend to compensate so that the resulting total engine weight is essentially constant.

The baseline weight for the LOX/CH_4 methane cooled engine is based on the initial Task IV weight statements, i.e. scaled historical weights and estimates from conceptual designs. Because of the low density of methane, the baseline weight includes a scale factor which accounts for the volumetric flow rate difference between CH_4 and RP-1 engine components.

C. PARAMETRIC WEIGHT DATA

With the baseline engine weight established, engine component weight scaling relationships were derived as functions of thrust, thrust chamber pressure and nozzle area ratio. These scaling relationships were used to calculate the weights over the parametric ranges of interest. The scaling equations were established through geometry considerations and empirical data fits of historical data. These techniques have proven to be satisfactory in past parametric studies of this nature such as, the OOS Engine Study (Contract F04611-71-C-0040), the Space Tug Storable Engine Study (Contract NAS8-29806), and the parametric analyses conducted for the early Phase B, Study (Contract NAS8-26188).

1. Mode 1 Staged Combustion Cycle

Figure 46, shows the Mode 1 staged combustion cycle engine weight as a function of thrust chamber pressure for a nozzle area ratio of 40:1. Weight variations with thrust are also shown on the figure.

The data on Figure 46 were calculated for the Mode 1 LOX cooled baseline engine but are also within the calculation accuracy for the practical candidate Mode 1 fuel cooled staged combustion cycles except for LOX/CH_4. Practical chamber pressure limits for each of the cycles were shown on Table XLI of the previous section.

Minimum engine weight occurs between 190 and 231 atm (2800 and 3400 psia) depending upon the thrust level. The lower thrust level has a corresponding higher chamber pressure. However, a chamber pressure increase to 272 atm (4000 psia) results in only a modest engine weight increase.

It can also be established from the data shown on Figure 46 that the engine thrust to weight ratio decreases as the engine thrust level increases. This would indicate that it may be desirable to cluster more small engines (i.e., four 2.70 MN (607,000 lb) thrust engines rather than three 3.6 MN (809,000 lb thrust) engines.

The effect of area ratio upon the Mode 1 staged combustion cycle engine weights is shown on Figure 47. The data are plotted for the baseline thrust chamber pressure of 272 atm (4000 psia). The engines are heavier at an area ratio of 10:1 than at 20:1 because a 10:1 nozzle at 272 atm (4000 psia) is well underexpanded and low performing at sea-level. This results in a large throat size and correspondingly large surface areas for the combustion chamber and nozzle.

The trends shown on Figure 47 are similar for the other engines considered in this study.

2. Hydrogen Cooled, Gas Generator Cycle

The hydrogen cooled, gas generator cycle engine weight as a function of chamber pressure and thrust level is shown on Figure 48. This engine is schematically depicted on Figure 37 of the previous section. The trends with chamber pressure and thrust are similar to those discussed for the Mode 1 staged combustion cycles. However, the chamber pressure resulting in minimum engine weight is higher for this cycle.

This engine weighs approximately 318 kg (700 lb) less than the baseline LOX cooled, LOX/RP-1 engine at a thrust of 2.7 MN (607K lb) and chamber pressure of 272 atm (4000 psia).

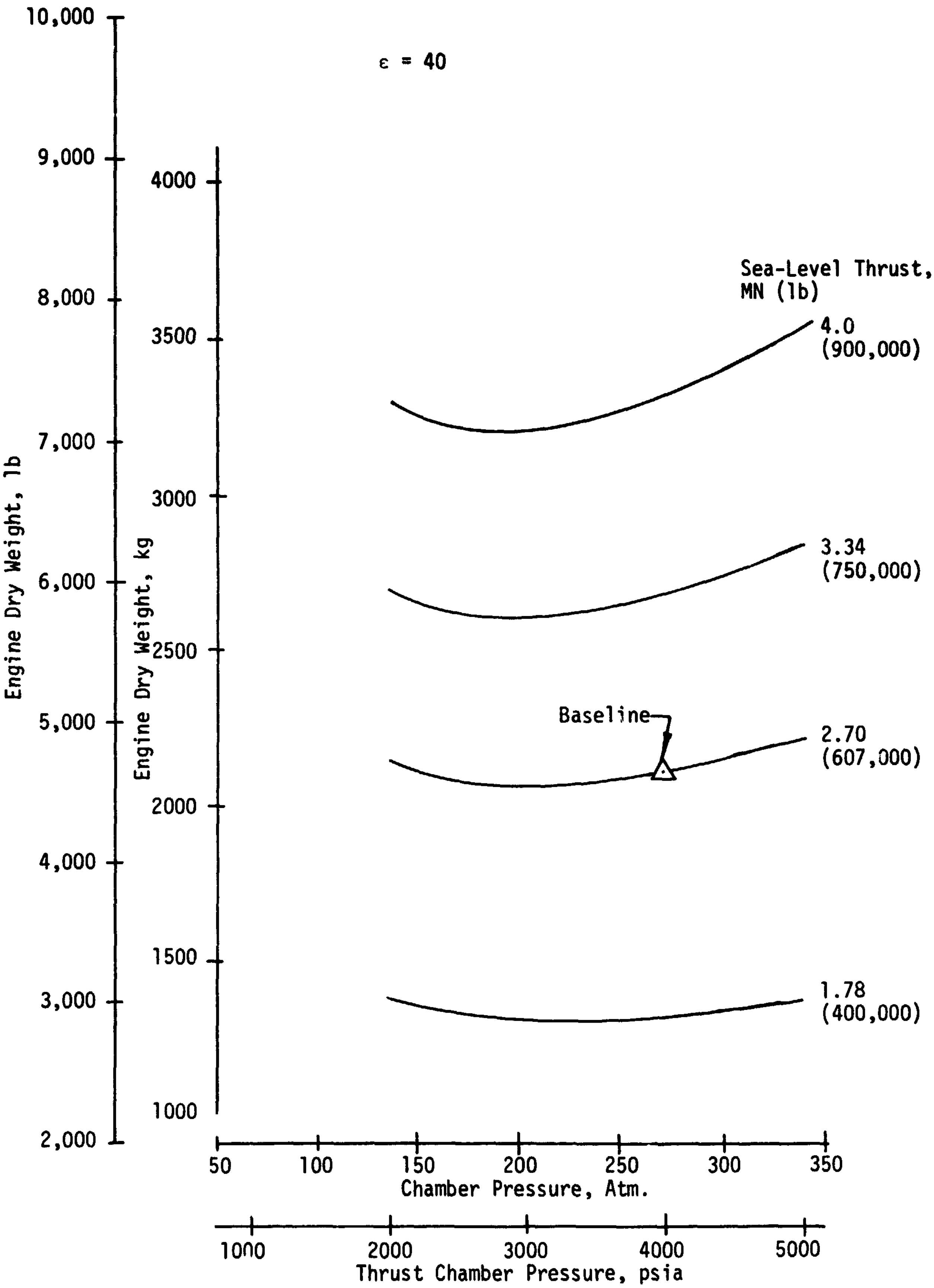

Figure 46. Mode 1 Staged Combustion Cycle Engine Weight Parametrics

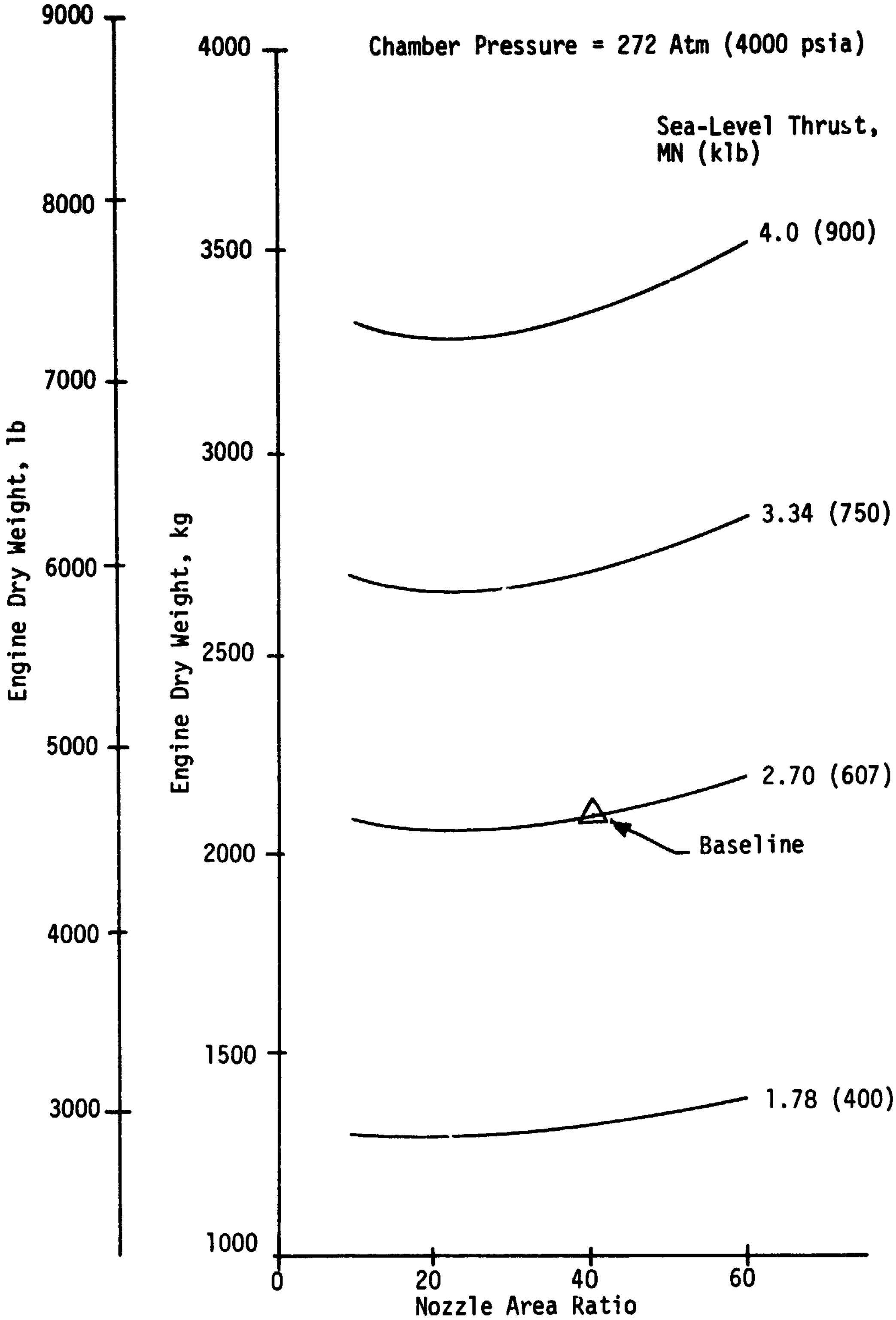

Figure 47. Effect of Area Ratio Upon Mode 1 Staged Combustion Cycle Engine Weight

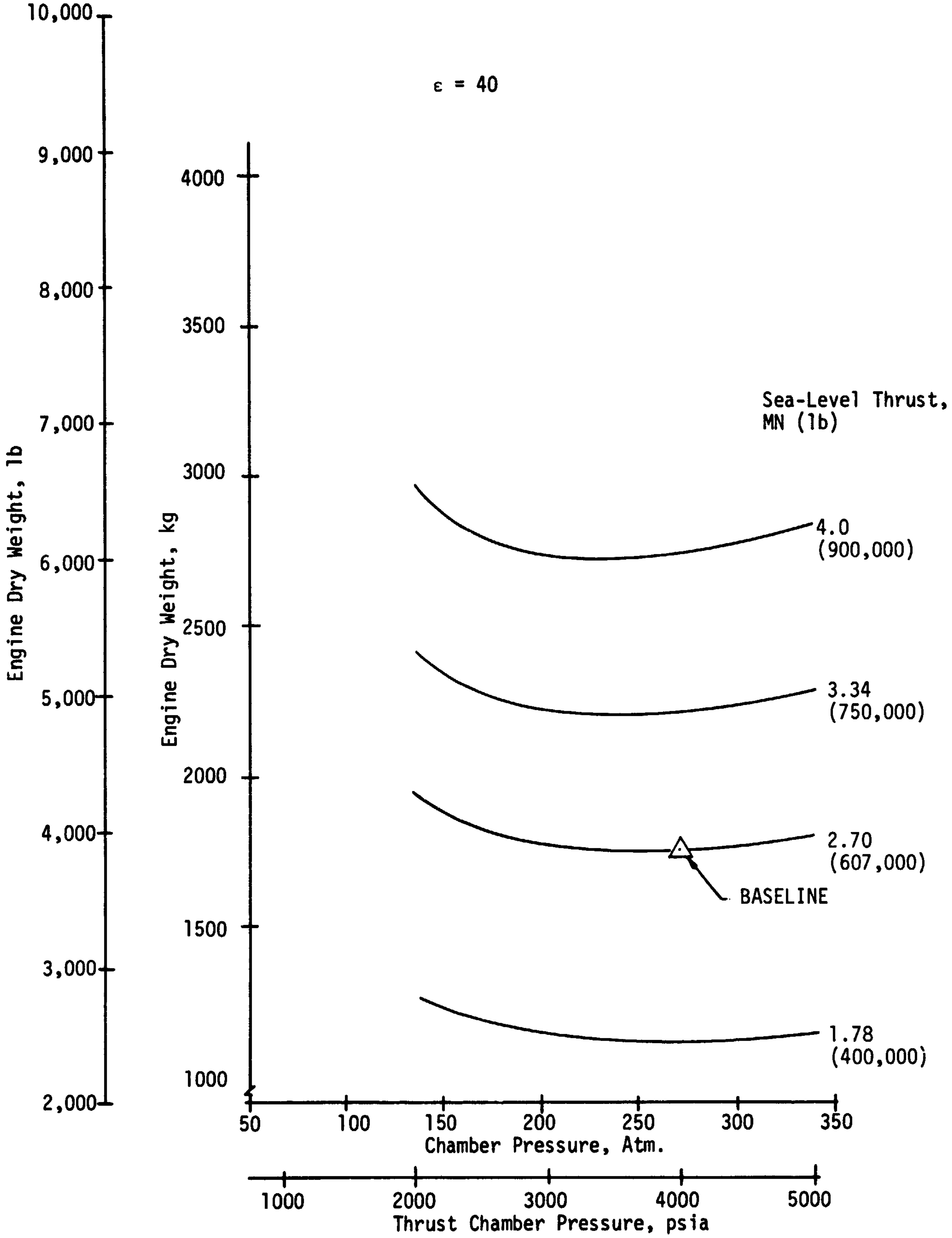

Figure 48. Mode 1 Hydrogen Cooled Gas Generator Cycle Engine Weight Parametrics

The effect of area ratio upon the hydrogen cooled gas generator cycle engine weight is shown on Figure 49. The data are plotted for a thrust chamber pressure of 272 atm (4000 psia). As with the Mode 1 staged combustion cycle engines, the GG cycle engines are heavier at an area of 10:1 than at 20:1 because of the nozzle underexpansion and low performance at sea level which results in a large throat size and correspondingly large surface areas for the combustion chamber and nozzle.

3. Dual-Fuel Engine

The dual-fuel engine concept is shown schematically on Figure 38. Oxygen is used to cool the engine in both modes of operation. Because the chamber cooling problem is more severe for the Mode 2 LOX/LH_2 operation, the Mode 2 chamber pressure and thrust is lower than Mode 1. The parametric weight data for this engine is shown on Figure 50 as a function of the extendible nozzle area ratio and Mode 1 thrust level. The data are shown for the recommended operating chamber pressures of 272 atm (4000 psia) for Mode 1 and 204 atm (3000 psia) for Mode 2.

For a given Mode 1 sea-level thrust, the Mode 2 vacuum thrust will vary with the nozzle area ratio because the throat area of the dual-fuel combustion chamber is fixed. The thrust varies as follows:

Mode 1 Sea-Level Thrust, MN	Mode 1 Sea-Level Thrust, (Klb)	Nozzle Area Ratio	Mode 2 Vacuum Thrust, MN	Mode 2 Vacuum Thrust, (Klb)
2.70	(607)	100	2.25	(505)
↓	↓	↓	2.78	(624)
			3.33	(749)
3.34	(750)	200	2.30	(517)
↓	↓	↓	2.84	(638)
			3.41	(766)
4.0	(900)	300	2.32	(522)
↓	↓	↓	2.87	(645)
			3.44	(774)

4. Mode 1 LOX/CH_4 Engine

The Mode 1 LOX/CH_4, methane cooled engine weight parametrics are shown on Figure 51. The data are presented as a function of thrust chamber pressure and thrust level for the baseline nozzle area ratio of 40:1.

Because of the lower density of methane, the base point fuel components are heavier. This results in lower pressures for minimum engine weight. However, the weight penalty for operating at a thrust chamber pressure of 272 atm (4000 psia) remains modest.

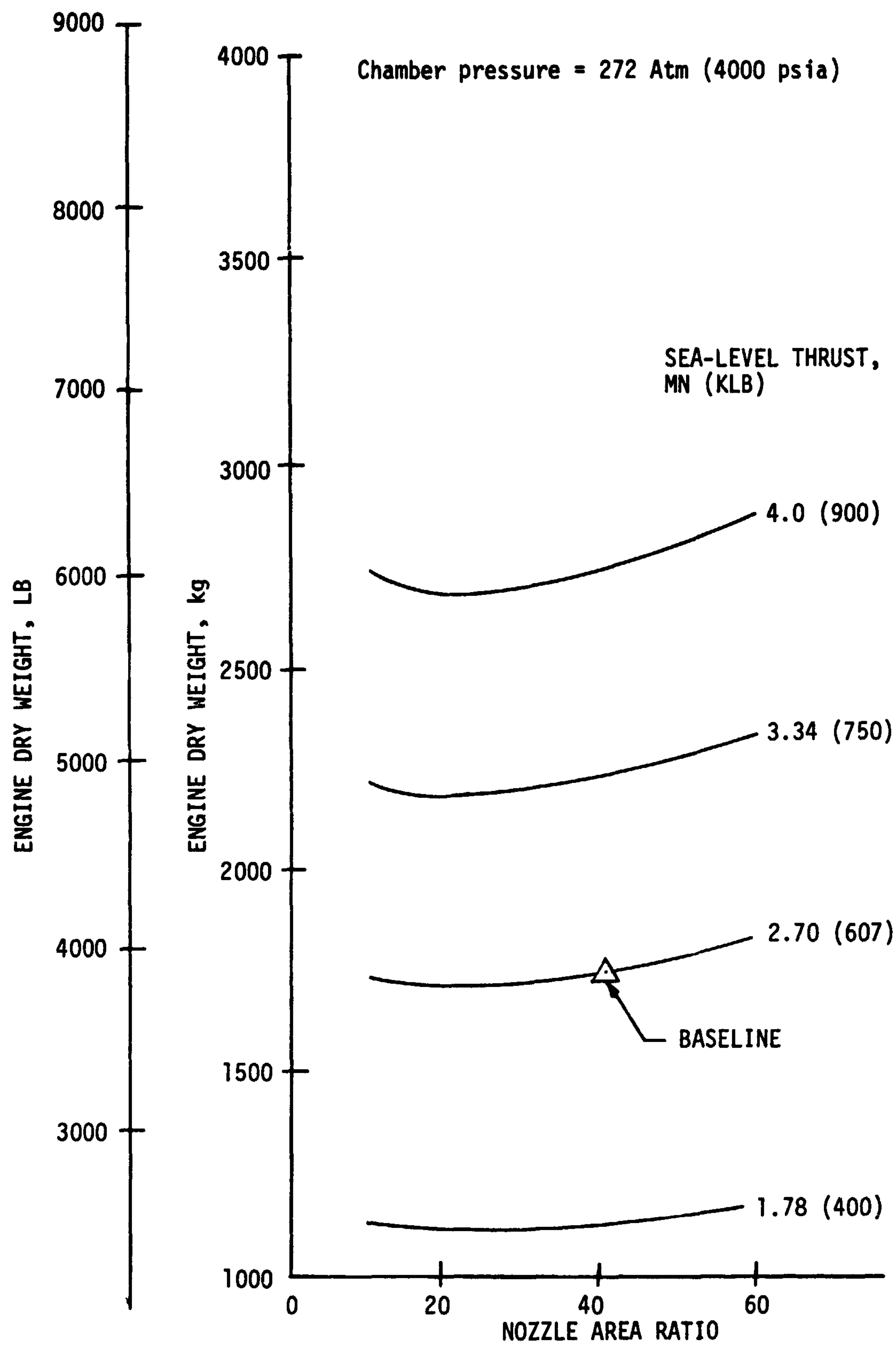

Figure 49. Effect of Area Ratio Upon Mode 1 Hydrogen Cooled Gas Generator Cycle Engine Weight

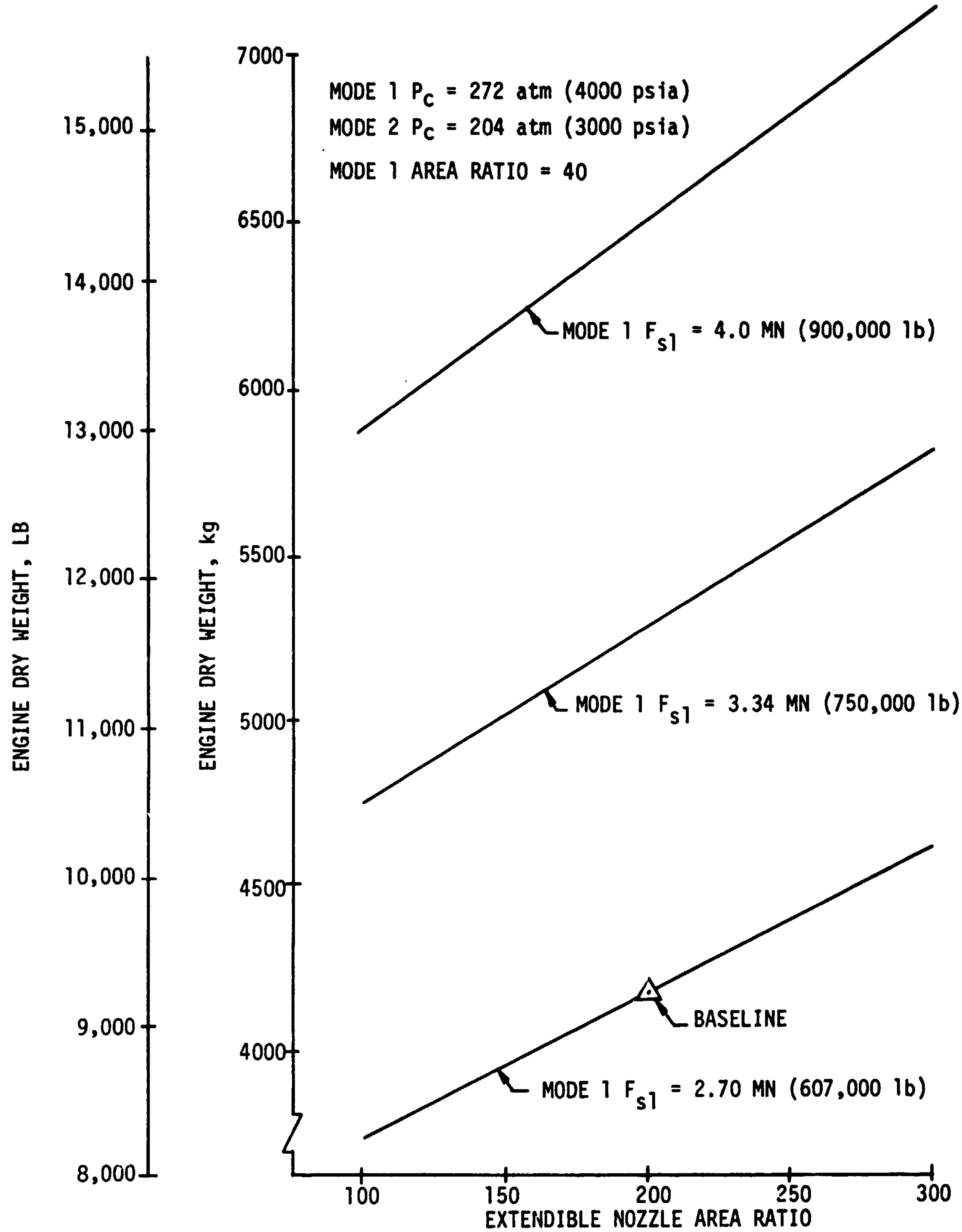

Figure 50. Dual-Fuel Engine Weight Parametrics

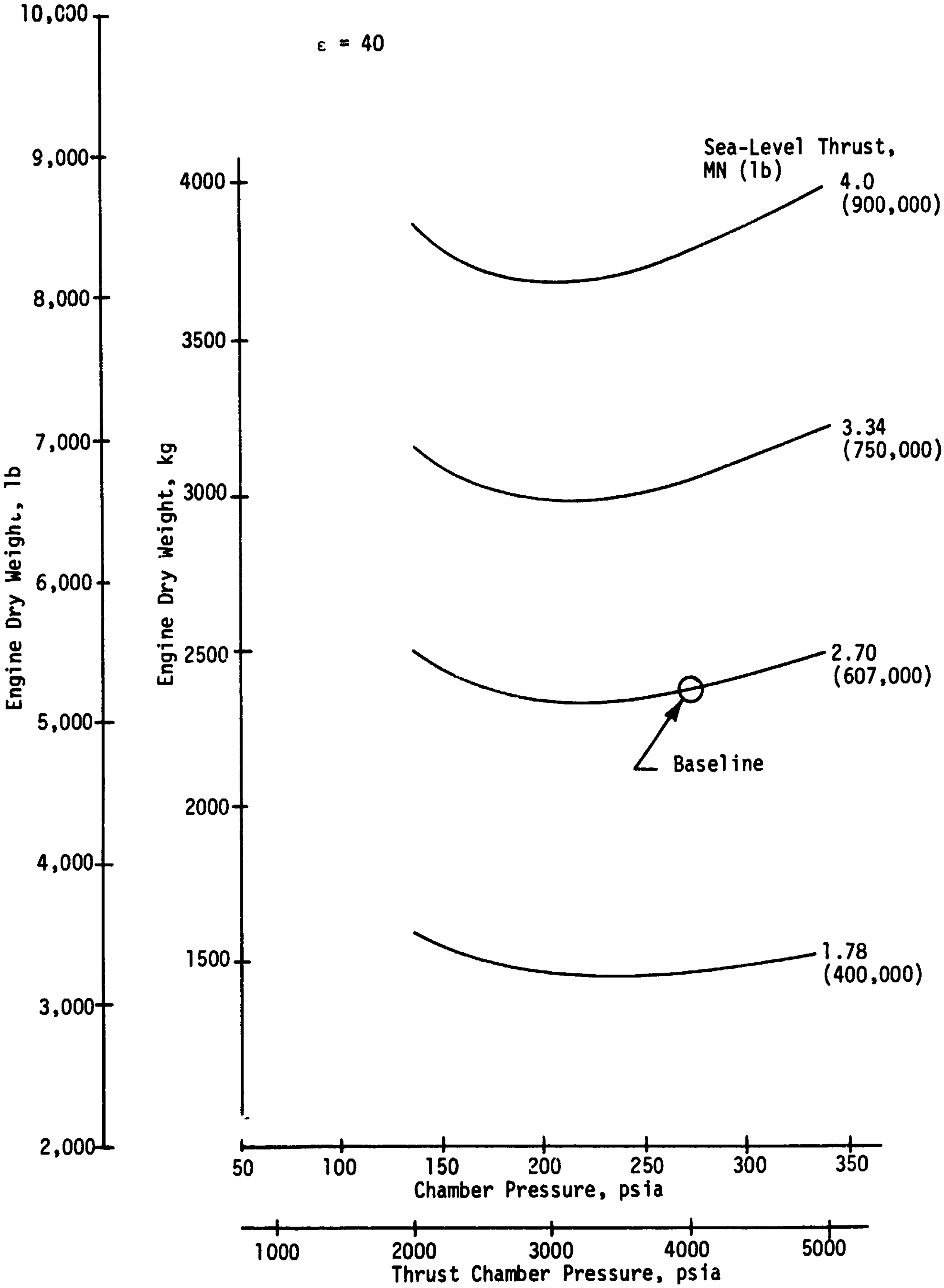

Figure 51. Mode 1 LOX/CH_4 Engine Weight Parametrics

5. Mode 2 LOX/LH_2 Engine

The LOX/LH_2 Mode 2 engine description follows:

- Scaled SSME
- Engine Cycle: Staged combustion with dual fuel-rich preburners.
- Propellant State at Thrust Chamber Injector Inlet: Fuel-rich gas and liquid oxygen.
- Combustion Chamber: Regeneratively cooled with hydrogen.
- Nozzle: Fixed bell to ϵ = 40 for sea-level operation; extendible nozzle for vacuum operation.

The weight data for this engine is shown on Figure 52 for a baseline nozzle area ratio of 200:1. The data are shown as a function of thrust chamber pressure and thrust level. The minimum engine weight occurs at a thrust chamber pressure of approximately 136 atm (2000 psia). At a baseline thrust of 3.32 MN (746K lb), the weight increase between 136 atm and 204 atm (2000 to 3000 psia) is only 227 kg (500 lb).

From the data shown on this figure, it can be established that the engine thrust to weight ratio decreases as the engine thrust level is increased.

The effect of area ratio upon the engine weight parametrics is shown on Figure 53. The data are presented for the baseline operating pressure of 204 atm (3000 psia).

D. PARAMETRIC ENVELOPE DATA

The elements of engine length include:

- Gimbal
- Injector and hot gas manifold
- Chamber
- Fixed Nozzle
- Nozzle Extension (Mode 2)

Scaling equations based upon geometric considerations were formulated as functions of thrust, thrust chamber pressure and area ratio. The diameter and length parametrics for the Mode 1 and dual-fuel engines were calculated using the envelopes established during the Task VI preliminary design effort

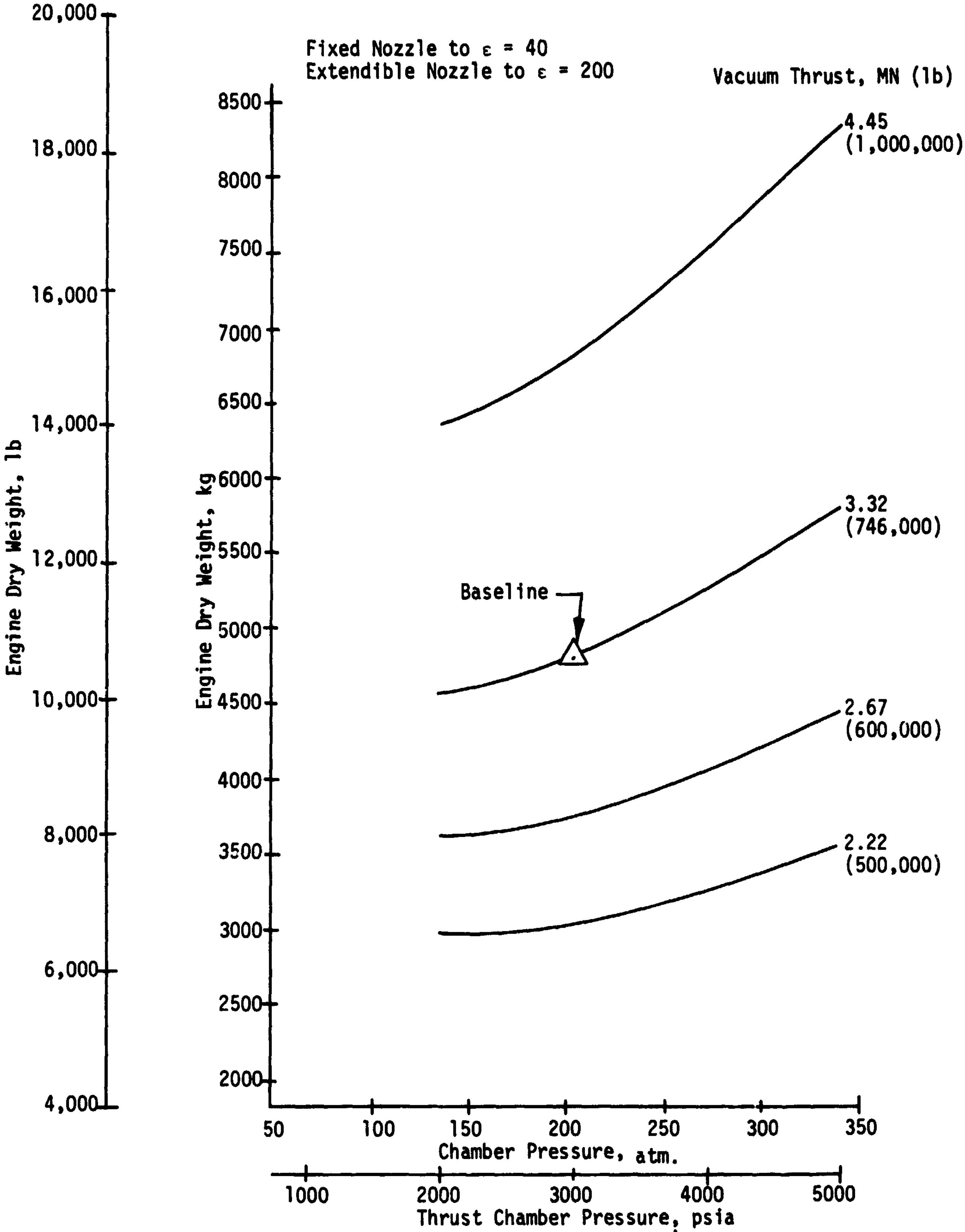

Figure 52. Mode 2 LOX/LH_2 Engine Weight Parametrics

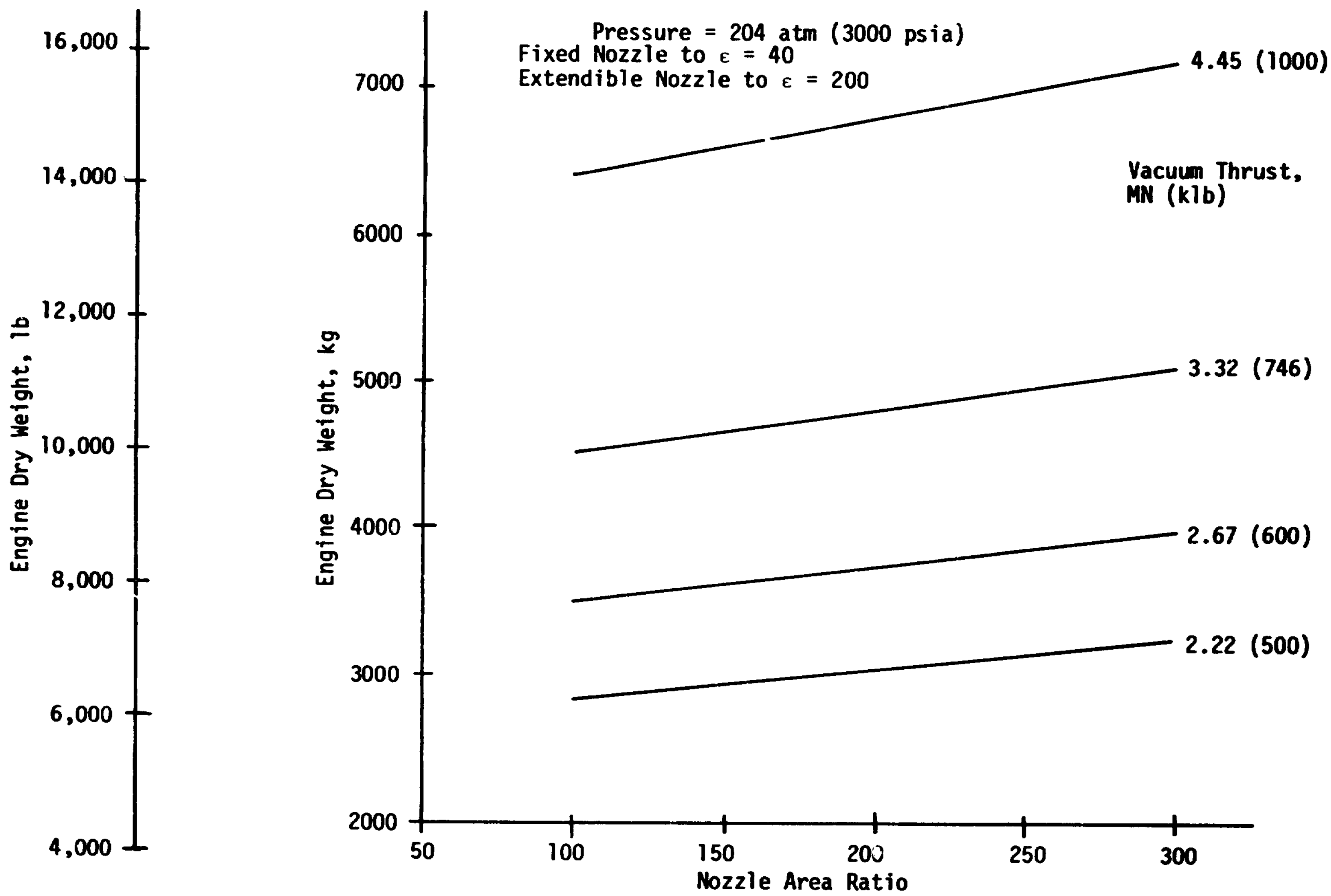

Figure 53. Effect of Area Ratio Upon Mode 2 LOX/LH_2 Engine Weight

as a base. Thus, the parametrics assume a similar engine packaging arrangement and the same percentage bell nozzle lengths.

The diameter parametrics include an estimation of the powerhead diameter (pump envelope) to establish whether the nozzle exit or this envelope is greater. For the Mode 2 engines, the powerhead diameter must be established to determine if the nozzle at the split will fit over the pump in order to reduce the stowed nozzle engine length.

The envelope parametrics do not include an allowance for gimballing.

1. Candidate Mode 1 Engines

The data shown in this section are valid for all Mode 1 staged combustion engine cycle candidates, including LOX/CH_4 when modified as noted in the tables. This is true because the maximum variation in thrust coefficient between all Mode 1 propellant combinations considered in this study is 3%. This has only a 1-1/2% influence upon the engine linear dimensions which is well within preliminary design calculation accuracy.

The overall effect of thrust and chamber pressure upon the Mode 1 engine dimensions is summarized on Table XLV at the design point area ratio of 40:1. The effect of area ratio upon the dimensions is summarized on Table XLVI at the design point thrust chamber pressure of 272 atm (4000 psia). Small variations in powerhead diameter (less than 1 cm) resulting from engine flowrate variations for the different area ratios at a given thrust level and chamber pressure were neglected.

2. Hydrogen Cooled, Gas Generator Cycle Engine

The Mode 1 hydrogen cooled, gas generator cycle engine envelope data is summarized on Tables XLVII and XLVIII. The engine length is different from the staged combustion cycle data because the chamber length required to achieve a given energy release efficiency is longer for liquid-liquid propellant injection. The powerhead diameter and nozzle exit outside diameters also vary from the Mode 1 engine data previously presented because of differences in engine packaging and the manifolding for the hydrogen coolant at the nozzle exit.

3. Dual-Fuel Engine

The dual-fuel engine envelope parametrics are shown on Table XLIX for the maximum recommended operating pressure of 272 atm (4000 psia) in Mode 1 and 204 atm (3000 psia) for Mode 2. The data are presented for the nozzle extension in the deployed and stowed positions. The Mode 1 nozzle area ratio was fixed at 40:1 for this study. Because the resulting powerhead diameters were larger than the nozzle exit diameter at 40:1, the nozzle will not stow over the turbomachinery. Therefore, it

TABLE XLV. - CANDIDATE MODE 1 ENGINE ENVELOPE

Parametrics (ϵ = 40)

Sea-Level Thrust		Thrust Chamber Pressure		Engine Length,		Nozzle Exit O.D.		Powerhead Diameter[a]	
MN	(Klb)	atm	(psia)	cm	(in.)	cm	(in.)	cm	(in.)
1.78	(400)	136	(2000)	330	(130)	211	(83)	221	(87)
↓	↓	204	(3000)	264	(104)	168	(66)	211	(83)
↓	↓	272	(4000)	226	(89)	142	(56)	203	(80)
↓	↓	340	(5000)	201	(79)	127	(50)	201	(79)
2.70	(607)	136	(2000)	409	(159)	262	(103)	246	(97)
↓	↓	204	(3000)	323	(127)	206	(81)	231	(91)
↓	↓	272	(4000)	277	(109)	178	(70)	224	(88)
↓	↓	340	(5000)	246	(97)	157	(62)	218	(86)
3.34	(750)	136	(2000)	450	(177)	290	(114)	262	(103)
↓	↓	204	(3000)	358	(141)	229	(90)	244	(96)
↓	↓	272	(4000)	307	(121)	196	(77)	236	(93)
↓	↓	340	(5000)	274	(108)	175	(69)	231	(91)
4.0	(900)	136	(2000)	490	(193)	318	(125)	277	(109)
↓	↓	204	(3000)	391	(154)	251	(99)	257	(101)
↓	↓	272	(4000)	335	(132)	216	(85)	249	(98)
↓	↓	340	(5000)	300	(118)	191	(75)	241	(95)

[a]For LOX/CH_4 engines, increase powerhead diameter by 11%.

TABLE XLVI. - CANDIDATE MODE 1 ENGINE ENVELOPE

Parametrics P_c = 272 atm (4000 psia)

Sea-Level Thrust		Nozzle Area Ratio	Engine Length,		Nozzle Exit O.D.		Powerhead Diameter[a]	
MN	(K lb)		cm	(in.)	cm	(in.)	cm	(in.)
1.78	(400)	10	127	(50)	74	(29)	203	(80)
↓	↓	20	168	(66)	102	(40)	↓	↓
		40	226	(89)	142	(56)		
		60	274	(108)	178	(70)		
2.70	(607)	10	155	(61)	89	(35)	224	(88)
↓	↓	20	203	(80)	302	(49)	↓	↓
		40	277	(109)	178	(70)		
		60	335	(132)	218	(86)		
3.34	(750)	10	170	(67)	99	(39)	236	(93)
↓	↓	20	226	(89)	140	(55)	↓	↓
		40	307	(121)	196	(77)		
		60	373	(147)	244	(96)		
4.0	(900)	10	188	(74)	109	(43)	249	(98)
↓	↓	20	246	(97)	152	(60)	↓	↓
		40	335	(132)	216	(85)		
		60	406	(160)	267	(105)		

[a] For LOX/CH_4 engines, increase powerhead diameter by 11%.

TABLE XLVII. - HYDROGEN COOLED GAS GENERATOR CYCLE

Engine Envelope Parametrics ($\epsilon = 40$)

Sea-Level Thrust		Thrust Chamber Pressure		Engine Length		Nozzle Exit O.D.		Powerhead Diameter	
MN	(K lb)	atm	(psia)	cm	(in.)	cm	(in.)	cm	(in.)
1.78	(400)	136	(2000)	373	(147)	206	(81)	216	(85)
↓	↓	204	(3000)	302	(119)	165	(65)	188	(74)
↓	↓	272	(4000)	262	(103)	140	(55)	173	(68)
↓	↓	340	(5000)	236	(93)	124	(49)	160	(63)
2.70	(607)	136	(2000)	452	(178)	254	(100)	264	(104)
↓	↓	204	(3000)	363	(143)	203	(80)	229	(90)
↓	↓	272	(4000)	315	(124)	173	(68)	208	(82)
↓	↓	340	(5000)	284	(112)	152	(60)	193	(76)
3.34	(750)	136	(2000)	498	(196)	282	(111)	292	(115)
↓	↓	204	(3000)	401	(158)	224	(88)	254	(100)
↓	↓	272	(4000)	348	(137)	193	(76)	229	(91)
↓	↓	340	(5000)	312	(123)	170	(67)	213	(84)
4.0	(900)	136	(2000)	544	(214)	310	(122)	318	(125)
↓	↓	204	(3000)	437	(172)	246	(97)	277	(109)
↓	↓	272	(4000)	378	(149)	211	(83)	251	(99)
↓	↓	340	(5000)	338	(133)	185	(73)	234	(92)

TABLE XLVIII. - HYDROGEN COOLED GAS GENERATOR CYCLE

Engine Envelope Parametrics P_c = 272 atm (4000 psia)

Sea-Level Thrust MN	Sea-Level Thrust (K lb)	Nozzle Area Ratio	Engine Length cm	Engine Length (in.)	Nozzle Exit O.D. cm	Nozzle Exit O.D. (in.)	Powerhead Diameter cm	Powerhead Diameter (in.)
1.78	(400)	10	163	(64)	71	(28)	173	(68)
↓	↓	20	203	(80)	99	(39)	↓	↓
↓	↓	40	262	(103)	140	(55)	↓	↓
↓	↓	60	310	(122)	173	(68)	↓	↓
2.70	(607)	10	193	(76)	89	(35)	208	(82)
↓	↓	20	241	(95)	122	(48)	↓	↓
↓	↓	40	315	(124)	173	(68)	↓	↓
↓	↓	60	376	(148)	213	(84)	↓	↓
3.34	(750)	10	211	(83)	97	(38)	231	(91)
↓	↓	20	267	(105)	137	(54)	↓	↓
↓	↓	40	348	(137)	193	(76)	↓	↓
↓	↓	60	414	(163)	236	(93)	↓	↓
4.0	(900)	10	229	(90)	107	(42)	251	(99)
↓	↓	20	287	(113)	150	(59)	↓	↓
↓	↓	40	378	(149)	211	(83)	↓	↓
↓	↓	60	450	(177)	259	(102)	↓	↓

TABLE XLIX. - DUAL-FUEL ENGINE ENVELOPE PARAMETRICS

Mode 1 P_C = 272 atm (4000 psia)
Mode 2 P_C = 204 atm (3000 psia)
Mode 1 Area Ratio = 40

Mode 1 Sea-Level Thrust		Extendible Nozzle Area Ratio	Stowed Nozzle Engine Length		Extended Nozzle Engine Length		Extendible Nozzle Exit I.D.		Powrrhead Diameter	
MN	(K lb)		cm	(in.)	cm	(in.)	cm	(in.)	cm	(in.)
2.70	(607)	100	498	(196)	640	(252)	277	(109)	394	(155)
↓	↓	200	734	(289)	879	(346)	394	(155)	↓	↓
		300	917	(361)	1062	(418)	480	(189)		
3.34	(750)	100	551	(217)	711	(280)	307	(121)	411	(162)
↓	↓	200	815	(321)	975	(384)	437	(172)	↓	↓
		300	1019	(401)	1179	(464)	533	(210)		
4.0	(900)	100	602	(237)	777	(306)	338	(133)	429	(169)
↓	↓	200	892	(351)	1069	(421)	478	(188)	↓	↓
		300	1115	(439)	1290	(508)	584	(230)		

NOTE: Parametrics are based on the Task VI preliminary design which consisted of a 75% bell nozzle to 40:1 (fixed) combined with a 110% bell nozzle to 200:1 (extendible). This results in a Mode 2 engine with an overall 119% bell nozzle length.

was assumed in the parametrics that the nozzle could be retracted to the relative position established for the Task VI dual-fuel engine preliminary design.

4. Mode 2 Engine

The Mode 2 engine consists of the same elements of length as the Mode 1 engine plus the addition of an extendible bell nozzle. For all cases, the overall nozzle (fixed plus extension) was assumed to be a 90% bell truncated at the fixed 40:1 area ratio.

Lengths of other components are based upon scaling of values typical of the SSME (Ref. 53). These are:

- Length from gimbal center to injector face = 20"
- Chamber length = 14"

Engine envelope data, as a function of extendible nozzle area ratio and thrust level, are presented on Table L for the extendible nozzle in both the extended and stowed positions. These data are summarized for the baseline chamber pressure of 204 atm (3000 psia). For all cases, the calculated pump envelope exceeds the exit diameter of the 40:1 fixed nozzle. Therefore, the nozzle extension cannot be retracted over the turbomachinery and associated components. It has been assumed that all of these components are packaged above the throat plane and that the nozzle extension can be retracted to this point. This results in the fixed nozzle portion being greater than the nozzle extension at ε = 100:1 but smaller than the nozzle extension at 200:1 and 300:1. Therefore, the stowed length is equal to:

- Length of gimbal, injector and hot gas manifold, chamber and the fixed 40:1 nozzle at ε = 100
- Length of gimbal, injector and hot gas manifold, chamber and the extendible nozzle at ε = 200 and 300.

Based upon the geometry and scaling equations, the area ratio at which the nozzle extension and fixed nozzle lengths are exactly equal is 136:1. Hence, stowed length below this area ratio is governed by the fixed nozzle.

The exit diameter of the extendible nozzle exceeds the pump envelope over the entire range of variables. Therefore, this nozzle exit diameter defines the maximum engine diameter for the Mode 2 engines.

TABLE L. - MODE 2 ENGINE ENVELOPE PARAMETRICS

P_c = 204 atm (3000 psia)

Mode 2 Vacuum Thrust		Extendible Nozzle Area Ratio	Stowed Nozzle Engine Length		Extended Nozzle Engine Length		Extendible Nozzle Exit I.D.		Powerhead Diameter	
MN	(K lb)		cm	(in.)	cm	(in.)	cm	(in.)	cm	(in.)
2.22	(500)	100	323	(127)	483	(190)	262	(103)	191	(75)
↓	↓	200	427	(168)	658	(259)	368	(145)	↓	↓
		300	564	(222)	792	(312)	447	(176)		
2.67	(600)	100	351	(138)	528	(208)	287	(113)	206	(81)
↓	↓	200	465	(183)	719	(283)	401	(158)	↓	↓
		300	615	(242)	866	(341)	490	(193)		
2.32	(746)	100	389	(153)	584	(230)	320	(126)	226	(89)
↓	↓	200	516	(203)	800	(315)	447	(176)	↓	↓
		300	681	(268)	963	(379)	546	(215)		
4.45	(1000)	100	445	(175)	673	(265)	371	(146)	254	(100)
↓	↓	200	594	(234)	922	(363)	518	(204)	↓	↓
		300	785	(309)	1113	(438)	632	(249)		

NOTE: Parametrics are based on an overall 90% bell nozzle (fixed plus extension) which is truncated at the fixed 40:1 area ratio.

SECTION VII

TASK V - AUXILIARY COOLANT FEASIBILITY

A. OBJECTIVES AND GUIDELINES

The objectives of this study were to: (1) determine the relative merit of auxiliary cooled Mode 1 engine concepts, (2) provide cycle power balance data for the maximum recommended chamber pressure, and (3) estimate engine weight and envelope data.

The engine cycle schematic analyzed is shown on Figure 54. The baseline propellants were specified as LOX/RJ-5. Liquid oxygen, rather than RJ-5 is used in the heat exchanger to avoid the gumming and coking problems which severely limited the operating pressure of the RJ-5 cooled chamber in Task II.

Additional study guidelines are as follows:

- Baseline Sea-Level Thrust = 2.70 MN (607K lb)
- Engine Mixture Ratio = 2.7
- Chamber Guidelines - Same as Task II
- Cycle Evaluation Guidelines - Same as Task III
- Auxiliary Coolants - Water, Lithium, and Sodium-Potassium (NaK 56%)
- Coolant Jacket Inlet Temperatures:
  - Water - 311°K (560°R)
  - Lithium - 456°K (820°R)
  - NaK - 311 (560°R)
- Liquid Oxygen Heat Exchanger
  - Inlet Temperature - 111°K (200°R)

B. AUXILIARY COOLANT PROPERTIES

Analyses and literature surveys were completed and the physical and thermodynamic property data for the candidate auxiliary coolants accumulated. A summary of this data is shown on Table LI.

The primary source of data for water is the ASME Steam Tables. Properties for Lithium and NaK (56%) are discussed in the paragraphs which follow:

1. Thermophysical Properties of Lithium

The primary source of data on lithium is an Aerojet-General Nucleonics report (Ref. 55). This reference is cited as the AGN report in this discussion.

a. Density

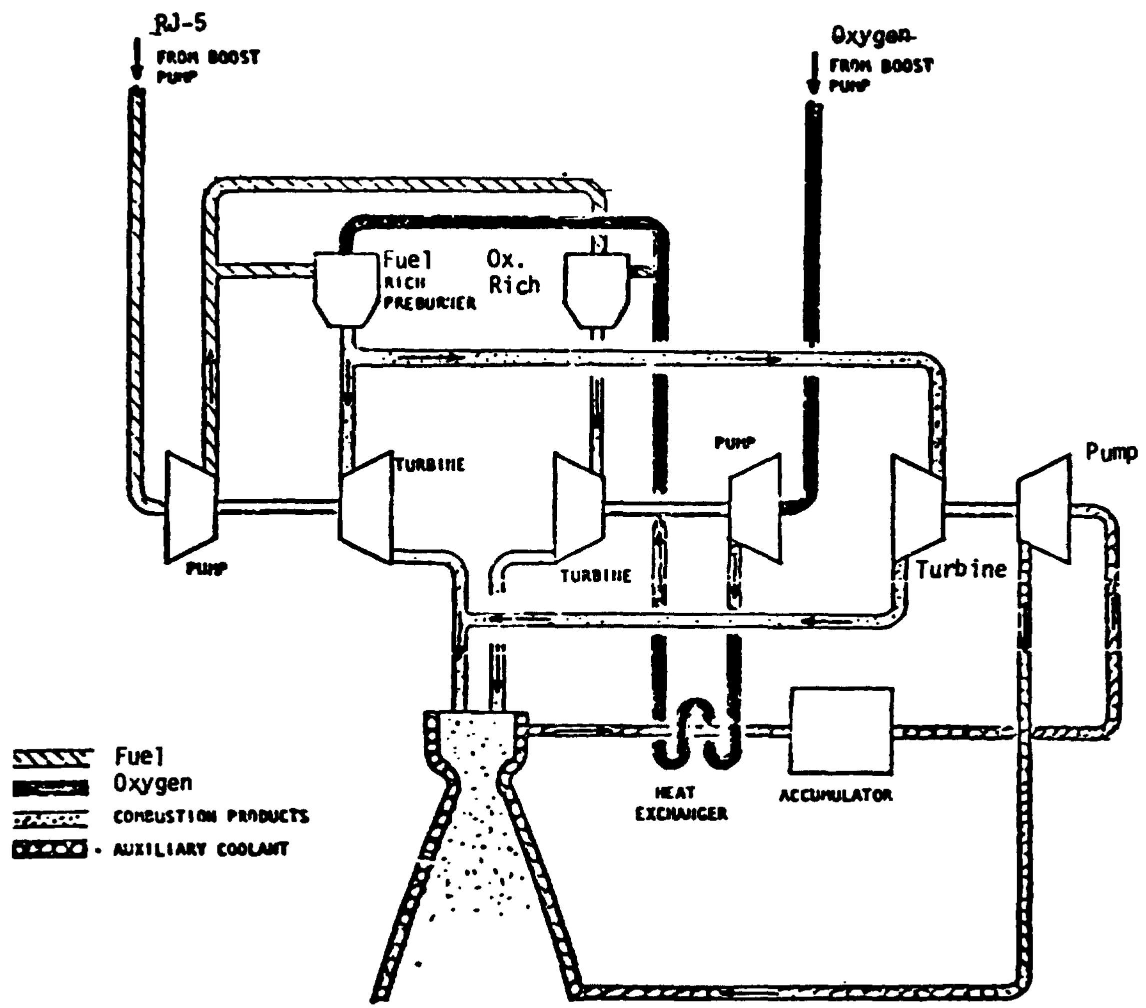

Figure 54. Mode 1 Auxiliary Cooled Engine Cycle Schematic

TABLE LI. - PROPERTIES OF CANDIDATE AUXILIARY COOLANTS

	Water	Sodium-Potassium (NaK 56%)	Lithium
Formula	H_2O	$Na_{.572}K_{.428}$	Li
Molecular Weight	18.01534	29.886	6.939
Freezing Point, °K	273.16	∿278.16	453.69
(°F)	(32.0)	(∿41)	(356.95)
Boiling Point, °K	373.16	∿1086	∿1615
(°F)	(212)	(∿1494)	(∿2448)
Critical Temperature, °K	647.31	∿2542 ± 40**	3173 ± 400
(°F)	(705.47)	(∿4116 ± 72**)	(5252 ± 720)
Critical Pressure, MN/m^2	22.120	∿30.9**	--
(psia)	(3208.2)	(∿4480**)	--
Critical Density, kg/m^3	315.4	∿153**	124 ± 25
(lb/ft^3	(19.69)	(∿9.57**)	7.74 ± 1.56
Vapor Pressure, Liquid at 298.15K, kN/m^2)	3.166	$\sim 9.6 \times 10^{-10}$	$\sim 1.9 \times 10^{-5}$*
(at 77°F, psia)	(0.4592)	($\sim 1.4 \times 10^{-10}$)	($\sim 2.7 \times 10^{-6}$*)
Density, Liquid			
at 298.15K, kg/m^3	997.1	893.8	513.1*
(at 77°F, lb/ft^3)	(62.247)	(55.80)	(32.03*)
Heat Capacity, liquid			
at 298.15K, J/g.K	4.177	1.090	4.341*
(at 77°F, Btu/lb°F)	(0.9983)	(0.2606)	(1.038*)
Viscosity, Liquid			
at 298.15K, $mN.S/m^2$	.8904	∿.888	.609*
(at 77°F, lb_m/ft-sec)	($.5983 \times 10^{-4}$)	($\sim .596 \times 10^{-4}$)	(4.09×10^{-4}*)
Thermal Conductivity, Liquid			
at 298.15K, W/m.K	.6095	∿22.5	42.8*
(at 77°F, Btu/ ft.sec°F)	(9.783×10^{-5})	($\sim 3.61 \times 10^{-3}$)	(6.87×10^{-3}*)

*Values at the freezing point.
**Psuedocritical value calculated by Kay's rule.

(1) Solid Lithium

The density of solid lithium has been obtained over the temperature range of -269°C to the melting point (180.54°C). The data developed by three investigators were combined by AGN to develop a correlating equation covering the entire temperature range. The recommended equation is given below:

$$\rho(s) = 0.560 + 9.243 \times 10^{-6}T \qquad (15)$$

where $\rho(s)$ is in g/cm^3 and T is in degrees Celsius. The standard deviation of the fit is 0.026 g/cm^3. The confidence range at the 95% confidence level is $\pm$ 0.048 g/cm^3 near the melting point, $\pm$ 0.028 g/cm^3 at 0°C, and $\pm$ 0.051 g/cm^3 at -273.15°C.

(2) Liquid Lithium

The density of liquid lithium has been measured over the temperature range from the melting point (180.54°C) to 1125°C. The data developed by four investigators are in very good agreement and were combined by AGN to develop a correlating equation covering the entire temperature range. The recommended equation is given below:

$$\rho_{(\ell)} = 0.124 + 5.306 \times 10^{-3}(2900-T)^{1/2} + 4.135 \times 10^{-5}(2900-T) \qquad (16)$$

where $\rho(\ell)$ is in g/cm^3 and T is in degrees Celsius. The standard deviation of the fit is 0.0018 g/cm^3. The confidence at the 95% confidence level is $\pm$ 0.0040 g/cm^3 near the melting point, $\pm$ 0.0032 g/cm^3 at midrange, and $\pm$ 0.0012 g/cm^3 is the highest temperature range.

b. Specific Heat

(1) Solid Lithium

Data on the specific heat of solid lithium have been collected by the Purdue University Thermophysical Properties Center and correlated to the following recommended equation for the temperature range of 200°K to the melting point (453.69°K).

$$Cp_{(s)} = 0.5248 + 1.2313 \times 10^{-3}\ T \qquad (17)$$

where $Cp_{(s)}$ is in cal/g.°K and T is in °K. The standard deviation of the fit is 0.0421 cal/g.°K.

(2) Liquid Lithium

The enthalpy of liquid lithium has been measured with reference to the ice point over various temperature ranges from near the melting point (180.54°C) to 1226.8°C. The data developed by three investigators are in good agreement and were combined by AGN to develop a correlating equation (third order polynomial) covering the entire temperature range. The recommended enthalpy equation is given below:

$$(H_t - H^\circ_{25^\circ C})_{(\ell)} = 67.184 + 1.0577T - 6.0759 \times 10^{-5}T^2 + 1.782 \times 10^{-8}T^3 \quad (18)$$

where $(H_t - H^\circ_{25^\circ C})_{(\ell)}$ is in cal/g and T is in degrees Celsius.

An equation for the heat capacity (specific heat) of liquid lithium was derived from the above equation by differentiation to give the following recommended equation:

$$C_{p(\ell)} = 1.0577 - 1.2152 \times 10^{-4}T + 5.3477 \times 10^{-8}T^2 \quad (19)$$

where $C_{p(\ell)}$ is in cal/g.°C and T is in degrees Celsius.

c. Thermal Conductivity

The available data on the thermal conductivity of solid and liquid lithium has been critically analyzed at the Thermophysical Properties Research Center at Purdue University. The recommended values developed from that analysis are presented on Page 360 of Ref. 56.

d. Viscosity

The viscosity of liquid lithium has been measured over the temperature range from the melting point (180.54°C) to 1181°C. The data developed by six investigators are in fair agreement and were combined by AGN to develop a correlating equation covering the entire temperature range. The recommended equation is:

$$\log \mu_{(\ell)} = 5.4192 - \frac{155.991}{T} - 1.61506 \log T \quad (20)$$

where $\mu(\ell)$ is in millipoise and temperature is in degrees Kelvin. The relative standard deviation of the fit is 9.1%. The confidence range at the 95% confidence level is ± 0.25 millipoise near the melting point, ± 0.11 millipoise at mid-range, and ± 0.10 millipoise in the highest range investigated.

e. Vapor Pressure

The vapor pressure of liquid lithium has been measured over the temperature range of 935 to 1608°C. The data developed by five investigators are in fair agreement and were combined by AGN to develop the correlating equation covering the entire temperature range. The recommended equation is:

$$\log P_{(\ell)} = -2.1974 - \frac{6499.1}{T} + 1.9390 \log T \quad (21)$$

where $P_{(\ell)}$ is in atmospheres and T is in degrees Kelvin. The relative standard deviation of the fit of the vapor pressure data is 3.3%. The confidence range at the 95% confidence level is ± 1.2×10^{-4} atm for the lowest temperature range, ± 8.2×10^{-4} atm in the mid-range and ± 4.5×10^{-3} atm in the highest temperature range.

The normal boiling point calculated from the above correlating equation is 1342.17°C ± 0.12°C at the 95% confidence level.

2. Thermophysical Properties of NaK (56)

a. Density of Liquid NaK (56)

The density of liquid NaK (56% wt K) is calculated from the following equation (Ref. 57):

$$\rho_{NaK(56)} = 1/1.003 \left(\frac{0.428}{\rho k} + \frac{0.572}{\rho_{Na}}\right) \quad (22)$$

Using data for ρ_k and ρ_{Na} from Ref. 57 the density of NaK (56) has been calculated accordingly. These data are summarized in Table LII.

The data in the table are closely fitted by the following linear equation:

$$\rho_{NaK(56)} = 0.8997-2.376 \times 10^{-4}T \text{ (T in °C)} \quad (23)$$

where ρ is in g/cm^3

b. Viscosity of Liquid NaK(56)

The viscosity of liquid NaK (56% wt K) is calculated from the following equation (Ref. 57):

$$\rho_{NaK(56)} = 1/\left(\frac{0.428}{\mu_k} + \frac{0.572}{\mu_{Na}}\right) \quad (24)$$

Using data for μ_k and μ_{Na} from Ref. 57 the viscosity of NaK(56) has been calculated accordingly. These data are summarized in Table LIII.

In the temperature region up to 400°C (673.16°K) the viscosity data of NaK(56) given in the table are closely fitted by the following equation:

$$\mu\text{(centipoise)} = (0.102079-2.0344 \times 10^{-5}T) \exp\left(0.10438 + \frac{632.01056}{T}\right) \quad (25)$$

where T is in °K and $\leq$ 673.16°K

c. Thermal Conductivity of NaK(56)

The thermal conductivity of a NaK very closely approximating NaK(56) has been published by Ewing, et. al. (Ref. 58) for the temperature range of 200 to 500°C. Ewing's data have been extended to higher and lower temperatures based on data for NaK(78) given in Ref. 57. The recommended thermal conductivity for NaK(56) can thus, be expressed by the following equation:

TABLE LII. - DENSITY OF LIQUID NaK(56)

Temp., °C	Density, g/cm^3	Temp., °C	Density, g/cm^3
50	(0.887)	400	0.8052
100	0.8750	450	0.7932
150	0.8636	500	0.7812
200	0.8521	550	0.7691
250	0.8405	600	0.7570
300	0.8288	650	0.7448
350	0.8170	700	0.7325

TABLE LIII. - VISCOSITY OF LIQUID NaK(56)

Temp., °C	Viscosity, Centipoise	Temp., °C	Viscosity, Centipoise
50	0.749	400	0.2506
100	0.5719	450	0.2296
150	0.4620	500	0.2127
200	0.3900	550	0.1957
250	0.3397	600	0.1818
300	0.3028	650	0.1702
350	0.2746	700	0.1602

$$K(W/cm.°C) = 0.220 + 2.07 \times 10^{-4} T - 2.2 \times 10^{-7} T^2 \quad (26)$$

where T is in °C

This equation represents Ewing's data within an average deviation of 0.4% and maximum deviation of 1.4%.

d. Specific Heat of NaK(56)

The specific heat of liquid NaK alloys can be calculated by the following equation according to (Ref. 57):

$$C_{p(NaK)} = X_{Na} C_{P(Na)} + X_K C_{P(K)} \quad (27)$$

where X_{Na} and X_k are the weight fractions of Na and K, respectively, and $C_{P(Na)}$ and $C_{P(k)}$ are the specific heats of Na and K, respectively.

Based upon the heat capacity equations for Na and K given in (Ref. 57), the heat capacity equation for liquid NaK(56) is evaluated to be as follows:

$$C_{P(NaK-56)} = 0.26325 - 1.1017 \times 10^{-4} T + 1.10026 \times 10^{-7} T^2 \quad (28)$$

where C_p is in cal/g.°C and T is in °C

e. Vapor Pressure of Liquid NaK(56)

The vapor pressure of NaK(56) can be calculated from that of its constituents assuming the validity of Raoult's law (Ref. 57). Based upon vapor pressure correlations for the constituents (Ref. 57), the vapor pressure of NaK(56) was calculated at 100°C increments from 100°C to 1200°C. Those calculated values were then curve-fitted to yield the following vapor pressure expression:

$$\log P(atm) = 4.168548 - \frac{4529.239}{T} \quad (29)$$

where T is in °K

The average deviation between the original calculated values and those calculated from the above equation is 2.44%. The maximum deviation is about 6% but occurs at a temperature where the vapor pressure is very low ($\sim 4 \times 10^{-6}$ atm at 200°C). The calculated normal boiling point is 1086.5°K which is in very good agreement with experimental values.

C. MATERIALS COMPATIBILITY

1. Water

Corrosion data most applicable to the advanced high pressure engine water cooling system is that determined for the structural materials in high pressure, water cooled nuclear reactors. Most of this testing has been conducted on steels, stainless steels and nickel base alloys in autoclaves and recirculating loop systems at temperatures to 617°K (650°F). It was noted that the recirculating systems required filters for the removal of insoluble corrosion products and that water purity is essential for adequate resistance of the austenitic stainless steels to stress corrosion cracking (Ref. 59). Both hydroxide and chloride contaminants will stress crack these materials. The stress corrosion cracking threshold temperature is 394°K (250°F) for 347 and 316 stainless steels in water containing 875 ppm NaCl (Ref. 60). The susceptibility of the austenitic stainless steels, including Incoloy 800, to stress corrosion cracking at 478°K (400°F) in water containing 10 ppm NaCl and 12-17 ppm O_2 is shown by Ref. 61. Nickel-chromium alloys must be utilized if water purity cannot be assured.

Of the high conductivity material candidates for the cooling system, i.e., aluminum alloys, coppers, and nickel, the latter two metals are considered satisfactory for service in high temperature water although stress corrosion data are not generally available and should be determined. Aluminum alloys have low strength at high operating temperatures, and are susceptible to pitting corrosion. The corrosion rates for copper at 373°K (212°F) and nickel at 422°K (300°F) are reported at less than 2 mils per year (MPY) in neutral pH water (Ref. 62). Tests conducted with copper base alloys, namely admiralty brass and cupronickels at 478°K (400°F) in neutral pH water containing less than 10 ppm O_2 indicated negligible corrosion rates (Ref. 62). However, over 90% of the metal in the corrosion product was released to the system.

Titanium alloys and 17-4PH H1025 steel are recommended for pump components where high fatigue strengths and cavitation resistance are required. The titanium alloys are preferred for a lightweight design and for high resistance to corrosion fatigue in the event of water contamination.

Galvanic corrosion effects should be minimal in the cooling system provided aluminum alloys are not utilized as materials of construction. Galvanic corrosion may be enhanced by water impurities other than O_2 through their activating of the passive surfaces of the stainless steels and the nickel-chromium alloys.

2. NaK

Two types of corrosion can occur in NaK coolant circuits; i.e., mass transfer and intergranular attack. The former corrosion mechanism involves the solution of the container material in the hot portion of the system and deposition in the cool portion and occurs when exposure times are sufficient to reach saturated solutions in the hot portion and supersaturated solutions in the cool portions. Intergranular attack involves the formation of corrosion products within the grain boundaries which embrittle and/or weaken the material. Mass transfer corrosion can result in restrictions or plugging of the coolant circuit.

The austenitic stainless steels and the nickel base alloys are satisfactory for long time service to 978°K (1300°F) (Ref. 63). OFHC copper is acceptable for long time service at (700°F) and 867°K (1100°F) for short time service (Ref. 64). Nickel is acceptable as a high conductivity material in sodium (Ref. 65). Titanium is rated as acceptable for long term use to 867°K (1100°F) and for short time use to 1144°K (1600°F) (Ref. 64).

Data on the effect of NaK on the low cycle fatigue life of the engineering alloys is not generally available. Na does not impair the low cycle fatigue life of 316 stainless steel (Ref. 63). Tests conducted on austenitic stainless steels and nickel base alloys to determine their susceptibility to long term cavitation damage in 1089°K (1500°F) Na indicated that the materials were satisfactory with the nickel base alloys sustaining the least cavitation damage (Ref. 66).

3. Lithium

Metals in molten lithium are subject to the same type of attack experienced in Na and NaK. The austenitic stainless steels exhibit severe solution corrosion, intergranular attack and mass transfer above 9/8°K (1300°F) (Ref. 63) and appear to be suitable for limited service at 867°K (1100°F) (Ref. 64). The nickel base alloys are more severly attacked and are not recommended for lithium service. Stress corrosion tests conducted on a number of alloys in lithium at 589°K (600°F) and 756°K (900°F) showed that titanium and the austenitic stainless steels are highly resistant to stress corrosion while the nickel base alloys are highly susceptible (Ref. 67). Copper and its alloys are listed as possessing poor resistance to lithium at 575°K (575°F), only 378°K (220°F) above the melt point of lithium (Ref. 64). Copper is readily dissolved in lithium as evidenced by the copper-lithium phase diagram. The use of copper or its alloys in molten lithium will be limited to short time service, and corrosion rates and mass transfer characteristics must be determined to establish the ti and temperature limits.

D. CHAMBER COOLING

Chamber thermal design analyses studies were conducted for the three candidate auxiliary coolants. The chamber pressure range considered was 272 to 340 atm (4000 to 5000 psia). The Task II results indicated that chamber pressures of at least 272 atm (4000 psia) could be achieved using one of the main engine propellants as coolants. Therefore, if the auxiliary cooled cycle is to be competitive, high chamber pressure must be achieved because of the added system weight and complexity.

The chamber designs differed from those of the Task II studies in two ways. In order to provide simpler designs for Task V, the coolant was assumed to flow in one pass from the injector end to the exit at area ratio 40:1. The number of coolant channels upstream of area ratio 7.6:1 was fixed at 300 for all Task V designs in order to prov... channel widths greater than about 1.52 mm (0.060 in.) As a result, all channel depth/width ratios in the high heat flux regions are well below the 4:1 limit specified in the Task II guidelines.

Design criteria and heat transfer correlations used for the auxiliary coolants are described below.

1. Water Cooling

An inlet pressure of 190 atm (2800 psia) was selected in order to provide subcritical operation with high saturation temperatures, without getting so close to the critical pressure that the heat transfer correlations used might be invalid. Operation at supercritical pressures provides no advantages without considering in detail the reduced heat transfer coefficients and ultimate heat flux limits which occur when the coolant-side wall temperature exceeds the critical temperature; such considerations were beyond the scope of the present study. In order to maintain nucleate boiling, local coolant velocities in the combustion chamber were determined such that maximum coolant heat fluxes did not exceed 80 percent of the burnout heat flux. The burnout correlation used herein was taken from Ref. 68. With nucleate boiling controlling the coolant-side wall temperature to a maximum of 275°K (35°F) above the local saturation temperature, gas-side wall temperatures were below 867°K (1100°F) for all chamber pressures considered. The Dittus-Boelter correlation (Table I of Ref. 45) with bulk coolant properties was used for forced convection heat transfer to water, i.e., when the coolant-side wall temperature was less than the saturation temperature.

A water flow rate of 59 kg/sec (130 lb/sec) was selected based on providing an exit subcooling of at least 272°K (30°F) with 10 percent flow maldistribution. A water inlet temperature of 311°K (100°F) was assumed.

2. Liquid Metal Cooling

A review of the liquid metal heat transfer literature indicated that the most popularly accepted correlation is of the form:

$$Nu_b = Nu_{min} + 0.025\,(Re_b\ Pr_b)^{0.8} \qquad (30)$$

where:

N_u = Nusselt number
R_e = Reynolds number
P_r = Prandtl number
b = Bulk
min = Minimum

with Nu_{min} varying from 4.3 to 7.0. The present studies are based on a Nu_{min} of 5.0 as recommended in Ref. 69 for a number of liquid metals, including dium-potassium alloys. No experimental studies of lithium heat transfer were found.

Gas-side wall temperatures were limited to 867°K (1100°F), as in Task II, due to the significant reduction in zirconium-copper alloy mechanical properties at higher temperatures. In order to meet this limit at area ratio 40:1 with small pressure gradients, outlet bulk temperatures were limited to 756°K (900°F). Based on inlet temperatures of 456°K (360°F) for lithium and 311°K (100°F) for NaK, the resulting flow rates were 54 and 154 kg/sec (120 and 340 lb/sec) respectively.

3. Results and Conclusions

Channel depth profiles and resultant pressure drops were generated based on the above flow rates, heat transfer correlations and design criteria. Pressure drop, coolant bulk temperature rise and maximum wall temperature results are shown on Table LIV.

All three auxiliary coolants were found to be acceptable from a chamber cooling standpoint for chamber pressures as high as 340 atm (5000 psi). Table LIV shows that water and NaK pressure drops are similar and are in the 20 to 48 atm (300-700 psi) range for the chamber pressure range studied. Lithium pressure drops are in the 7 to 20 atm (100-300 psi) range. Note that the nucleate boiling in the water cooled designs maintains the maximum wall temperature below the limit imposed on the liquid metal cooled designs. Although the lithium requires the lowest flow rate and pressure drop, its temperature must be maintained above 454°K (357°F) to prevent freezing. In addition, it should also be emphasized that lithium is incompatible with copper and its alloys at temperatures above 575°K (575°F) for long term use.

E. ENGINE DATA

In addition to the coolant jacket pressure drop data and cycle evaluation guidelines, it was necessary to conduct preliminary heat exchanger analyses to evaluate the pressure drop of this component prior to conducting the engine power balances. The ΔP estimates resulting from this analyses are as follows:

	HEAT EXCHANGER, ΔP	
AUX. COOLANT	LOX, atm (psi)	AUX. COOLANT atm (psi)
Water	15.6 (230)	102 (1500)
Lithium	5.4 (80)	2.0 (30)
NaK	14.3 (210)	5.4 (80)

The pressure drop of each coolant through the heat exchanger was calculated by determining the design velocity necessary to avoid freezing the coolant. LOX, at a 367°K (200°R) inlet temperature, is the other heat exchanger fluid.

For each of the auxiliary coolants, engine cycle power balances were conducted which resulted in the following main pump discharge pressure requirements.

TABLE LIV. - SUMMARY OF TASK V CHAMBER DESIGNS

Coolant	Water		Lithium		NaK	
Flow Rate, kg/sec (lb/sec)	59	(130)	54	(120)	154	(340)
Bulk Temperature Rise, °K, (°F)						
Pc = 272 atm (4000 psia)	518	(473)	547	(525)	689	(781)
Pc = 340 atm (5000 psia)	516	(468)	543	(517)	682	(767)
Outlet Temperature, °K (°F)						
Pc = 272 atm (4000 psia)	574	(573)	747	(885)	745	(881)
Pc = 340 atm (5000 psia)	571	(568)	743	(877)	737	(867)
Pressure Drop, atm (psi)						
Pc = 272 atm (4000 psia)	23.6	(347)	5.6	(82)	18.7	(275)
Pc = 306 atm (4500 psia)	32.4	(477)		--		--
Pc = 340 atm (5000 psia)	43.6	(641)	20	(294)	49.0	(720)
Maximum Wall Temperature, °K (°F)						
Pc = 272 atm (4000 psia)	803	(986)	867	(1100)	867	(1100)
Pc = 340 atm (5000 psia)	831	(1035)	867	(1100)	867	(1100)

Pump Discharge Pressure, atm (psia)

Coolant		LOX		RJ-5		Aux. Coolant	
Water,	Pc = 272 atm (4,000 psia)	497	(7,300)	478	(7,030)	145	(2126)
	Pc = 340 atm (5,000 psia)	748	(11,000)	702	(10,320)	165	(2420)
NaK,	Pc = 272 atm (4,000 psia)	495	(7,280)	478	(7,030)	37	(545)
	Pc = 340 atm (5,000 psia)	762	(11,200)	710	(10,440)	67	(990)
Lithium,	Pc = 272 atm (4,000 psia)	483	(7,100)	475	(6,980)	19.7	(290)
	Pc = 340 atm (5,000 psia)	714	(10,500)	692	(10,170)	34.1	(502)

With the discharge pressure requirements determined, engine weight and envelope estimates were made. For the same LOX pump discharge pressure as the baseline LOX cooled, Mode 1 engine, the auxiliary cooled cycles can achieve a higher thrust chamber pressure (i.e., 313 atm (4600 psia) vs 272 atm (4000 psia)). However, for comparative purpose to the other Mode 1 engines considered in Task III, a chamber pressure of 272 atm (4000 psia) was selected for the data summary.

Table LV summarizes pertinent auxiliary cooled engine cycle data. At a thrust chamber pressure of 272 atm (4000 psia), the engine performance is identical to the baseline engine. The maximum difference in auxiliary cooled system weights is about 136 kg (300 lbs.) The auxiliary cooled system weight includes the following components:

- Pump and Turbine
- Heat Exchanger
- Accumulator
- Lines
- Coolant

Because the main pump discharge pressures are reduced compared to the baseline, the basic LOX/RJ-5 components weigh 2058 kg (4537 lbs.). However the weight of the auxiliary components result in increased engine weight compared to the baseline as shown below:

Coolant	Baseline LOX		Water		Lithium		NaK	
	Weight, kg (lbs.)							
Basic Engine	2130	(4696)	2058	(4537)	2058	(4537)	2058	(4537)
Aux. Coolant System	-	-	277	(610)	177	(390)	310	(683)
Total	2130	(4696)	2335	(5147)	2235	(4927)	2368	(5220)

TABLE LV. - TASK V AUXILIARY COOLED ENGINE SUMMARY

Engine Sea-Level Thrust, MN (lb)	2.07	(607,000)
Engine Specific Impulse, sec		
Sea-Level		321.3
Vacuum		347.4
Chamber Pressure, atm (psia)	272	(4000)
Nozzle area ratio		40
Engine Length, cm (in.)	312	(123)
Nozzle Exit Dia, cm (in.)	168	(66)
Pump Envelope Dia, cm (in.)	191	(75)
Engine Weight, kg (lb)		
Water	2335	(5147)(1)
Lithium	2235	(4927)
NaK	2368	(5520

(1)Most viable candidate.

This data shows that the weight differences between auxiliary cooled systems are minor and the NaK system is the heaviest because flow rate requirements are the highest. This results in a greater wet weight.

Although the lithium cooled system results in the lightest engine weights, operational problems would seem to preclude its use. For example, the melting point of lithium is 454°K (357°F). This means that upon engine shutdown, the lithium will solidify in the system unless it is heated. This, of course, would create a severe power drain on the vehicle. Because of handling and safety considerations, it is advisable to maintain a closed environment with both lithium and NaK. Therefore, dumping of these coolants upon engine shutdown is not feasible. Water can be dumped to avoid its freezing. This can result in some equivalent weight saving since the weight of the water, approximately 72.6 kg (160 lbs), need not be carried throughout the entire vehicle trajectory.

Because of the handling, operational and corrosivity problems associated with using lithium and NaK and weight differences are relatively minor, water is obviously the superior auxiliary coolant.

SECTION VIII

TASK VI - ENGINE PRELIMINARY DESIGN

Based on the results of the parametric studies, three engine concepts were selected to be investigated and characterized further in a preliminary engine design effort. In addition, RP-1, rather than RJ-5, was selected as the baseline fuel for all three engines.

The three selected engine concepts are:

1. Baseline LOX/RP-1 Mode 1 Engine
2. Dual-Fuel Engine
3. Alternate Mode 1 Hydrogen Cooled, Gas Generator Cycle Engine

A. OBJECTIVES AND GUIDELINES

The objectives of this task were to provide engine preliminary designs and data for the three candidate engine concepts. The designs include preliminary layouts of the engine assemblies and the major engine components. The data includes the performance, mass property, envelope, and operational characteristics of the engines and their components.

The guidelines used in this preliminary design study are:

- Engine Performance

  Based upon JANNAF Methodology

- Engine System Pressure Losses

  Same as Task III

- Thrust Chamber

  Same as Task II (Table XXXIII).

- High Pressure Pumps

  Inducers and/or impellers utilized in the high pressure pumps shall be designed for operation above incipient cavitation.

  Impeller burst speed shall be at least 20% above the maximum operating speed.

  Impeller effective stress at 5% above the maximum operating speed shall not exceed the allowable .2% yield stress. (Does not apply to areas in which local yielding is permitted.)

- <u>Low Pressure Pumps</u>

  Inlet Flow Coefficient: .06 (Minimum)
  Inlet Flow Maximum Velocity:

$$LH_2,\ C_m = \sqrt{\frac{2gNPSH}{1.3}} \tag{31}$$

$$LOX,\ C_m = \sqrt{\frac{2gNPSH}{2.3}} \tag{32}$$

$$\text{MODE 1 FUELS},\ C_m = \sqrt{\frac{2gNPSH}{3.0}} \tag{33}$$

- <u>Turbines</u>

Blade root steady-state stress shall not exceed the allowable 1% 50 hour creep stress.

Stress state at the blade root as defined by the steady-state stress and an assumed vibratory stress equal to the gas bending stress shall be within the allowable stress range diagram or modified Goodman diagram.

No blade natural frequencies within ± 15% of known sources of excitation at steady-state operating speeds.

Disk burst speed shall be at least 20% above the maximum operating speed.

Disk maximum effective stress at 5% above the maximum operating speed shall not exceed the allowable .2% yield stress. (Does not apply to areas in which local yielding is permitted.)

- <u>Bearings</u>

  Turbopump designs shall utilize rolling element bearings.

  Maximum DN: Same as Task III (Table XXXVIII)

- <u>Seals</u>

  Turbopump designs shall utilize conventional type seals.

Face Contact Seal Maximum PV, FV, and P_fV Factors: Same as Task III (Table XXXIX).

- General

Components which are subject to a low cycle fatigue mode of failure shall be designed for a minimum of 250 cycles times a safety factor of 4.

Components which are subject to a fracture mode of failure shall be designed for a minimum of 250 cycles times a safety factor of 4.

Components which are subject to a high cycle fatigue mode of failure shall be designed within the allowable stress range diagram (based on the material endurance limit.) If stress range material property data are not available, modified Goodman diagrams constructed as shown below shall be utilized.

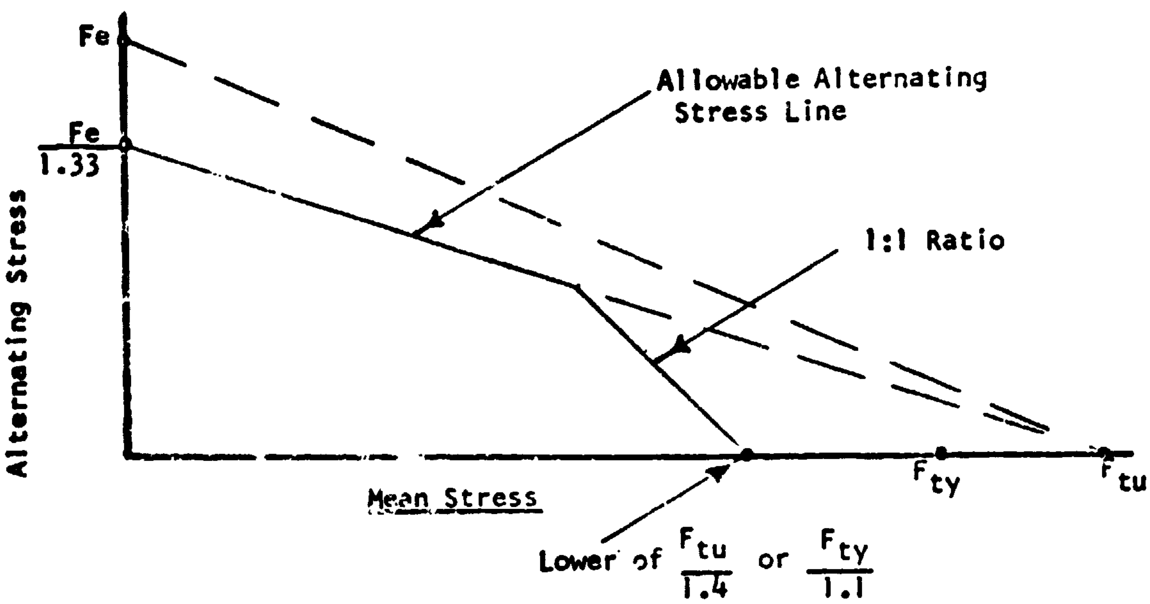

Fe = Material Endurance Limit
F_{ty} = Material Yield Strength (.2% offset)
F_{tu} = Material Ultimate Strength

Effective stress shall be based on the Mises-Hencky constant energy of distortion theory.

Unless otherwise noted under component ground rules specified herein, the following minimum factors of safety shall be utilized:

Factor of Safety (.2% yield) = 1.1 x Limit Load
Factor of Safety (Ultimate) = 1.4 x Limit Load
Limit Load: The maximum predicted load or pressure at the most critical operating condition.

Components subject to pressure loading shall be designed to the following minimum proof and burst pressures:

Proof Pressure = 1.2 x Limit Pressure
Burst Pressure = 1.5 x Limit Pressure

B. BOOST PUMP DRIVE SELECTION

1. Low Speed Pump Drive Method

In order to minimize turbomachinery weight, a low speed boost pump is used to permit the main or high speed turbopump to operate at its optimum speed. The purpose of this study was to determine the most appropriate drive method for the low speed boost pump. This included trade-offs to determine the effect of alternate boost pump drive methods and design point net positive suction head levels on engine weight, complexity, performance, start transient characteristics and boost pump inlet diameter.

The boost pump drive methods considered are:

a. Gear Drive
b. Hydraulic Turbine Drive
c. Gas Turbine Drive

The hydraulic turbine is powered by fluid tapped off from an interstage station of the high speed pump.

The gas turbine is powered by hot gas from the preburner. In order to avoid complex seal problems, gas from the fuel-rich preburner is used in the low speed fuel pumps and gas from the oxidizer-rich preburner to drive the low speed LOX pump. No other gas supply was considered in the study.

Only single reduction gear train configurations were considered in the gear train study.

The engine boost pump trade study was initiated prior to the selection of RP-1 as the baseline fuel. Therefore, much of the effort was concentrated on the original LOX/RJ-5 baseline engine. However, the results and selections made are not affected by the fuel change to RP-1.

a. Cycle and Engine Performance Considerations

As anticipated, the low speed pump power requirement is quite small compared to the high speed pump power requirement. This is illustrated below for the original baseline LOX/RJ-5 engine:

FLUID	NPSH M (ft)	Pump Head Requirement, M (ft) LOW * SPEED	HIGH SPEED	RATIO LOW SPEED HEAD / TOTAL HEAD
LOX	4.0 (16)	99.1 (325)	5608 (18,400)	0.0174
RJ-5	14.0 (46)	77.4 (254)	4785 (15,700)	0.0159

*Estimated low speed pump head rise required for a high speed pump suction specific speed of 4.14 RPMX $(M^3/sec)^{1/2}xM^{-3/4}$ (20,000 RPM x $GPM^{1/2}$ x $Ft^{-3/4}$)

The energy extraction from the cycle required to drive the boost pumps is directly dependent on the efficiency of the drive system. Estimated drive efficiencies are:

DRIVE METHOD	DRIVE EFFICIENCY
Gears	0.98
Hydraulic Turbine	0.50 - 0.65
Gas Turbine	0.50 - 0.70

Although the gear drive is the most efficient, the efficiency of the turbine drives are high enough to warrant further consideration. A range of efficiencies is indicated for the turbine drives to illustrate the effect of the turbine type on efficiency. For the gas turbines, turbine tip speed and the number of stages are the principle variables. Due to the low speed of the boost pump, optimum tip speeds require relatively large diameter turbines and consequently result in high weight.

For the hydraulic turbine drive, the efficiency indicated is the product of the turbine efficiency and the efficiency of the pump supplying the working fluid. As with the gas turbine, the efficiency achievable is dependent primarily on tip speed and number of stages.

Because the boost pump drive system power requirement is small, differences between the boost pump drive methods on the engine cycle balance and performance is negligible for any reasonably achievable drive efficiency. Therefore, the choice of a boost pump drive method must be based on other considerations.

b. Start Transient and System Complexity

A gas turbine drive, in which the hot gas is bled from the preburner, would undoubtedly require hot gas valves for flow control during the engine start transient. As presently conceived, a hydraulic turbine drive would not require any flow control device other than a trim orifice in the turbine supply line to assure a specific operating speed. A gear drive is ideal in the sense that speed control is definite. The gear drive, however, requires that the low speed and high speed pump are attached. This restricts the pump packaging and mounting arrangements with the thrust chamber and preburner assemblies.

Although significant development problems would not be anticipated with gears operating in RJ-5 (or RP-1) and possibly LH_2, the use of gears in LOX would undoubtedly require comprehensive design studies and experimental development.

c. Engine Weight Considerations

The relative weights of the low speed LOX pump drive system which are based upon comparisons of preliminary sizes to historical data are:

DRIVE METHOD	DRIVE WEIGHT, kg (lb)
Gear	13.6 (30)
Liquid Turbine	36.3 (80)
Gas Turbine*	544 (1200)

*Drive gas from preburner

The gear drive is clearly the lightest in weight, but for the LOX sys ·n a devel‿pment program would be required to validate the concept feasibility.

The gas turbine drive is unacceptably heavy. The weight is high because of the very high turbine inlet pressures, 340 to 408 atm (5000 to 6000 psi), and high inlet temperature, 867 to 922°K (1560 to 1660°R).

d. Low Speed Pump Drive Method Selection

In order to maintain flexibility in the turbomachinery packag g arrangement, while still achieving a good low speed pump drive effici :y, the hydraulic turbine drive was selected for all propellants. Figure illustrates the manner in which fluid is tapped from the high pressure pump t drive the hydraulic turbine.

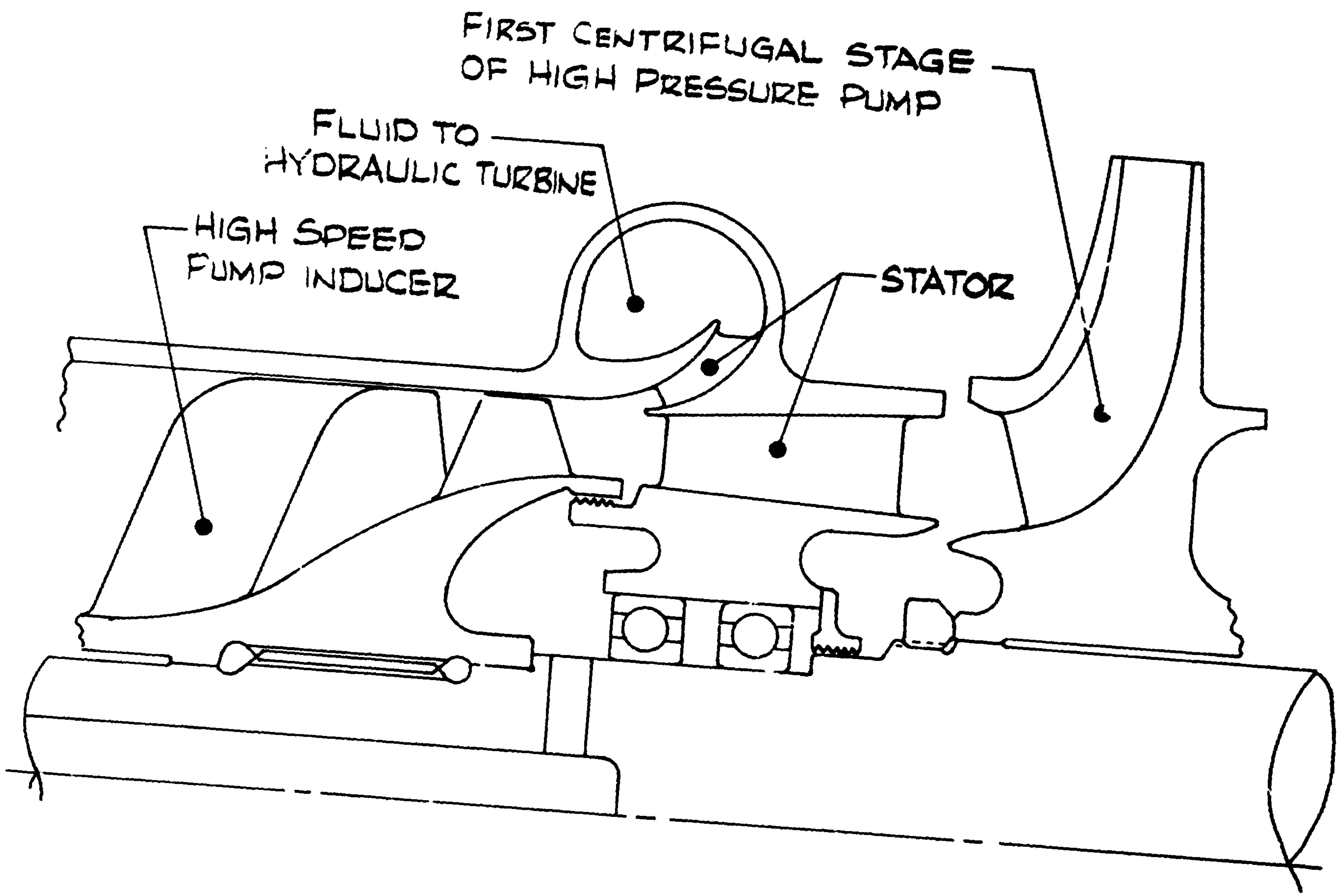

Figure 55. High Speed Pump Configuration Concept for Tap-Off of Hydraulic Turbine Drive Fluid

C. BOOST PUMP NPSH EFFECTS

Low speed hydraulic turbine driven boost pump preliminary designs which were generated for each of the three engine concepts are discussed in Section VIII.E. For each of the boost pumps, analyses were conducted to determine the effect of varying design point NPSH on boost pump operating characteristics, weight, and diameters. The following net positive suction head levels were investigated:

	NPSH, M (ft)		
LOX	0.61 (2)	2.4 (8)	4.9 (16)
LH_2	10.1 (33)	39.6 (130)	78.6 (258)
RP-1	13.7 (45)	16.2 (53)	19.8 (65)

1. Boost Pump Design Point Conditions

Design point suction specific speeds were selected to minimize the likelyhood of encountering cavitation induced flow and pressure oscillations. Magnitudes selected for the preliminary design effort were as follows:

Propellant	Suction Specific Speed(1) $\frac{RPM\ (M^3/sec)^{1/2}}{M^{3/4}}$	$\frac{RPM\ (GPM)^{1/2}}{Ft^{3/4}}$
RP-1	5.2	25,000
LOX	6.2	30,000
LH_2 (Dual-Fuel)	8.9	43,000
LH_2 (Alternate Mode 1)	6.0	29,000

(1) These units will be used throughout this section without further identification.

Head rise requirements of the boost pumps were determined by specifying high speed pump operating suction specific speeds of 4.14 (20,000) along with allowance for ducting pressure losses. This resulted in the following magnitudes:

Propellant	Boost Pump Head, ΔH M	(Ft.)
RP-1	112.8	370
LOX	99.1	326
LH_2 (Dual-Fuel)	613	1800
LH_2 (Alternate Mode 1)	324	950

Boost pump inlet diameters were established within the criteria for inlet velocity as a function of NPSH specified in the guidelines, i.e.,

Propellant	Max, Inlet Velocity, C_m
RP-1	$C_m = \sqrt{\frac{(NPSH)\ 2g}{3.0}}$
LOX	$C_m = \sqrt{\frac{(NPSH)\ 2g}{2.3}}$
LH_2	$C_m = \sqrt{\frac{(NSPH)\ 2g}{1.3}}$

Hydraulic turbine flow was selected to be 20 percent of the low speed pump flow. The head of the high speed pump inducer (and turbine head) was selected commensurate with hydraulic turbine efficiency, line losses, and trim orifice requirements. This was estimated to be approximately eight times the low speed pump head.

2. Analysis and Results

In conducting the analysis, flow, head rise, inlet flow coefficient, inlet hub-tip ratio, and suction specific speed were held constant at the design point magnitudes. Pump speed was determined from the suction specific speed relationship as a function of NPSH. The inlet diameter was then calculated for the design point inlet flow coefficient and hub-tip ratio. The impeller discharge tip speed was calculated as a function of head rise by establishing the head coefficient as a function of stage specific speed (Figure 56). The mean impeller outlet diameter was then calculated from the tip speed/pump speed relationship. For the constant flow, constant head boost pump conditions, weight was estimated to vary with the cube of inlet diameter.

Figures 57, 58, and 59 show the effects of NPSH on the low speed turbopump weights and figures 60 and 61 show the effects on inlet and outlet diameters. The NPSH range for each pump corresponds to an inlet pressure range of approximately 1.07 atm (15.7 psia) to 1.54 atm (22.7 psia). As indicated in the figures, significant increases in LOX and LH_2 boost pump weight and impeller diameters occur as NPSH is reduced. Because of the lower vapor pressure of RP-1, the NPSH is relatively high even at the lower inlet pressures and the change in RP-1 pump weight and diameter is much smaller.

D. ENGINE DESIGN AND OPERATING SPECIFICATIONS

This section describes the engine system characteristics of all three engine concepts selected for preliminary design efforts.

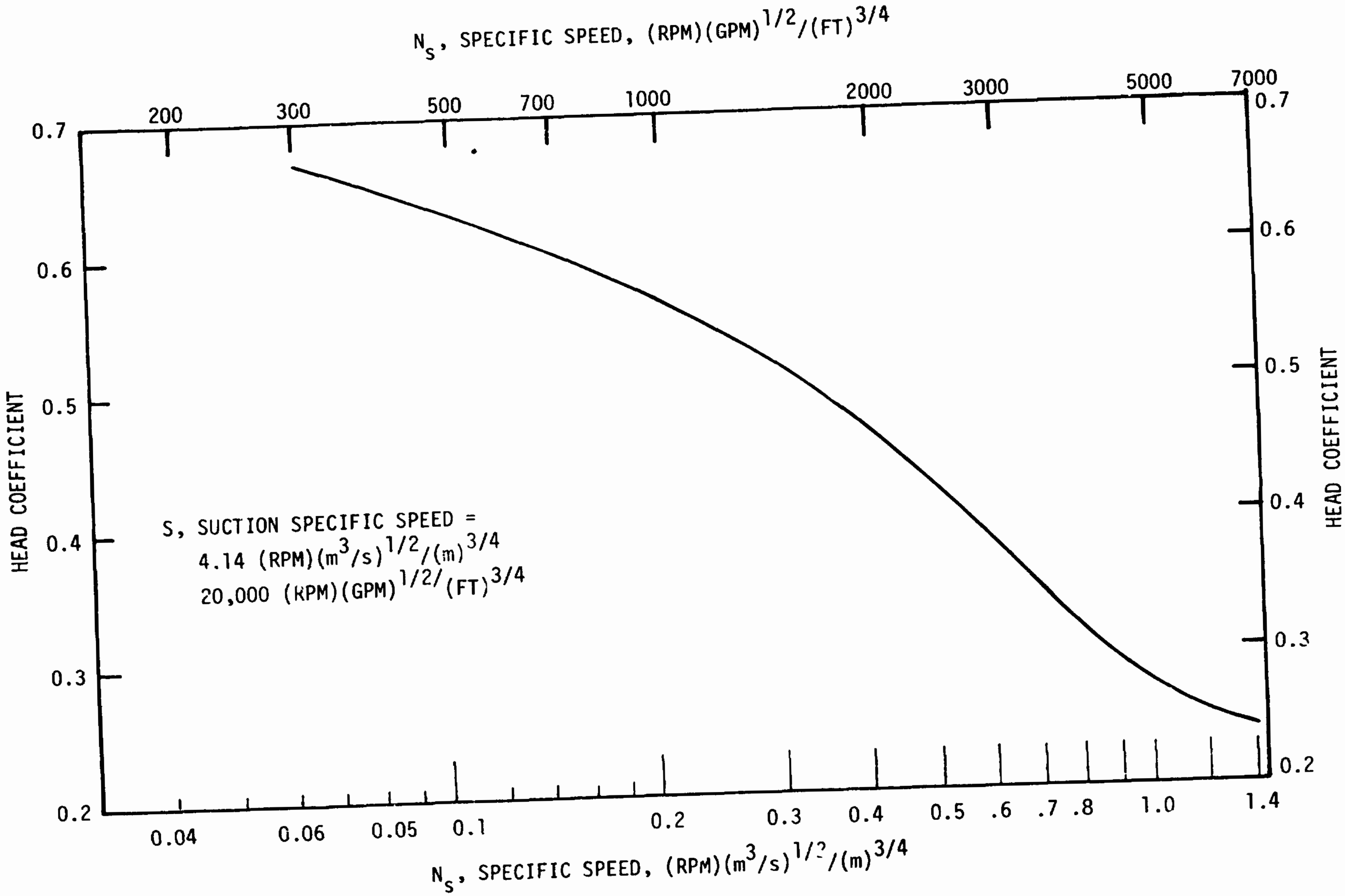

Figure 56. Head Coefficient vs Specific Speed

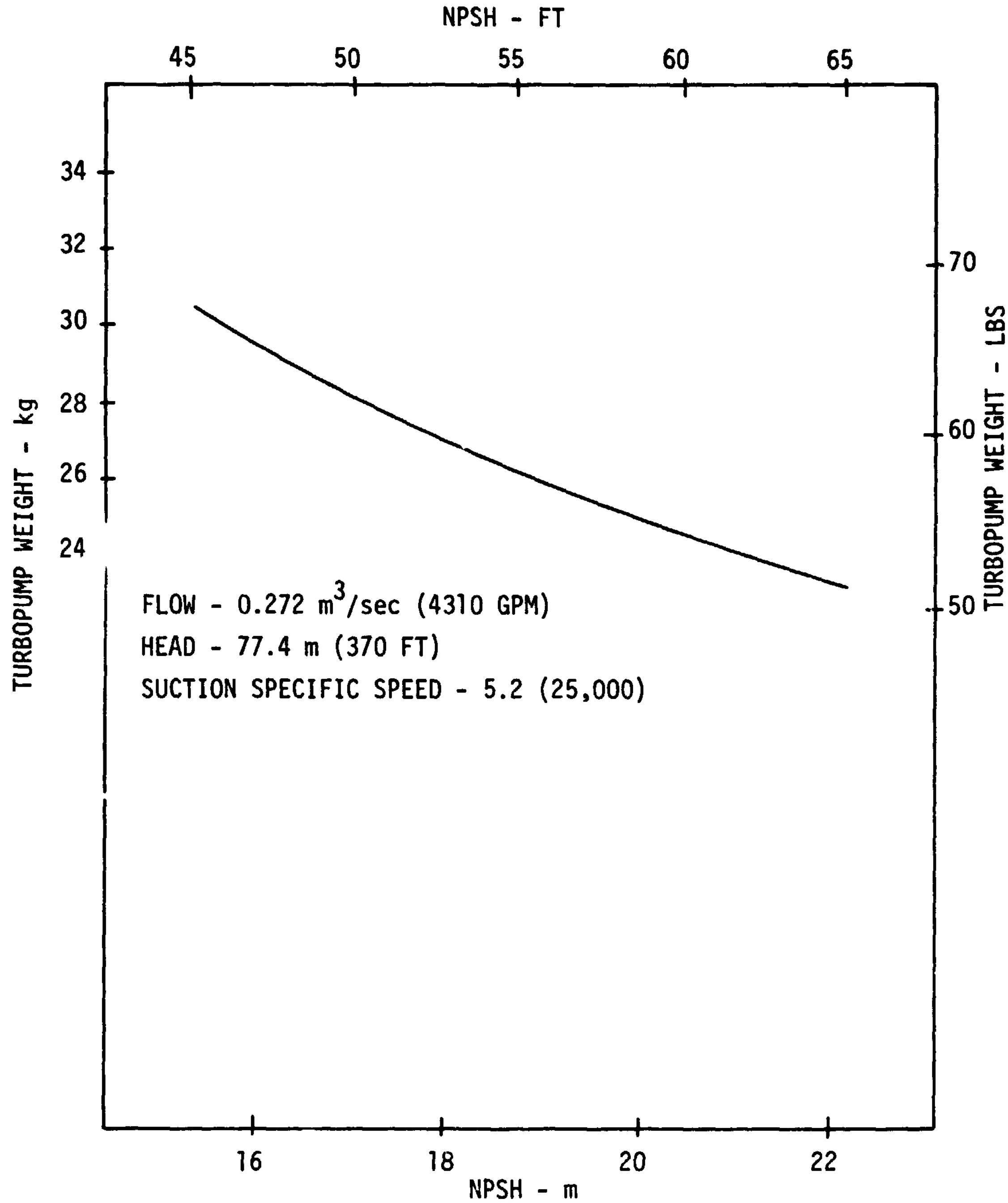

Figure 57. Effect of NPSH on Low Speed RP-1 Turbopump Weight

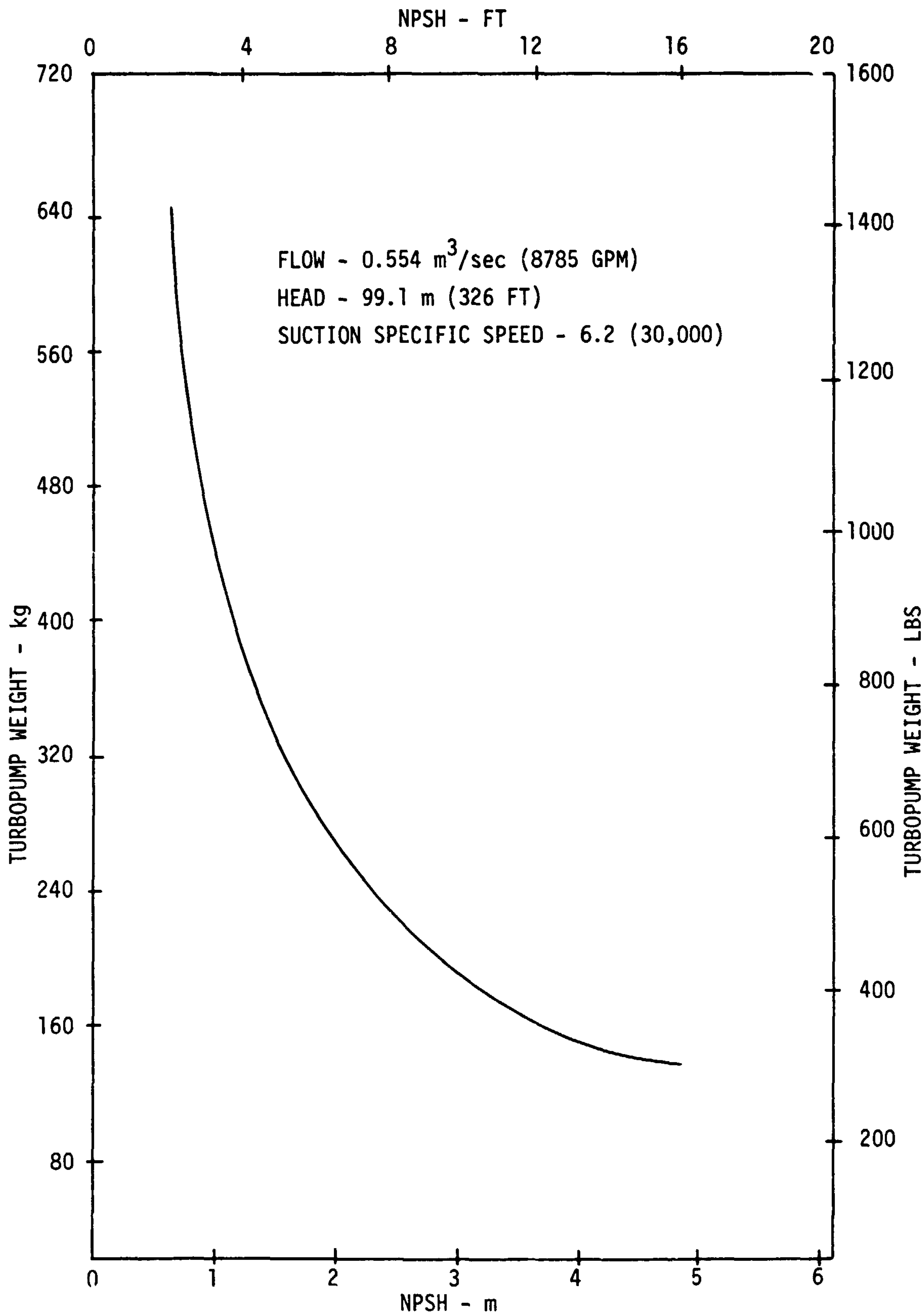

Figure 58. Effect of NPSH on Low Speed LOX Turbopump Weight

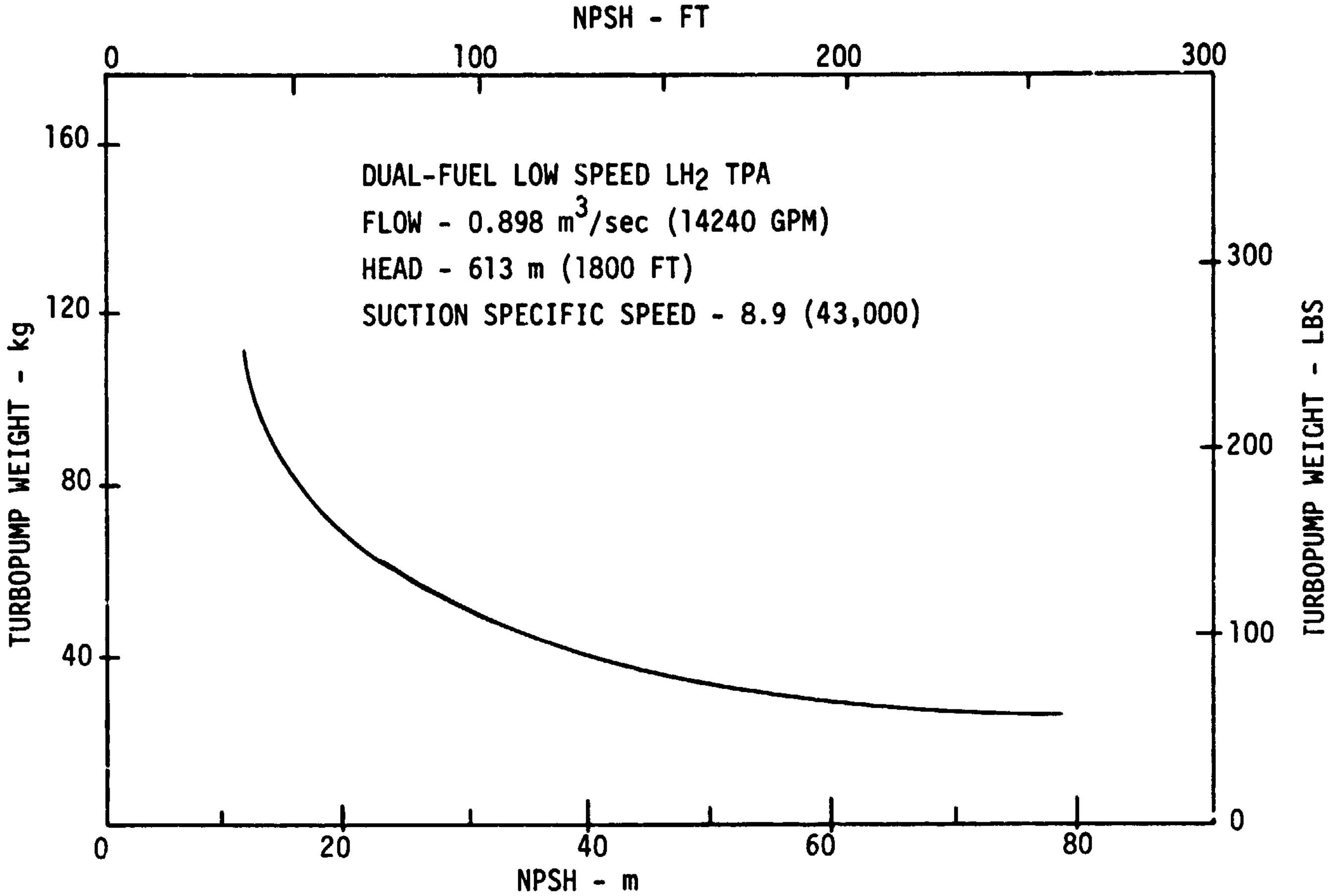

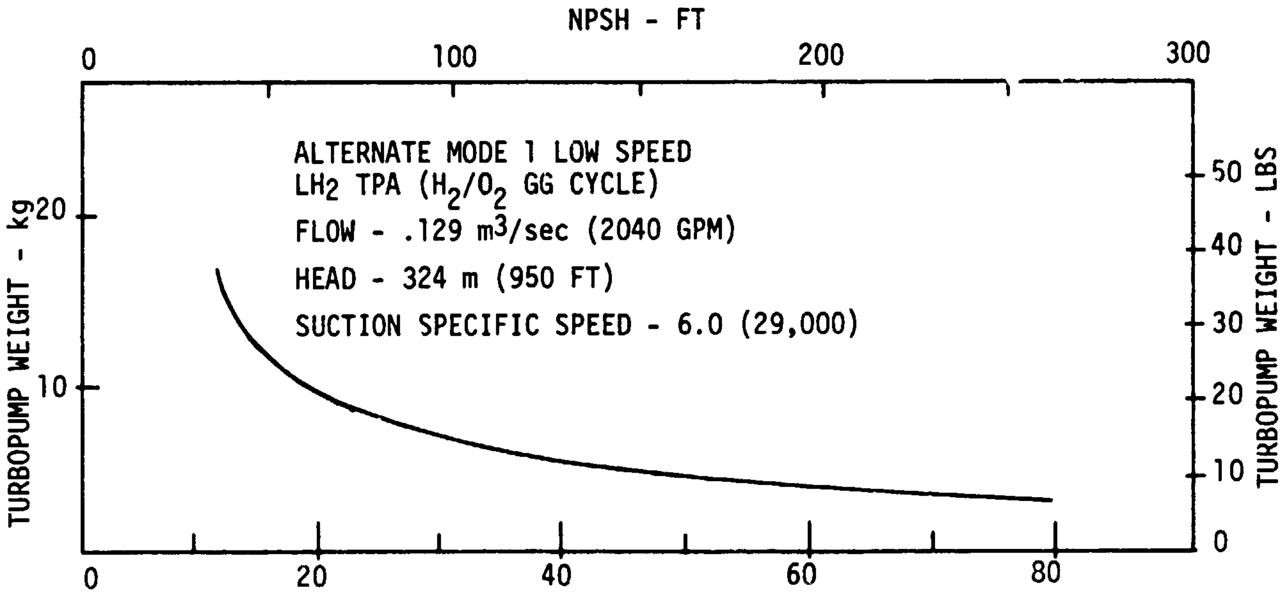

Figure 59. Effect of NPSH on Low Speed LH_2 Turbopump Weight

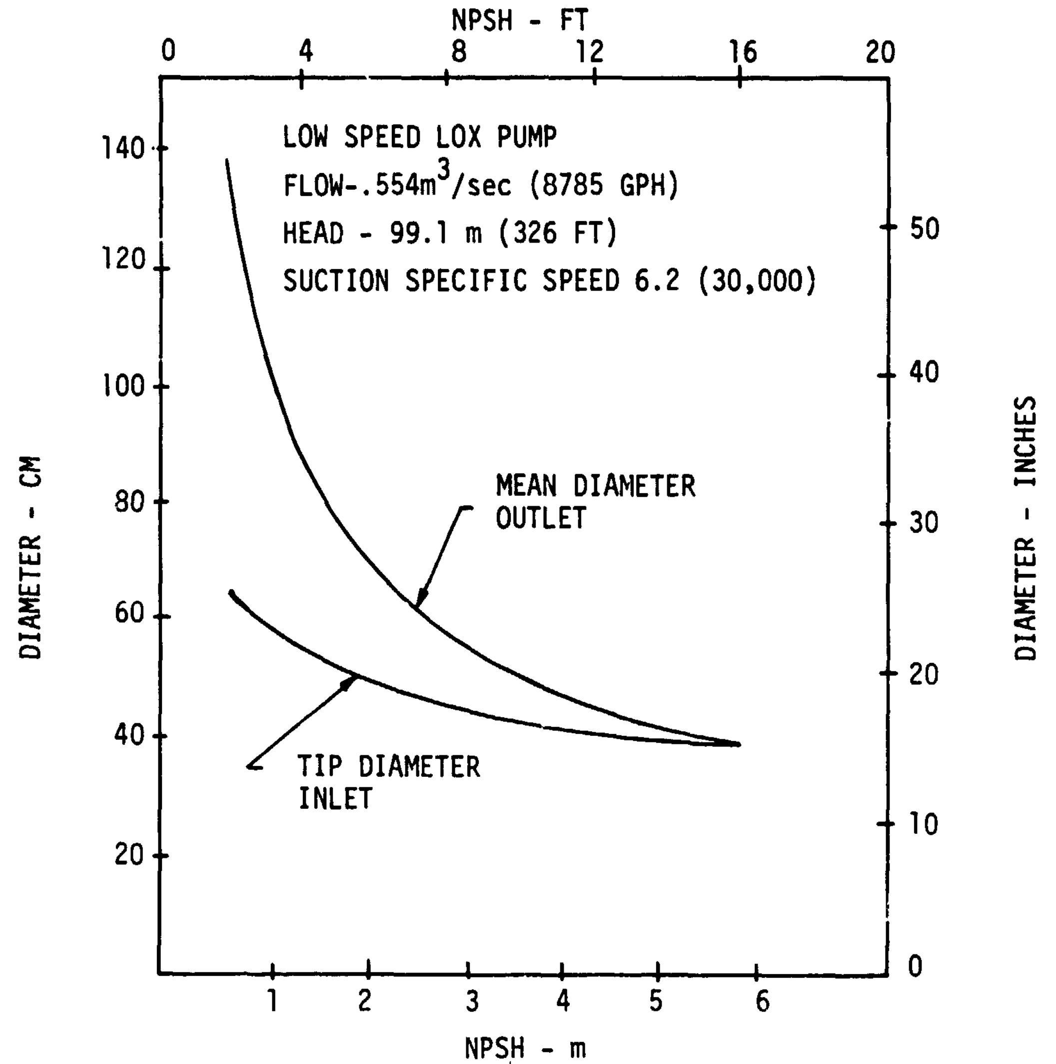

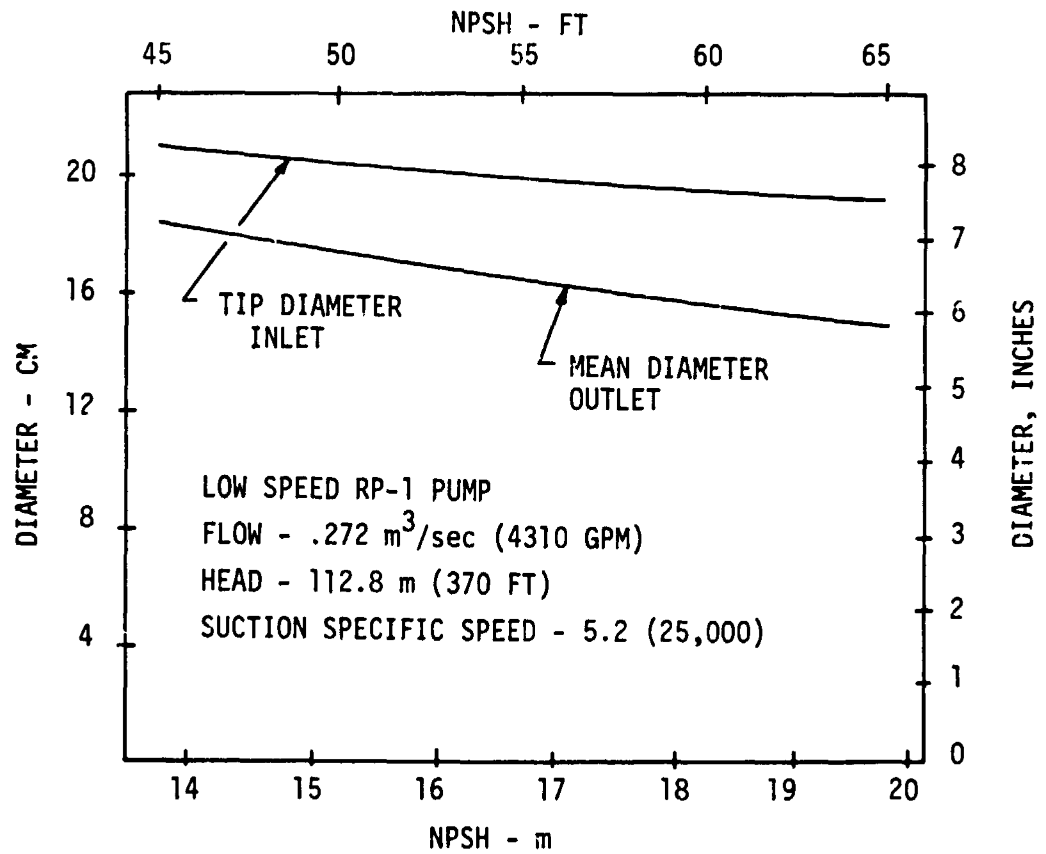

Figure 60. Effect of NPSH on Low Speed LOX & RP-1 Pump Impeller Diameters

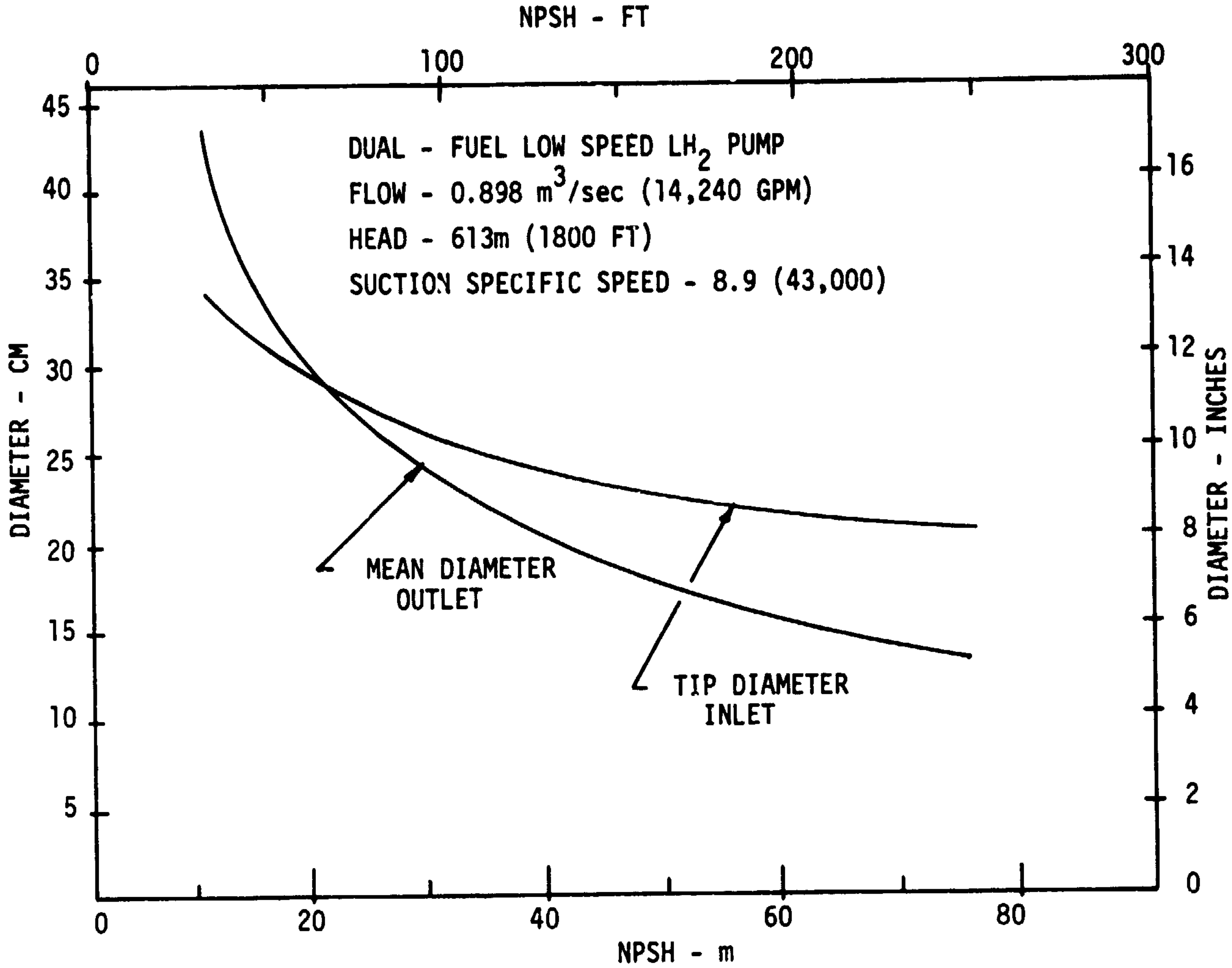

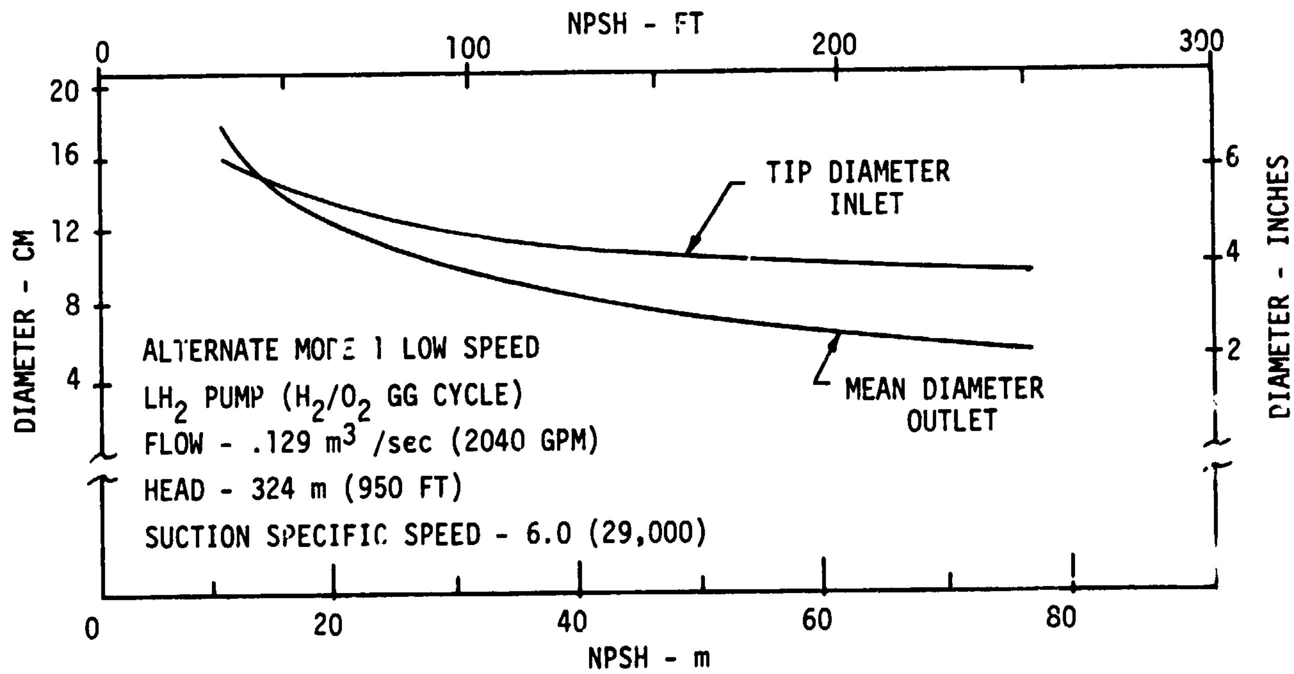

Figure 61. Effect of NPSH on Low Speed LH_2 Pump Impeller Diameters

1. Mode 1 LOX/RP-1 Baseline Design

a. Configuration and Nominal Operating Conditions

The engine cycle for the Mode 1 Baseline engine design is a dual preburner staged combustion cycle with a LOX cooled thrust chamber. The engine schematic is shown on Figure 62 including the engine control requirements which basically consist of main fuel and oxidizer valves. Cycle balance is obtained by orifices in the fuel-rich preburner propellant lines.

The preliminary assembly drawing of the baseline engine is shown on Figures 63 and 64. The main feature is the sidemounted TPA's and boost pump assemblies Hot gas ducting is minimized through completely integrated TPA's which are mounted to the engine by means of the hot gas cross-over ducts. The TCA is totally regeneratively cooled with LOX. The TCA design incorporates a slotted zirconium copper chamber to a nozzle area ratio of 15:1. A two pass Inconel 718 tube bundle is used from here to the 40:1 nozzle exit area ratio. The coolant is introduced at an area ratio of 1.5:1 and flows up to the plane of the injector face. The coolant is collected and introduced at the area ratio of 1.5 to cool the nozzle. The coolant exits from the tube bundle at an area ratio of 15:1 and is then introduced into the preburners.

The design details for the principal components are presented in appropriate paragraphs of this section.

The gimballed envelope was evaluated for a 10° square pattern and is also shown on Figure 63. The results indicated a 240.2 cm (94.6 in.) square requirement.

The Mode 1 baseline engine nominal operating specifications are shown on Table LVI and an engine pressure schedule for nominal operation is shown on Table LVII.

b. Engine Operation and Control

Each of the engine cycles were examined to establish the main control requirements. Particular attention was given to the start and shutdown sequences. The LOX/RP-1 modes of operation are patterned after F-1 (Ref. 70) and Titan I (Ref. 71) engine experience. The primary concern with these propellants is to keep contaminants out of the LOX manifolds. Therefore, all LOX/RP-1 combustors are started oxidizer-rich to reduce the chance of RP-1 entering the oxidizer circuits.

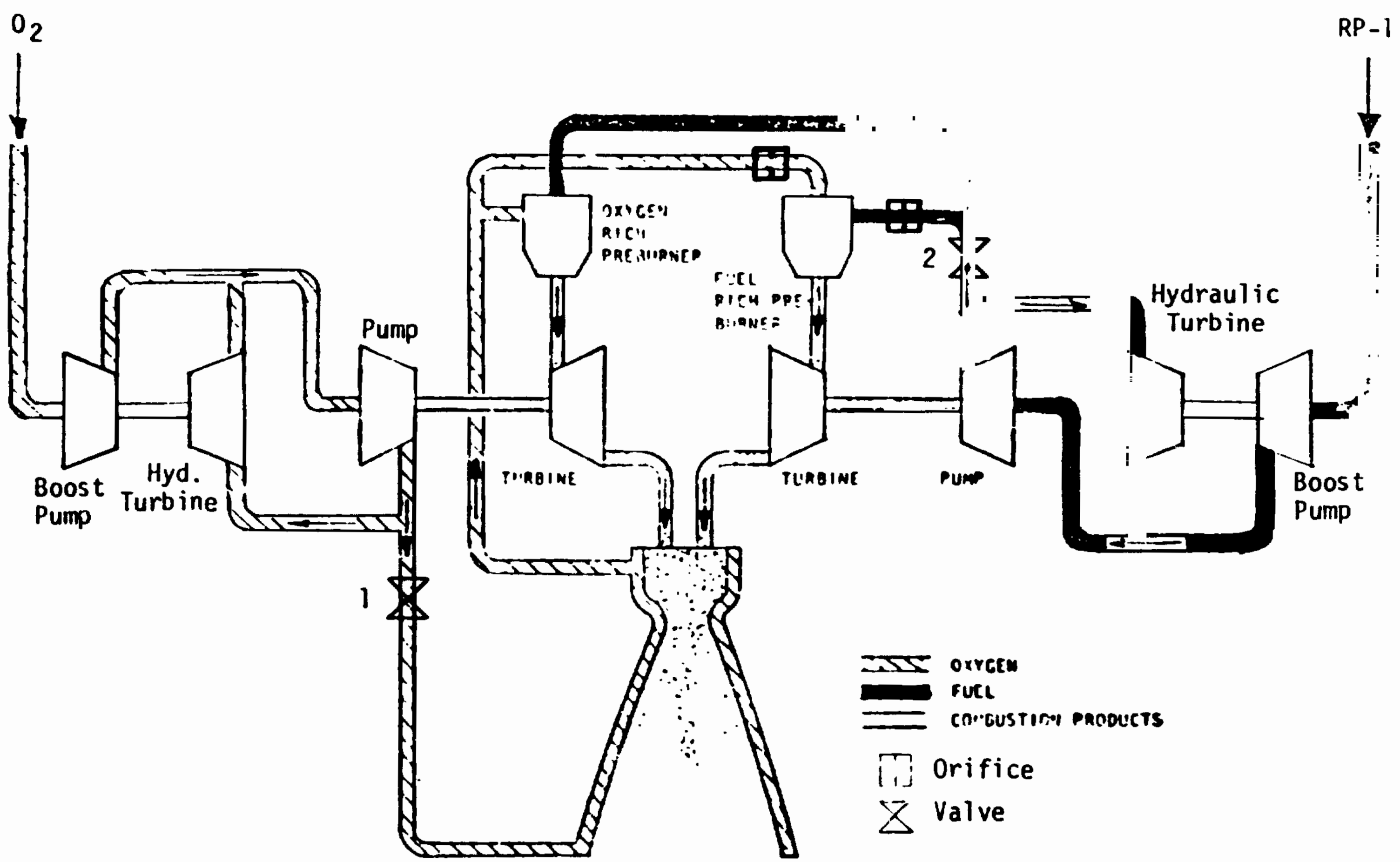

Figure 62. Baseline LOX/RP-1 Mode 1 Engine Cycle Schematic

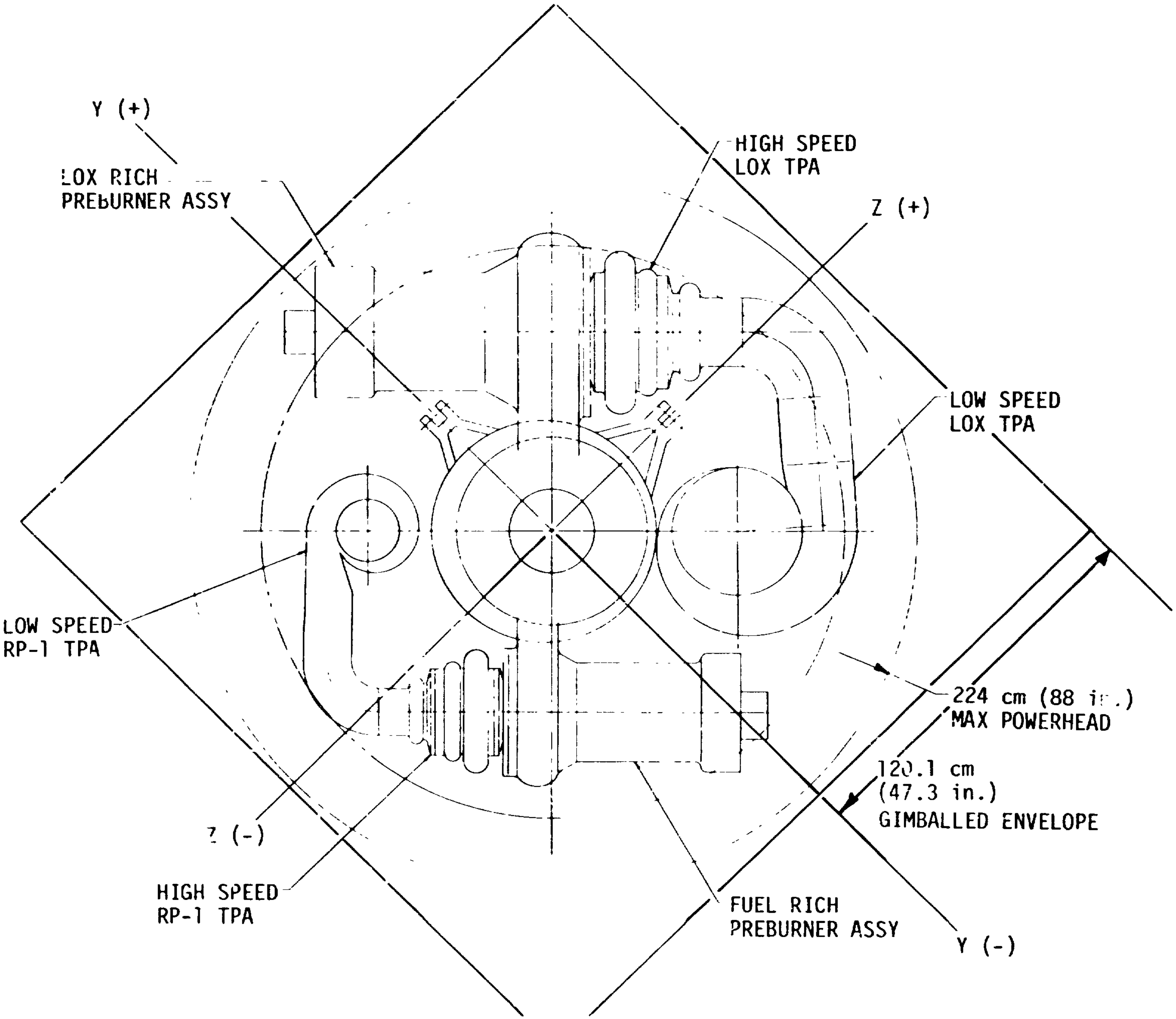

Figure 63. Mode 1 LOX/RP-1 Baseline Engine Assembly (Top View)

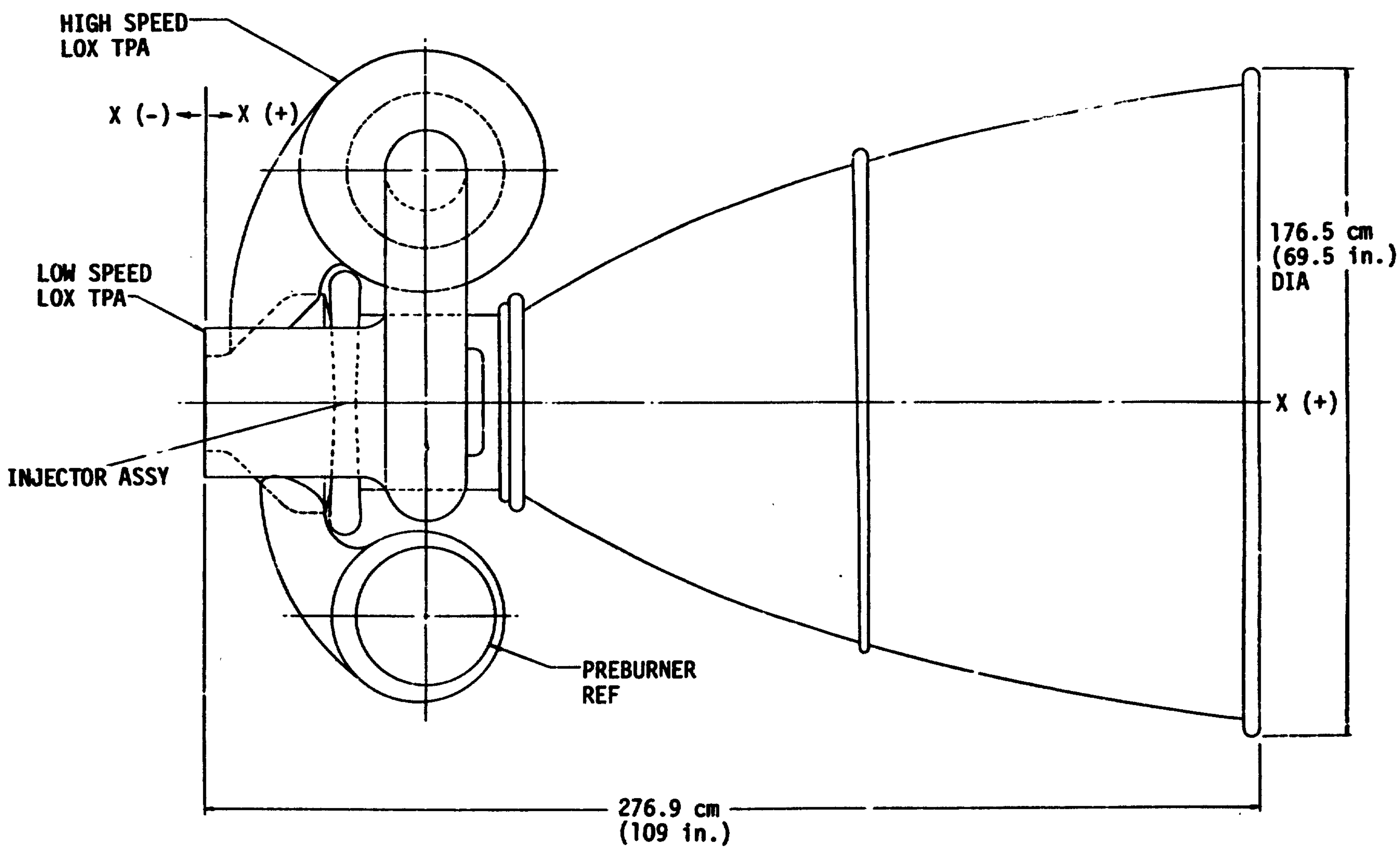

Figure 64. Mode 1 LOX/RP-1 Baseline Engine Assembly (Side View)

TABLE LVI. - MODE 1 LOX/RP-1 ENGINE OPERATING SPECIFICATIONS

Nominal MR = 2.9

Engine		
Sea-Level Thrust, MN (lb)	2.70	(607,000)
Vacuum Thrust, MN (lb)	2.926	(657,700)
Sea-Level Specific Impulse, sec	323.6	
Vacuum Specific Impulse, sec	350.6	
Total Flow Rate, kg/sec (lb/sec)	850.9	(1,875.8)
Mixture Ratio	2.9	
Oxidizer Flow Rate, kg/sec (lb/sec)	632.7	(1,394.8)
Fuel Flow Rate, kg/sec (lb/sec)	218.2	(481.0)
Thrust Chamber		
Sea-Level Thrust, MN (lb)	2.70	(607,000)
Vacuum Thrust, MN (lb)	2.926	(657,700)
Sea-Level Specific Impulse, sec	323.6	
Vacuum Specific Impulse, sec	350.6	
Chamber pressure, atm (psia)	272.2	(4,000)
Nozzle Area Ratio	40	
Mixture Ratio	2.9	
Throat Diameter, cm (in.)	26.314	(10.36)
Nozzle Exit Diameter, cm (in.)	166.421	(65.52)
Coolant Jacket Flow Rate (LOX), kg/sec (lb/sec)	632.7	(1,394.8)
Coolant Jacket ΔP, atm (psi)	126.9	(1,865)
Coolant Inlet Temp., °K (°R)	111.1	(200)
Coolant Exit Temp., °K (°R)	202.8	(365)
Injector Ox.-Rich Gas Flow Rate, kg/sec (lb/sec)	600.6	(1,324.1)
Injector Fuel-Rich Gas Flow Rate, kg/sec (lb/sec)	250.3	(551.7)
Chamber Length, cm (in.)	24.765	(9.75)
Chamber Diameter, cm (in.)	41.605	(16.38)

TABLE LVI (cont.)

Preburners	LOX/RP-1 Ox.-Rich		RP-1/LOX Fuel-Rich	
Chamber Pressure, atm (psia)	440.8	(6,479)	439	(6,452)
Combustion Temperature, °K (°R)	922	(1,660)	867	(1,560)
Mixture Ratio	45.0		0.22	
Oxidizer Flow Rate, kg/sec (lb/sec)	587.5	(1,295.3)	45.1	(99.5)
Fuel Flow Rate, kg/sec (lb/sec)	13.1	(28.8)	205.1	(452.2)
Turbines	LOX Pump		RP-1 Pump	
Inlet Pressure, atm (psia)	440.8	(6,479)	439	(6,452)
Inlet Temperature, °K (°R)	922	(1,660)	867	(1,560)
Total Gas Flow Rate, kg/sec (lb/sec)	600.6	(1,324.1)	250.3	(551.7)
Gas Properties				
C_p, specific heat @ constant pressure, J/kg °K (Btu/lb °R)	1100	(0.263)	3209	(0.767)
γ, Ratio of specific heats	1.31		1.095	
Shaft Horsepower mhp (HP)	59,725	(58,900)	25,502	(25,150)
Efficiency, %	80		80	
Speed, rpm	15,100		25,300	
Pressure Ratio (total to static)	1.49		1.484	
Main Pumps	LOX		RP-1	
Total Outlet Flow Rate, kg/sec (lb/sec)	632.7	(1,394.8)	218.2	(481.0)
Volumetric Flow Rate, m^3/sec (gpm)	0.556	(8,820)	0.273	(4,330)
NPSH, m (ft.)	89.3	(293)	110.9	(364)
Suction Specific Speed (RPM)$(m^3/sec)^{1/2}/(m)^{3/4}$	4.14	(20,000)[a]	4.14	(20,000)[a]
Speed, rpm	15,100		25,300	

TABLE LVI (cont.)

Main Pumps (cont.)	LOX		RP-1	
Discharge Pressure, atm (psia)	632.8	(9,300)	551.1	(8,100)
Number of Stages	2		2	
Specific Speed, (RPM)$(m^3/sec)^{1/2}/(m)^{3/4}$	0.31	(1,500)[a]	0.31	(1,500)[a]
Total Head Rise, m (ft)	5660	(18,570)	7013	(23,010)
Efficiency, %	82		82	
Low Speed TPA				
Pumps				
NPSH, m (ft)	4.88	(16)	19.81	(65)
Inlet Flow Rate, kg/sec (lb/sec)	632.7	(1,394.8)	218.2	(481.0)
Outlet Flow Rate, kg/sec (lb/sec)	759.2	(1,673.8)	261.8	(577.2)
Discharge Pressure, atm (psia)	12.4	(182)	10.2	(150)
Hydraulic Turbine				
Inlet Pressure, atm (psia)	92.9	(1,365)	77.6	(1,140)
Outlet Pressure, atm (psia)	12.4	(182)	10.2	(150)
Flow Rate, kg/sec (lb/sec)	126.6	(279.0)	43.6	(96.2)
Speed, rpm	2560		8715	

[a] $(RPM \times GPM^{1/2} \times FT^{-3/4})$

TABLE LVII. - MODE 1 LOX/RP-1 BASELINE ENGINE PRESSURE SCHEDULE

Nominal MR = 2.9

Preburner	Ox-Rich				Fuel-Rich			
Propellant	LOX		RP-1		LOX		RP-1	
Pressure, atm (psia)								
Main Pump Discharge	632.8	(9,300)	551.1	(8,100)	632.8	(9,300)	551.1	(8,100)
Main Shutoff Valve Inlet	632.8	(9,300)	551.1	(8,100)	632.8	(9,300)	551.1	(8,100)
ΔP Shutoff Valve	6.33	(93)	5.51	(81)	6.33	(93)	5.51	(81)
Valve Outlet	626.4	(9,207)	545.6	(8,019)	626.4	(9,207)	545.6	(8,019)
ΔP Line	2.72	(40)	2.72	(40)	2.72	(40)	2.72	(40)
Coolant Jacket Inlet	623.7	(9,167)		--	623.7	(9,167)		--
ΔP Coolant Jacket	127.6	(1,875)		--	127.6	(1,875)		--
Coolant Jacket Outlet	496.1	(7,292)		--	496.1	(7,292)		--
ΔP Line	2.72	(40)		--	2.72	(40)		--
Preburner Control Inlet		--		--	493.4	(7,252)	542.9	(7,979)
ΔP Control		--		--	5.65	(83)	26.4	(388)
Preburner Inlet	493.4	(7,252)	542.9	(7,979)	487.8	(7,169)	516.5	(7,591)
ΔP Preburner	52.6	(773)	102.1	(1,500)	48.9	(717)	77.5	(1,139)
Turbine Inlet	440.8	(6,479)			439	(6,452)		
ΔP Turbine (Total to Static)	145	(2,131)			143.2	(2,104)		
Main Injector Inlet (Total)	295.8	(4,348)			295.8	(4,348)		
ΔP Injector	23.7	(348)			23.7	(348)		
Chamber Pressure	272.2	(4,000)			272.2	(4,000)		

The engine start and shutdown sequence is presented on Table LVIII. The sequence of operations listed are assumed to occur after the vehicle prevalves have been opened and the cryogenic components have been chilled down to the main engine shutoff valves.

c. Start and Shutdown Data

The engine start and shutdown transients were also estimated. The staged combustion cycle engines were assumed to be chilled down and bled-in to the main chamber valves prior to receipt of the fire signal. These engines were then assumed to be started under tank head. The transient estimates are based upon the analytical modeling of similar engine configurations on the ALRC Liquid Engine Transient Simulation (LETS) model.

The start and shutdown transient data is summarized on Table LVIX. Start to 90% of rated thrust and shutdown down to 5% of rated thrust are generally specified values to establish transient times.

d. Design and Off-Design Engine Performance

The design and off-design engine performance at the design thrust level for $\pm$ 10% MR excursions are presented on Table LX. The nominal engine operating mixture ratio is 2.9. A requirement for the engine to operate over the entire mixture ratio range inflight was not identified during the course of this study. Therefore, for this analysis, it was assumed that the preburner flow orifice sizes are changed to operate at the various mixture ratios. Continuous inflight operation over the entire MR range would result in higher engine pressure drop requirements.

e. Engine Mass Properties Data

The engine mass properties data, consisting of the engine weight breakdown, gimballed moments of inertia and center of gravity location, were computed from the preliminary engine and component layout drawings.

The weight breakdown for the baseline engine is shown on Table LX1.

The center of gravity in the axial direction was calculated to be 62 cm (24.4 inches) from head-end of the gimbal.

TABLE LVIII. - SEQUENCE OF OPERATIONS BASELINE LOX/RP-1

Start

1. Purge Oxidizer Lines and Manifolds in Fuel and Ox. Rich Preburners.
2. Energize Spark Igniters.
3. Open Main Ox. Valve (#1).*
4. Open Igniter Valves on Fuel and Ox. Rich Preburners.
5. Open Main (RP-1) Fuel Valve (#2).

Shutdown

1. Close Main Ox. Valve (#1).
2. Initiate Ox. Purge.
3. Close Main (RP-1) Fuel Valve (#2).
4. Close Igniter Valves on Fuel and Ox. Rich Preburners.
5. Cutoff Igniter Spark Energy.

*Note: Numbers refer to valves on Figure 62.

TABLE LIX. - MODE 1 LOX/RP-1 BASELINE START AND SHUTDOWN TRANSIENT DATA SUMMARY

Start to 90% F		
Time, sec	2.52	
Total Start Impulse, kg-sec (lb-sec)	69,000	(152,000)
LOX Consumption, kg (lb)	129.3	(285)
RP-1 Consumption, kg (lb)	120.2	(265)
Shutdown to 5% F		
Time, sec	0.50	
Total Shutdown Impulse, kg-sec (lb-sec)	80,800	(178,200)
LOX Consumption, kg (lb)	162.4	(358)
RP-1 Consumption, kg (lb)	73.0	(161)

TABLE LX. - MODE 1 LOX/RP-1 BASELINE ENGINE DESIGN AND OFF-DESIGN MR PERFORMANCE

$\epsilon = 40$

Engine	Mixture Ratio 2.61		Mixture Ratio 2.90		Mixture Ratio 3.19	
Sea-Level Thrust, MN (lb)	2.70	(607,000)	2.70	607,000	2.70	(607,000)
Vacuum Thrust, MN (lb)	2.93	(658,700)	2.926	657,700	2.924	(657,300)
Sea-Level Specific Impulse, sec	321.7		323.6		321.1	
Vacuum Specific Impulse, sec	349.1		350.6		347.7	
Total Flow Rate, kg/sec (lb/sec)	855.9	(1886.9)	850.9	(1875.8)	875.5	(1890.4)
Fuel Flow Rate, kg/sec (lb/sec)	237.1	(522.7)	218.2	(481.0)	204.7	(451.2)
Oxidizer Flow Rate, kg/sec (lb/sec)	618.8	(1364.2)	632.7	(1394.8)	652.8	(1439.2)
Chamber Pressure, atm (psia)	277.5	(4,078)	272.2	(4,000)	270.3	(3,973)

TABLE LXI. - MODE 1 LOX/RP-1 BASELINE ENGINE WEIGHT STATEMENT

Component	Weight kg	Weight (lb)
Gimbal	95.7	(211)
Main Injector	293.0	(646)
Copper Chamber and Nozzle (ε = 14.7)	124.3	(274)
Tube Bundle Nozzle (ε = 14.7 to 40)	112.9	(249)
Fuel Rich Preburner	80.7	(178)
Oxidizer Rich Preburner	99.8	(220)
Fuel Valves and Actuation	36.3	(80)
Oxidizer Valves and Actuation	54.4	(120)
Low Speed LOX TPA	136.1	(300)
Low Speed RP-1 TPA	23.1	(51)
High Speed LOX TPA	382.8	(844)
High Speed RP-1 TPA	145.2	(320)
Hot Gas Manifold	91.6	(202)
Low Pressure Lines	89.8	(198)
High Pressure Lines	118.8	(262)
Ignition System	27.2	(60)
Miscellaneous	200.5	(442)
TOTAL	2112.2	(4657)

The center of gravity and gimballed moments of inertia for the engine are summarized below.

	Axis					
	X		Y		Z	
Center of Gravity	cm	(in)	cm	(in)	cm	(in)
	62	(24.4)	3.50	(1.2)	10.4	(4.1)

	X - X		Y - Y		Z - Z	
Gimballed Inertia	$kg\text{-}m^2$	($slug\text{-}ft^2$)	$kg\text{-}m^2$	($slug\text{-}ft^2$)	$kg\text{-}m^2$	($slug\text{-}ft^2$)
	661.2	(487.8)	862.5	(636.3)	760.5	(561.1)

The coordinate system is defined on Figures 63 and 64.

2. Dual-Fuel Engine Design

a. Configuration and Nominal Operating Conditions

This engine concept is peculiar to mixed mode propulsion systems since the Mode 1 and Mode 2 propellants utilize a common thrust chamber and LOX feed system. A schematic (without boost pumps) is shown on Figure 65. The engine uses a LOX cooled thrust chamber, gaseous propellant main injection and dual preburners in both operating modes. The LOX TPA has two preburners; one for each mode of operation. Mode 1 operation utilizes a nozzle area ratio of 40:1 and Mode 2 a 200:1 retractable nozzle extension.

The TCA design uses a slotted zirconium copper chamber to a nozzle area ratio of 15:1. An Inconel 718, two pass, tube bundle is used from 15:1 to an area ratio of 40:1. The coolant flow path is the same as the baseline design. The nozzle extension is regeneratively cooled with LOX from the 40:1 point to an area ratio of 132:1 and radiation cooled from here to the exit. Columbium is used as the material throughout the radiation cooled section.

The schematic identifies the control valves required for engine operation in both Mode 1 and Mode 2. This engine concept is exclusively used for a series burn application and the Mode 2 feed system has to be isolated during Mode 1 operation. This affected the number and location of the valves.

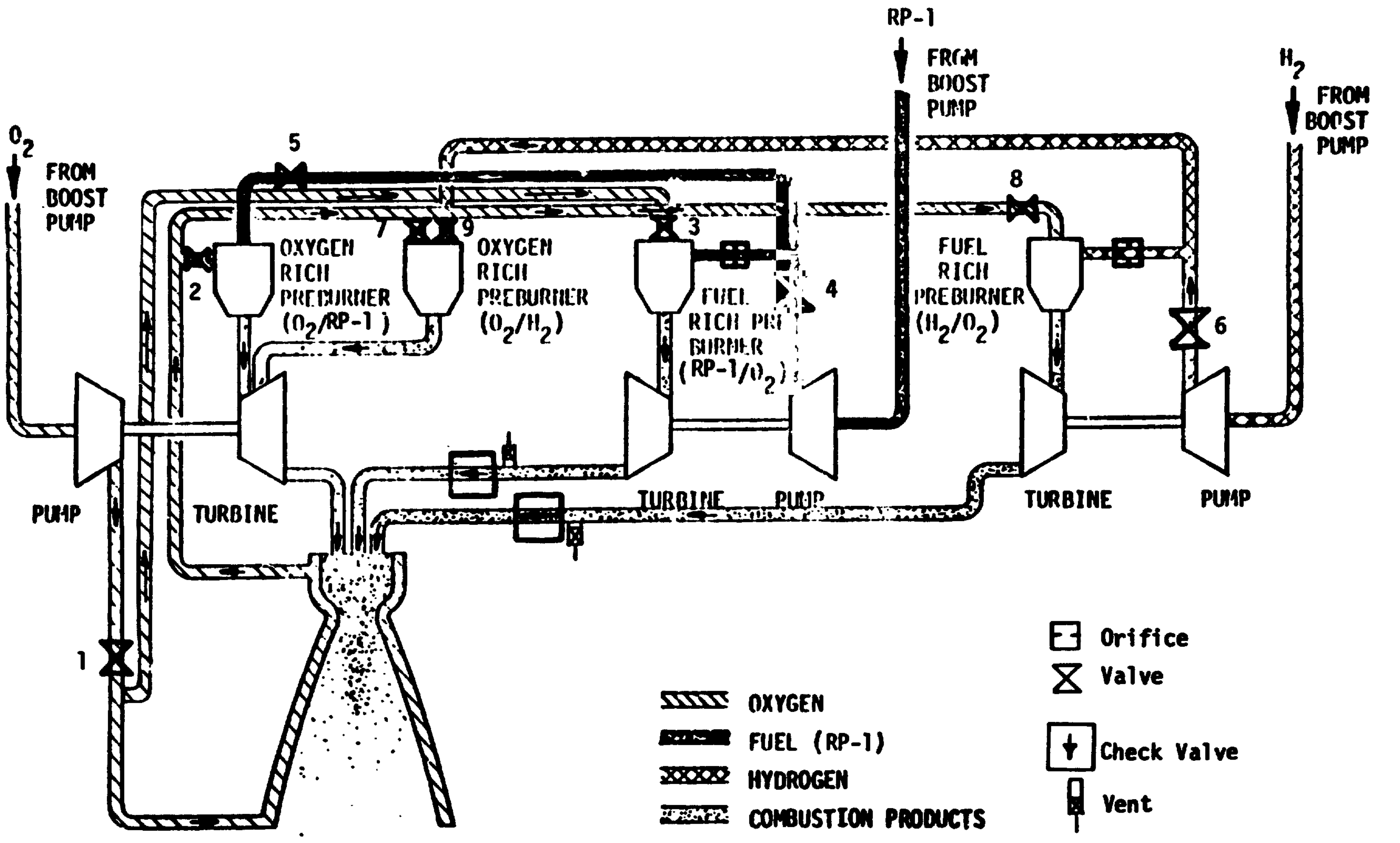

Figure 65. Dual-Fuel, Oxygen Cooled Engine Cycle Schematic

The preliminary layout of the dual-fuel engine is shown on Figures 66 and 67. The engine features fixed boost pumps for all three propellants clustered around the engine gimbal center. The TPA's are side mounted with their axis perpendicular to the thrust axis in order to obtain favorable center of gravity location. The preliminary layout indicates the split and stored length of the extendible nozzle.

The engine envelope data is summarized below.

Engine Length, cm (in.)	
Fixed Nozzle	307 (121)
Extendible Nozzle Retracted	734 (289)
Extendible Nozzle Deployed	879 (346)
Nozzle Exit Diameter, cm (in.)	176.5/392 (69.5/154.5)

The gimballed envelope was evaluated for a 10° square pattern in Mode 1 and a 7° square pattern in Mode 2. The resulting square dimensions are:

	GIMBAL ANGLE	ENVELOPE CM (in.)
Fixed Nozzle	10°	433 (170.6)
Retracted Nozzle	10°	504 (198.4)
Deployed Nozzle	7°	494 (194.6)

The engine operating conditions for the engine nominal design point are presented in Table LXII for both the Mode 1 and Mode 2 engine operation.

The engine pressure schedules for Mode 1 and Mode 2 nominal engine operation are presented in Table LXIII and Table LXIV.

b. Engine Operation and Control

The study of the dual-fuel engine resulted in the identification of additional controls for not only operational purposes but to prohibit the flow of hot gases through inactive components. For example, when the oxygen-rich preburner is operating with LOX/RP-1, valves 7 and 9 (Figure 65) must be closed to keep the LOX/RP-1 preburner exhaust products from backing through the LOX and LH_2 propellant feed systems. The combustion products of both fuel-rich preburners (RP-1/LOX and H_2/O_2) are exhausted into a common main injector manifold. Therefore, there is an open flow path through the inactive system when the other is operating. Closing off this flow with preburner valves does not solve the problem

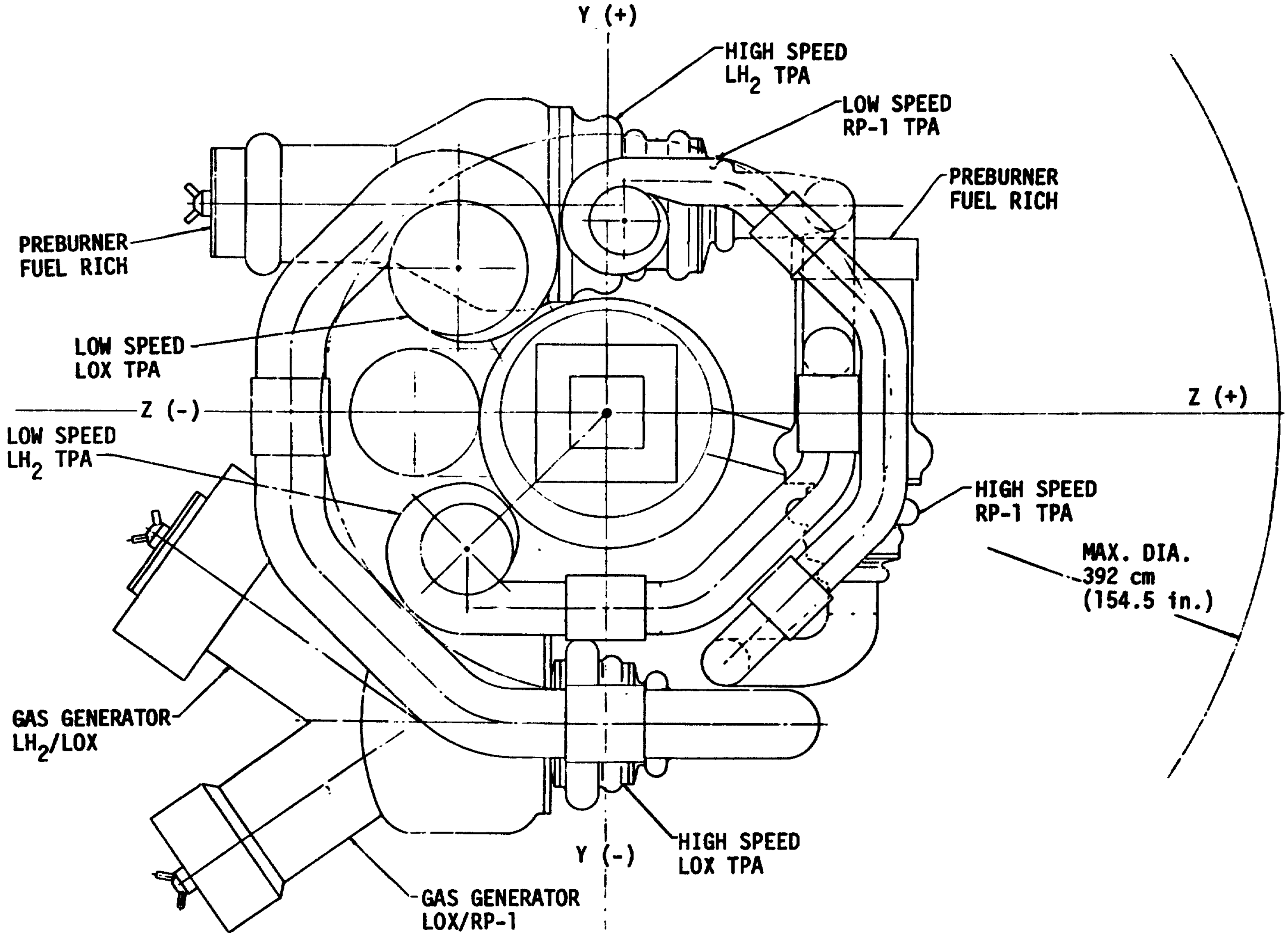

Figure 66. Dual-Fuel Engine Assembly (Top View)

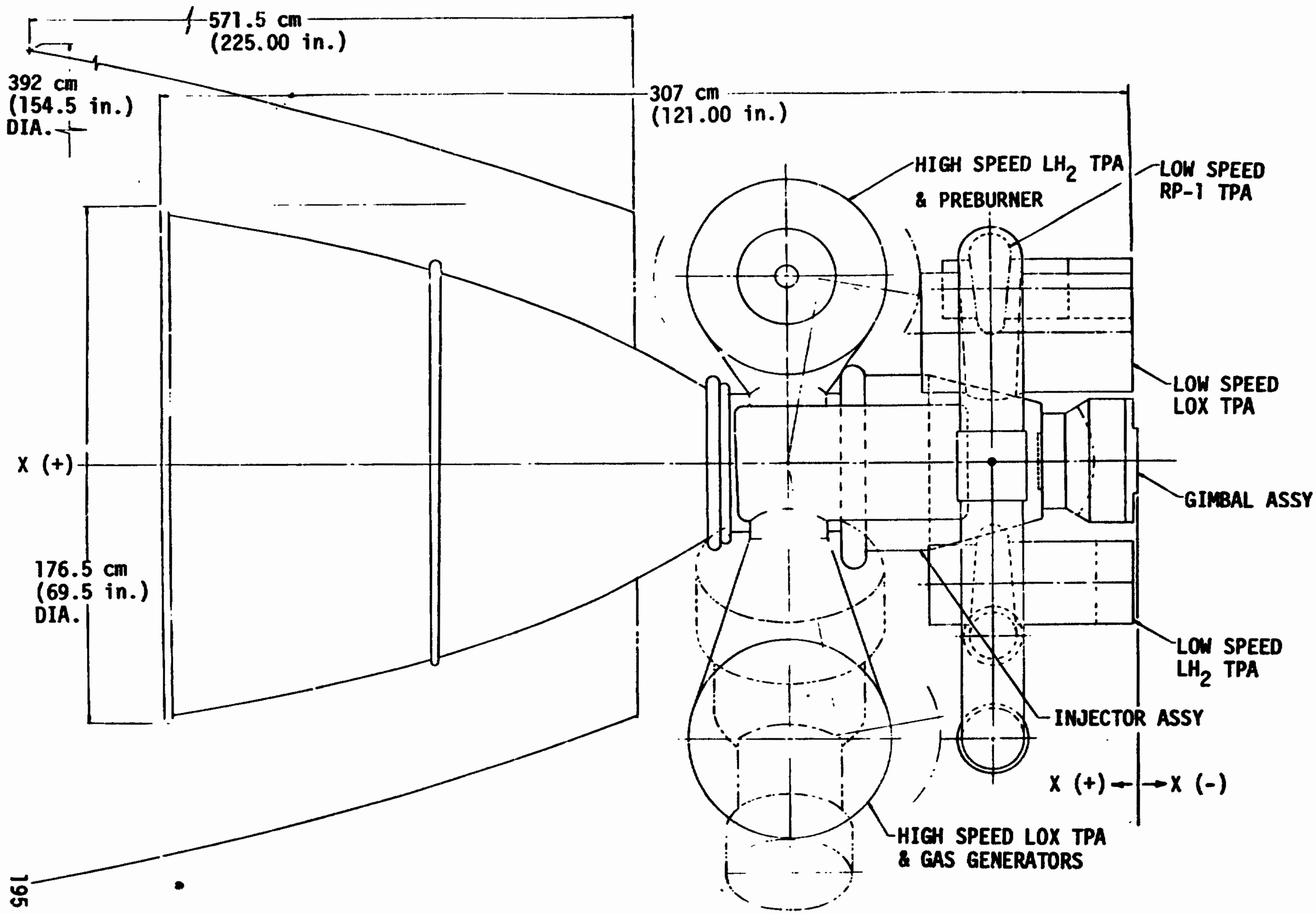

Figure 67. Dual-Fuel Engine Assembly (Side View)

TABLE LXII. - DUAL-FUEL NOMINAL ENGINE OPERATING SPECIFICATIONS

Engine	LOX/RP-1 Mode 1		LOX/LH_2 Mode 2	
Sea-Level Thrust, MN (lb)	2.70	(607,000)		--
Vacuum Thrust, MN (lb)	2.926	(657,700)	2.292	(515,250)
Sea-Level Specific Impulse, sec	322.9			--
Vacuum Specific Impulse, sec	349.9		459.2	
Total Flow Rate, kg/sec (lb/sec)	852.7	(1,879.8)	509.0	(1,122.1)
Mixture Ratio	2.9		7.0	
Oxidizer Flow Rate, kg/sec (lb/sec)	634.0	(1,397.8)	445.3	(981.8)
Fuel Flow Rate, kg/sec (lb/sec)	218.6	(482.0)	63.6	(140.3)
Thrust Chamber				
Sea-Level Thrust, MN (lb)	2.70	(607,000)		--
Vacuum Thrust, MN (lb)	2.926	(657,700)	2.292	(515,250)
Sea-Level Specific Impulse, sec	322.9			--
Vacuum Specific Impulse, sec	349.9		459.2	
Chamber Pressure, atm (psia)	272.2	(4,000)	204.1	(3,000)
Nozzle Area Ratio	40		200	
Mixture Ratio	2.9		7.0	
Throat Diameter, cm (in.)	26.31	(10.36)	26.31	(10.36)
Nozzle Exit Diameter, cm (in.)	166.42	(65.52)	372.11	(146.5)
Coolant Jacket Flow Rate (LOX), kg/sec (lb/sec)	588.8	(1,298.1)[a]	445.3	(981.8)
Coolant Jacket ΔP, atm (psi)	132.0	(1,940)	84.0	(1,235)
Coolant Inlet Temp., °K (°R)	111.1	(200)	111.1	(200)
Coolant Exit Temp., °K (°R)	203.3	(366)	231.1	(416)
Injector Ox.-Rich Gas Flow Rate, kg/sec (lb/sec)	601.9	(1,326.9)	394.8	(870.3)

[a] $\sim$7% of the LOX flow bypasses the coolant jacket in Mode 1 operation and supplies the fuel-rich preburner.

TABLE LXII (cont.)

Thrust Chamber (cont.)	LOX/RP-1 Mode 1		LOX/LH_2 Mode 2	
Injector Fuel-Rich Gas Flow Rate, kg/sec (lb/sec)	250.8	(552.9)	114.2	(251.8)
Chamber Length, cm (in.)	24.77	(9.75)	24.77	(9.75)
Chamber Diameter, cm (in.)	41.61	(16.38)	41.61	(16.38)
Preburners	**LOX/RP-1 Ox.-Rich**		**RP-1/LOX Fuel-Rich**	
Chamber Pressure, atm (psia)	440.8	(6,479)		(6,714)
Combustion Temperature, °K (°R)	922	(1,660)	867	(1,560)
Mixture Ratio	45.0		0.22	
Oxidizer Flow Rate, kg/sec (lb/sec)	588.8	(1,298.1)	45.2	(99.7)[a]
Fuel Flow Rate, kg/sec (lb/sec)	13.1	(28.8)	205.6	(453.2)
Turbines	**LOX Pump**		**RP-1 Pump**	
Inlet Pressure, atm (psia)	440.8	(6,479)		(6,714)
Inlet Temperature, °K (°R)	922	(1,660)	867	(1,560)
Total Gas Flow Rate, kg/sec (lb/sed)	601.9	(1,326.9)	250.8	(552.9)
Gas Properties				
C_p, Specific Heat @ Constant Pressure, J/kg °K (Btu/lb °R)	1100	(0.263)	3209	(0.767)
γ, Ratio of Specific Heats	1.31		1.095	
Shaft Horsepower, mHp (HP)	59,826	(59,000)	25,553	(25,200)
Efficiency, %	80		80	
Speed, rpm	15,100	(15,100)	25,300	(25,300)
Pressure Ratio (Total to Static)	1.490		1.484	

[a]Coolant jacket bypass flow.

TABLE LXII (cont.)

Main Pumps	LOX		RP-1	
Total Outlet Flow Rate, kg/sec (lb/sec)	634.0	(1,397.8)	218.6	(482.0)
Volumetric Flow Rate, m^3/sec (gpm)	0.558	(8,840)	0.274	(4,340)
NPSH, m (ft)	89.3	(293)	110.9	(364)
Suction Specific Speed, $(RPM)(m^3/s)^{1/2}/(m)^{3/4}$	4.14	(20,000)[a]	4.14	(20,000)[a]
Speed, rpm	15,100		25,300	
Discharge Pressure, atm (psia)	632.8	(9,300)	551.1	(8,100)
Number of Stages	2		2	
Specific Speed, $(RPM)(m^2/s)^{1/2}/(m)^{3/4}$	0.31	(1,500)[a]	0.31	(1,500)[a]
Total Head Rise, m (ft)	5660	(18,570)	7013	(23,010)
Efficiency, %	82		82	

LOW SPEED TPA	LOX		RP-1	
Pumps				
NPSH, m (ft)	4.48	(16)	19.81	(65)
Inlet Flow Rate, kg/sec (lb/sec)	634.0	(1,397.8)	218.6	(482.0)
Outlet Flow Rate, kg/sec (lb/sec)	761.0	(1,677.8)	262.4	(578.4)
Discharge Pressure, atm (psia)	12.4	(182)	10.2	(150)
Hydraulic Turbine				
Inlet Pressure, atm (psia)	92.9	(1,365)	77.6	(1,140)
Outlet Pressure, atm (psia)	12.4	(182)	10.2	(150)
Flow Rate, kg/sec (lb/sec)	127.0	(280.0)	43.7	(96.4)
Speed, rpm	2560		8715	

[a] $(RPM \times GPM^{1/2} \times Ft^{-3/4})$

TABLE LXII (cont.)

Dual-Fuel, Mode 2 Nominal

Preburners	LOX/LH_2 OX.-Rich		LOX/LH_2 Fuel-Rich	
Chamber Pressure, atm (psia)	301.1	(4,425)	315.2	(4,632)
Combustion Temperature, °K (°R)	922	(1,660)	922	(1,660)
Mixture Ratio	110		0.9	
Oxidizer Flow Rate, kg/sec (lb/sec)	391.2	(862.5)	54.1	(119.3)
Fuel Flow Rate, kg/sec (lb/sec)	3.54	(7.8)	60.1	(132.5)

Turbines	LOX Pump		LH_2 Pump	
Inlet Pressure, atm (psia)	301.1	(4,425)	315.2	(4,632)
Inlet Temperature, °K (°R)	922	(1,660)	922	(1,660)
Total Gas Flow Rate, kg/sec (lb/sec)	394.8	(870.3)	114.2	(251.8)
Gas Properties				
C_p, Specific Heat @ Constant Pressure, J/kg °K (Btu/lb °R)	1159	(0.277)	8242	(1.97)
γ, Ratio of Specific Heats	1.312		1.357	
Shaft Horsepower, mHp (HP)	32,347	(31,900)	58,305	(57,500)
Efficiency, %	77		81	
Speed, rpm	12,600	(12,600)	33,200	(33,200)
Pressure Ratio (Total to Static)	1.37		1.27	

Main Pumps	LOX		LH_2	
Total Outlet Flow Rate, kg/sec (lb/sec)	445.3	(981.8)	63.6	(140.3)
Volumetric Flow Rate, m^3/sec (gpm)	0.392	(6,210)	0.903	(14,310)
NPSH, m (ft)	67.4	(221)	518.2	(1,700)
Suction Specific Speed, (RPM) $(m^3/sec)^{1/2}/(m)^{3/4}$	3.581	(17,300)[a]	3.105	(15,000)[a]

TABLE LXII (cont.)

Main Pumps (cont.)	LOX		LH_2	
Speed, rpm	12,600		33,200	
Discharge Pressure, atm (psia)	469.5	(6,900)	381.0	(5,600)
Number of Stages	2		3	
Specific Speed, $(RPM)(m^3/sec)^{1/2}/(m)^{3/4}$	0.269	(1,300)[a]	0.217	(1,050)[a]
Total Head Rise, m (ft)	4197.1	(13,770)	54,102	(177,500)
Efficiency, %	79		80	

Low Speed TPA	LOX		LH_2	
Pumps				
NPSH, m (ft)	4.88	(16)	30.48	(100)
Inlet Flow Rate, kg/sec (lb/sec)	445.3	(981.8)	63.6	(140.3)
Outlet Flow Rate, kg/sec (lb/sec)	534.4	(1,178.2)	76.4	(168.4)
Discharge Pressure, atm (psia)	9.19	(135)	4.76	(70)
Hydraulic Turbine				
Inlet Pressure, atm (psia)	65.73	(966)	33.34	(490)
Outlet Pressure, atm (psia)	9.19	(135)	4.76	(70)
Flow Rate, kg/sec (lb/sec)	89.1	(196.4)	12.75	(28.1)
Speed, rpm	2150		11,420	

[a] $(RPM \times GPM^{1/2} \times Ft^{-3/4})$

TABLE LXIII. - DUAL-FUEL, MODE 1 NOMINAL ENGINE PRESSURE SCHEDULE

Preburner Propellant Pressure, atm (psia)	Ox-Rich				Fuel-Rich			
	LOX		RP-1		LOX(1)		RP-1	
Main Pump Discharge	632.8	(9,300)	551.1	(8,100)	632.8	(9,300)	551.1	(8,100)
Main Shutoff Valve Inlet	632.8	(9,300	551.1	(8,100)	632.8	(9,300)	551.1	(8,100)
ΔP Shutoff Valve	6.33	(93)	5.51	(81)	6.33	(93)	5.51	(81)
Valve Outlet	626.4	(9,207)	545.6	(8,019)	626.4	(9,207)	545.1	(8,019)
ΔP Line	2.72	(40)	2.72	(40)	2.72	(40)	2.72	(40)
Coolant Jacket Inlet	623.7	(9,167)		--		--		--
ΔP Coolant Jacket	132.0	(1,940)		--		--		--
Coolant Jacket Outlet	491.7	(7,227)		--		--		--
ΔP Line	2.72	(40)		--		--		--
Preburner Control Inlet	489.0	(7,187)	542.9	(7,979)	623.7	(9,167)	542.9	(7,979)
ΔP Control	4.90	(72)	5.44	(80)	86.3	(1,268	5.44	(80)
Preburner Inlet	484.1	(7,115)	537.4	(7,899)	537.4	(7,899)	537.4	(7,899)
ΔP Preburner	43.3	(636)	96.6	(1,420)	80.6	(1,185)	80.6	(1,185)
Turbine Inlet	440.8	(6,479)			456.8	(6,714)		
ΔP Turbine (Total to Static)	145.0	(2,131)			149.0	(2,190)		
Check Valve Inlet		--			307.8	(4,524)		
ΔP Check Valve		--			12.0	(176)		
Main Injector Inlet	295.8	(4,348)			295.8	(4,348		
ΔP Injector	23.7	(348)			23.7	(348)		
Chamber Pressure	272.2	(4,000)			272.2	(4,000)		

(1) TCA By-Pass Flow.

TABLE LXIV. - DUAL-FUEL, MODE 2 NOMINAL ENGINE PRESSURE SCHEDULE

Preburner	Ox-Rich				Fuel-Rich			
Propellant	LOX		LH_2		LOX		LH_2	
Pressure, atm (psia)								
Main Pump Discharge	469.5	(6,900)	381.0	(5,600)	469.5	(6,900)	381.0	(5,600)
Main Shutoff Valve Inlet	469.5	(6,900)	381.0	(5,600)	469.5	(6,900)	381.0	(5,600)
ΔP Shutoff Valve	3.2	(46)	3.8	(56)	3.2	(46)	3.8	(56)
Valve Outlet	466.3	(6,854)	377.2	(5,544)	466.3	(6,854)	377.2	(5,544)
ΔP Line	1.6	(23)	2.7	(40)	1.6	(23)	2.7	(4[illegible]
Coolant Jacket Inlet	464.7	(6,831)		--	464.7	(6,831)		--
ΔP Coolant Jacket	84.0	(1,235)		--	84.0	(1,235)		--
Coolant Jacket Outlet	380.7	(5,596)		--	380.7	(5,596)		--
ΔP Line	2.7			--	2.7	(40)		--
Preburner Control Inlet	378.0	(5,556)	374.5	(5,504)	378.0	(5,556)	374.5	(5,504)
ΔP Control	19.0	(278)	20.3	(298)	19.0	(278)	3.8	(55)
Preburner Inlet	359.0	(5,278)	354.2	(5,206)	359.0	(5,278)	370.7	(5,449)
ΔP Preburner	58.0	(853)	53.2	(781)	43.9	(646)	55.6	(817)
Turbine Inlet	301.0	(4,425)			315.1	(4,632)		
ΔP Turbine (Total to Static)	81.3	(1,195)			67.0	(985)		
Check Valve Inlet		--			248.1	(3,647)		
ΔP Check Valve		--			4.8	(71)		
Main Injector Inlet	219.7	(3,230)			243.3	(3,576)		
ΔP Injector	15.6	(230)			39.2	(576)		
Chamber Pressure	204.1	(3,000)			204.1	(3,000)		

of leakage through the turbopump shaft and up the suction line. Turbopump shaft seals and vents or hot gas check valves and vents are required. The hot gas check valve has been preliminarily selected as the most reasonable approach.

The LOX/RP-1 combustors are again sequenced to start oxidizer-rich. The LOX/LH_2 combustor sequences are based upon test experience with both fuel and oxidizer-rich modes of operation. The fuel-rich LOX/LH_2 combustors are started fuel-rich and the oxidizer-rich combustors are started oxidizer-rich. Experience has shown that it is possible to start fuel-rich LOX/LH_2 combustors oxidizer-rich but attempts, both planned and inadvertent, to start oxidizer-rich combustors fuel-rich resulted in destruction of the hardware (Ref. 72 and 73).

The cryogenic components, both LOX and LH_2, for this dual-fuel engine are assumed to be chilled down on the launch pad.

The start and shutdown sequence for the dual-fuel engine is shown in Table LXV.

c. Start and Shutdown Data

The dual-fuel engine was also assumed to be chilled down and bled-in to the main chamber valves prior to receipt of the fire signal and started under tank head. The transient estimates are based upon the analytical modeling of similar engine configurations such as, the ARES and ALRC SSME design.

The start and shutdown data is summarized on Table LXVI.

d. Design and Off-Design Engine Performance

Engine cycle balances and performance were evaluated at the design thrust level over a mixture ratio range encompassing the design point mixutre ratio ± 10%. These data are summarized on Tables LXVII and LXVIII for Mode 1 and 2 operation, respectively.

e. Engine Mass Properties Data

The engine mass properties data were computed from the preliminary engine and component layout drawings.

The weight breakdown for the dual-fuel engine is shown on Table LXIX.

The center of gravity in the axial direction was calculated to be 199 cm (78.2 in.) from the head-end of the gimbal with the nozzle extension deployed.

TABLE LXV. - SEQUENCE OF OPERATION DUAL-FUEL ENGINE

Mode 1

Start

1. Purge Oxidizer Lines and Manifold.
2. Energize Spark Igniters.
3. Open Main Ox. Valve (#1).*
4. Open Igniter Valves on Fuel and Ox. Rich Preburners.
5. Open Ox. Valves on Fuel and Ox. Rich Preburners (#2 and #3).
6. Open Main Fuel (RP-1) Valve (#4).
7. Open Ox. Rich Preburner Fuel (RP-1) Valve (#5).

Shutdown

1. Close Ox. Rich Preburner Fuel (RP-1) Valve (#5).
2. Close Main Ox. Valve (#1).
3. Initiate Ox. Purge.
4. Close Main Fuel (RP-1) Valve (#4).
5. Close Igniter Valves on Fuel and Ox. Rich Preburners.
6. Cutoff Igniter Spark Energy.
7. Close Fuel and Ox. Rich Preburner Ox. Valves (#2 and #3).

Mode 2

Start

1. Energize Spark Igniters.
2. Open Igniter Valves on Fuel and Ox. Rich Preburners.
3. Open Main Fuel Valve (#6).*
4. Open Main Ox. Valve (#1).
5. Open Ox. Valves on Fuel and Ox. Rich Preburners (#7 and #8).
6. Open Ox. Rich Preburner Fuel-Valve (#9).

*Numbers refer to valves on Figure 65.

TABLE LXV (cont.)

Mode 2 (cont.)

Shutdown

1. Close Igniter Valves.
2. Cutoff Igniter Spark Energy.
3. Close Ox. Rich Preburner Fuel Valve (#9).
4. Close Main Ox. Valve #1.
5. Initiate Ox. Purge.
6. Close Main Fuel Valve.
7. Close Ox. Valves on Fuel and Ox. Rich Preburners (#7 and #8).

TABLE LXVI. - DUAL-FUEL ENGINE START AND SHUTDOWN TRANSIENT DATA SUMMARY

	Mode 1		Mode 2	
Start to 90% F				
Time, sec	2.52		2.52	
Total Start Impulse, kg-sec (lb-sec)	69,000	(152,000)	58,500	(129,000)
LH_2 Consumption, kg (lb)		--	35.4	(78)
LOX Consumption, kg (lb)	129.3	(285)	93.0	(205)
RP-1 Consumption, kg (lb)	120.2	(265)		--
Shutdown to 5% F				
Time, sec	0.50		0.50	
Total Shutdown Impulse, kg-sec (lb-sec)	80,800	(178,200)	63,400	(139,700)
LH_2 Consumption, kg (lb)		--	23.1	(51)
LOX Consumption, kg (lb)	162.9	(358)	113.9	(251)
RP-1 Consumption, kg (lb)	73.0	(616)		--

TABLE LXVII. - DUAL-FUEL, MODE 1 DESIGN AND OFF-DESIGN MR PERFORMANCE

$\varepsilon = 40$

Engine	Mixture Ratio 2.61		Mixture Ratio 2.90		Mixture Ratio 3.19	
Sea-Level Thrust, MN (lb)	2.70	(607,000)	2.70	(607,000)	2.70	(607,000)
Vacuum Thrust, MN (lb)	2.93	(658,800)	2.926	(657,700)	2.924	(657,400)
Sea-Level Specific Impulse, sec	321.0		322.9		320.4	
Vacuum Specific Impulse, sec	348.4		349.9		347.0	
Total Flow Rate, kg/sec (lb/sec)	857.8	(1891.0)	852.7	(1879.8)	859.3	(1894.5)
Fuel Flow Rate, kg/sec (lb/sec)	237.6	(523.8)	218.6	(482.0)	205.1	(452.1)
Oxidizer Flow Rate, kg/sec (lb/sec)	620.2	(1367.2)	634.0	(1397.8)	654.3	(1442.4)
Chamber Pressure, atm (psia)	277.5	(4,078)	272.2	(4,000)	270.3	(3,973)

TABLE LXVIII. - DUAL-FUEL, MODE 2 DESIGN AND OFF-DESIGN MR PERFORMANCE

$\varepsilon = 200$

Engine	Mixture Ratio 6.3		7.0		7.7	
Vacuum Thrust, MN (lb)	2.29	(515,250)	2.29	(515,250)	2.29	(515,250)
Vacuum Specific Impulse, sec	461.6		459.2		455.4	
Total Flow Rate, kg/sec (lb/sec)	506.3	(1116.2)	508.9	(1122.1)	513.2	(1131.4)
Fuel Flow Rate, kg/sec (lb/sec)	69.4	(152.9)	63.6	(140.3)	59.0	(130.0)
Oxidizer Flow Rate, kg/sec (lb/sec)	463.9	(963.3)	445.3	(981.8)	454.2	(1001.4)
Chamber Pressure, atm (psia)	205.0	(3,014)	204.1	(3,000)	201.5	(2,962)

TABLE LXIX. - DUAL-FUEL ENGINE WEIGHT STATEMENT

Component	Weight kg	(lb)
Gimbal	95.7	(211)
Main Injector	293.0	(646)
Copper Chamber and Nozzle (ε = 14.7)	124.3	(274)
Tube Bundle Nozzle (ε = 14.7 to 40)	89.4	(197)
Extendible Nozzle*	592.4	(1306)
Extendible Nozzle Deployment System	292.1	(644)
Fuel-Rich Preburners		
O_2/H_2	107.5	(237)
O_2/RP-1	80.7	(178)
Oxidizer-Rich Preburners		
O_2/H_2	122.5	(270)
O_2/RP-1	99.8	(220)
Fuel Valves and Actuation	91.6	(202)
Oxidizer Valves and Actuation	172.4	(380)
Hot Gas Check Valves	40.8	(90)
Low Speed LOX TPA	136.1	(300)
Low Speed RP-1 TPA	23.1	(51)
Low Speed LH_2 TPA	49.9	(110)
High Speed LOX TPA	382.8	(844)
High Speed RP-1 TPA	145.2	(320)
High Speed LH_2 TPA	458.1	(1010)
Hot Gas Manifold	91.6	(202)
Low Pressure Lines	133.8	(295)
High Pressure Lines	314.8	(694)
Ignition System	45.4	(100)
Miscellaneous	200.5	(442)
TOTAL	4183.5	(9223)

*Tube bundle to ε = 132 and columbium to the exit.

The center of gravity and gimballed moments of inertia for the engine are:

	AXIS X	AXIS Y	AXIS Z
Center of Gravity, cm (in.)			
Nozzle Retracted	176 (69.2)	6.35 (-2.5)	20.3 (-8.0)
Nozzle Deployed	199 (78.2)	6.35 (-2.5)	20.3 (-8.0)
	X-X	Y-Y	Z-Z
Gimballed Inertia, kg-m^2 (slug-ft^2)			
Nozzle Retracted	2659 (1972)	16,700 (12,300)	16,500 (12,160)
Nozzle Deployed	2635 (1944)	25,700 (18,960)	25,500 (18,800)

The coordinate system is defined on Figures 66 and 67.

3. Alternate Mode 1 Engine Design

a. Configuration and Nominal Operating Conditions

Based upon the results of Task I through V, the hydrogen cooled, gas generator cycle engine was selected as the alternate Mode 1 candidate. The cycle schematic (without boost pumps) is shown in Figure 68. This cycle uses LH_2 to cool the combustion chamber and nozzle and a fuel-rich LOX/LH_2 gas generator to drive the turbines of the main propellant pumps. LOX/RP-1 are injected as liquids in the main injector. The engine cycle features the hydrogen turbine in series with the LOX and RP-1 turbines which operate in parallel.

The preliminary engine layouts are shown in Figures 69 and 70.

The TCA design uses a slotted zirconium copper chamber to a nozzle area ratio of 25:1. A single pass A-286 tube bundle is used from 25:1 to the nozzle exit (area ratio of 42.7:1). The coolant flow path is shown on Figure 70.

The nominal engine operating conditions and pressure schedule is presented on Tables LXX and LXXI, respectively.

The gimballed envelope was evaluated for a 10° square pattern and is also shown on Figure 69. The square dimension is 264.6 cm (104.2 in.).

b. Engine Operation and Control

The engine control requirements are primarily governed by the engine start and shutdown sequences. The sequence of operation for the LOX/RP-1 components is again patterned after the F-1. The start and shutdown sequences are described on Table LXXII.

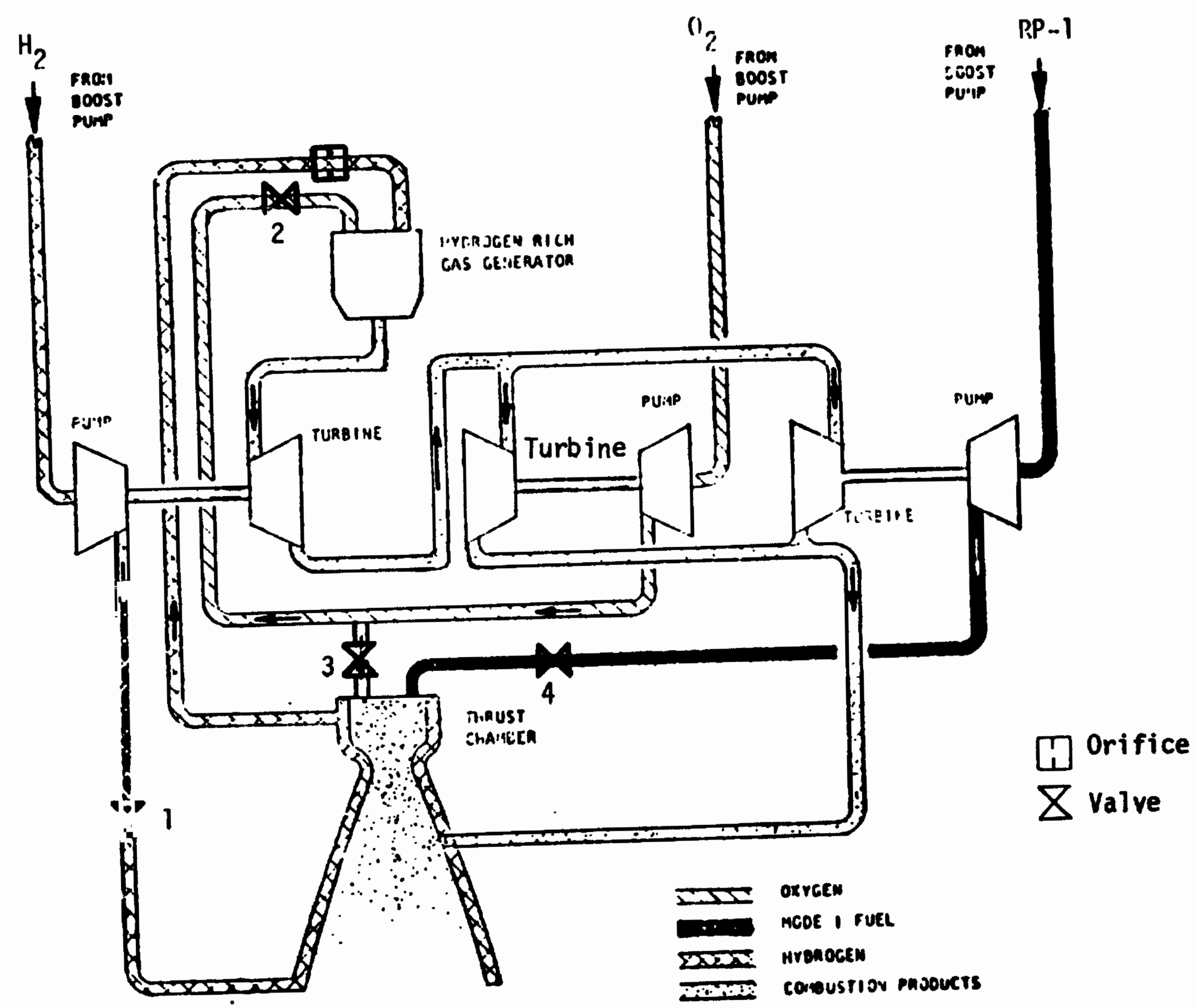

Figure 68. Mode 1 Hydrogen Cooled, Gas Generator Cycle Schematic

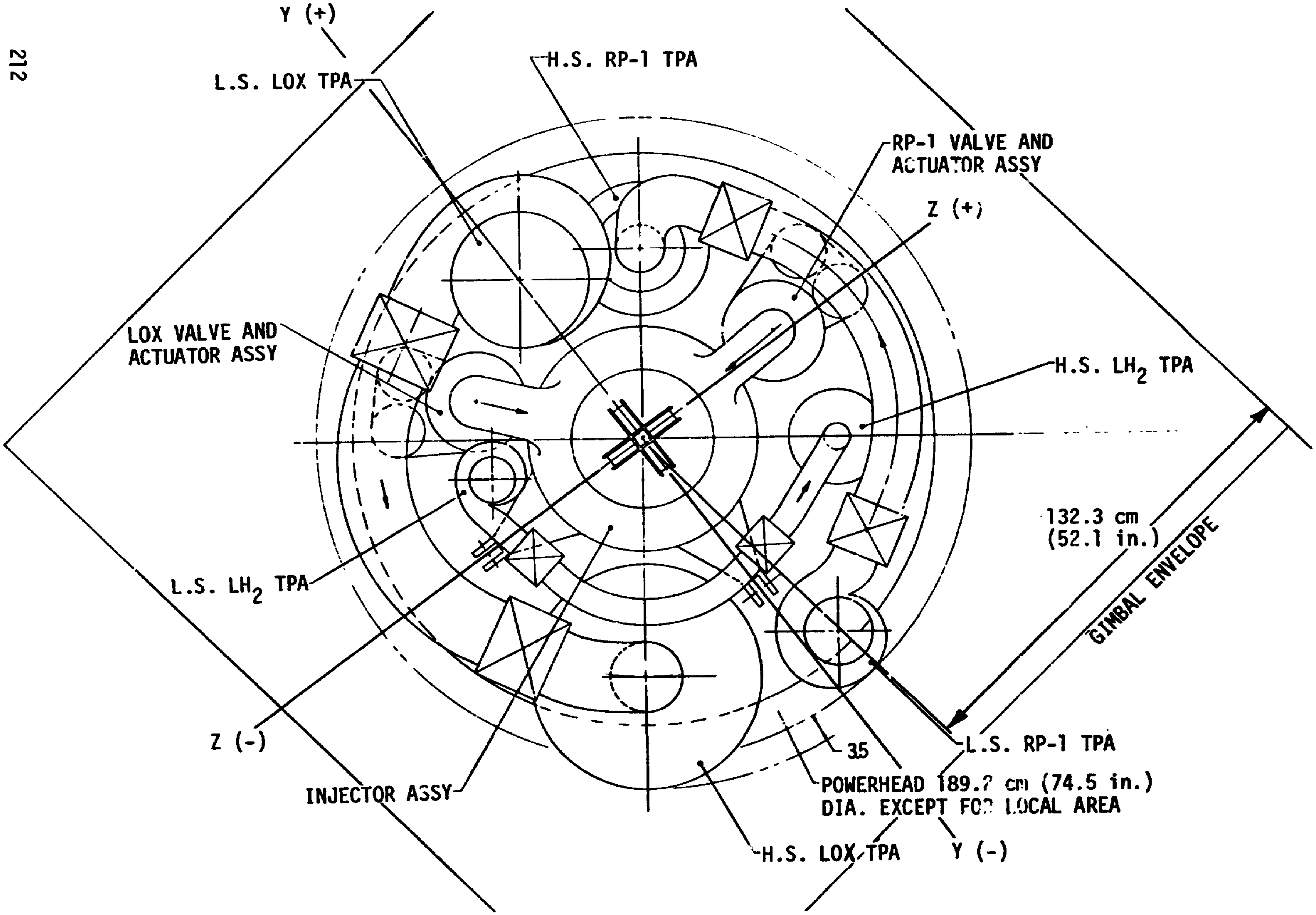

Figure 69. Mode 1 Hydrogen Cooled, Gas Generator Cycle Engine Assembly (Top View)

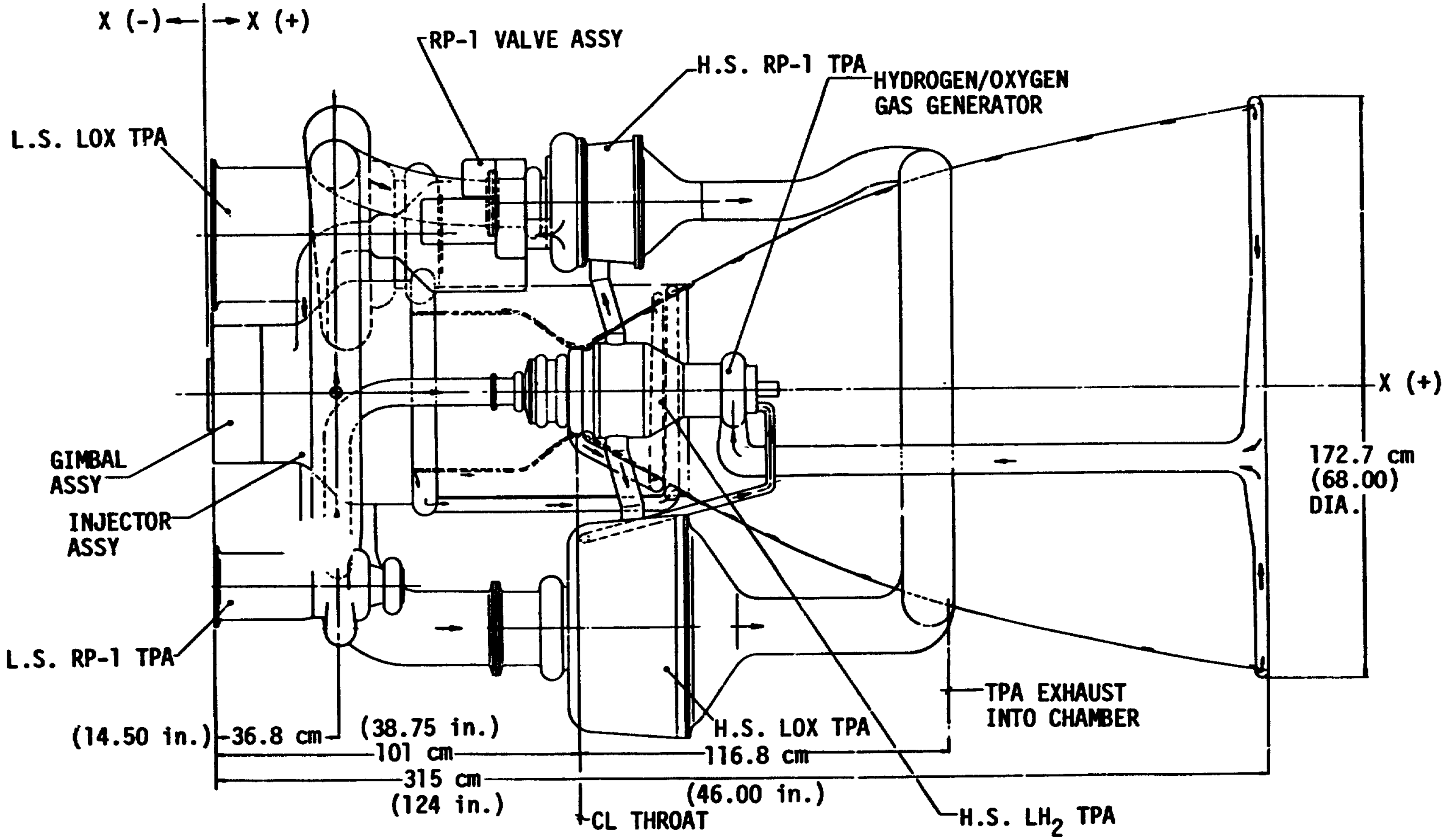

Figure 70. Mode 1 Hydrogen Cooled, Gas Generator Cycle Engine Assembly (Side View)

TABLE LXX. - ALTERNATE MODE 1 HYDROGEN COOLED, GAS GENERATOR CYCLE ENGINE OPERATING SPECIFICATIONS

Nominal MR = 2.9

Engine		
Sea-Level Thrust, MN (lb)	2.70	(607,000)
Vacuum Thrust, MN (lb)	2.93	(658,000)
Sea-Level Specific Impulse, sec	323.5	
Vacuum Specific Impulse, sec	350.7	
Total Flow Rate, kg/sec (lb/sec)	851.1	(1,876.4)
Mixture Ratio ($\dot{W}_{LOX}/\dot{W}_{RP-1}$)	2.9	
LOX Flow Rate, kg/sec (lb/sec)	626.1	(1,380.4)
RP-1 Flow Rate, kg/sec (lb/sec)	215.9	(476.0)
Hydrogen Flow Rate, kg/sec (lb/sec)	9.07	(20.0)
Thrust Chamber		
Sea-Level Thrust, MN (lb)	2.67	(599,990)
Vacuum Thrust, MN (lb)	2.89	(650,200)
Sea-Level Specific Impulse, sec	325.3	
Vacuum Specific Impulse, Sec	352.5	
Chamber Pressure, atm (psia)	289.2	(4,250)
Nozzle Area Ratio	42.7	
Mixture Ratio ($\dot{W}_{LOX}/\dot{W}_{RP-1}$)	2.88	
Throat Diameter, cm (in.)	25.30	(9.96)
Nozzle Exit Diameter, cm (in.)	165.35	(65.1)
Coolant Jacket Flow Rate (LH_2), kg/sec (lb/sec)	9.07	(20.0)
Coolant Jacket ΔP, atm (psi)	75.2	(1,105)
Coolant Inlet Temp., °K (°R)	61.1	(110)
Coolant Exit Temp., °K (°R)	811.1	(1,460)
LOX Flow Rate, kg/sec (lb/sec)	620.7	(1,368.4)
RP-1 Flow Rate, kg/sec (lb/sec)	215.9	(476.0)
Chamber length, cm (in.)	46.99	(18.5)
Chamber Diameter, cm (in.)	40.01	(15.75)

TABLE LXX (cont.)

Turbine Exhaust Performance		
Sea-Level Thrust, N (lb)	31,582	(7,100)
Vacuum Thrust, N (lb)	35,008	(7,870)
Sea-Level Specific Impulse, Sec	222	
Vacuum Specific Impulse, sec	246	
Gas Flow Rate, kg/sec (lb/sec)	14.5	(32.0)
Gas Generator		
Chamber Pressure, atm (psia)	272.5	(4,005)
Combustion Temperature, °K (°R)	922.2	(1,660)
Mixture Ratio	0.60	
LOX Flow Rate, kg/sec (lb/sec)	5.44	(12.0)
Hydrogen Flow Rate, kg/sec (lb/sec)	9.07	(20.0)

TABLE LXX (cont.)

Turbines	LOX		RP-1		LH_2	
Inlet Pressure, atm (psia)	174.9	(2,571)	174.9	(2,571)	272.5	(4,005)
Inlet Temperature, °K (°R)	859.4	(1,547)	859.4	(1,547)	922.2	(1,660)
Total Gas Flow Rate, kg/sec (lb/sec)	9.66	(21.3)	4.85	(10.7)	14.52	(32.0)
Gas Properties						
C_p, Specific Heat @ Constant Pressure, J/kg °K (Btu/lb °R)	9665	(2.31)	9665	(2.31)	9665	(2.31)
γ, Ratio of Specific Heats	1.364		1.364		1.364	
Shaft Horsepower, mHp (hP)	33,726	(33,260)	17,035	(16,800)	11,915	(11,750)
Efficiency, %	60		60		72	
Speed, rpm	16,100		29,900		70,000	
Pressure Ratio (Total to Static)	15.1		15.1		1.448	
Turbine Exit Static Pressure, atm (psia)	11.57	(170)	11.57	(170)	188.2	(2,766)
Turbine Exit Total Temp., °K (°R)	593.3	(1,068)	593.3	(1,068)	859.4	(1,547)
Main Pumps						
Total Outlet Flow Rate, kg/sec (lb/sec)	626.1	(1,380.4)	215.9	(476.0)	9.07	(20.0)
Volumetric Flow Rate, m^3/sec (gpm)	0.553	(8,730)	0.270	(4,280)	0.129	(2,040)
NPSH, m (ft.)	96.3	(316)	137.2	(450)	260.6	(855)
Suction Specific Speed, $(RPM)(m^3/sec)^{1/2}/(m)^{3/4}$	4.14	(20,000)[a]	4.14	(20,000)[a]	4.14	(20,000)[a]
Speed, rpm	16,100		29,900		70,000	
Discharge Pressure, atm (psia)	374	(5,100)	347	(5,100)	408.2	(6,000)
Number of Stages	1		1		3	
Specific Speed, $(RPM)(m^3/sec)^{1/2}/(m)^{3/4}$	0.310	(1,500)[a]	0.310	(1,500)[a]	0.163	(786)[a]

[a] $(RPM \times GPM^{1/2} \times Ft^{-3/4})$

TABLE LXX (cont.)

Main Pumps (cont.)	LOX		RP-1		LH_2	
Total Head Rise, m (ft)	3057.1	(10,030)	4349.5	(14,270)	58,522	(192,000)
Efficiency, %	80		75		60	
Low Speed TPA						
Pumps						
NPSH, m (ft)	4.88	(16)	19.81	(65)	30.48	(100)
Inlet Flow Rate, kg/sec (lb/sec)	626.1	(1,380.4)	215.9	(476.0)	9.07	(20)
Outlet Flow Rate, kg/sec (lb/sec)	751.3	(1,656.4)	259.1	(571.2)	9.98	(22)
Discharge Pressure, atm (psia)	12.25	(180)	12.25	(180)	3.13	(46)
Hydraulic Turbine						
Inlet Pressure, atm (psia)	95.3	(1,400)	95.3	(1,400)	33.3	(490)
Outlet Pressure, atm (psia)	12.25	(180)	12.25	(180)	3.13	(46)
Flow Rate, kg/sec (lb/sec)	125.2	(276.0)	43.2	(95.2)	0.907	(2.0)

TABLE LXXI. - ALTERNATE MODE 1 HYDROGEN COOLED, GAS GENERATOR CYCLE ENGINE PRESSURE SCHEDULE

Nominal MR = 2.90

Thrust Chamber Flows

Propellant Pressure, atm (psia)	LOX		RP-1	
Main Pump Discharge	347.0	(5,100)	347.0	(5,100)
ΔP Line	3.33	(49)	3.33	(49)
Shutoff Valve Inlet	343.7	(5,051)	343.7	(5,051)
ΔP Shutoff Valve	3.47	(51)	3.47	(51)
Main Injector Inlet	340.2	(5,000)	340.2	(5,000)
ΔP Injector	51.0	(750)	51.0	(750)
Chamber Pressure	289.2	(4,250)	289.2	(4,250)

Gas Generator Flows

Propellant Pressure, atm (psia)	LOX		LH_2	
Main Pump Discharge	347.0	(5,100)	408.2	(6,000)
Shutoff Valve Inlet		--	408.2	(6,000)
ΔP Shutoff Valve		--	4.08	(60)
Valve Outlet		--	404.2	(5,940)
ΔP Line	6.80	(100)	2.72	(40)
Coolant Jacket Inlet		--	401.4	(5,900)
ΔP Coolant Jacket		--	75.2	(1,105)
Coolant Jacket Outlet			326.3	(4,795)
ΔP Line			4.08	(60)
G.G. Control Inlet	340.2	(5,000)	322.2	(4,735)
ΔP Gas Generator	19.60	(288)	25.99	(382)
G.G. Injector Inlet	320.6	(4,712)	296.2	(4,353)
ΔP Gas Generator	48.1	(707)	23.7	(348)
Turbine Inlet	272.5	(4,005)	272.5	(4,005)

TABLE LXXII. - SEQUENCE OF OPERATION HYDROGEN COOLED, GAS GENERATOR CYCLE

Start

1. Purge Gas Generator and Thrust Chamber Oxidizer Lines and Manifold.
2. Energize Spark Igniters.
3. Open Gas Generator Igniter Valves.
4. Open Main LH_2 Valve (#1).*
5. Open Gas Generator Ox. Valve (#2).
6. Open Thrust Chamber Ox. Valve (#3).
7. Open Thrust Chamber Igniter Valves.
8. Open Thrust Chamber RP-1 Valve (#4).

Shutdown

1. Cutoff Gas Generator Spark Energy.
2. Close Gas Generator Igniter Valves.
3. Close Ox. Gas Generator Valve (#2).
4. Close Ox. Thrust Chamber Valve (#3).
5. Initiate Ox. Purge.
6. Close Main LH_2 Valve.
7. Close Thrust Chamber RP-1 Valve (#4).
8. Close Thrust Chamber Igniter Valves.
9. Cutoff Thrust Chamber Spark Energy.

*Numbers refer to the valves on Figure 68.

c. Start and Shutdown Data

The engine is assumed to be bled-in and the hydrogen and oxygen components chilled down to the main propellant shutoff valves prior to receipt of the start signal. The thrust, total impulse, and propellant consumptions during transient operation are summarized in Table LXXIII from 90% of rated thrust to shutdown at 5% of rated thrust. Transient estimates are modeled after the F-1 engine start and shutdown.

d. Design and Off-Design Engine Performance

Engine performance at the design thrust level over a mixture ratio range encompassing the design point mixture ratio $\pm$ 10% is summarized on Table LXXIV.

A requirement for this engine to operate over this range in flight has not as yet, been identified. Therefore, the power balances assume that the engine orifice sizes are changed to operate at the various mixture ratios. The operating points are representative of those that would be required with a variable control valve although some penalty would be incurred at the points where no orifice is required.

e. Engine Mass Properties Data

The mass properties dated for the alternate Mode 1 engine were calculated from the preliminary engine and component layout drawings.

The weight breakdown for this engine is shown on Table LXXV.

The center of gravity in the axial direction was calculated to be 93.7 cm (36.9 in.) from the head-end of the gimbal.

The center of gravity and gimballed moments of inertia for the engine are:

	AXIS		
	X	Y	Z
Center of Gravity, cm (in.)	93.7 (36.9)	-1.78 (-0.7)	-3.8 (-1.5)
	X-X	Y-Y	Z-Z
Gimballed Inertia, kg-m^2 (slug-ft^2)	431 (318)	1301 (960)	1313 (969)

The coordinate system is defined on Figures 69 and 70.

TABLE LXXIII. - ALTERNATE MODE 1 ENGINE START AND SHUTDOWN TRANSIENT DATA SUMMARY

Start to 90% F		
Time, sec	0.80	
Total Start Impulse, kg-sec (lb-sec)	69,030	(152,200)
LH_2 Consumption, kg (lb)	52.6	(116)
LOX Consumption, kg (lb)	166.5	(367)
RP-1 Consumption, kg (lb)	3.2	(7)
Shutdown to 5% F		
Time, sec	0.50	
Total Shutdown Impulse, kg-sec (lb-sec)	80,800	(178,200)
LH_2 Consuption, kg (lb)	3.2	(7)
LOX Consumption, kg (lb)	160.1	(353)
RP-1 Consumption, kg (lb)	72.1	(159)

TABLE LXXIV. - ALTERNATE MODE 1 HYDROGEN COOLED GAS GENERATOR CYCLE ENGINE DESIGN AND OFF-DESIGN MR PERFORMANCE

$\varepsilon = 42.7$

	Engine Mixture Ratio ($\dot{W}_{LOX}/\dot{W}_{RP-1}$)					
Engine	2.61		2.90		3.19	
Sea-Level Thrust, MN (lb)	2.70	(607,000)	2.70	(607,000)	2.70	(607,000)
Vacuum Thrust, MN (lb)	2.931	(658,900)	2.927	(658,000)	2.926	(657,700)
Sea-Level Specific Impulse, sec	321.6		323.5		321.0	
Vacuum Specific Impulse, sec	349.1		350.7		347.8	
Total Flow Rate, kg/sec (lb/sec)	856.1	(1887.4)	851.1	(1876.4)	857.8	(1891.0)
LOX Flow Rate, kg/sec (lb/sec)	612.4	(1350.1)	626.1	(1380.4)	646.2	(1424.5)
RP-1 Flow Rate, kg/sec (lb/sec)	234.6	(517.3)	215.9	(476.0)	202.5	(446.5)
Hydrogen Flow Rate, kg/sec (lb/sec)	9.07	(20.0)	9.07	(20.0)	9.07	(20.0)
Thrust Chamber						
Sea-Level Thrust, MN (lb)	2.67	(599,900)	2.67	(599,900)	2.67	(599,900)
Vacuum Thrust, MN (lb)	2.896	(651,000)	2.892	(650,200)	2.890	(649,800)
Sea-Level Specific Impulse, sec	323.3		325.3		322.7	
Vacuum Specific Impulse, sec	350.9		352.5		349.6	
Chamber pressure, atm (psia)	294.7	(4,331)	289.2	(4,250)	287.4	(4,224)

TABLE LXXV. - ALTERNATE MODE 1 HYDROGEN COOLED, GAS GENERATOR CYCLE ENGINE WEIGHT STATEMENT

Component	Weight kg	Weight (lb)
Gimbal	95.7	(211)
Main Injector	348.8	(769)
Copper Chamber and Nozzle (ϵ = 25)	157.4	(347)
Tube Bundle Nozzle (ϵ = 25 to 42.7)	92.1	(203)
Fuel-Rich Gas Generator	9.1	(20)
Fuel Valves and Actuation	59.0	(130)
Oxidizer Valves and Actuation	73.9	(163)
Low Speed LOX TPA	136.1	(300)
Low Speed RP-1 TPA	23.1	(51)
Low Speed LH_2 TPA	7.7	(17)
High Speed LOX TPA	266.7	(588)
High Speed RP-1 TPA	79.8	(176)
High Speed LH_2 TPA	47.6	(105)
Low Pressure Lines	70.8	(156)
High Pressure Lines	89.4	(197)
Ignition System	27.2	(60)
Miscellaneous	200.5	(442)
TOTAL	1784.9	(3935)

E. TURBOMACHINERY DESIGN

Preliminary designs for the high speed and low speed turbopumps were established for the three candidate engine designs.

1. Baseline Mode 1
2. Dual-Fuel
3. Alternate Mode 1

The turbomachinery was designed in general accordance with the engine cycle balance data presented in Section VIIID. Some modifications to the data would be required for the next design iteration.

1. Baseline Mode 1 Engine

The low speed LOX turbopump for the baseline Mode 1 engine is shown on Figure 71. This pump uses a scroll type discharge to accommodate the engine assembly. The shaft is supported by two spring loaded angular contact ball bearings. At the design point, the estimated pump efficiency is 85%. The hydraulic turbine is driven by flow from the high speed pump. Low speed pump and turbine design data are shown on Table LXXVI.

The high speed LOX pump is shown in Figure 72. Significant design features include:

- High head inducer with tap-off flow for the low speed pump turbine.
- Two centrifugal pump stages.
- Axial thrust reacted by self-compensating thrust balancer.
- Each bearing package consists of two spring loaded angular contact ball bearings, one located between inducer and first stage impeller, and the second between the last impeller and turbine.
- Single stage turbine; configured for zero reaction at the rotor hub with free vortex-velocity distribution from hub to tip.

The pump and turbine design parameters are listed in Table LXXVII. The pump performance at the design point is estimated to be 82%. The turbine was configured as a single stage with free vortex velocity diagrams (approximately 10% reaction at the mean diameter). Based on the information in Reference 74 and the design ratio of mean blade speed to nozzle spouting velocity, the turbine efficiency at the design point, is estimated to be 80% based on the total to static pressure ratio.

The RP-1 turbopumps designed for the baseline Mode 1 engine are shown on Figures 73 and 74.

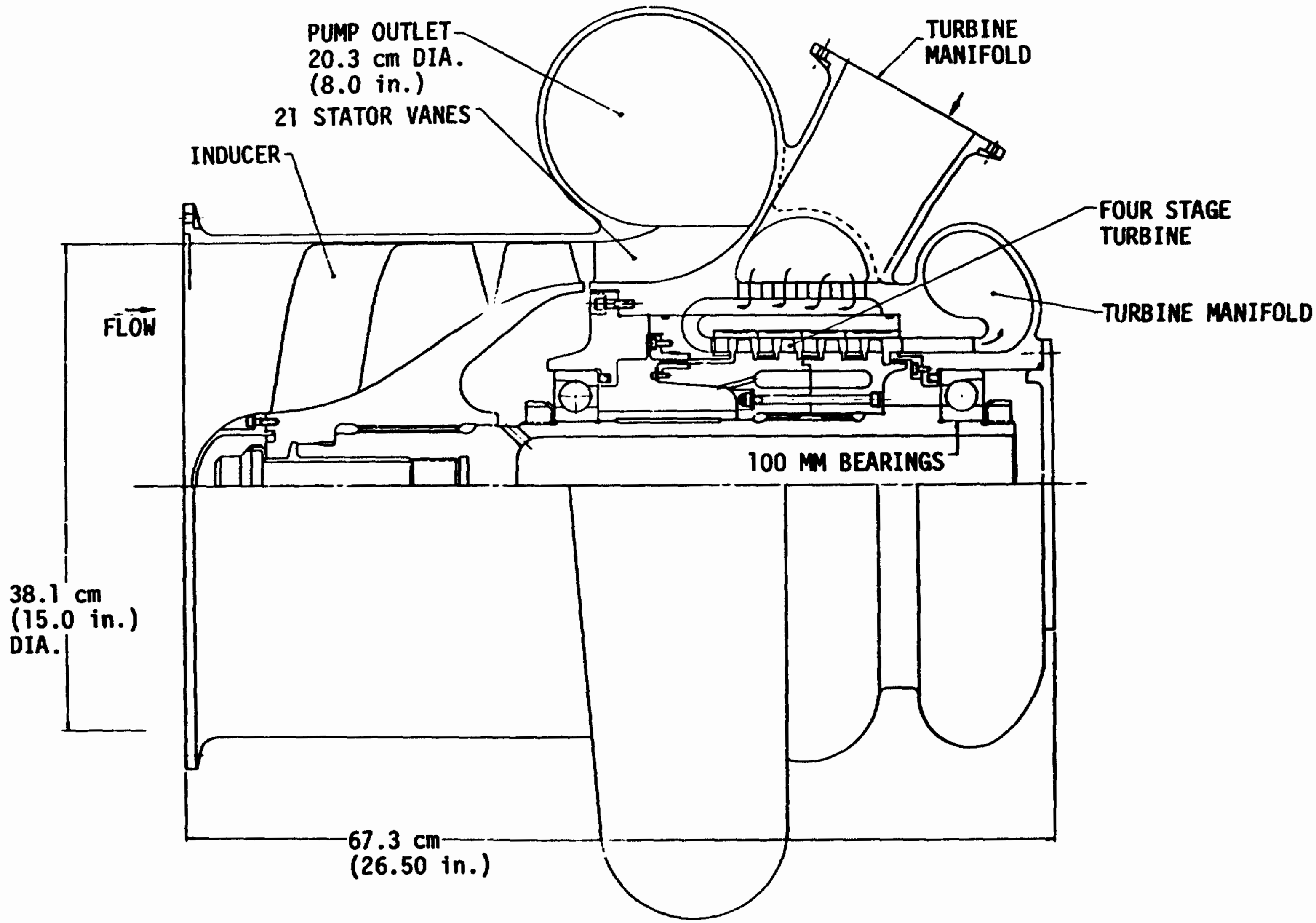

Figure 71. Baseline Mode 1, Dual-Fuel and Alternate Mode 1 Low Speed LOX TPA

TABLE LXXVI. - BASELINE MODE 1 AND DUAL-FUEL ENGINE
LOW SPEED LOX TPA DESIGN POINT

	Pump		Turbine	
Speed, rpm	2560		2560	
Flow, m^3/sec (gpm)	0.554	(8,785)	0.111	(1,755)
Head, m (ft)	99.4	(326)	762.0	(2,500)
Power, mHp (hp)	1014	(1,000)	1014	(1,000)
NPSH, m (ft)	4.88	(16)		--
Suction Specific Speed	6.210	(30,000)		--
Specific Speed	0.647	(3,127)	0.177	(857) (Stage)
No. of Stages	1		4	
Efficiency, %	85		81	

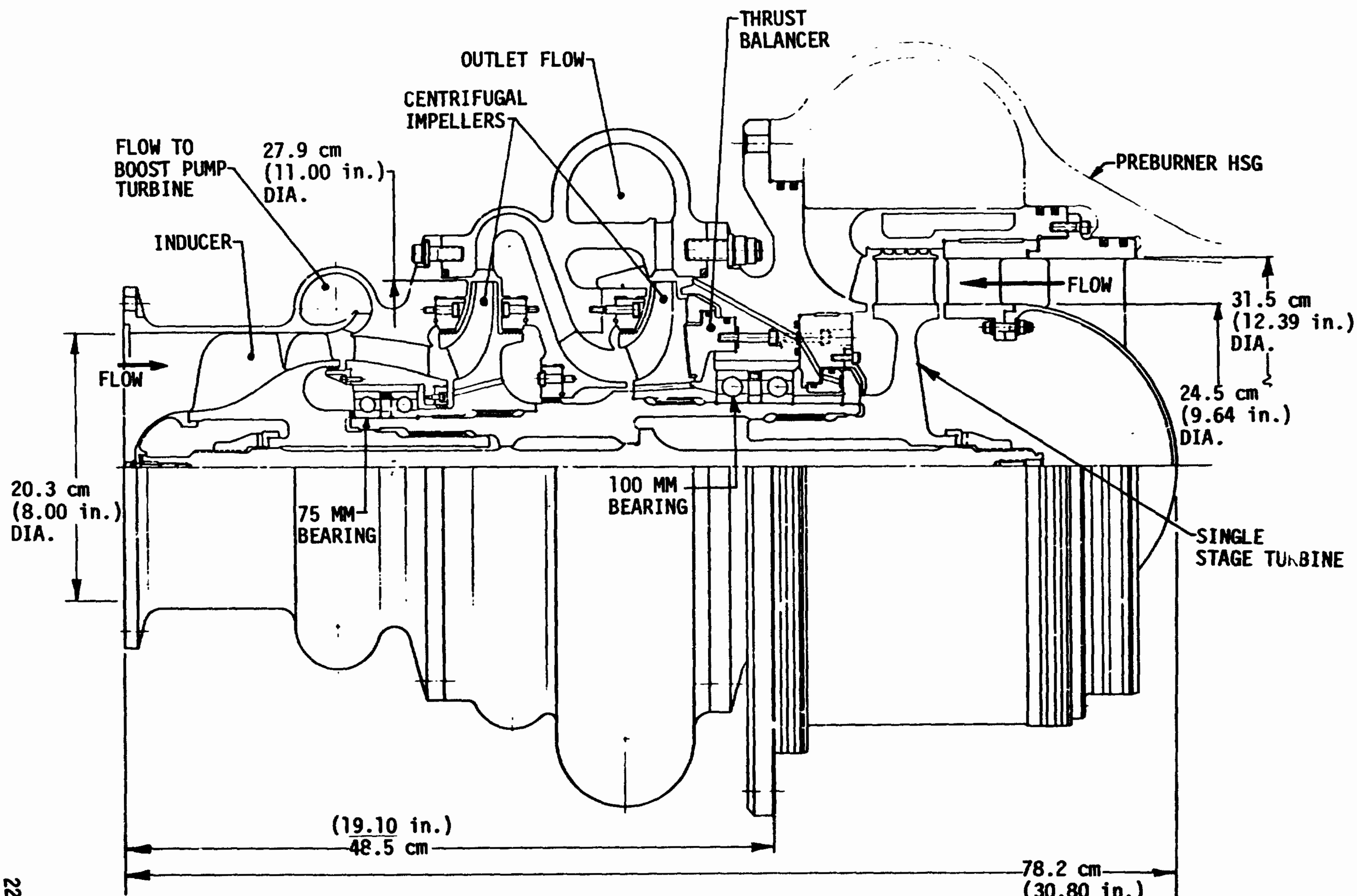

Figure 72. Baseline Mode 1 and Dual-Fuel High Speed LOX TPA

TABLE LXXVII. - BASELINE MODE 1 AND DUAL-FUEL ENGINE HIGH SPEED LOX TPA DESIGN POINT

Pump

Speed, rpm	15,000	
Inlet Flow, m^3/sec (gpm)	0.665	(10,540)
Exit Flow, m^3/sec	0.554	(8,785)
Inducer Head, m (ft)	823.0	(2,700)
Stage Head, m (ft)	2418.6	(7,935)
Overall Head, m (ft)	5660.1	(18,570)
No. of Stages		2 + Inducer
Power, mHp (hp)	60,434	(59,600)
Inducer Suction Specific Speed	4.14	(20,000)
NPSH, m (ft)	99.4	(326)
Inducer Specific Speed	0.849	(4,100)
Stage Specific Speed	0.346	(1,670)
Overall Efficiency, %	82	

TABLE LXXVII (cont.)

<u>Turbine</u>

No. of Stages	1	
Speed, rpm	15,000	
Flow, kg/sec (lb/sec)	598.4	(1319.2)
Inlet Pressure, atm (psia)	438.4	(6444)
Pressure Ratio	1.49	
Inlet Temperature, °K (°R)	922.2	(1660)
Nozzle Outlet Velocity, m/sec (ft/sec)	435.9	(1430)
Blades Speed (mean), m/sec (ft/sec)	218.8	(718)
Efficiency, %	80	
Rotor Tip Dia, cm (in.)	31.50	(12.40)
Hub Dia, cm (in.)	24.13	(9.50)
Annular Area, Aa, cm^2 ($in.^2$)	321.96	(49.9)
AaN^2 (Annular Area x Speed Squared)	72.26×10^9	(11.2×10^9)

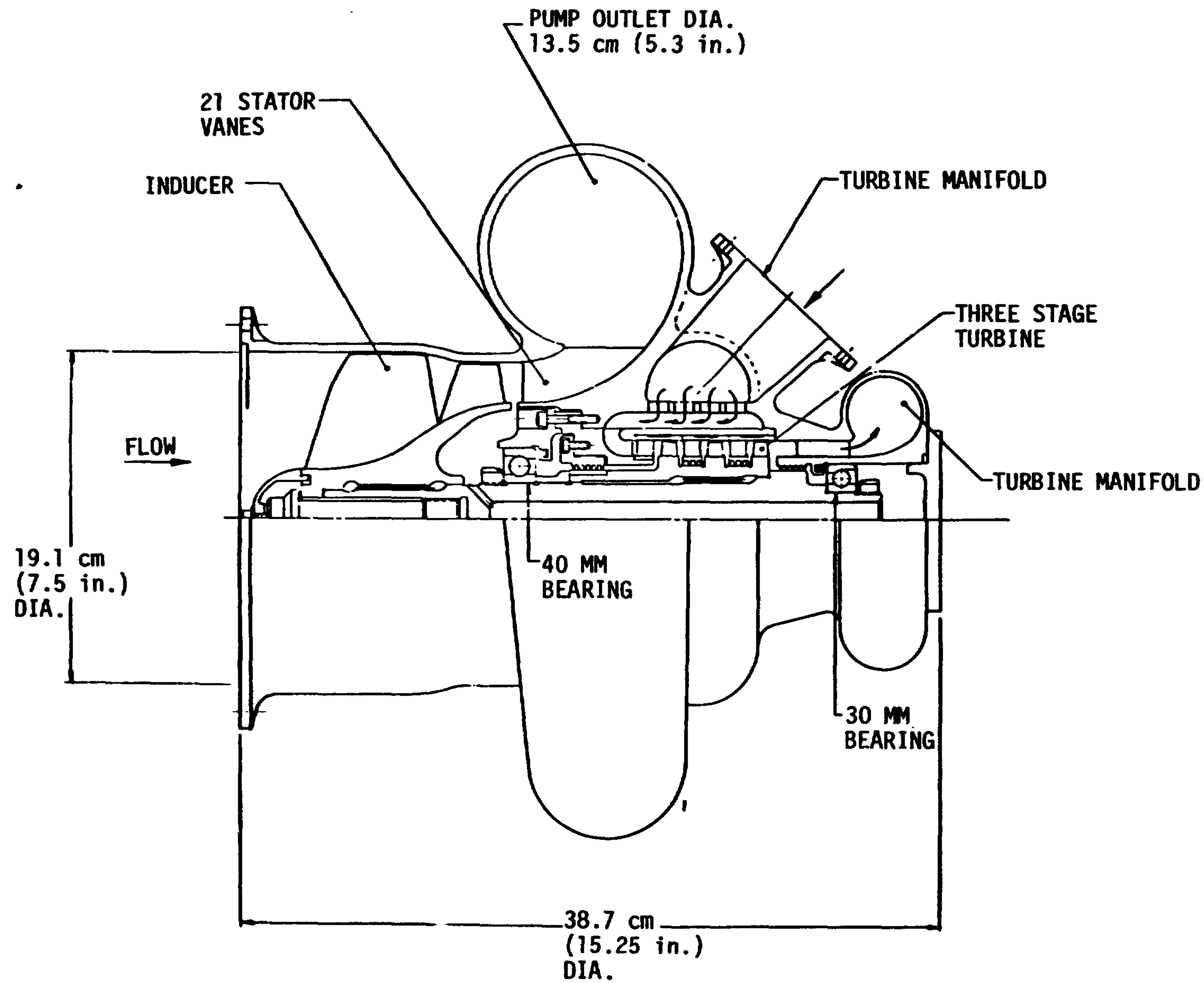

Figure 73. Baseline Mode 1, Dual-Fuel and Alternate Mode 1 Low Speed RP-1 TPA

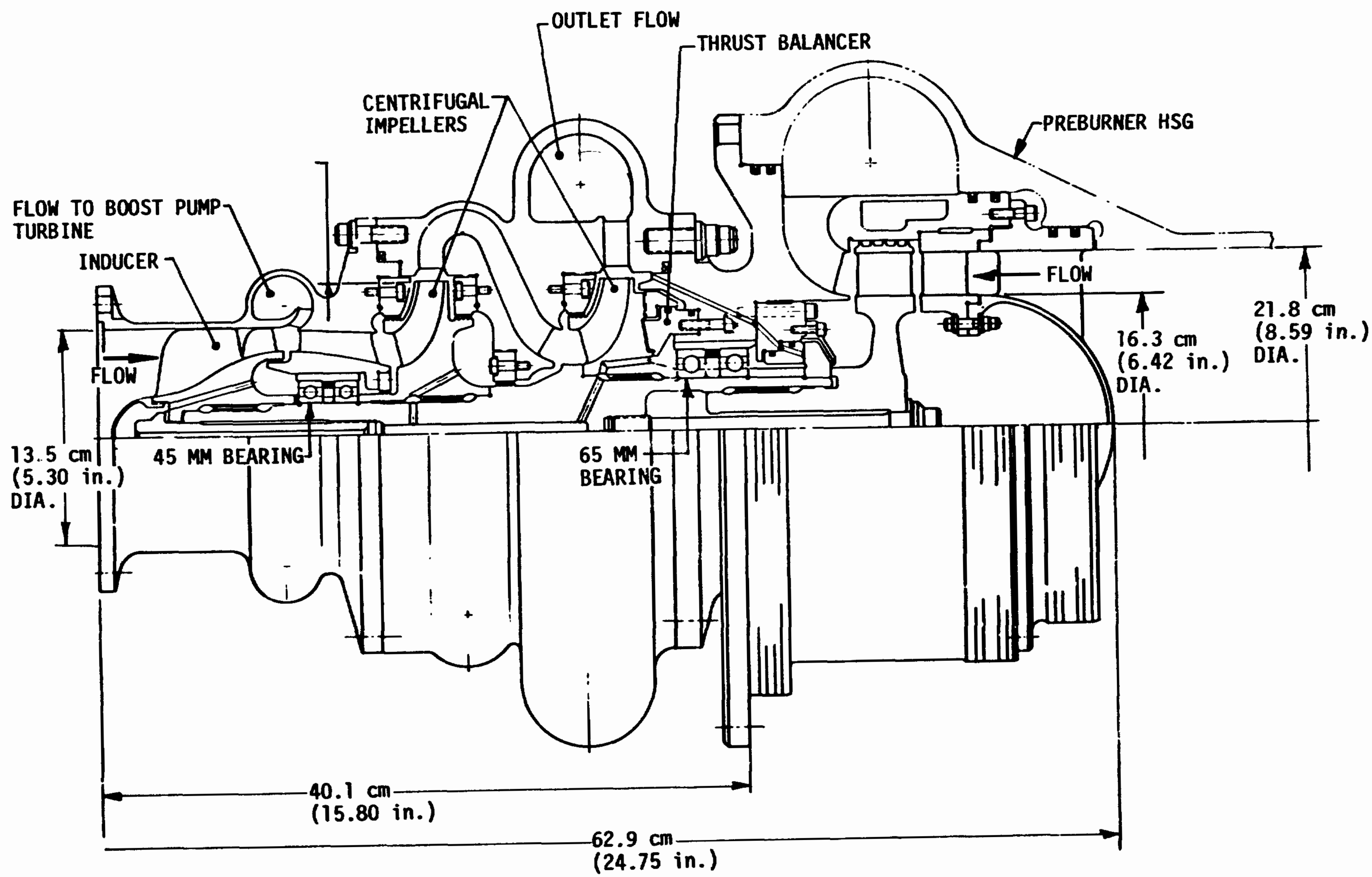

Figure 74. Baseline Mode 1 and Dual-Fuel High Speed RP-1 TPA

The design parameters for the low speed RP-1 pump are listed in Table LXXVIII. The low speed pump incorporates a scroll discharge design to accommodate the engine installation. The estimated pump performance at the design point is 83%. The turbine vector diagrams were selected for a ratio of mean blade speed to nozzle discharge velocity of approximately 0.5 (near optimum for an impulse turbine). The hydraulic turbine is driven by propellant flow from the main pump.

The high speed fuel turbopump is shown in Figure 74. The configuration is basically the same as the LOX turbopump and incorporates essentially the same design features. The pump and turbine design parameters are listed in Table LXXIX. The estimated pump performance at the design point is 82%. The turbine was configured for free vortex blading with approximately 10 percent reaction at the rotor mean diameter. The turbine efficiency is estimated from Ref. 74 to be at least 75 percent. The blading centrifugal stress will be quite conservative based on AaN^2 (see Fig. 30, Page 45 of Ref. 74).

2. <u>Dual-Fuel Engine</u>

The LOX and RP-1 turbopumps used for the dual-fuel engine are the same as those designed for the baseline Mode 1 engine.

The low speed LH_2 pump for use on the dual-fuel engine is shown on Figure 75. The configuration consists of a high head inducer stage driven by a four stage hydraulic turbine. The design point parameters are listed in Table LXXX. The pump performance at the design point is 85%. The rotating assembly is supported by spring loaded angular contact bearings as indicated in Figure 75. The axial thrust on the bearings is kept low by placement of the labyrinth seal between the pump and turbine.

The high speed LH_2 turbopump configuration is shown in Figure 76. As with the PP-1 and LOX high speed pumps, the inducer stage supplies the fluid to drive the hydraulic turbine. A three-stage centrifugal pump was necessary to maintain the stage specific speed above 1000. The turbine end bearing package is outboard of the turbine to avoid either high shaft stress or an excessive value of bearing DN.

The pump and turbine design parameters are listed in Table LXXXI. Although the turbopump configuration satisfies all the stipulated design criteria; further design refinements would be desirable to reduce weight. Further studies would be required to explore potential shaft critical speed and vibration problems.

3. <u>Alternate Mode 1 Engine</u>

The alternate Mode 1 hydrogen cooled, gas generator cycle engine has lower pump discharge requirements than the other candidates as discussed

TABLE LXXVIII. - BASELINE MODE 1 AND DUAL-FUEL ENGINE
LOW SPEED RP-1 TPA DESIGN POINT

	Pump		Turbine	
Speed, rpm	8715		8715	
Flow, m^3/sec (gpm)	0.272	(4310)	0.054	(862)
Head, m (ft)	112.8	(370)	871.7	(2860)
Power, mHp (hp)	390	(385)	390	(385)
NPSH, m (ft)	19.81	(65)		
Suction Specific Speed	5.175	(25,000)		
Specific Speed	1.387	(6700)	0.308	(1490)(Stage)
Stages	1		3	
Efficiency, %	83		78	

TABLE LXXIX. - BASELINE MODE 1 AND DUAL FUEL ENGINE
HIGH SPEED RP-1 TPA DESIGN POINT

<u>Pump</u>		
Speed, rpm	25,370	
Inlet flow, m^3/sec (gpm)	0.326	(5,172)
Exit flow, m^3/sec (gpm)	0.272	(4,310)
Inducer Head, m (ft)	961.3	(3,154)
Stage Head, m (ft)	3026.1	(9,928)
Overall head, m (ft)	7013.4	(23,010)
Number of stages		2 + Inducer
Power, mHp (hp)	26,567	(26,200)
Inducer Suction		
Specific speed	4.14	(20,000)
NPSH, m (ft)	125.3	(411)
Inducer Specific Speed	0.897	(4,335)
Stage Specific Speed	0.346	(1,670)
Overall Efficiency, %	82	

TABLE LXXIX (cont.)

Turbine

No. of Stages	1	
Speed, rpm	25,370	
Flow, kg/sec (lb/sec)	249.3	(549.6)
Inlet Pressure, atm (psia)	4615.2	(6,783)
Pressure Ratio	1.56	
Inlet Temperature, °K (°R)	866.7	(1,560)
Nozzle Outlet Velocity, m/sec (ft/sec)	449.3	(1,474)
Blade Speed (mean), m/sec (ft/sec)	253.3	(831)
Efficiency, %	75	
Rotor Tip Dia, cm (in.)	21.82	(8.59)
Hub Dia, cm (in.)	16.31	(6.42)
Annular Area, cm^2 ($in.^2$)	165.2	(25.6)
Aa N^2 (Annular Area x Speed Squared)	106.46×10^9	(16.5×10^9)

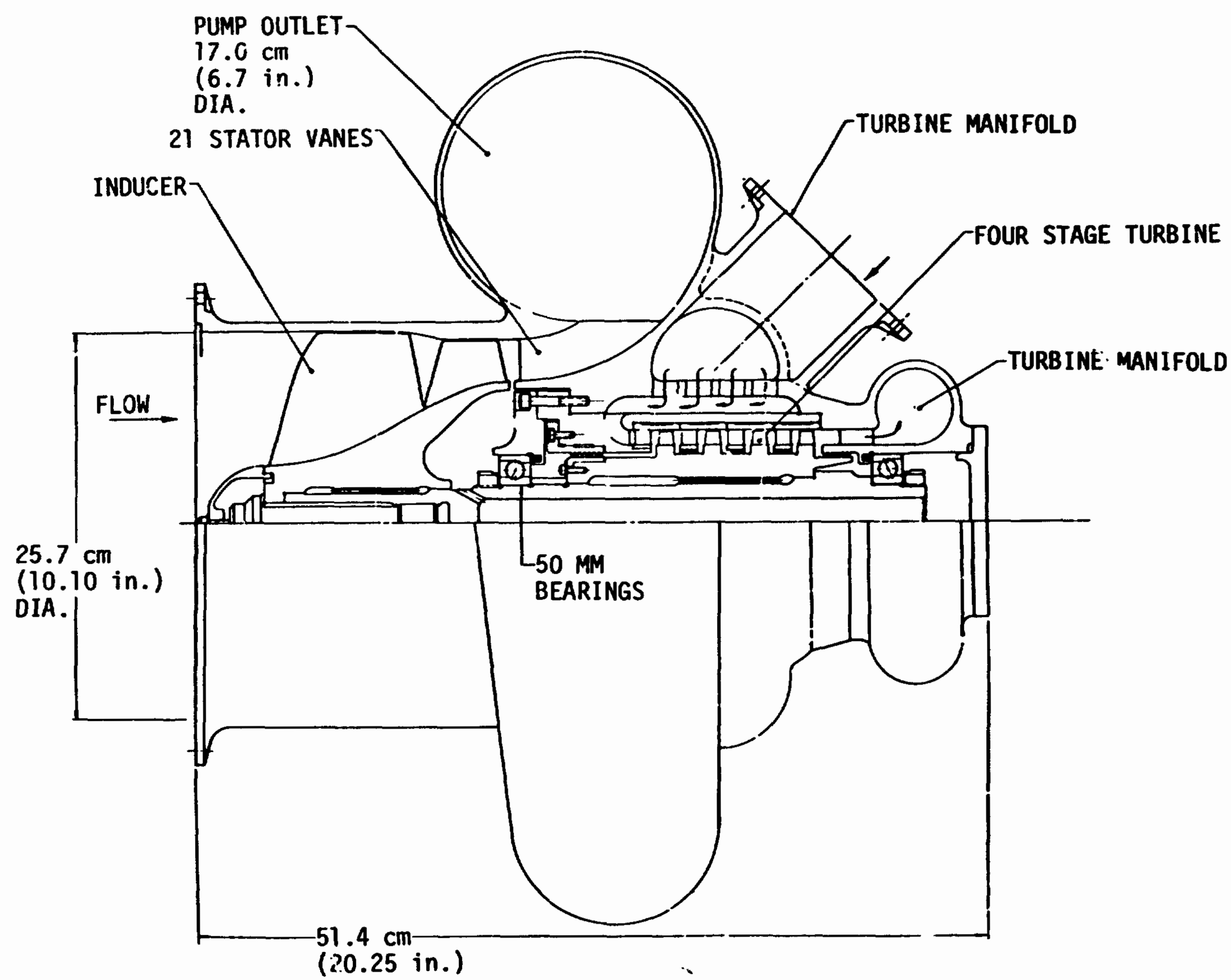

Figure 75. Dual-Fuel Low Speed LH_2 TPA

TABLE LXXX. - DUAL-FUEL ENGINE LOW SPEED LH_2 TPA DESIGN POINT

	Pump		Turbine	
Speed, rpm	11,420		11,420	
Flow, m^3/sec (gpm)	0.898	(14,240)	0.180	(2,848)
Head, m (ft)	549	(1,800)	4145	(13,600)
Power, mhp (hp)	545.5	(538)	545.5	(538)
NPSH	30.5	(100)		--
Suction Specific Speed	11.8	(43,100)		--
Specific Speed	1.02	(4,930)	0.283	(1,369)(Stage)
Stages	1		4	
Efficiency, %	85		78	

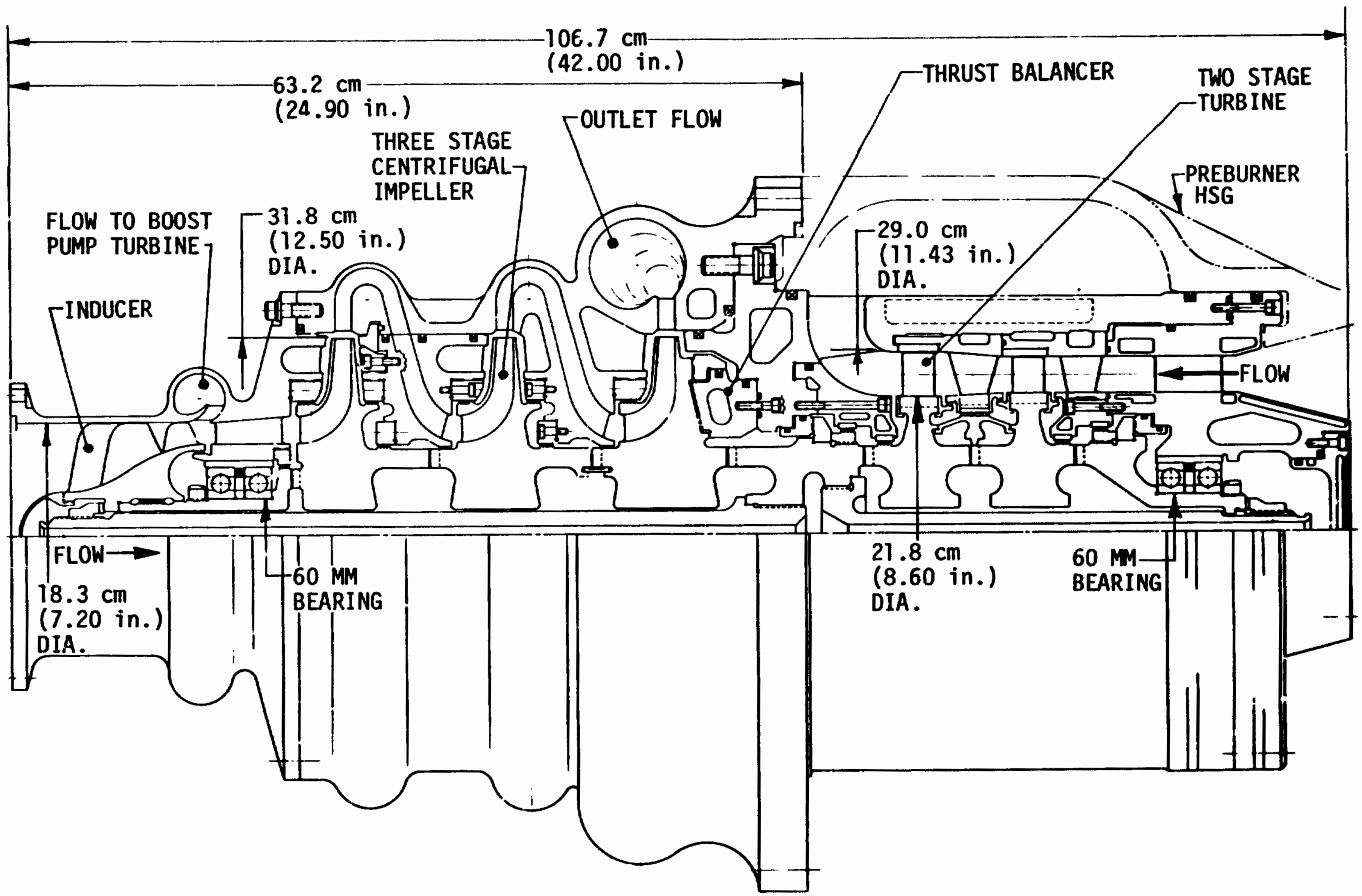

Figure 76. Dual-Fuel High Speed LH_2 TPA

TABLE LXXXI. - DUAL-FUEL ENGINE HIGH SPEED LH_2 TPA DESIGN POINT

<u>Pump</u>		
Speed, rpm	33,000	
Inlet flow, m^3/sec (gpm)	1.078	(17,090)
Exit Flow, m^3/sec (gpm)	0.898	(14,240)
Inducer Head, m (ft)	4572	(15,000)
Stage Head, m (ft)	16,805	(55,133)
Overall Head, m (ft)	54,986	(180,400)
No. of Stages		3 + Inducer
Power, mHp (hp)	59,826	(59,000)
Inducer Suction Specific Speed	4.14	(20,000
NPSH, m (ft)	30.48	(100)
Inducer Specific Speed	0.659	(3,183)
Stage Specific Speed	0.227	(1,095)
Overall Efficiency, %	80	

TABLE LXXXI (cont.)

Turbine

No. of Stages	2	
Speed, rpm	33000	
Flow, kg/sec	113.6	(250.4)
Inlet Pressure, Atm (psia)	311.1	(4572)
Pressure Ratio	1.27	
Inlet Temperature, °K (°R)	922.2	(1660)
First Stage Nozzle Outlet Velocity, m/sec (ft/sec)	762.0	(2500)
Rotor Blade Speed (mean), m/sec (ft/sec)	439.2	(1441)
Overall Efficiency, %	81	
Second Stage Rotor Tip Dia., cm (in.)	28.96	(11.4)
Hub Dia., (in.)	21.84	(8.6)
Annular Area, Aa, cm^2 ($in.^2$)	283.9	(44.0)
AaN^2 (Annular Area X Speed Squared)	309.1×10^9	(47.9×10^9)

in Section VC. However, two more pumps are required for the LH_2 flow. Because of the reduced pump discharge pressure requirement, the main LOX and RP-1 pumps can operate at higher speeds than the baseline Mode 1 engine pumps. Consequently, the required NPSH for the high speed pump inducers is greater. The Mode 1 engine low speed LOX and RP-1 pumps meet these requirements with a slight increase in speed. The LH_2 turbopumps are essentially scaled down versions of the dual-fuel engine LH_2 turbopumps.

The low speed LOX turbopump selected for the alternate Mode 1 engine (Figure 71) is the same as that selected for the baseline Mode 1 and dual-fuel engines. However, the operating speed is increased from 2,560 rpm to 2,650 rpm. The small increase in rotational speed does not significantly affect the low speed pump NPSH requirement and the design point performance is reduced by only approximately 0.1%.

The high speed LOX pump configuration is shown on Figure 77 and the design parameters are listed in Table LXXXII. The turbopump consists of a high head inducer, a single stage centrifugal pump and a velocity compounded turbine (Curtis Stage). The rotor is supported by two bearing packages, each of which consists of two spring loaded angular contact ball bearings. Rotor thrust is balanced by a balance piston. Fluid is tapped-off of the high head inducer to supply the hydraulic turbine which drives the low speed LOX pump. A preliminary design for the hot gas seal between the pump and the fuel-rich turbine is also shown on the figure. The pump configuration shown has not been optimized from the standpoint of critical speeds and rotor dynamics at design speed. Further refinements in the configuration would be required to achieve an optimum reliable design. The weight, however, would not change appreciably from the weight of the configuration shown.

The low speed RP-1 turbopump selected for the alternate Mode 1 engine is identical with that selected for the Mode 1 and dual-fuel engines (Figure 73). Its operating speed, however, was increased from 8715 rpm to approximately 8800 rpm to increase the head from 112M (366 feet) to 123M (405 feet). The small increase in speed does not significantly affect the NPSH requirement or the pump performance.

The high speed (RP-1) pump configuration is shown on Figure 78, and the design parameters are listed in Table LXXXIII. The turbopump consists of a high head inducer, a single stage centrifugal pump, and a velocity compounded turbine (Curtis Stage). The rotor is supported by two bearing packages each of which consists of two spring loaded angular contact ball bearings. Rotor thrust is balanced by a hydrostatic balance piston. As with the LOX TPA for the alternate Mode 1 engine, rotor dynamics studies and critical speed estimates should be made in the next design iteration.

The low speed LH_2 turbopump is shown in Figure 79, and is essentially a scaled version of the low speed pump configured for the dual-fuel engine. The pump and hydraulic turbine design parameters are listed in

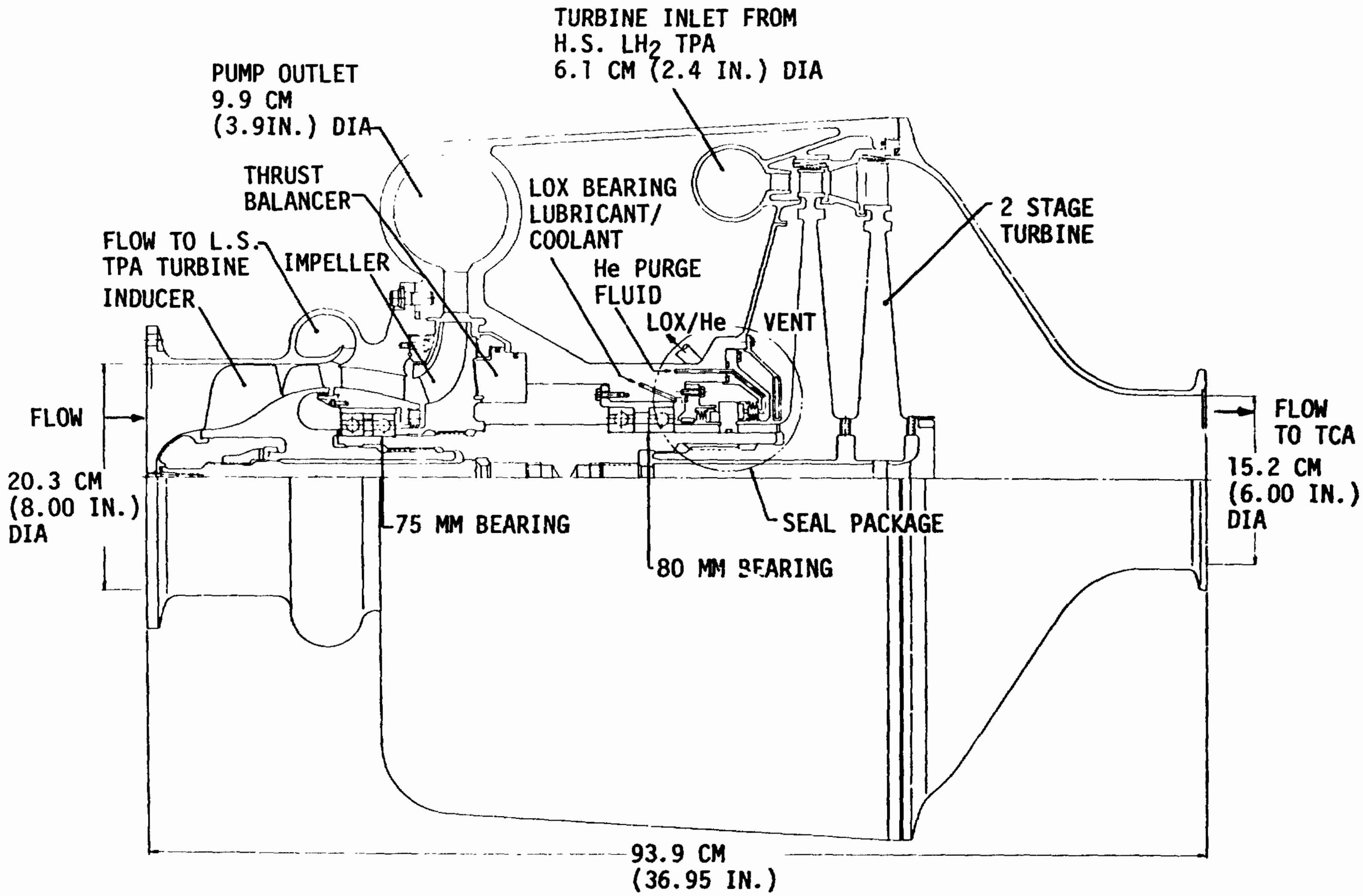

Figure 77. Alternate Mode 1 High Speed LOX TPA

TABLE LXXXII. - ALTERNATE MODE 1 ENGINE HIGH SPEED
LOX TPA DESIGN POINT

Pump		
Speed, RPM	16,100	
Inlet Flow, m^3/sec (gpm)	0.661	(10,476)
Outlet Flow, m^3/sec (gpm)	0.551	(8,730)
Inducer Head, m (ft)	883.9	(2,900)
Stage Head, m (ft)	2173.2	(7,130)
Overall Head, m (ft)	3157.1	(10,030)
No. of Stages		1 + Inducer
Power, mHp (hp)	33,766	(33,300)
Inducer Suction Specific	4.14	(20,000)
NPSH, m (ft)	109.7	(360)
Inducer Specific Speed	0.863	(4,170)
Centrifugal Stage Specific Speed	0.401	(1,939)
Overall Efficiency, %	80	
Turbine		
Number of Stages	1	
Stage Type		Velocity Compounded (Curtis Stage)
Speed, rpm	16,100	
Flow, kg/sec (lb/sec)	9.53	(21)
Inlet Pressure, atm (psia)	173.4	(2,549)
Pressure Ratio (Total to Static)	12.7	
Inlet Temp., °K (°R)	859.4	(1,547)
Nozzle Velocity (Ideal), m/sec (ft/sec)	2859.0	(9,380)
Mean Blade Speed, m/sec (ft/sec)	457.2	(1,500)
Overall Efficiency, %	60	
Second Rotor Tip Dia, cm (in.)	56.64	(22.3)
Hub Dia, cm (in.)	51.56	(20.3)
Annular Area, cm^2 ($in.^2$)	432.3	(67)
AaN^2 *Annular Area x Speed Squared)	111.6×10^9	(17.3×10^9)

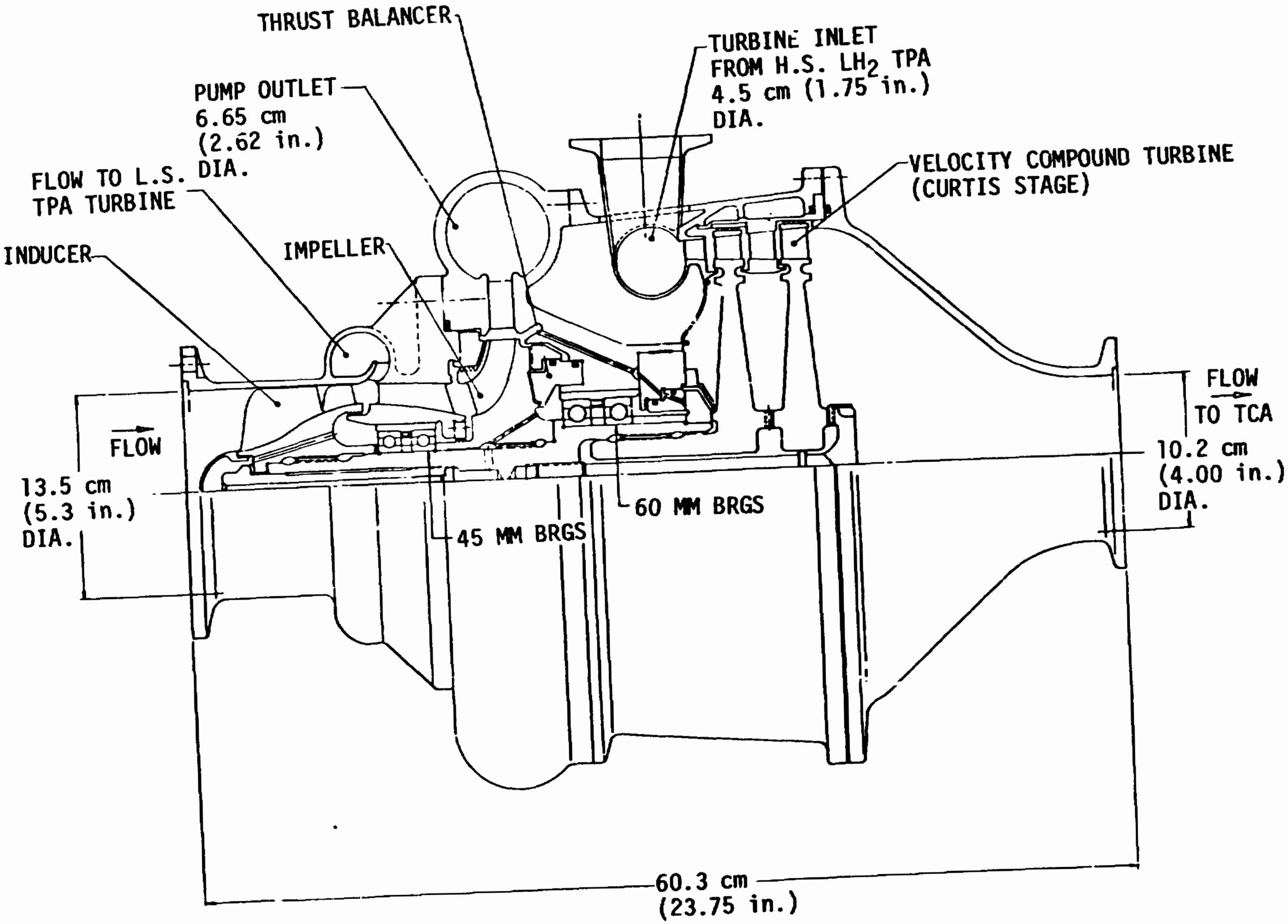

Figure 78. Alternate Mode 1 High Speed RP-1 TPA

TABLE LXXXIII. - ALTERNATE MODE 1 ENGINE HIGH SPEED RP-1 TPA DESIGN POINT

Pump		
Speed RPM	29,900	
Inlet, Flow m^3/sec (gpm)	0.324	(5,136)
Outlet Flow, m^3/sec (gpm)	0.270	(4,280)
Inducer Head, m (ft)	1219.2	(4,000)
Centrifugal Stage Head, m (ft)	3130.3	(10,270)
Overall Head, m (ft)	4349.5	(14,270)
No. of Stages		1 + Inducer
Power, mHp (hp)	17,035	(16,800)
Inducer Suction Specific Speed	4.14	(20,000)
NPSH, m (ft)	137.2	(450)
Inducer Specific Speed	0.882	(4,260)
Centrifugal Stage Specific Speed	0.393	(1,900)
Overall Efficiency, %	75	
Turbine		
Number of Stages	1	
Stage Type		Velocity Compounded (Curtis Stage)
Speed, RPM	29,900	
Flow, kg/sec (lb/sec)	4.99	(11)
Inlet Pressure, atm (psia)	177.7	(2,612)
Pressure Ratio (Total to Static)	12.7	
Inlet Temp., °K (°R)	859.4	(1,547)
Nozzle Velocity (Ideal), m/sec (ft/sec)	2859.0	(9,380)
Mean Blade Speed, m/sec (ft/sec)	457.2	(1,500)
Overall Efficiency, %	60	
Second Rotor Tip Dia, cm (in.)	30.48	(12.0)
Hub Dia, cm (in.)	25.40	(10.0)
Annular Area, cm^2 ($in.^2$)	219.4	(34)
AaN^2 (Annular Area x Speed Squared)	193.6×10^9	(30×10^9)

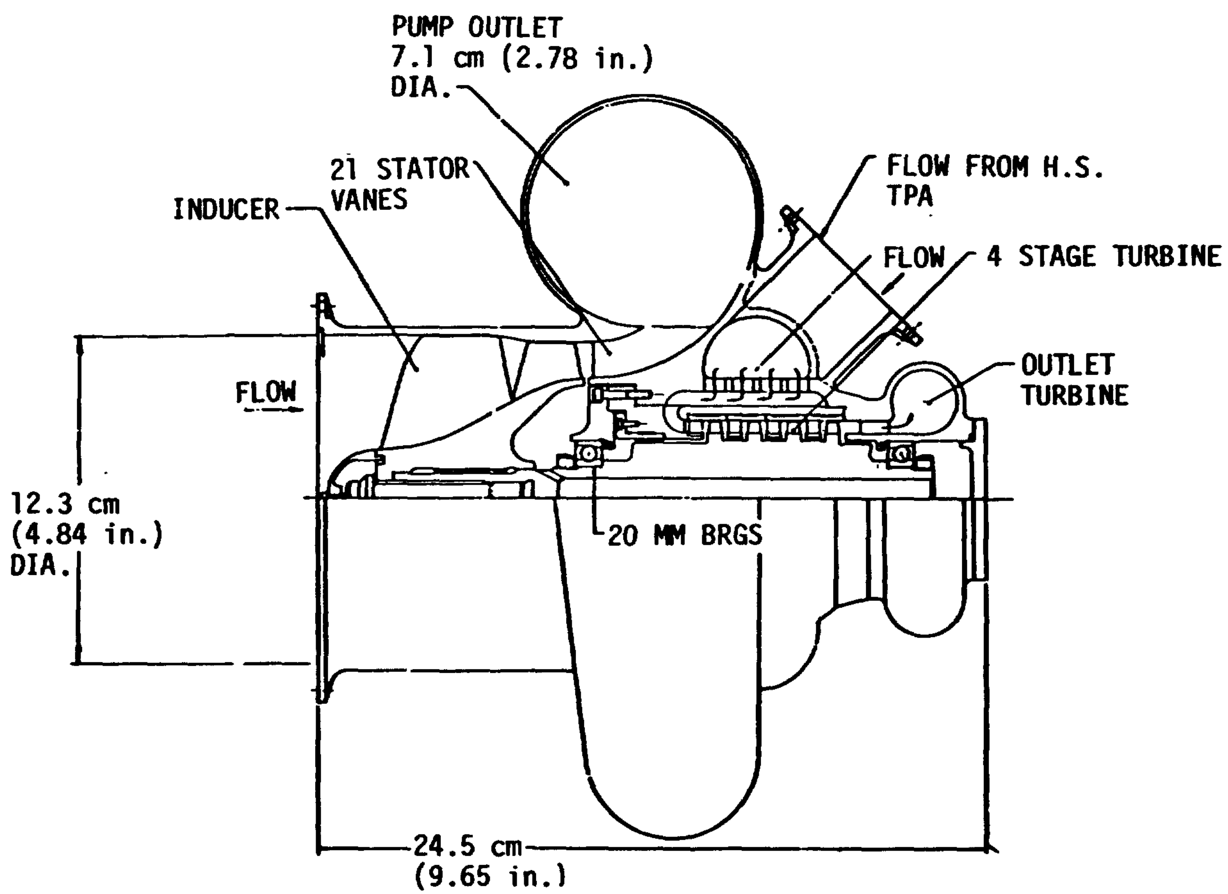

Figure 79. Alternate Mode 1 Low Speed LH_2 TPA

Table LXXXIV. The pump exit scroll configuration was selected for ease of mounting on the engine.

The high speed LH_2 turbopump configuration is shown in Figure 80, and the design parameters are listed in Table LXXXV. The configuration is a scaled version of the high speed LH_2 pump configured for the dual-fuel engine.

F. THRUST CHAMBER DESIGN ANALYSES

1. Performance

The objective of the performance analysis was to predict the delivered specific impulse performance of the candidate engines using JANNAF methodology. As part of this analysis, it was necessary to establish an "optimum" compromise nozzle contour for the two modes of operation of the dual-fuel engine.

a. Dual-Fuel Nozzle Contour Analysis

The objective of the dual-fuel contour analysis was to determine relative performance tradeoffs and to select a nozzle for the dual-fuel engine which offers the best performance in both modes of operation. In the analysis, 40:1 and 200:1 expansion ratio nozzles of various lengths were generated with a RAO optimum nozzle contour program. For combinations of these contours, the TDK computer program (Ref. 51) was utilized to evaluate the performance for various Mode 1 and Mode 2 engine configurations.

The Mode 1 performance was evaluated with a LOX/RP-1 propellant combination at a mixture ratio of 2.9 with gamma equal to 1.129. Mode 2 performance is based on a LOX/LH_2 nozzle combination at a mixture ratio of 7.0 with gamma equal to 1.210.

A less than optimum Mode 2 contour results from combining an optimum 40:1 Mode 1 contour with an optimum 200:1 contour. The opposite is also true. In general, a performance tradeoff exists between the various Mode 1 and Mode 2 nozzle combinations. The results of the study are summarized on Table LXXXVI.

Case 1 illustrates the relative performance values for the shortest possible optimum 200:1 nozzle contour (73.2% bell based on RAO criteria) combined with an optimum 40:1 contour of sufficient length (83.7% bell) to provide a 90% bell nozzle for the Mode 2 engine configuration. Case 2 illustrates the relative performance values for the shortest possible optimum 40:1 nozzle contour (57.9% bell based on RAO criteria) combined with an optimum 200:1 contour of sufficient length (85.4% bell) to provide a 90% bell nozzle for the Mode 2 engine configuration. Case 1 results in the best performance at ε = 40:1 at the expense of the performance at ε = 200:1. Conversely, Case 2 gives the best performance at ε = 200:1 at the expense of

TABLE LXXXIV. - ALTERNATE MODE 1 ENGINE LOW SPEED LH_2 TPA DESIGN POINT

	Pump		Turbine	
Speed, RPM	18,790		18,790	
Flow, m^3/sec (gpm)	0.129	(2,040)	0.026	(408)
Head, m (ft)	289.6	(950)	2438.4	(8,000)
Power, mHp (hp)	41.6	(41)	41.6	(41)
NPSH, m (ft)	27.43	(90)		--
Suction Specific Speed	6.003	(29,000)		--
Specific Speed	1.027	(4,960)	0.263	(1,270)(Stage)
No. of Stages	1		4	
Efficiency, %	85		71	

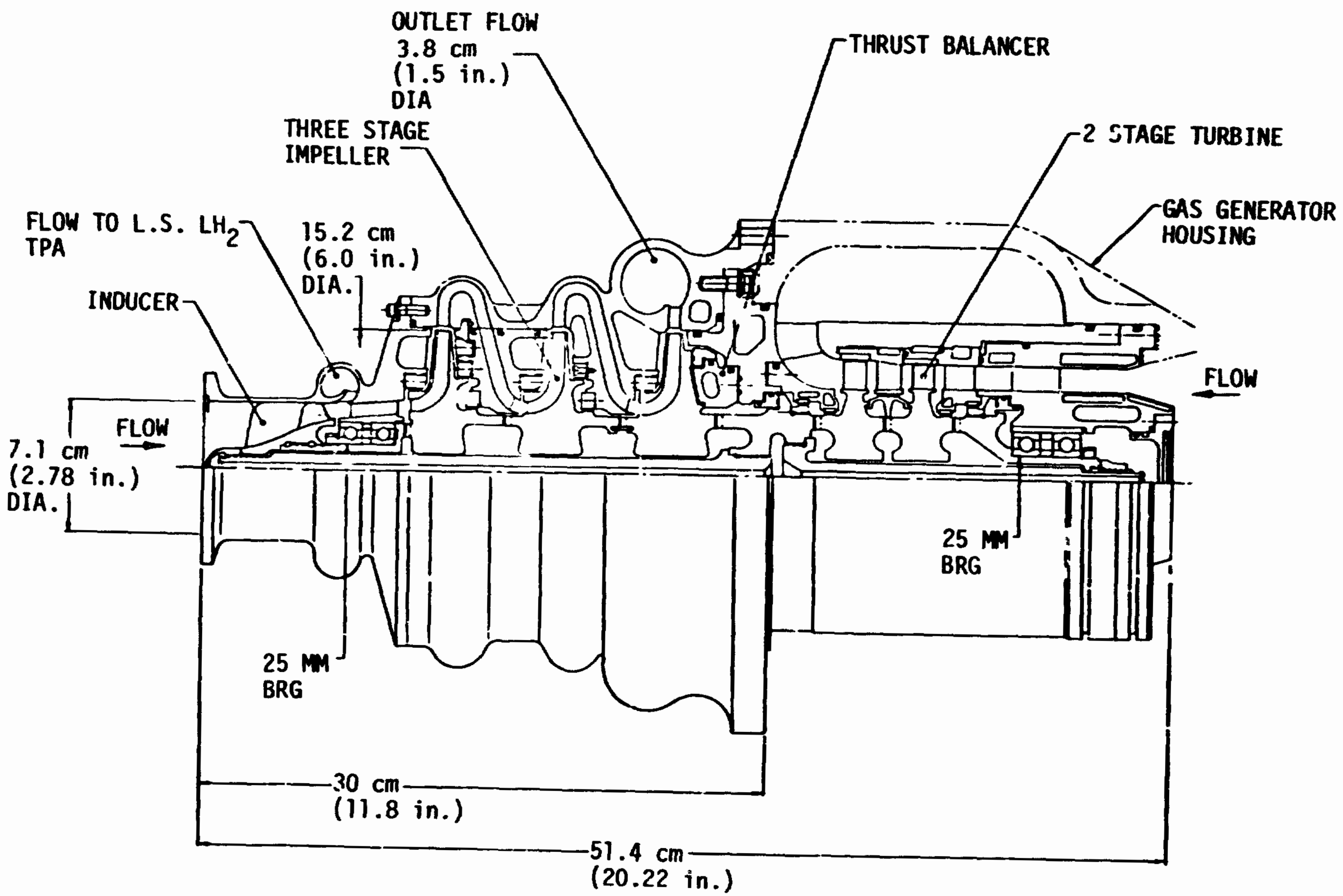

Figure 80. Alternate Mode 1 High Speed LH_2 TPA

TABLE LXXXV. - ALTERNATE MODE 1 ENGINE HIGH SPEED LH_2 TPA DESIGN POINT

Pump		
Speed, RPM	70,000	
Inlet Flow, m^3/sec (gpm)	0.154	(2,448)
Outlet Flow, m^3/sec (gpm)	0.129	(2,040)
Inducer Head, m (ft)	2743.2	(9,000)
Stage Head, m (ft)	17,883	(58,670)
Overall Head, m (ft)	56,388	(185,000)
No. of Stages		3 + Inducer
Power, mHp (hp)	11,478	(11,320)
Inducer Suction Specific Speed	4.14	(20,000)
NPSH, m (ft)	292.6	(960)
Inducer Specific Speed	0.708	(3,420)
Stage Specific Speed	0.174	(840)
Overall Efficiency, %	60	
Turbine		
No. of Stages	2	
Speed, RPM	70,000	(70,000)
Flow, kg/sec (lb/sec)	14.52	(32)
Inlet pressure, atm (psia)	272.5	(4,005)
Pressure Ratio (Total to Static)	1.43	(1.43)
Inlet Temp., °K (°R)	922.2	(1,660)
Nozzle Velocity, m/sec (ft/sec)	898.6	(2,948)
Mean Blade Speed, m/sec (ft/sec	404.5	(1,327)
Efficiency, %	72	(72)
Last Stage Rotor Tip Dia, cm (in.)	12.62	(4.97)
Hub Dia, cm (in.)	9.45	(3.72)
Annular Area, Aa, cm^2 ($in.^2$)	54.84	(8.5)
N^2 Aa	271×10^9	(42×10^9)

TABLE LXXXVI. - DUAL-FUEL NOZZLE CONTOUR EVALUATION

$\varepsilon_1 = 40$
$\varepsilon_2 = 200$

Case		% Bell Length	Performance Change, %*	
1	Mode 1	83.7	0	
	Mode 2 (Overall)	90.0	-1.97	
2	Mode 1	57.9	-2.30	
	Mode 2	90.0	-0.73	
3	Mode 1	80.0	0	
	Mode 2	121.0	-0.85	
4	Mode 1	75.0	-0.21	Design
	Mode 2	119.0	-0.68	

*Compared to Optimum 80% Mode 1 and 90% Mode 2 Bells.

the performance at ϵ = 40:1 (within the design constraint of a 90% bell length for the ϵ = 200:1 nozzle). Note that in either case, the Mode 2 nozzle results in a performance loss from the single Mode 2 baseline nozzle and as the Mode 2 nozzle performance loss is minimized, the Mode 1 performance loss is significantly increased.

As a result, longer Mode 2 nozzle contours were investigated in order to improve the Mode 2 performance without changing the Mode 1 performance.

Case 3 illustrates the relative performance for an 80% bell Mode 1 nozzle combined with an optimum 110% bell nozzle for the Mode 2 engine. In this arrangement, a 0.85% specific impulse performance loss occurs in the Mode 2 engine with no loss for the Mode 1 engine. The Mode 2 overall nozzle length for this concept is equivalent to a 121% bell nozzle.

The best overall engine performance appears to be obtained by sacrificing some performance for both the Mode 1 and Mode 2 configurations as illustrated in Case 4. In this case, an optimum 75% bell nozzle (Mode 1) is combined with an optimum 110% bell, which results in a Mode 2 engine with an overall 119% bell nozzle length. This combination effects a 0.21% and 0.68% drop in Mode 1 and Mode 2 vacuum specific impulse, respectively, compared with the baseline 80% bell Mode 1 and 90% bell Mode 2 nozzles. This case was selected for design. The nozzle is heavier but the performance loss is reduced to 0.7 sec in Mode 2.

b. Delivered Performance

Tables LXXXVII through XC present delivered Isp at nominal and $\pm$ 10% of nominal mixture ratio for various engine candidates.

The delivered performance values were calculated using the JANNAF simplified calculation technique described in Section 3 of CPIA publication 246. The ODK (One Dimensional Kinetic) computer program was used to determine the theoretical vacuum specific impulse and kinetic performance loss, for the respective propellant combinations and mixture ratios. Delivered Isp was obtained by correcting the ODK performance for the following losses: (1) injector energy release efficiency, (2) nozzle divergence efficiency, (3) nozzle and chamber boundary layer loss, and (4) where applicable, a sea-level Isp correction. For the gas generator cycle, an additional calculated 1.5 second loss was subtracted as a result of the gas-generator flow being dumped downstream of the throat. To make up for this loss such that the delivered vacuum and sea-level delivered specific impulse are nearly equivalent to the baseline performance, the gas generator nozzle expansion ratio and chamber pressure were increased to 42.7:1 and 289 atm (4250 psia), respectively.

An injector energy release efficiency of 0.985 was used. This is based on a 24.8 cm (9.75 in.) chamber length for the baseline Mode 1 and

TABLE LXXXVII. - MODE 1 BASELINE DELIVERED SPECI¯˙C IMPULSE

$\varepsilon = 40:1$ — $P_c = 272$ atm (4000 psia)

80% Bell Length — Propellant LOX/RP-1

		(Nominal)	
Mixture Ratio (O/F)	2.61	2.90	3.19
ODK Vacuum I_{sp}(sec)	358.8	360.3	357.3
Energy Release Efficiency	.9850	.9850	.9850
Divergence Efficiency	.9935	.9935	.9935
Corrected I_{sp} (sec)	351.1	352.6	349.7
Boundary Layer Loss (sec)	2.0	2.0	2.0
Delivered Vacuum I_{sp} (sec)	349.1	350.6	347.7
Sea Level I_{sp} Correction (sec)	27.4	27.0	26.6
Delivered Sea Level I_{sp} (sec)	321.7	323.6	321.1

TABLE LXXXVIII. - MODE 1 GAS GENERATOR CYCLE DELIVERED SPECIFIC IMPULSE

ε = 42.7:1 | P_c = 289 atm (4250 psi)

80% Bell Length | Propellant = LOX/RP-1

		(Nominal)	
Mixtur Ratio (O/F)	2.61	2.90	3.19
ODK Vacuum I_{sp} (sec)	360.0	361.6	358.7
Energy release efficiency	.9850	.9850	.9850
Divergence efficiency	.9946	.9946	.9946
Corrected I_{sp} (sec)	352.7	354.3	351.4
Boundary layer loss (sec)	2.1	2.1	2.1
Gas Generator loss (sec)	1.5	1.5	1.5
Delivered Vacuum I_{sp} (sec)	349.1	350.7	347.8
Sea level I_{sp} Correction (sec)	27.5	27.2	26.8
Delivered Sea Level I_{sp} (sec)	321.6	323.5	321.0

TABLE LXXXIX. - MODE 1 DUAL-FUEL DELIVERED SPECIFIC IMPULSE

$\varepsilon = 40:1$ $P_c = 272$ atm (4000 psia)

75% Bell Length Propellant LOX/RP-1

Mixture Ratio (O/F)	2.61	(Nominal) 2.90	3.19
ODK Vacuum I_{sp} (sec)	358.8	360.3	357.3
Energy release efficiency	.9850	.9850	.9850
Divergence efficiency	.9915	.9915	.9915
Corrected I_{sp} (sec)	350.4	351.9	349.0
Boundary layer loss (sec)	2.0	2.0	2.0
Delivered Vacuum I_{sp} (sec)	348.4	349.9	347.0
Sea Level I_{sp} Correction (sec)	27.4	27.0	26.6
Delivered Sea Level I_{sp} (sec)	321.0	322.9	320.4

TABLE XC. - MODE 2 DUAL FUEL DELIVERED SPECIFIC IMPULSE

$\epsilon = 200:1$ | P_c = 204 atm (3000 psia)

119% Bell Length (See Enclosure 4) | Propellant LOX/LH_2

		(Nominal)	
Mixture Ratio (O/F)	6.3	7.0	7.7
ODK Vacuum I_{sp} (sec)	477.5	475.0	471.1
Energy release efficiency	.9850	.9850	.9850
Divergence efficiency	.9902	.9902	.9902
Corrected I_{sp} (sec)	465.7	463.3	459.5
Boundary Layer Loss (sec)	4.1	4.1	4.1
Delivered Vacuum I_{sp} (sec)	461.6	459.2	455.4

dual-fuel engines and a 72.8 cm (18.50) length for the alternate Mode 1 engines. The nozzle divergence efficiency is based on the value computed with the TDK program (Ref. 51) using the ideal gas option.

The chamber boundary layer friction loss was calculated with an ALRC computerized formulation of the JANNAF boundary layer chart technique (Ref. 52). Sea-level performance was calculated by subtracting the ambient pressure nozzle exit force from the delivered vacuum performance.

2. Thermal Analysis

Heat transfer and hydraulic analyses were conducted to formulate regeneratively cooled thrust chamber designs for the three candidate engine concepts. The analyses were conducted using the Task VI performance governed nozzle contour results of the previous paragraphs, updated cycle life governed thermal limits, and chamber curvature enhancement of the liquid side heat transfer coefficient.

The results from the cycle life criterion and wall strength limits are presented on Figures 81 and 82. Figure 81 presents two curves showing the allowable temperature differential ΔT, from the maximum gas-side wall temperature (T_{wg}) to the average external wall temperature (T_{BS}) as a function of the latter temperature for the barrel section of the chamber and for the remainder of the chamber and nozzle. Figure 82 presents the allowable channel width to wall thickness ratio as a function of the chamber gas-side wall temperature for three pressure differential values across the gas-side wall. This curve is applicable to zirconium-copper slotted chambers which are proposed for use in all three engine concepts.

The curvature enhancement effects were treated in the same manner as that used in Reference 75. This correction for the effects of curvature on friction coefficients is also applicable to local heat transfer coefficients. For the purposes of this analysis, only the heat transfer coefficients of the gas side liquid wall was corrected, the other walls of the passage were exempted from curvature effects.

The coolant heat transfer correlation used for the baseline and the dual-fuel engine concepts where LOX cooling is employed was the same as used in the Task II analysis, with curvature enhancement effects added. The use of the supercritical oxygen correlation developed at ALRC has been previously described in Section IVD along with the correlation used for the hydrogen cooled gas generator cycle concept. This correlation, developed for superciritical hydrogen by Hess and Kunz (Ref. 48) in 1964, was also modified to include curvature enhancement effects.

Gas side heat transfer correlations were the same as those used in Task II.

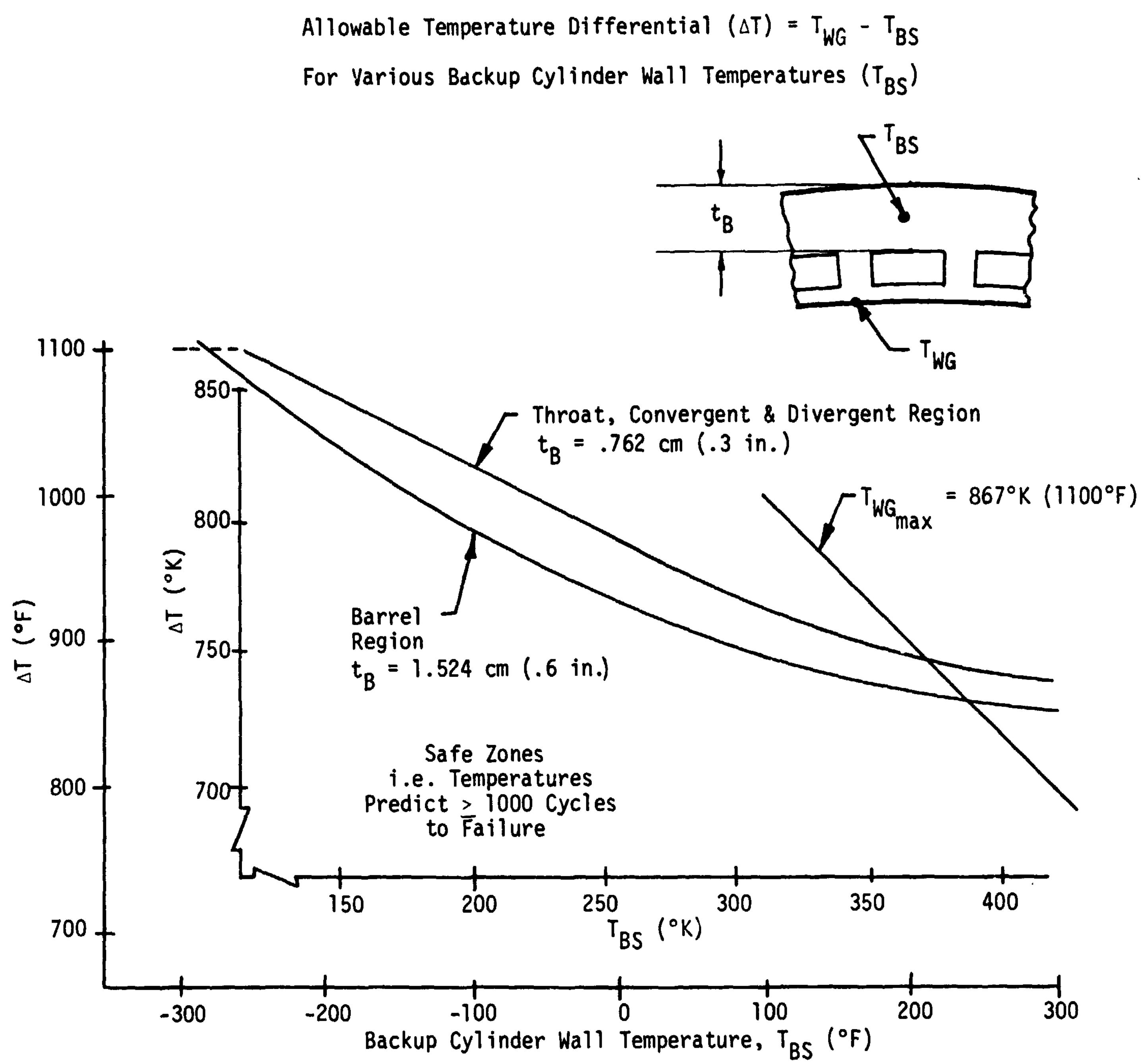

Figure 81. ZrCu Slotted Chamber Life Limits

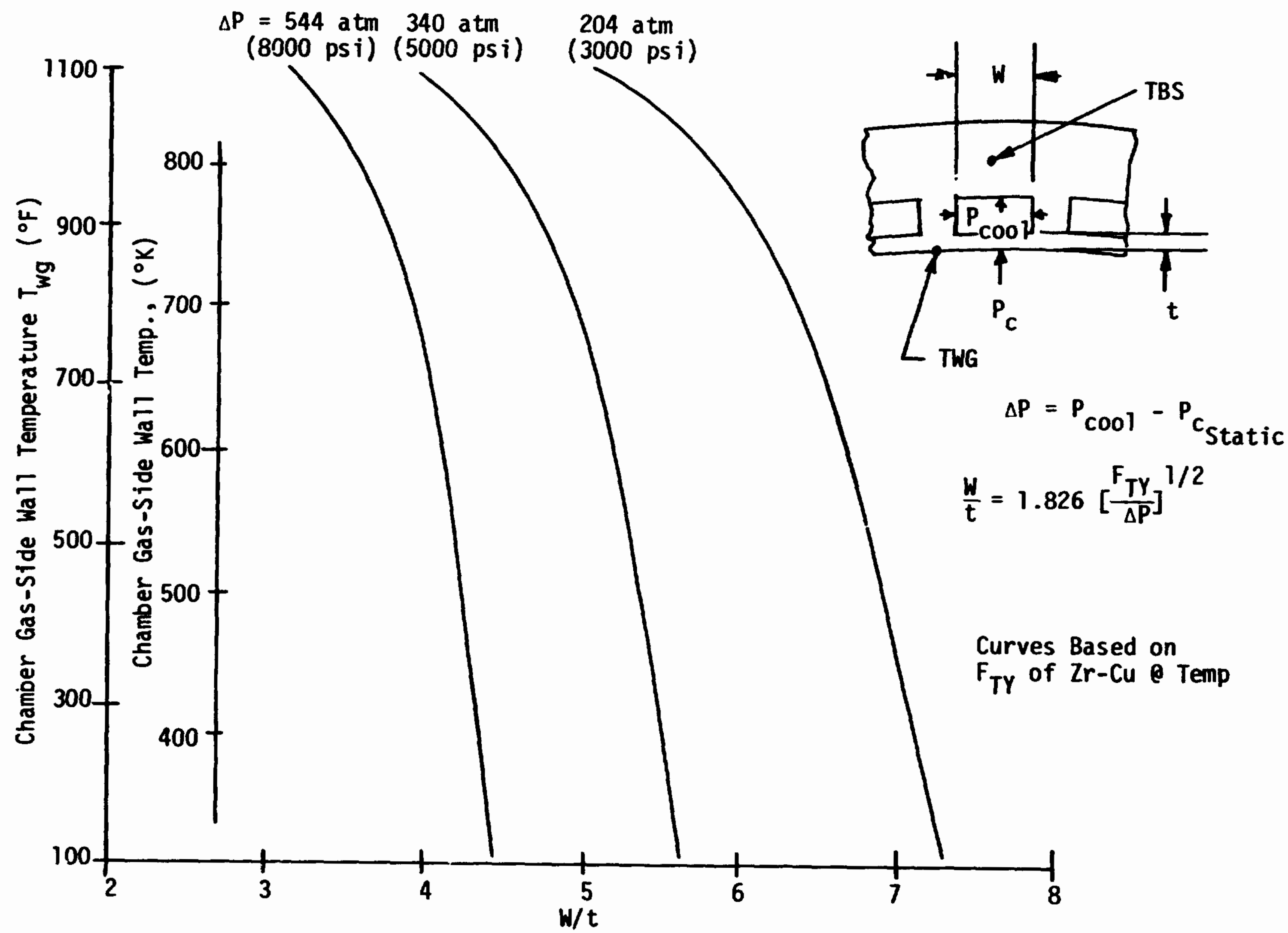

Figure 82. ZrCu Slotted Chamber Pressure and Temperature Wall Thickness Limits

All three of the engine chamber designs generated utilized a similar coolant flow pattern. In all three designs the coolant was initially introduced into a slotted zirconium-copper chamber just downstream from the throat at an area ratio of 1.5:1 and flowed through the throat region up to the plane of the injector face. From here the coolant is gathered, brought externally back to just downstream of the entry point at 1.5:1 and flows on down through the nozzle. This basic flow path was chosen because it results in the minimum coolant pressure drop. More conventional (injector-throat-nozzle) flow paths were analyzed, but resulted in higher pressure drops by 10 to 25%. The pressure drop is minimized by the chosen flow path primarily because the coolant passes through the highest heat flux (throat) region while at the lowest bulk temperature. This has two advantageous effects; it allows the temperature differential between the external wall and the hot wall to be maximized in the most critical cooling region, and the lower bulk temperature results in a higher O_2 heat transfer coefficient. This results in lower coolant velocity requirements and thus lower pressure drop.

All three engine chamber designs were analyzed for both full slotted chamber configurations and for tube bundles to be attached at optimized area ratios. The three primary tube materials considered were: Zr-Cu, A-286, and Inconel 718. Structural analysis were used to determine the required tube wall thickness as a function of the tube radius for the three materials mentioned at their cycle life temperature limits. Zr-Cu was eliminated because it requires a high wall thickness to radius ratio. Inconel 718 was chosen for use on the LOX cooled designs becuase it has a higher maximum temperature limit and lower thickness to radius ratio. Because of its incompatibility with hydrogen, Inconel was not used for the gas generator cycle design, and thus A-286 tubes were used.

The results of the heat transfer analyses are summarized on Table XCI.

a. LOX/RP-1, Mode 1 Baseline Engine, LOX Cooled

The approved baseline Mode 1 engine analyzed during the Task VI effort utilized a LOX/RP-1 propellant combination as opposed to the original Task II Baseline LOX/RJ-5 engine. This propellant combination change resulted in higher chamber heat fluxes than those of the LOX/RJ-5 engine, and therefore higher coolant velocity requirements and resulting pressure drop. The chosen operating conditions for the engine included: P_C = 272 atm (4000 psia), MR = 2.9, with a coolant inlet temperature set at 111°K (200°R). The design incorporates a zirconium-copper slotted chamber design to a nozzle area ratio of 15:1 and a two pass Inconel 718 tube bundle to the nozzle exit area ratio of 40:1. The coolant flow path is as follows: coolant inlet at nozzle area ratio = 1.5:1 flows to the injector end, is collected, brought externally back to ε = 1.5:1, re-enters chamber channels, flows to ε = 15:1 where tube bundle starts, flows in half the tubes to ε_{exit} = 40:1, turns and flows in the other half of the tubes back up to ε = 15:1 where it is collected. The resultant total pressure drop for the chamber-tube bundle design was evaluated as 126.9 atm (1865 psi).

TABLE XCI. TASK VI - COOLANT JACKET SUMMARY (PRESSURE DROP)

	Baseline Mode 1 Oxygen Cooled LOX/RP-1		Engine Concept Dual Fuel, Oxygen Cooled: Mode 1 LOX/RP-1		Engine Concept Dual Fuel, Oxygen Cooled: Mode 2 LOX/LH_2		Gas Generator Cycle Hydrogen Cooled LOX/RP-1	
Slotted Chamber ΔP, atm (psi	118.7	(1745)	123.1	(1809)	76.9	(1130)	55.3	(813)
Tube Bundle ΔP, atm (psi)	8.2	(120)	8.9	(131)	7.1	(105)	19.9	(292)
Combined Slotted & Tube Bundle ΔP, atm (psi)	126.9	(1865)	132.0	(1940)	84.0	(1235)	75.2	(1105)

(CHAMBER SECTION GEOMETRY)

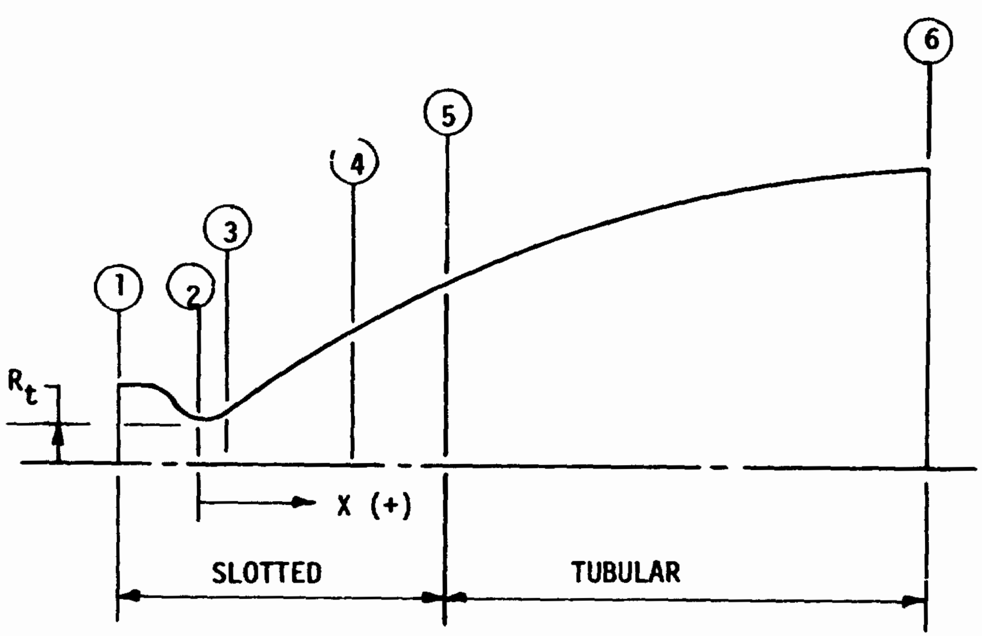

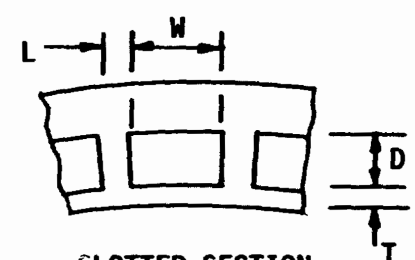

SLOTTED SECTION

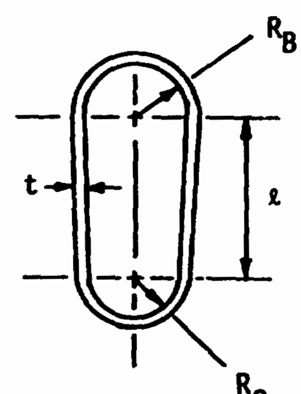

TUBULAR SECTION

TABLE XCI. - COOLANT JACKET SUMMARY (cont.)
(BASELINE MODE 1 GEOMETRY)

Parameter	Station 1	2	3	4	4	5	5	6
X/R_t	-1.88	0	5[illegible]9	3.064	3.064	5.454	5.454	15.867
Area Ratio	2.50	1.00	1.5[illegible]	7.65	7.65	14.74	14.74	40.00
No. of Channels or Tubes	270	270	270	270	540	540	277	277
W cm (in.)	.384 (.151)	.206 (.081)	.277 (.109)	.749 (.295)	.323 (.127)	.488 (.192)		
D cm (in.)	.599 (.236)	.8[illegible] (.32[illegible])	1.102 (.434)	1.295 (.510)	1.295 (.510)	1.875 (.738)		
L cm (in.)	.102 (.040)	.102 (.040)	.102 (.040)	.102 (.040)	.102 (.040)	.102 (.040)		
T cm (in.)	.064 (.025)	.064 (.025)	.076 (.030)	.191 (.075)	.191 (.075)	.191 (.075)		
R_B cm (in.)							.297 (.117)	.490 (.193)
R_G cm (in.)							.287 (.113)	.472 (.186)
ℓ cm (in.)							1.478 (.582)	2.835 (1.116)
t cm (in.)							.025 (.010)	.051 (.020)

R_t = 13.157 cm (5.18 in.)

Nomenclature Defined on Page 261

TABLE XCI. - COOLANT JACKET SUMMARY (cont.)
(DUAL-FUEL GEOMETRY)

Parameter	Station							
	1	2	3	4	4	5	5	6
X/R_t	-1.88	0	.473	2.988	2.988	5.309	5.309	14.875
Area Ratio	2.50	1.00	1.46	7.65	7.65	14.93	14.93	40.0
No. of Channels or Tubes	270	270	270	270	540	540	277	277
W cm (in.)	.384 (.151)	.206 (.081)	.269 (.106)	.749 (.295)	.323 (.127)	.495 (.195)		
D cm (in.)	.544 (.214)	.818 (.322)	1.072 (.422)	1.245 (.490)	1.245 (.490)	1.854 (.730)		
L cm (in.)	.102 (.040)	.102 (.040)	.102 (.040)	.102 (.040)	.102 (.040)	.102 (.040)		
T cm (in.)	.064 (.025)	.064 (.025)	.076 (.030)	.191 (.075)	.191 (.075)	.191 (.075)		
R_B cm (in.)							.297 (.117)	.488 (.192)
R_G cm (in.)							.290 (.114)	.472 (.186)
ℓ cm (in.)							1.323 (.521)	2.380 (.937)
t cm (in.)							.025 (.010)	.051 (.020)

R_T = 13.157 cm (5.18 in.)

Nomenclature Defined on Page 261

TABLE XCI. - COOLANT JACKET SUMMARY (cont.)
(H_2/O_2 GG CYCLE - HYDROGEN COOLED GEOMETRY)

Parameter	Station							
	1	2	3	4	4	5	5	6
X/R_t	-3.723	0	.534	2.803	2.803	8.807	8.807	16.568
Area Ratio	2.50	1.00	1.54	6.90	6.90	24.98	24.98	42.7
No. of Channels or Tubes	390	390	390	390	7.80	780	1900	1900
W cm (in.)	.224 (.088)	.104 (.041)	.155 (.061)	.439 (.173)	.168 (.066)	.411 (.162)		
D cm (in.)	.178 (.070)	.279 (.110)	.610 (.240)	.378 (.149)	.378 (.149)	.589 (.232)		
L cm (in.)	.102 (.040)	.102 (.040)	.102 (.040)	.102 (.040)	.102 (.040)	.102 (.040)		
Γ cm (in.)	.064 (.025)	.064 (.025)	.064 (.025)	.114 (.045)	.114 (.045)	.152 (.060)		
R_B cm (in.)							.107 (.042)	.137 (.054)
R_G cm (in.)							.107 (.042)	.137 (.054)
ℓ cm (in.)							.056 (.022)	.018 (.007)
t cm (in.)							.018 (.007)	.018 (.007)

R_t = 12.649 cm (4.98 in.)

Nomenclature Defined on Page 261

b. Dual-Fuel, LOX Cooled, (LOX/RP-1, LOX/LH_2) Engine

Previous analyses indicated that the Mode 2 operation heat transfer characteristics dictated the coolant channel configurations. Therefore, the Mode 2 operating conditions were used to generate the chamber coolant passage design parameters. After the design was generated based on Mode 2 operation, the Mode 1 operation was analyzed to determine the amount of allowable coolant bypass flow which would meet the cycle life criterion and minimize the chamber pressure drop. This bypass flow rate was determined as approximately 40.8 kg/sec (90 lb/sec).

This design also incorporates a slotted Zr-Cu chamber to ε = 15:1, and an Inconel two pass tube bundle to ε_{exit} = 40:1. It also has the same coolant flow path as the baseline design. Mainly, inlet at 1.5:1, to injector, 1.5:1 to 15:1, tube bundle to 40:1 and back to 15:1. The resultant total pressure drop for the Mode 2 operation was 84 atm (1235 psi), and for the Mode 1 operation, 132 atm (1940 psi). The Mode 2 pressure drop is significantly lower than the Mode 1 pressure drop primarily because of the pressure effects associated with the O_2 heat transfer correlation. The lower coolant pressures of the Mode 2 operation require lower mass velocities for the same oxygen heat transfer coefficient as Mode 1.

c. Hydrogen Cooled, Gas Generator Cycle

The chamber design consists of a Zr-Cu slotted chamber to a nozzle area ratio of 25:1, and a one pass A-286 tube bundle to ε_{exit} = 42.7:1. The coolant flow path is as follows: coolant inlet at nozzle area ratio of 1.5:1, flows to injector end, is collected and brought externally back to 1.5:1, flows downstream to 25:1 where tube bundle starts, and then on out to the exit area ratio of 42.7:1, where it is collected and brought to the hydrogen-rich gas generator. The large bulk temperature rise associated with the 9.07 kg/sec (20 lbm/sec) hydrogen flow rate, results in hydrogen exit temperatures near 811°K (1000°F). These high bulk temperatures in the nozzle, preclude the use of a two pass tube bundle because of the resulting high velocities required to limit the gas-side wall temperature. A one pass tube bundle design was thus conceived which provides successively higher coolant velocities as the coolant flows through the nozzle to the larger area ratios and finally to the exit. The resultant total pressure drop for the chamber-tube bundle design was evaluated as 75.2 atm (1105 psi).

G. MAIN INJECTOR DESIGN

The main thrust chamber injector for the Mode 1 LOX/RP-1 baseline and dual-fuel engines is shown on Figure 83. The injector uses a coaxial-type element which was selected on the basis of Task II results. An acoustic cavity, whose size has been estimated, is shown as the combustion instability supression device. The injector design parameters are summarized on Table XCII.

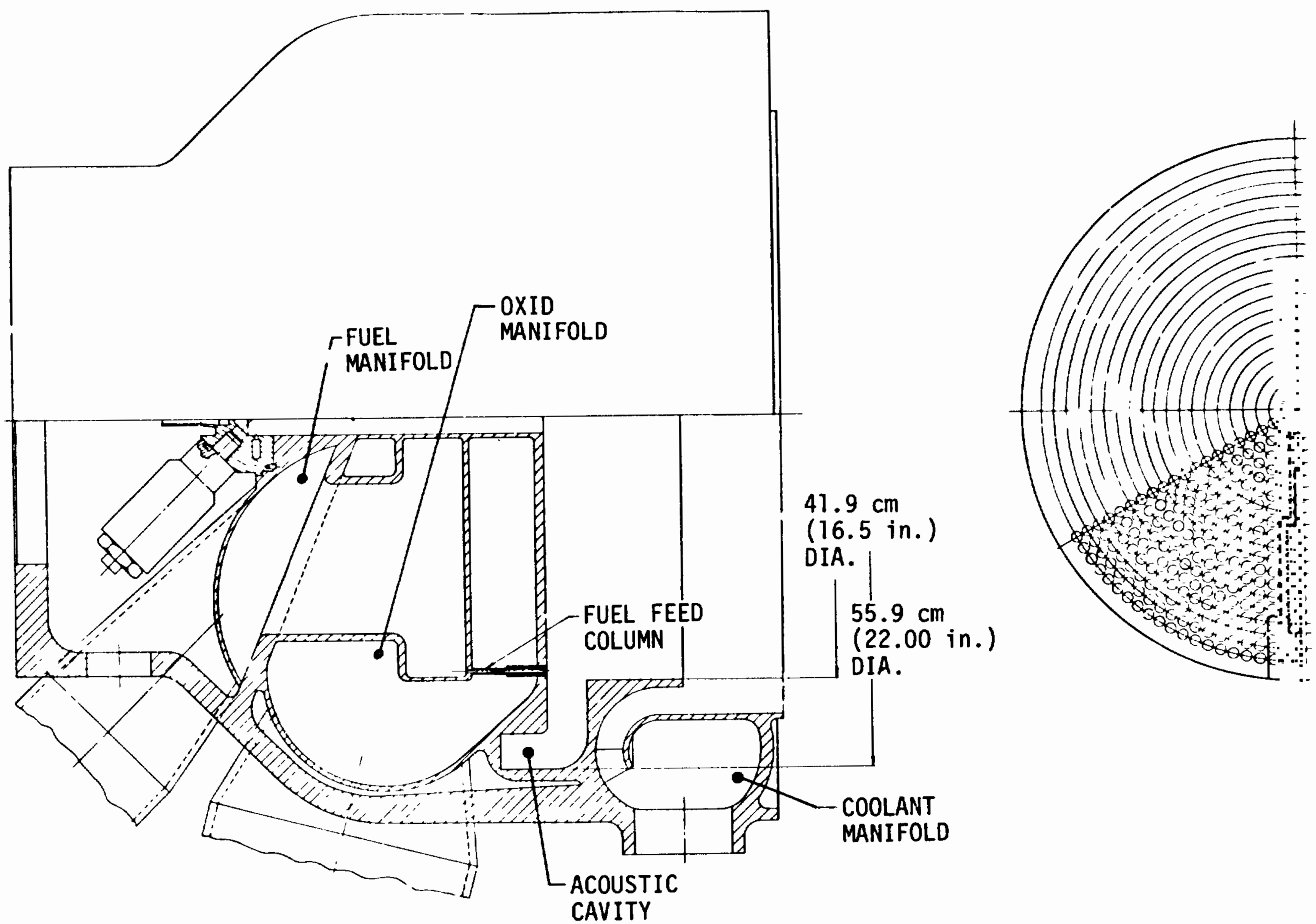

Figure 83. Mode 1 LOX/RP-1 Baseline and Dual-Fuel Thrust Chamber Injector

TABLE XCII. - MODE 1 LOX/RP-1 BASELINE AND DUAL-FUEL ENGINE MAIN, INJECTOR DESIGN DATA

	Fuel Circuit		Oxid. Circuit	
Flow Rate, kg/sec (lb/sec)	249.3	(549.6)	598.4	(1,319.2)
MR		2.9		
Type of Element	Co-Axial			
No. of Rings	19			
No. of Elements	1254		1254	
Element				
Element Size, cm (in.)	.330	(.130) dia	.681	(.268) O.D.
			.465	(.183) I.D.
Velocity, m/sec (ft/sec)	178	(583.8)	173	(566.5)
ΔP, atm (psi)	23.7	(348)	23.7	(348)
Manifold & Inlet				
Velocity, m/sec (ft/sec)	66.4	(218)	54.9	(180)
ΔP, atm (psi)	2.70	(40)	2.0	(30)
Inlet dia, cm (in.)	15.2	(6.0)	31.8	(12.5)
Injector O.D. cm (in.)	51.2	(20.15)		

If acoustic cavities are not required to stabilize the gaseous propellant combustion process, the design shown on Figure 84 indicates the size decrease and potential weight savings that would result. The coaxial element is detailed on this drawing, and is based upon the Task II thrust per element recommendation. This injector design is similar to that of the main injector of the SSME, although it is shorter because the oxidizer does not have to be vaporized.

The alternate Mode 1, gas generator cycle engine main liquid/liquid injector design is shown on Figure 85. This injector uses quadlet-like doublet self impinging elements. The element selection is based on recent results of ALRC liquid/liquid injection development for programs such as OMS, MX, and Improved Transtage (ITIP). A summary of the alternate Mode 1 injector design parameters is presented on Table XCIII.

H. PREBURNER DESIGN

The Mode 1 baseline engine uses both fuel and oxidizer-rich preburners. The LOX/RP-1 oxidizer-rich preburner design is shown on Figure 86 and the fuel-rich RP-1/LOX preburner design is shown on Figure 87. The injectors use a platelet design with like-on-like impinging doublet elements with the adjacent unlike fans canted into each other. Acoustic cavities are shown as the combustion instability suppression devices although in-depth sizing of the cavity is beyond the scope of the current study. The preburner design parameters are presented on Tables XCIV and XCV.

For the dual-fuel engine, the fuel and oxidizer-rich LOX/RP-1 preburners are the same as those shown for the baseline Mode 1 engine. The hydrogen/oxygen preburner designs are similar to these and are shown on Figures 88 and 89. The preburner design parameters are presented on Tables XCVI and XCVII.

The fuel-rich gas generator design for the alternate Mode 1 engine is shown on Figure 90. This injector design is based upon the design developed during the M-1 engine program (Ref. 76). The injector uses a coaxial element which injects gaseous hydrogen and liquid oxygen and achieved a 98% combustion efficiency during M-1 testing. M-1 testing was conducted over a mixture ratio range from 0.6 to 1.0 and a chamber pressure range of 51 to 77.9 atm (750 to 1145 psia).

Principal element dimensions for the design shown on Figure 90 are:

Oxidizer Flow Diameter	=	0.31 cm (.122")
Fuel Slot Width	=	0.208 cm (.082")
Element Wall Thickness	=	0.184 cm (.0725")

A summary of the preburner design parameters is shown on Table XCVIII.

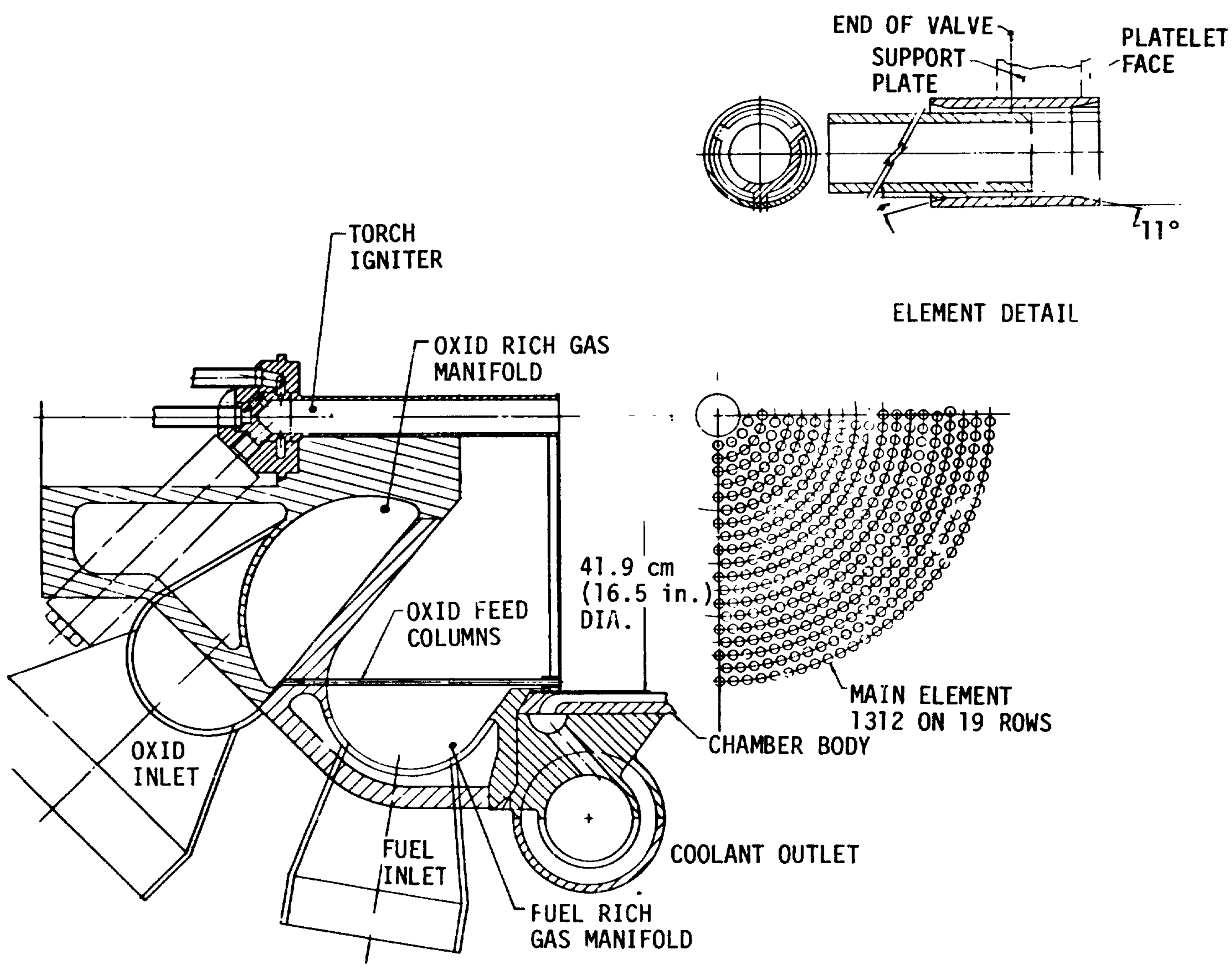

Figure 84. Mode 1 LOX/RP-1 Baseline Backup Main Injector

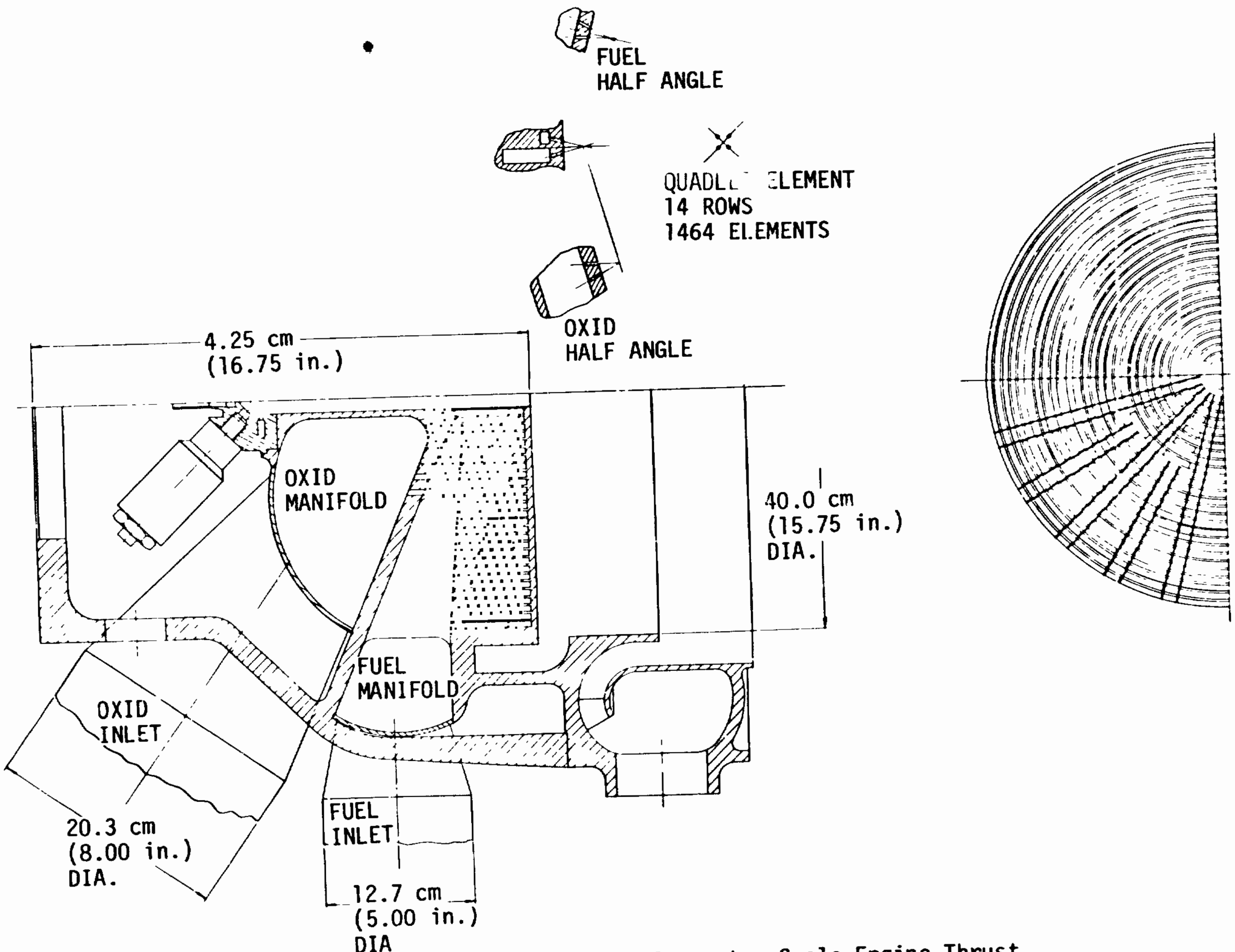

Figure 85. Alternate Mode 1 Gas Generator Cycle Engine Thrust Chamber Injector

TABLE XCIII. - ALTERNATE MODE 1 GAS GENERATOR CYCLE ENGINE MAIN INJECTOR DESIGN DATA

	Fuel Circuit		Oxid. Circuit	
Flow Rate, kg/sec (lb/sec)	216	(476.0)	621	(1368.4)
MR		2.88		
Type of Element		Quadlet-Like Doublet Self Impinging		
No. of Rows		14		
No. of Elements		1464		1464
No. of Channels		14		14
Orifice size, cm (in.)	.109	(.043)	.191	(.075)
Injection Velocity, m/sec (ft/sec)	71.3	(234)	72.8	(239)
Orifice ΔP, atm (psi)	34.0	(500)	34.0	(500)
Inlet Velocity, m/sec (ft/sec)	15.8	(51.8)	18.6	(60.9)
Manifold Velocity, m/sec (ft/sec)	5.5	(18)	5.5	(18)
Manifold ΔP, atm (psi)	6.8	(100)	5.2	(77.0)
Inlet Dia, cm (in.)	12.7	(5.0)	20.3	(8.0)
Injector O.D., cm (in.)		63.5 (25.0)		

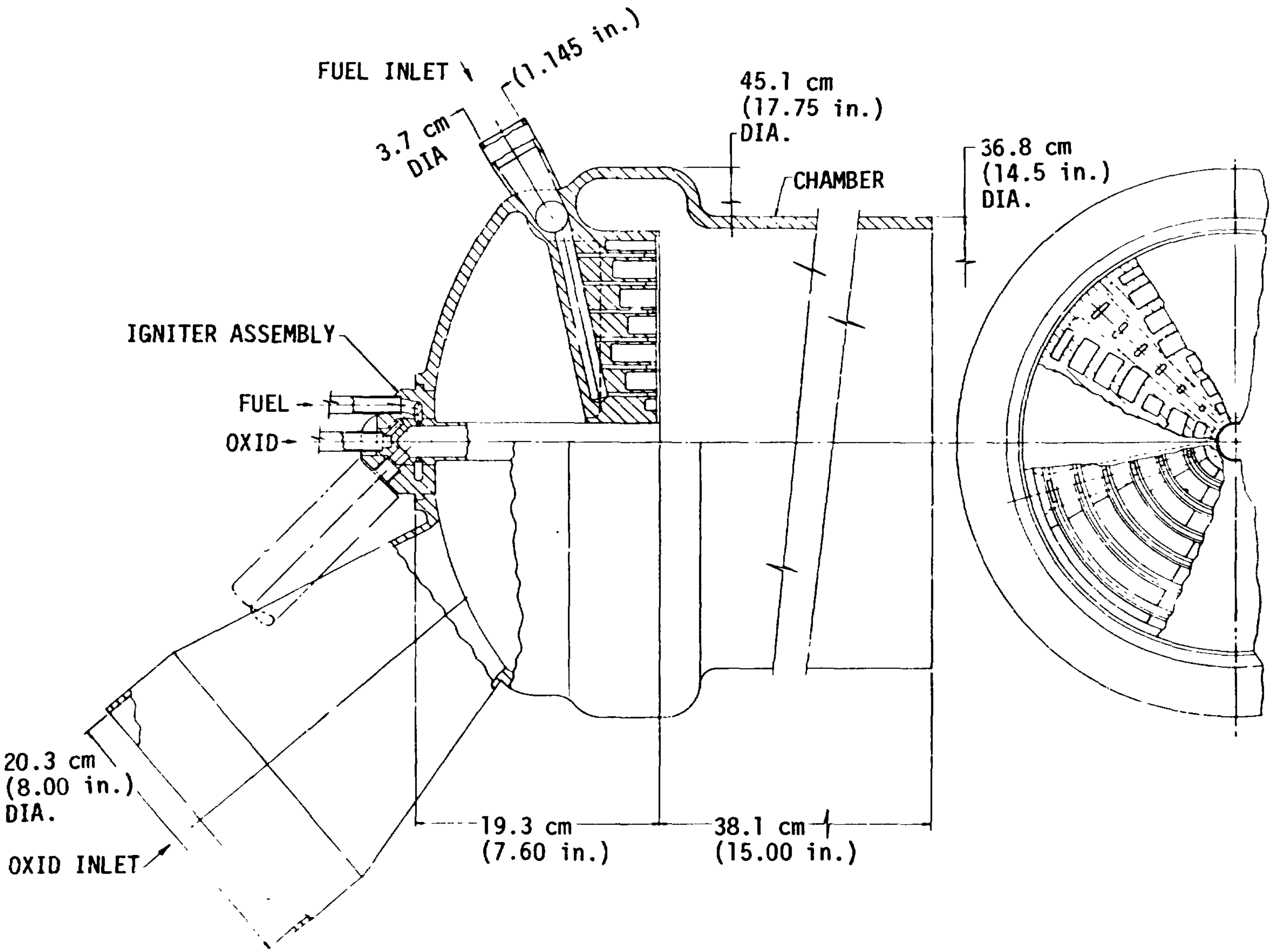

Figure 86. Mode 1 LOX/RP-1 Baseline Oxidizer-Rich Preburner

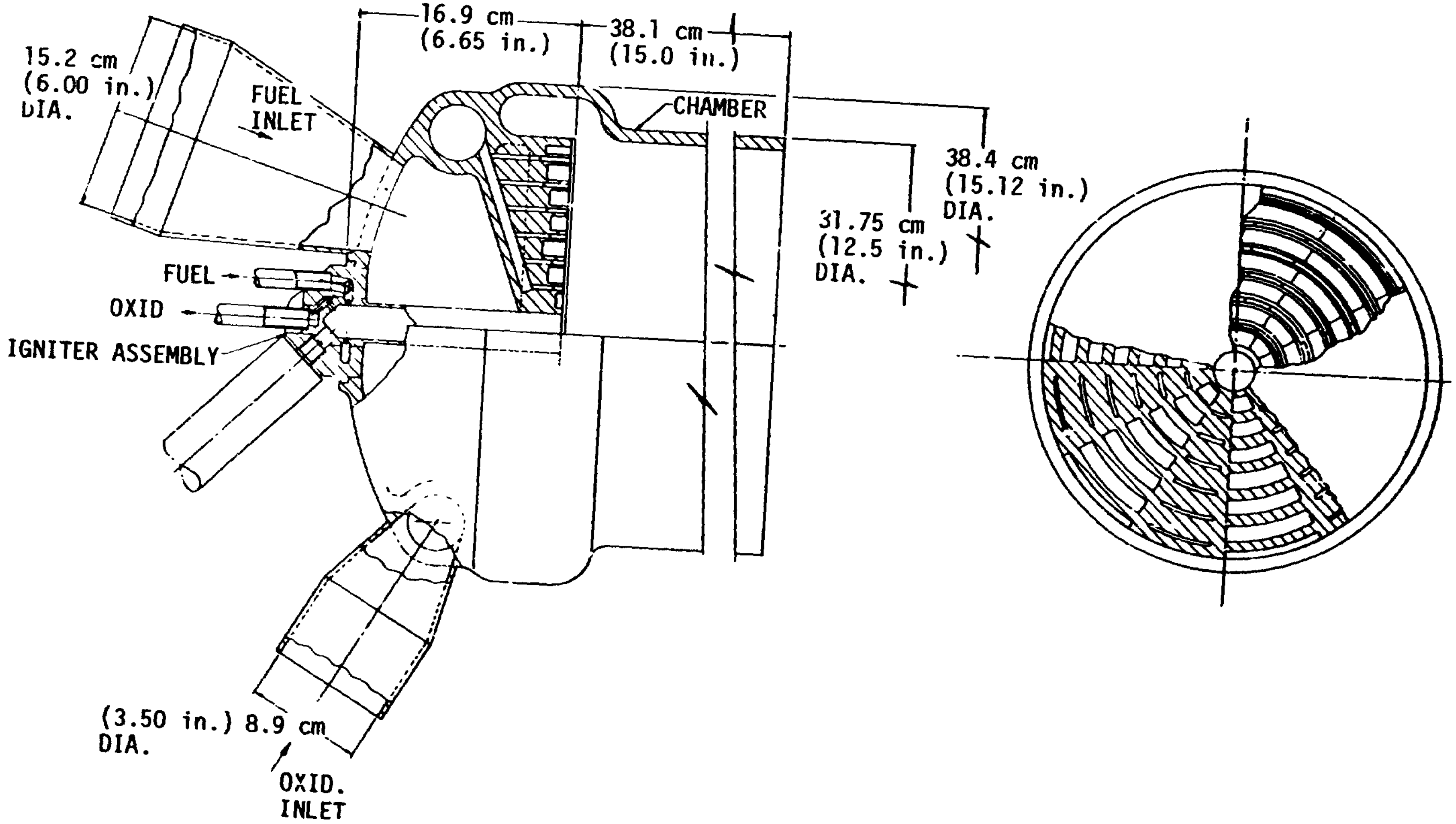

Figure 87. Mode 1 LOX/RP-1 Baseline Fuel-Rich Preburner

TABLE XCIV. - OXIDIZER-RICH PREBURNER DESIGN DATA SUMMARY, LOX/RP-1 BASELINE

	Fuel Circuit RP-1		Oxid. Circuit LOX	
Flow Rate, kg/sec (lb/sec)	13.0	(28.7)	585.4	(1290.5)
MR		45		45
Type of Elements		X-Doublet		V-Doublet
No. of Rings		6		7
No. of Elements		492		984
<u>Element</u>				
Element Size, cm (in.)	.038 x .097	(.015 x .038) Slot	.330	(.130) Square
Velocity, m/sec (ft/sec)	65.2	(214)	47.5	(155.8)
ΔP, atm (psi)	61.2	(900)	34.0	(500)
<u>Manifold</u>				
Velocity, m/sec (ft/sec)	10.7	(35)	10.7	(35)
ΔP, atm (psi)	1.36	(20)	1.36	(20)
Inlet dia, cm (in.)	3.7	(1.45)	20.3	(8.00)
Injector O.D., cm (in.)	41.4	(16.3)	41.4	(16.3)

TABLE XCV. - FUEL-RICH PREBURNER DESIGN DATA SUMMARY, LOX/RP-1 BASELINE

	Fuel Circuit RP-1		Oxid. Circuit LOX	
Flow Rate, kg/sec (lb/sec)	204.3	(450.5)	45.0	(99.1)
MR		0.22		0.22
Type of Elements		V-Doublet		X-Doublet
No. of Rings		7		6
No. of Elements		972		486
Element				
Element Size, cm (in.)	.173	(.068) Square	.051 x .335	(.020 x .132) Slot
Velocity, m/sec (ft/sec)	65.2	(214)	47.5	(155.8)
ΔP, atm (psi)	61.2	(900)	34.0	(500)
Manifold				
Velocity, m/sec (ft/sec)	10.7	(35)	10.7	(35)
ΔP, atm (psi)	1.36	(20)	1.36	(20)
Inlet Dia, cm (in.)	15.2	(6.0)	8.9	(3.5)
Injector O.D., cm (in.)	36.5	(14.36)	36.5	(14.36)

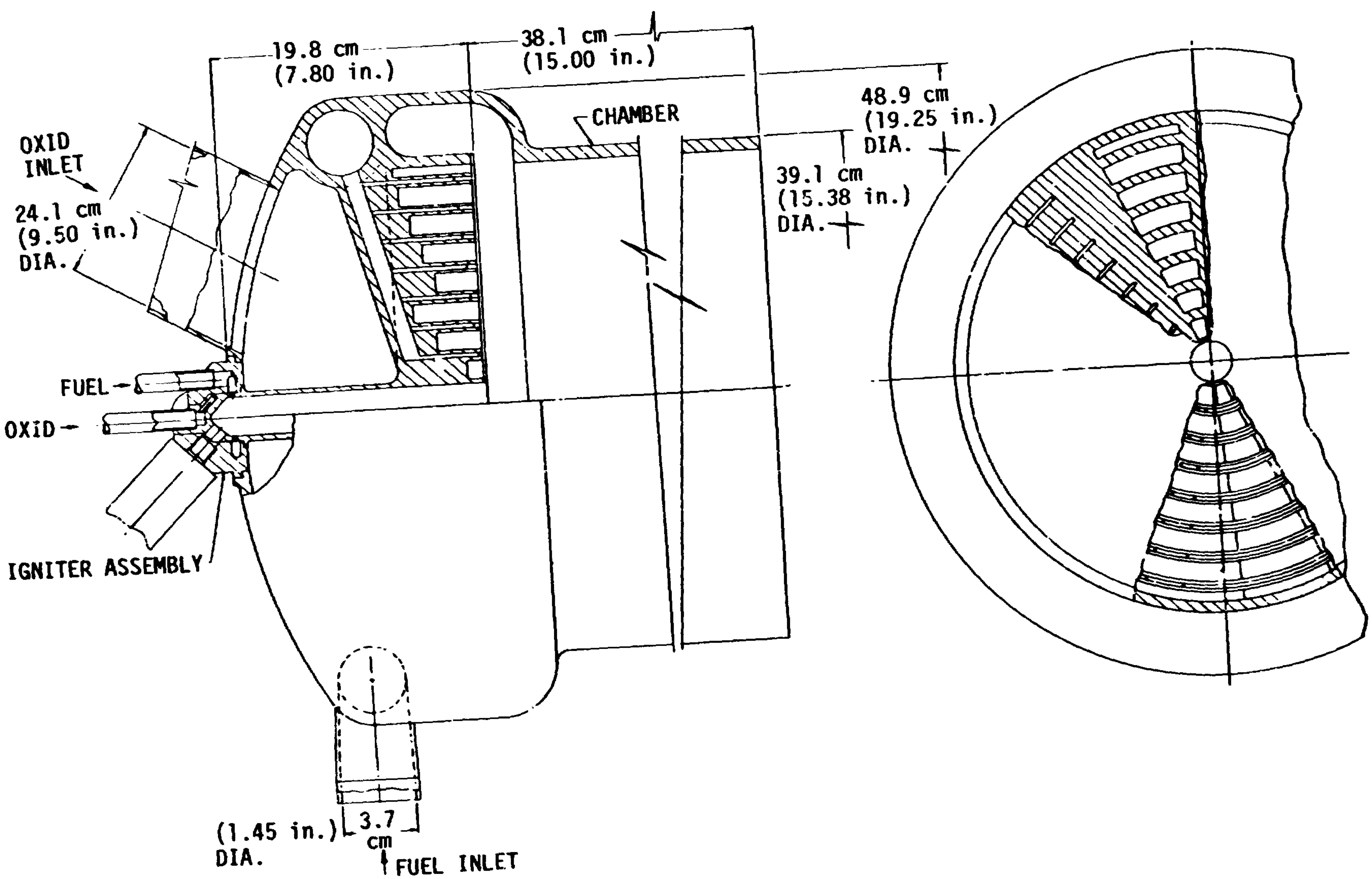

Figure 88. O_2/H_2 Oxidizer-Rich Preburner, Dual-Fuel

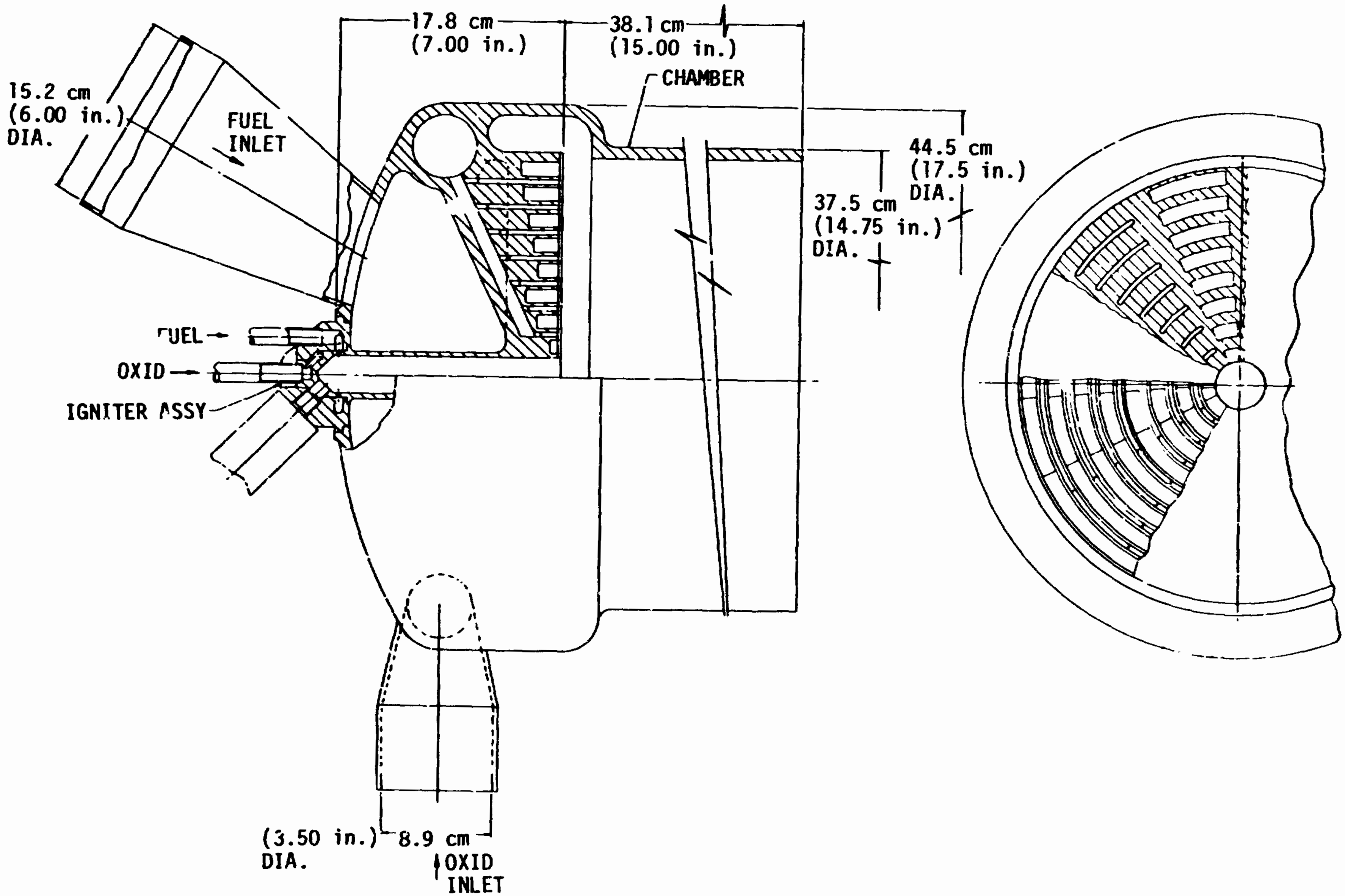

Figure 89. H_2/O_2 Fuel-Rich Preburner, Dual-Fuel

TABLE XCVI. - O_2/H_2 OXIDIZER-RICH PREBURNER DESIGN SUMMARY, DUAL-FUEL

	Fuel Circuit H_2		Oxid. Circuit O_2	
Flow Rate, kg/sec (lb/sec)	3.54	(7.8)	389.3	(858.3)
MR		110		110
Type of Element		X-Doublet		V-Doublet
No. of Rings		7		8
No. of Elements		642		1284
<u>Element</u>				
Element Size, cm (in.)	.038 x .102	(.015 x .040) Slot	.295	(.116) Square
Velocity, m/sec (ft/sec)	322	(1057)	43.3	(142)
ΔP, atm (psi)	36.9	(543)	20.1	(296)
<u>Manifold</u>				
Velocity, m/sec (ft/sec)	45.7	(150)	10.7	(35)
ΔP, atm (psi)	1.36	(20)	1.36	(20)
Inlet Dia, cm (in.)	3.7	(1.45)	24.1	(9.50)
Injector O.D., cm (in.)	44.9	(17.68)	44.9	(17.68)

TABLE XCVII. - H_2/O_2 FUEL-RICH PREBURNER DESIGN DATA SUMMARY, DUAL-FUEL

	Fuel Circuit H_2		Oxid. Circuit O_2	
Flow Rate, kg/sec (lb/sec)	59.8	(131.8)	53.8	(118.6)
MR		0.9		0.9
Type of Element		V-Doublet		X-Doublet
No. of Rings		8		7
No. of Elements		1272		636
Element				
Element Size, cm (in.)	.173	(.068) Square	.076 x .267	(.030 x .105) Slot
Velocity, m/sec (ft/sec)	219	(720)	51.5	(169)
ΔP, atm (psi)	46.1	(677)	28.2	(414)
Manifold				
Velocity, m/sec (ft/sec)	45.7	(150)	10.7	(35)
ΔP, atm (psi)	1.36	(20)	1.36	(20)
Inlet Dia, cm (in.)	15.2	(6.0)	8.9	(3.5)
Injector O.D., cm (in.)	42.2	(16.6)	42.2	(16.6)

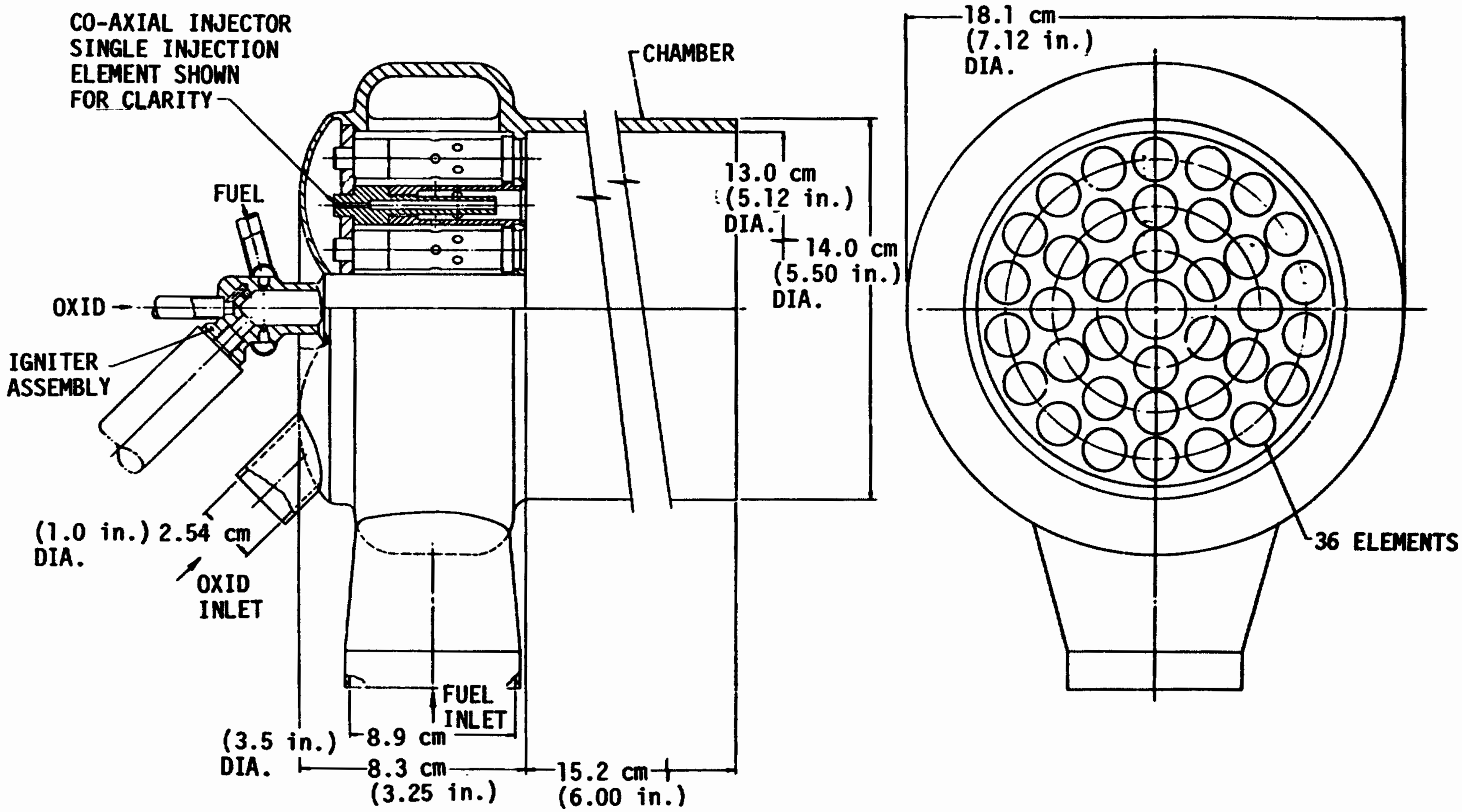

Figure 90. Alternate Mode 1 Co-Axial Gas Generator

TABLE XCVIII. - ALTERNATE MODE 1 CO-AXIAL GAS GENERATOR DESIGN DATA SUMMARY

	Fuel Circuit H_2		Oxid. Circuit O_2	
Flow Rate, kg/sec (lb/sec)	9.07	(20)	5.44	(12)
MR		0.6		0.6
Type of Element		Co-Axial		
No. of Rings		3 {18, 12, 6}		
No. of Elements		36		36
<u>Element</u>				
Element Size, cm (in.)	1.095 .678	(.431) O.D. (.267) I.D.	0.31	(.122) Dia
Velocity, m/sec (ft/sec)	457	(1498)	72.9	(239.3)
ΔP, atm (psi)	11.4	(168)	32.4	(476)

I. VALVE SELECTION AND SIZING

Based upon the controls identified by the start and shutdown sequence analyses, a valve sizing study was performed. These components are shutoff valves of varying size and type. Considering the parameters involved, the majority of the valves selected were the poppet type. These valves are actuated from full-closed to full-open position in the presence of tank head pressure during engine start and are closed during engine shutdown once valve inlet pressure has decayed to a reduced level.

Translating sleeve valves were selected for operation in the high pressure environment associated with valve closure to initiate the engine shutdown. A sleeve valve configuration can be virtually pressure force balanced by matching the diameter of the sleeve seal with that of the shutoff seal which results in a reduction in power requirements.

The estimated pressure drop and weight flow requirements for each valve were defined and converted to a fluid K_w requirement.* An array of historical data regarding the use of LOX, LH_2, and RP-1 valves on past engine programs was likewise arranged as a function of K_w and provided the basis for the valve diameter, weight, and envelope estimates shown in Tables XCVIX, C, and CI.

The dual-fuel engine cycle exhibits the need for preventing the backflow of main combustion gases into the nonoperating fuel-rich preburner discharge circuit. An approach to preventing this backflow is to provide check valves in the fuel-rich preburner circuits. These large, ∿15.2 cm (∿6"), check valves are required to operate at high pressures, 272 atm (4000 psia), in hot gases that are the product of LOX/RP-1 and LOX/LH_2 combustion. The weight and dimensions for a 15.2 cm (6") check valve were estimated from historical data and are listed on Table CII.

1. Valve Materials

The basic valve materials for the valves were defined which are compatible with the propellants designated for these engine cycles. Specific considerations are embrittlement, metallurgical stability, and chemical compatibility. The basic valve materials are listed as follows:

Part	Material: LOX	Material: LH_2	Material: RP-1
Valve Body	Inconel 718	Inconel 718	A-286 CRES
Seat	Inconel 718	Inconel 718	Inconel 718
Shutoff Seal	Phosphor Bronze	Phosphor Bronze	Beryllium Nickel
Spring	Inconel 750	Inconel 750	Inconel 750
Sleeve	Inconel 718	A-286 CRES	A-286 CRES
Bellows	Inconel 718	Inconel 718	Inconel 718

*K_w = Weight flow/(pressure drop x specific gravity)$^{1/2}$

TABLE XCVIX. - VALVE SIZING: MODE 1 LOX COOLED BASELINE

Valve	Type	Configuration	Fluid K_w Requirement	Approx. Valve Diameter cm (in.)	Approx. Valve & Actuator Weight kg (lb)	Approximate Valve & Actuator Envelope Dimensions: Diameter cm (in.)	Approximate Valve & Actuator Envelope Dimensions: Length cm (in.)
Main LOX Valve	Shutoff	Poppet	132	14.5 5.7	54.4 (120)	38.1 (15)	58.4 (23)
Main RP-1 Valve	Shutoff	Poppet	59.3	9.7 3.8	36.3 (80)	30.5 (12)	48.3 (19)

TABLE C. - VALVE SIZING: HYDROGEN COOLED, GAS GENERATOR CYCLE

Valve	Type	Configuration	Fluid K_w Requirement	Approx. Valve Diameter cm (in.)	Approx. Valve & Actuator Weight kg (lb)	Approx. Valve & Actuator Envelope: Diameter cm (in.)	Approx. Valve & Actuator Envelope: Length cm (in.)
Main LOX Valve	Shutoff	Poppet	178.4	17.1 (6.75)	68.0 (150)	40.6 (16)	61.0 (24)
Main RP-1 Valve	Shutoff	Poppet	73.5	10.8 (4.25)	40.8 (90)	33.0 (13)	50.8 (20)
Main LH_2 Valve	Shutoff	Poppet	10.4	5.1 (2.0)	18.1 (40)	21.6 (8.5)	33.0 (13)
LOX GGV	Shutoff	Sleeve	0.65	1.8 (0.7)	5.9 (13)	20.3 (8)	27.9 (11)

TABLE CI. - VALVE SIZING: DUAL-FUEL ENGINE
(MODE 1: LOX/RP-1)
(MODE 2: LOX/LH_2)

Valve	Type	Configuration	Fluid K_w Requirement	Approx. Valve Diameter cm (in.)	Approx. Valve & Actuator Weight kg (lb)	Approx. Valve & Actuator Envelope Diameter cm (in.)	Approx. Valve & Actuator Envelope Length cm (in.)
Main LOX Valve (Mode 1)	Shutoff	Poppet	132	14.5 (5.7)	54.4 (120)	38.1 (15)	58.4 (23)
Main RP-1 Valve	Shutoff	Poppet	59.3	9.7 (3.8)	36.3 (80)	30.5 (12)	48.3 (19)
Main LH_2 Valve	Shutoff	Poppet	70	10.2 (4)	38.6 (85)	31.8 (12.5)	49.5 (19.5)
Ox Rich Preburner (O_2/RP-1)							
LOX Valve	Shutoff	Poppet	67	10.2 (4)	38.6 (85)	31.8 (12.5)	49.5 (19.5)
RP-1 Valve	Shutoff	Sleeve	1.6	2.3 (0.9)	8.2 (18)	22.9 (9)	30.5 (12)
Fuel Rich Preburner (RP-1/O2)							
LOX Valve	Shutoff	Poppet	12	5.8 (2.3)	20.4 (45)	22.9 (9)	34.3 (13.5)
Ox Rich Preburner (O_2/H_2)							
LOX Valve	Shutoff	Poppet	59.4	9.7 (3.8)	36.3 (80)	30.5 (12)	48.3 (19)
LH_2 Valve	Shutoff	Sleeve	1.76	2.4 (0.95)	8.6 (19)	22.9 (9)	30.5 (12)
Fuel Rich Preburner (H_2/O_2)							
LOX Valve	Shutoff	Poppet	18	6.4 (2.5)	22.7 (50)	22.9 (9)	35.6 (14)

TABLE CII. - HOT GAS CHECK VALVE WEIGHT AND ENVELOPE ENGINE CYCLE - DUAL-FUEL, OXYGEN COOLED

(Mode 1: LOX/RP-1)
(Mode 2: LOX/LH_2)

Valve	Type	Configuration	Approx. Valve Diameter cm (in.)	Approx. Valve Weight kg (lb)	Approx. Valve Diameter cm (in.)	Envelope Length cm (in.)
Mode 1 - Fuel Rich Preburner Discharge Circuit	Check	Poppet	15.2 (6)	20.4 (45)	27.2 (10.7)	32.3 (12.7)
Mode 2 - Fuel Rich Preburner Discharge Circuit	Check	Poppet	15.2 (6)	20.4 (45)	27.2 (10.7)	32.3 (12.7)

2. Valve Actuation Forces

The forces to be overcome include pressure forces, flow forces, friction forces and inertial forces of moving parts. The inertial forces become significant for the typical actuation time response requirements associated with engine start and shutdown. A representative set of actuator loads were obtained by comparison to the ALRC Space Shuttle Main Engine (AJ-550) study.

The actuation system should be capable of producing the following approximate linear forces for the following valves.

- 14,230N (3200 Pounds)

  Main LOX Valves
  Main RP-1 Valves
  LOX Valves - Ox Rich Preburners
  LOX Valves - Fuel Rich Preburners

- 7560N (1700 Pounds)

  Main LH_2 Valves
  RP-1 and LH_2 Valves - Ox Rich Preburners
  LOX GGV

3. Valve Actuation Methods

Electromechanical valve actuation has been selected for the valves considered in this study. This selection is based upon a trade study conducted early in the ALRC SSME program to select the method of engine control valve actuation. Electrical, hydraulic and pneumatic systems were evaluated on the basis of seventeen design considerations; the primary factors being weight, contamination susceptibility, power requirements, fabrication cost and lead time, maintainability, reliability and safety. The results of this study indicated the three systems were relatively equal in their ability to satisfy the overall design requirements.

Due to the close results of the initial trade study, a more extensive review was conducted in which greater consideration was given to vehicle integration and system maintenance. This review clearly revealed the advantages of the electrical system which can be summarized as follows:

- Single Interface: The electrical system requires only an electrical interface, an item also required by hydraulic and pneumatic systems in addition to their actuation fluid interfaces.

- Reliability: Due to its single interface, the electrical system represents the least complex system. The large number of lines associated with conveying the hydraulic or pneumatic fluids throughout the engine are deleted along with their numerous leak paths. Although the electrical system requires more electrical control components, the power levels are sufficiently low to permit the use of well developed switches and control components. A completely redundant electrical system can be provided with fewer components than the other systems and a single point failure is isolated without its affecting other components, a condition not necessarily true in the case of a hydraulic or pneumatic component leakage failure.

- Contamination Free: The electrical system is not exposed to the contamination problems associated with hydraulic and pneumatic systems, problems which are a primary cause of hydraulic and pneumatic system failures. This is more significant as the number of components in an overall system is increased as, for example, is the case when using the vehicle hydraulic system for a power source.

- Ease of Maintenance: The electrical system is easier to maintain. No hydraulic or pneumatic fluid leakage inspection or cleanliness checkouts are required. Basic component checkout is easier since items such as hydraulic system bleed-in are deleted. The electrical system also provides for easier overall engine system maintenance through the deletion of fluid lines which could interfere with engine component installation or removal.

- Safety: A double malfunction consisting of hydraulic fluid and propellant leakage could result in loss of a hydraulic system due to freezing or a potential fire hazard.

- Electrical Power Required: The electrical system requires more electrical power than the hydraulic or pneumatic systems, however, the total energy from the vehicle power source is not significantly different. The overall power efficiency is higher for the electrical system.

The estimated power requirements are shown on Table CIII.

J. MATERIALS SELECTION

The materials selected for the major engine components are listed on Table CIV. These materials were selected to achieve lightweight engines with consideration of the design and long life requirements and the environmental and propellant compatibility aspects.

TABLE CIII. - ESTIMATED POWER REQUIREMENTS FOR ELECTROMECHANICAL VALVE ACTUATION

Valve	Estimated Nominal Opening Actuation Time (sec)	Estimated Average Opening Power (Watts)
Main LOX Valve	1.5	200
Main RP-1 Valve	0.4	450
LOX Valve - Ox Rich Preburner	1.4	125
LOX Valve - Fuel Rich Preburner	1.4	125
Main LH_2 Valve	0.4	450
RP-1 Valve - Ox Rich Preburner	1.0	50
LH_2 Valve - Ox Rich Preburner	1.0	50
LOX GGV	1.0	50

TABLE CIV. - MATERIALS SELECTION

Component	Baseline LOX/RP-1	Dual-Fuel	Alternate Mode 1
1. Low Speed LOX TPA			
a. Shaft	Inconel 718	Same	Same
b. Impeller & Turbine	7075 T-37 Aluminum Alloy	Same	Same
c. Housing	A356T-6 Al Alloy	Same	Same
d. Bolts	A-286	Same	Same
e. Housing Liner	FEP Teflon Fused Coating	Same	Same
f. Bearings	CRES 440C; Alternate Haynes Star Alloy PM	Same	Same
2. Low Speed RP-1 TPA	All materials the same as low speed LOX TPA except Teflon Coating is not required.		
3. Low Speed LH_2 TPA	Not Applicable	All materials the same as low speed LOX TPA except Teflon Coating is not required.	
4. High Speed LOX TPA			
a. Shaft	A-286	Same	Same
b. Impeller	Inconel 718	Inconel 718	Inconel 718
c. High Pressure Pump & Turbine Housing	ARMCO Nitronic-50	Same	Same
d. Inducer Housing	Inconel 718	Same	Same
e. Turbine	Inconel 718	Inconel 718	UDIMET 630
f. Bolts (pump)	A-286	Same	Same
g. Bolts Turbine	Waspaloy	Same	Same
h. Bearings	CRES 440C or Alternate	Same	Same
5. High Speed RP-1 TPA			
a. Inducer Housing	5AL-2.5 SnEli Titanium Alloy	Same	Same
	All other material the same as High Speed LOX TPA		

TABLE CIV (cont.)

Component	Baseline LOX/RP-1	Dual-Fuel	Alternate Mode 1
6. High Speed LH_2 TPA			
a. Inducer Housing	N/A*	5AL-2.5 Sn Eli Titanium Alloy	Same as Dual-Fuel
b. High Pressure Pump Housing	N/A*	5AL-2.5 SnEli Titanium Alloy	Same
c. Turbine	N/A*	UDIMET 630	Same
d. Impeller	N/A*	A-286	Same
e. Turbine Housing	N/A*	ARMCO Nitronic-50	Same
f. Shaft	N/A*	A-286	Same
g. Bolts (pump)	N/A*	A-286	Same
h. Bolts (turbine)	N/A*	Waspaloy	Same
i. Bearings	N/A*	CRES 440C	CRES 440C
7. LOX/RP-1 Ox-Rich Preburner			
a. Injector Body	ARMCO Nitronic-50	Same	N/A*
b. Chamber	ARMCO Nitronic-50	Same	N/A*
8. RP-1/LOX Fuel-Rich Preburner			
a. Injector Body	ARMCO Nitronic-50	Same	N/A*
b. Chamber	Inconel 625	Same	N/A*
9. LOX/LH_2 Ox-Rich Preburner			
a. Injector Body	N/A*	ARMCO Nitronic-50	N/A*
b. Chamber	N/A*	ARMCO Nitronic-50	N/A*
10. LOX/LH_2 Fuel-Rich Preburner or Gas Generator			
a. Injector Body & Chamber	N/A*	ARMCO Nitronic-50	Same

*Not Applicable.

TABLE CIV (cont.)

	Component	Baseline LOX/RP-1	Dual-Fuel	Alternate Mode 1
11	Thrust Chamber Injector			
	a. Body	Inconel 625	Same	ARMCO Nitronic-50
	b. Manifolds	CRES 347	Same	ARMCO Nitronic-50
	c. Injector Face	Inconel 625	Same	Same
12.	Combustion Chamber	ZR Cu	ZR Cu	ZR Cu
13.	Tubes	Inconel 718	Inconel 718	A-286
14.	Nozzle Extension	N/A*	Columbium	N/A*
15.	Hot Gas Manifold	ARMCO Nitronic-50	Same	N/A*

*Not Applicable.

SECTION IX

CONCLUSIONS AND RECOMMENDATIONS

A. CONCLUSIONS

The conclusions which have been derived from the results of this advanced high pressure engine study are presented on Table CIV for easy reference. These conclusions cover all study tasks.

It should be noted that, because candidates are not recommended as coolants, this does not necessarily mean that the propellant combination is eliminated. LOX cooling would be feasible for any of the study propellant combinations. For example, RP-1 was eliminated as the coolant but selected as the baseline fuel in a LOX cooled engine. Operational problems may preclude the use of MMH and N_2H_4 in any case.

The dual-fuel engine nozzle is very long and heavy because the contour was performance optimized. That is, a two position nozzle contour which resulted in performance almost equal to the baseline Mode 1 and Mode 2 engines was selected. The nozzle length and engine weight could be significantly reduced if some performance penalty is acceptable.

B. RECOMMENDATIONS

The recommendations for technology and further study that were identified as a result of this high pressure engine study are tabulated on Table CV.

TABLE CV. - CONCLUSIONS

CANDIDATE	CONCLUSIONS
o Baseline LOX/RJ-5, LOX Cooled	o FEASIBLE CANDIDATE o Max Pc based upon power balance, ∿ 286 atm (4200 psia) with 20% margin.
o LOX/RJ, RJ-5 Cooled	o UNFEASIBLE Candidate for reusable, high pressure engine o Max Pc<136 atm (2000 psia); limited by coking in coolant channels.
o LOX/RP-1, RP-1 Cooled	o UNFEASIBLE Candidate for reusable, high pressure engine. o Max Pc < 136 atm (2000 psia); limited by coking in coolant channels.
o LOX/MMH, MMH Cooled	o NOT RECOMMENDED o Max Pc based upon power balance ∿ 306 atm (4500 psia) with 20% margin. o MMH incompatible with ZrCu for long term use. o Fuel-Rich Preburner Temp. ∿ 1333°K (2400°R) creates turbine life or design problem.
o LOX/N_2H_4, N_2H_4 Cooled	o NOT RECOMMENDED. o Max Pc > 340 atm (5000 psia); based upon power balance with 20% margin. o N_2H_4 incompatible with ZrCu for long term use. o Fuel-rich Preburner Temp. ∿ 1000°K (1800°R) creates turbine life or design problem. o N_2H_4 vapors create explosive hazard.
o LOX/CH_4, CH_4 Cooled	o FEASIBLE CANDIDATE o Max Pc ∿ 272 atm (4000 psia) based upon power balance with 20% margin o Delivered I_s approximately 13 secs greater than baseline. o Engine weight 248 kg (546 lb) heavier than baseline.

TABLE CV (cont.)

CONCLUSIONS

CANDIDATE	CONCLUSIONS
o Parallel Burn, Hydrogen Cooled, LOX/RJ-5	o VIABLE CANDIDATE BUT NOT RECOMMENDED o Max. Pc ~ 340 atm (5000 psia) based upon power balance with 20% margin. o Operationally limited to only parallel burn. o Operation affects Mode 2 engine development. o Gimbal potentially unfeasible
o Hydrogen Cooled, Gas-Generator Cycle (LOX/RJ-5)	o VIABLE CANDIDATE: RECOMMENDED FOR FURTHER STUDY o Max Pc > 340 atm (5000 psia) based upon coolant and power balance analyses. o Coolant flow rate ~ 9.07 kg/sec (20 lb/sec) requires increased LH_2 tank capacity. o Lighter engine weight, 327 kg (722 lb), compared to baseline for equivalent I_s. o Preliminary trade studies show potential payoff compared to baseline.
o Auxiliary Coolants	o NOT RECOMMENDED o WATER BEST CANDIDATE o No gains with NaK o Lithium corrosivity and operational problems o All systems heavier than baseline with equivalent I_s o Higher Pc potential than baseline. o Increased system complexity
o Baseline Fuel: RJ-5 or RP-1	o RP-1 RECOMMENDED o Unknown cost projection for RJ-5

TABLE CV (cont.)

CONCLUSIONS

CANDIDATE	CONCLUSIONS
Boost Pump Drive Method	
o Hydraulic Turbine	o Selected Concept: Simple control and light weight
o Gas Turbine	o Not Recommended: (1) Requires hot gas control valves, multi-stage turbine and high pressure hot gas housings (2) Very heavy
o Gear Drive	o Not Recommended: (1) Restricts engine packaging. (2) LOX cooled gears considered unfeasible
Preliminary Designs	
o Mode 1 LOX/RP-1	o Promising Concept: (1) Engine Weight = 2112 kg (4657 lb) (2) Engine I_s = 323.6 secs (sea-level) = 350.6 secs (vacuum) (3) Engine Length = 277 cm (109 in) (4) Requires advanced technology effort (5) Potentially simple control system
o Alternate Mode 1 (Gas Generator Cycle) Engine	o Promising Concept: (1) Engine Weight = 1758 kg (3935 lb) (2) Engine I_s = 323.5 secs (sea-level) = 350.7 secs (vacuum) (3) Engine Length = 315 cm (124 in) (4) Most technology has been demonstrated (5) Additional engine complexity

TABLE CV (cont.)

CONCLUSIONS

CANDIDATE		CONCLUSIONS
o Dual-Fuel Engine (Mode 1 and Mode 2)	o Advanced Concept:	(1) Lighter weight than a Mode 1 plus a Mode 2 engine (2) Engine Weight = 4183 kg (9223 lb) (3) Engine I_s — Mode 1 / Mode 2 Sea-level: 322.9 secs / - Vacuum: 349.9 secs / 459.2 secs (4) Engine Length: Mode 1 cm (in) / Mode 2 (cm) (in) 734 (289) / 878 (345.5) (5) Requires hot gas check valves (6) Greatest engine complexity (7) Requires advanced technology effort

TABLE CVI. - TECHNOLOGY RECOMMENDATIONS

Item	Technology Suggestion	Objectives
1. Propellants	o Extend investigation to include other fuels.	o Define low cost synthetic fuel for large quantity production.
	o Verification of propellant properties at high pressure	o Extend experimental data to 408 atm (6000 psia).
2. Combustion	o LOX/Hydrocarbon Preburner, Fuel-Rich	o Evaluate carbon formation, deposition and combustion properties at high pressure.
	o LOX/Hydrocarbon Preburner, Ox-Rich	o Investigate potential MR distribution problems and define combustion properties at high pressure.
	o LOX/Hydrocarbon TCA	o Verification of propellant properties at high pressure, 408 atm (6000 psia). Carbon deposition evaluation.
3. Performance	o Thrust chamber performance gas/gas injection	o Verification of chamber length requirements, performance levels and stability of gas/gas injection at high pressure.
4. TCA Heat Transfer	o LOX regeneratively cooled TCA for LOX/Hydrocarbon propellant	o LOX heat transfer heated tube testing. Demonstration of heat flux capability in ZrCu thrust chamber and material compatability.
	o LOX regeneratively cooled TCA for LOX/H_2 Propellants	o Same as above.
5. Thrust Chamber	o LOX regeneratively cooled TCA failure analysis	o Evaluation cf LOX leakage on TCA hot wall side without film cooling.
6. Turbomachinery	o Propellant cooled bearings	o Establish propellant lubricated rolling contact bearing life-load characteristics.
	o TPA Seal Evaluation	o Determine TPA seal wear and life data.

TABLE CVI (cont.)

TECHNOLOGY RECOMMENDATIONS

Item	Technology Suggestion	Objectives
7. System Analysis	o Extend of parametric range to 6.67 MN (1.5 Mil. lbs) thrust engines	o Obtain useful data for heavy lift vehicle mission studies
	o LOX/CH_4 Engine Preliminary Design	o Obtain baseline engine data for LOX/Methane engines
	o Evaluation of cost effective chamber life for SSTO mission	o Increase in payload through engine weight reduction
	o Definition of Advanced High Pressure Engine development and production plans and cost	o Define development lead times, hardware and funding rate requirements

REFERENCES

1. McCarty, R. D. and Weber, L. A., Thermophysical Properties of Oxygen From the Freezing Line to 600°R for Pressures to 5000 psia, NBS Tech. Note 384, National Bureau of Standards, Cryogenics Div., Boulder, Colorado, July 1971.

2. Roder, H. M. and Weber, L. A., ASRDI Oxygen Technology Survey: Volume I, Thermophysical Properties, NASA SP-3071, National Aeronautics and Space Administration, Washington, D. C., 1972.

3. Weber, L. A., Extrapolation of Thermophysical Properties Data for Oxygen to High Pressures (5000 to 10,000 psia) at Low Temperatures (100-600°R), NASA-CR-133858, NBS-10727, National Bureau of Standards, Cryogenics Div., Boulder, Colorado, November 1971.

4. Hanley, H. J., McCarty, R. D. and Sengers, J. V., Viscosity and Thermal Conductivity Coefficients of Gaseous and Liquid Oxygen, NASA-CR-2440, National Aeronautics and Space Administration, Washington, D. C., August 1974.

5. McCarty, R. D. and Weber, L. A., Thermophysical Properties of Parahydrogen from the Freezing Liquid Line to 5000°R for Pressures to 10,000 psia, NBS Tech. Note 617, National Bureau of Standards, Cryogenics Div., Boulder, Colorado, April 1972.

6. Liquid Propellants Manual, Unit 20, RP-1, Chemical Propulsion Information Agency, The Johns Hopkins University Applied Physics Laboratory, Silver Springs, Md., January 1966.

7. Dean, L. E. and Shurley, L. A., Characteristics of RP-1 Rocket Fuel, Tech. Report TCR-70, Contract F04(645)-8, Weapon System 107A, Aerojet-General Corporation, Sacramento, Calif., 14 February 1957.

8. USAF Propellant Handbook-Hydrazine Fuels-Volume 1, AFRPL-TR-69-149, Bell Aerospace Co., Buffalo, New York, Contract F04611-69-C-005, March 1970.

9. Rousar, D. C., et al, Heat Transfer Study of MHF-5 and MMH, AFRPL-TR-67-208, Part II, Aerojet-General Corporation, Sacramento, California, August 1967.

10. Constantine, M. T., Engineering Property Determination on Rocket Propellants, AFRPL-TR-70-147, Rocketdyne, Canoga Park, California, Nov. 1970.

11. Engineering Property Data on Rocket Propellants, AFRPL-TR-68-100, Rocketdyne, Canoga Park, California, May 1968.

12. Airbreathing Propulsion Manual, Unit 2, RJ-5, Air Force Aero Propulsion Laboratory, Wright-Patterson Air Force Base, Ohio, May 1974.

13. Schneider, A., et al, Air-Breathing Missile Fuel Development, AFAPL-TR-74-44, Sun Oil Company, Marcus Hook, Pa., May 1974.

14. Sargent, D. H., Advanced Fuel Systems for Ramjet-Powered Vehicles, AFAPL-TR-72-1, Vol. I, Atlantic Research, Alexandria, Va. February 1972.

15. Reicl, R. C., and Sherwood, T. K., The Properties of Gases and Liquids, Their Estimation and Correlation, McGraw and Hill, New York, 2nd Edition, 1966.

16. Nixon, A. C., et al., Vaporizing and Endothermic Fuels for Advanced Engine Applications: Part III, Studies of Thermal and Catalytic Reactions, Thermal Stability, and Combustion Properties of Hydrocarbon Fuels, AFAPL-TR-67-114, Part III, Volume, II, Shell Development Company, February 1970.

17. Goodwin, R. D., The Thermophysical Properties of Methane, from 90 to 500K at Pressures to 700 Bar, NBS Technical Note 653, Cryogenics Div., National Bureau of Standards, Boulder, Colorado (1974).

18. Stull, D. R., et al, JANAF Thermochemical Tables, The Dow Chemical Company, Midland, Michigan; Methane (CH_4), March 31, 1961.

19. Gambill, W. R., Generalized Gas Heat Capacities, Chem. Eng., 64 (10), 283-8 (1957).

20. Lydersen, A. L., Greenkorn, R. A. and Hougen, O. A., Generalized Thermodynamic Properties of Pure Liquids, Univ. Wisconsin Coll. Eng. Rept. 4, Madison, Wisconsin, October 1955.

21. Touloukian, Y. S., Saxena, S. C., and Hestermans, P., Thermophysical Properties of Matter, Vol. II, Viscosity, p. 189, IFI/Plenum, New York.

22. Huang, E.T.S., Swift, G. W., and Kurata, Fred., Viscosities of Methane and Propane at Low Temperatures and High Pressures, A.I.Ch.E. Journal, 12 (5), 932-6, 1966.

23. Swift, G. W., Lohrenz, John, and Kurata, Fred, Liquid Viscosities Above the Normal Boiling Point for Methane, Ethane, Propane, and n-Butane, A.I.Ch.E. Journal, 6 (3), 415-9, 1960.

24. Touloukian, Y. S., Liley, P. E., and Saxena, S. C., Thermophysical Properties of Matter, Vol. 3, Thermal Conductivity, Nonmetallic Liquids and Gases, p. 220, IFI/Plenum, New York (1970).

25. Ikenberry, L. D., and Rice, S. A., On the Kinetic Theory of Dense Fluids XIV. Experimental and Theoretical Studies of Thermal Conductivity in Liquid Ar, Kr, Xe, and CH_4, J. Chem. Phys., 39 (6), 1561 (1963).

26. Gregory, J. W., Propulsion Technology Needs for Advanced Space Transportation Systems, AIAA Paper No. 75-1246, October 1975.

27. Chemical Rocket-Propellant Hazards - Volume III, Liquid Propellant Handling, Storage and Transportation, CPIA Publication No. 194, JANNAF Propulsion Committee, The JANNAF Hazards Working Group, Chemical Propulsion Information Agency, The John Hopkins University Applied Physics Laboratory, Silver Springs, Md., May 1970.

28. Jet Fuel Thermal Stability Improvements Through Fuel Processing, AFAPL-TR-74-35, Air Force Aero Propulsion Laboratory, Wright-Patterson Air Force Base, Ohio, August 1974.

29. Pauckert, R. P., Space Storable Regenerative Cooling Investigation, NASA CR-72360, Contract NAS3-11191, Rocketdyne, Sept. 25, 1968.

30. Osborn, G. H. Gas Generator Coking Investigation, Report No. L1507SM-3, Aerojet-General Corporation, Sacramento, California, Contract AF04(645)-8, 11 February 1959.

31. VanderWall, E. M., Suder, J. K., Beegle, R. L., Jr., and Cabeal, J. A., Propellant/Material Compatibility Study, AFRPL-TR-71-41, Aerojet Liquid Rocket Company, Sacramento, California, Contract F04611-71-C-0094, December 1971.

32. A Survey of Compatibility of Materials with High Pressure Oxygen Service, Final Report 275.03-72-11, National Bureau of Standards, Cryogenics Division, Boulder, Colorado, NASA Order No. H-9 2180A, October 1972.

33. Pelouch, J. J., Jr., ASRDI Oxygen Technology Survey: Volume III, Characteristics of Metals that Influence System Safety, NASA SP-3077 National Aeronautics and Space Administration, Washington, D. C. (1974).

34. Space Shuttle Main Engine, Supporting Analysis, DR No. SE 278, Contract NAS8-26188, ALRC, 21 April 1971.

35. Effects of Environment and Complex Load History on Fatigue Life, STP 462, American Society for Testing Materials, January 1970.

36. Tiffany, C. F., et al., Investigation of Crack Growth Threshold of Inconel 718 Exposed to High Pressure Oxygen, Final Report NASA CR-108485, Contract NAS9-10913, The Boeing Company, August 1970.

37. Harris, J. A., Jr. and Van Wanderham, M. C., Properties of Materials in High Pressure Hydrogen at Cryogenic, Room, and Elevated Temperatures, Final Report FR-5768, Pratt and Whitney Aircraft, West Palm Beach, Florida, Contract NAS8-26191, 31 July 1973.

38. Walter, R. J. and Chandler, W. T., Influence of Gaseous Hydrogen on Metals, Final Report NASA CR-124410, Rocketdyne, Canoga Park, California, Contract NAS8-25579, October 1973.

39. Gray, H. R., Hydrogen Environment Embrittlement, NASA TMS-68088, Lewis Research Center, June 1972.

40. Stanley, J. K., Carburization of Four Austenitic Stainless Steels, Report No. TR-0066 (5250-10)-6, Aerospace Corporation, September 1969.

41. Gilbraeth, W. P. and Adamson, M. J., The Stress Corrosion Susceptibility of Several Alloys in Hydrazine Fuels, NASA TN D-7604, Ames Research Center, February 1974.

42. Svehla, R. A., and McBride, B. J., Fortran IV Computer Program for Calculation of Thermodynamic and Transport Properties of Complex Chemical Systems, NASA TN D-7056, January 1973.

43. Gas Generator Thermochemical Data, Project 107A Contract AF04(645)-8, ALRC Report No. TCR-5, March 1955.

44. Calhoon, et. al., Investigation of Gaseous Propellant Combustion and Associated Injector/Chamber Design Guidelines, NASA CR-121234, Contract NAS3-14379, ALRC, 31 July 1973.

45. Combustion Effects on Film Cooling, HOCOOL Users Manual, Contract NAS3-17813, ALRC, 15 July 1975.

46. Rousar, D., and Miller, F., Cooling with Supercritical Oxygen, AIAA Paper No. 75-1248, Sept. 1975.

47. Vasserman, A. A., and Rabinovich, V. A., Thermophysical Properties of Liquid Air and its Components, Translated from Russian, U. S. Dept. of Commerce Clearinghouse for Federal Scientific and Technical Information, 1968.

48. Hess, H. L., and Kunz, H. R., A Study of Forced Convection Heat Transfer to Supercritical Hydrogen, ASME Paper No. 63-WA-205, Nov. 1963.

49. Hines, W. S., Turbulent Forced Convection Heat Transfer to Liquids at Very High Heat Fluxes and Flowrates, Rocketdyne Research Report No. 61-14, Nov. 1961.

50. Rousar, D. C., et. al., Heat Transfer Study of MHF-5 and MMH, AFRPL-TR-67-208, Part I, August 1967.

51. Nickerson, G. R., et. al., Two Dimensional Kinetic (TDK) Reference Computer Program, Ultrasystems, Inc., December 1973.

52. Pieper, J. L., ICRPG Liquid Propellant Thrust Chamber Performance Evaluation Manual, CPIA Report 178, September 1968.

53. Design Verification Specification, Space Shuttle Main Engine, Volume II, DVS-SSME-101C, Rocketdyne, North American Rockwell, 9 April 1974.

54. Space Shuttle Main Engine, Phase C/D Program Definition Documentation, Volume I, Engine Design Definition Report, Engine System, DR No. SE-275, Contract NAS8-26188, ALRC, 21 April 1971

55. Achener, P. Y., et. al., Thermophysical and Heat Transfer Properties of Alkali Metals, AGN-8195 (Vol. 1), USAEC Contract AT (04-3)-368, Aerojet-General Corp., Nucleonics Div., San Ramon, Ca., April 1968.

56. Ho, C. Y., Powell, R. W., and Liley, P. E., Thermal Conductivity of the Elements, Reprint No. 7 from J. Phys. and Chem. Ref. Data, Vol. 1, No. 2, pp 279-421 (1972).

57. Foust, O. J., editor, Sodium-NaK Engineering Handbook, Vol. 1, Sodium Chemistry and Physical Properties, Gordon and Breach, Science Publishers, Inc., New York (1972).

58. Ewing, C. T., et. al., Thermal Conductivity of Mercury and Two Sodium-Potassium Alloys, J. Phys. Chem., 59, 524-528 (1955).

59. Berry, E., Testing Nuclear Materials in Aqueous Environments - Handbook for Corrosion Testing and Evaluation, John Wiley & Sons, 1971.

60. Beck, F. H., Fontana, M. G., and Kirk, W. W., Stress Corrosion Cracking of Austentic Stainless Steels in High Temperature Chloride Waters, "Physical Metalurgy of Stress Corrosion Fracture," Rhodin, T., ed., Interscience Publishers, Inc., New York, 1959.

61. Staehle, R. W., Materials Problems and Research Opportunities in Coal Conversion, Ohio State Univ., 1974.

62. Brush, E. G., and Pearl, W. L., Corrosion Behaviour of Nonferrous Alloy Feedwater-Heater Materials in Neutral Water with Low Oxygen Contents, Corrosion, Vol. 25, No. 3, March 1969

63. Strong, J. H., et. al., Compatibility of Liquid and Vapor Alkali Metals with Construction Materials, DMIC Report 227, April 15, 1966.

64. Lyon, R. N., Liquid Metals Handbook, Atomic Energy Commission and Department of Navy, June 1952.

65. Cheng, C. F., and Rurther, W. E., The Corrosion of Nickel in Liquid Sodium, Corrosion, Vol. 28, No. 1, January 1972.

66. Reemsnyder, D. C., et. al., Performance and Cavitation Damage of an Axial-Flow Pump in 1500°F Liquid Sodium, NASA TN D-5138, April 1969.

67. DeVries, G., The Corrosion of Metals by Molten Lithium, from "Corrosion of Liquid Metals," Plenum Press, 1970.

68. Rousar, D. C. and Van Huff, N. E., Heat Transfer Characteristics of 98% H_2O_2 at High Pressure and High Velocity, AFRPL-TR-66-263, August 1966.

69. Talanov, V. D., and Ushakov, P. A., Study of Heat Transfer in Liquid Metals in Round Pipes, NASA-TT-F-522, 1969.

70. Model Specification 1,500,000 lb. Thrust Liquid Oxygen RP-1 Liquid-Propellant Engine, Rocketdyne Model F-1, Rocketdyne Report R-1420cS dated 15 Jan. 1963.

71. Titan Engines and Applications, Aerojet-General Corp. Report Number CR128, 31 Oct. 1960.

72. A Preliminary Investigation of Oxidizer-Rich Oxygen-Hydrogen Combustion Characteristics, NASA TMX-53371, 20 Dec. 1965.

73. An Experimental Investigation of an Oxygen-Hydrogen Gas-Gas Cycle Engine System, Final Report IR&D 8709-40, Aerojet-General Corp., Jan. 1967.

74. Liquid Rocket Engine Turbines, NASA Space Vehicle Design Criteria (Chemical Propulsion) NASA SP-8110, Jan. 1974.

75. Taylor, M. F., Applications of Variable Property Heat-Transfer and Friction Equations to Rocket Nozzle Coolant Passages and Comparison with Nuclear Rocket Test Results, AIAA Paper No. 70-661, presented 15 June 1970.

76. Ito, J. I., Development of LO_2/LH_2 Gas Generators for the M-1 Engine, NASA CR5-4812, 1 June 1976.